2008

Mechanisms of Nickel-Based Coatings for Fretting Wear Mitigation of Ti6Al4V Interfaces

Carl H. Hager Jr.
Wright State University

MECHANISMS OF NICKEL-BASED COATINGS FOR FRETTING WEAR MITIGATION OF Ti6Al4V INTERFACES

A dissertation submitted in partial fulfillment of the
requirements for the degree of
Doctor of Philosophy

By

CARL H. HAGER, JR.
B.S., Pennsylvania State University, 2000
M.S., Pennsylvania State University, 2002

2008
Wright State University

August 29, 2008

I HEREBY RECOMMEND THAT THE DISSERTATION PREPARED UNDER MY SUPERVISION BY CARL HAGER, Jr. ENTITLED Mechanisms of Nickel-Based Coatings for Fretting Wear Mitigation of Ti6Al4V Interfaces BE ACCEPTED IN PARTIAL FULFILLMENT OF THE REQUIREMENTS FOR THE DEGREE OF Doctor of Philosophy.

_____
Ramana Grandhi, Ph.D.
Dissertation Director

_____
Ramana Grandhi, Ph.D.
Director, Ph.D. in Engineering

_____
Joseph F. Thomas, Jr., Ph.D
Dean, School of Graduate Studies

Committee on
Final Examination:

_____
Ramana Grandhi, Ph.D.

_____
Terry Murray, Ph.D

_____
Jeffrey Sanders, Ph.D

_____
Andrey Voevodin, Ph.D

_____
Joseph C. Slater, PE, Ph.D

_____
Daniel Young, Ph.D

ABSTRACT

Hager, Jr. Carl H. Ph.D. in Engineering, Department of Mechanical and Materials Engineering, Wright State University, 2008. Mechanisms of Nickel-Based Coatings for Fretting Wear Mitigation of Ti6Al4V Interfaces.

Fretting wear is an accumulation of damage that occurs at component interfaces that are subjected to high contact stresses coupled with low amplitude oscillation. The key to fretting wear reduction in metallic contacts is the mitigation of galling at the interface, followed by the control of debris production and the rheology of active wear debris. Once the thin surface species of the metallic interfaces is dispersed, adhesion between the contacting nascent surfaces causes the inception of severe surface deformation and material transfer or removal. This is extremely apparent in the fretting wear of aerospace materials such as titanium alloy and nickel alloy contacts. However, the literature suggests that nickel alloy contacts perform very well in sliding and reciprocating wear contacts at elevated temperatures due to the formation of what is often called a 'Glaze' oxide layer. The current state of literature describes the composition of the glaze layer as NiO. The focus of this dissertation was to provide experimentation and analysis of temperature effects on the lubricious tribofilm formation that occurs in nickel contacts. This was accomplished by testing commercially pure nickel coatings and thick nickel oxide surfaces. The enhanced understanding of the fretting performance of nickel oxides aided in the development of nickel graphite based self-lubricating coatings. These coatings were then proved to reduce fretting wear damage within Ti6Al4V mated surfaces over a wide temperature range.

TABLE OF CONTENTS

LIST OF FIGURES

LIST OF TABLES

ACKNOWLEDGEMENTS

First I would like to thank Dr. Jeffrey Sanders for bringing me into the Tribology group at Wright Patterson Air Force Base and for encouraging me to go back to school to earn my PhD. His insight and friendship help me start my career in the field of Tribology. I would also like to thank Dr. Andrey Voevodin for continuing to support my work, and for bringing me up to a new level. For years I was so focused on the surface mechanics, and it was Dr. Voevodin that really made me focus on the whole picture by equally analyzing the surface chemistry and material microstructure. To Dr. Joseph Slater, I would like to thank for his willingness to push students hard to make them learn. To Dr. Terry Murray and Dr. Daniel Young, I would like to thank them for their helpful insight and their willingness to serve on my committee at short notice. The completion of this work would not be possible without them. To Dr. Ramana Grandhi, I would like to thank for his leadership and passion to for me to put my best foot forward and complete everything that I started to the best of my ability. And last but of course not least, I would like to extend my appreciation to Alysoun Taylor for always keeping on top of things and helping me to complete things correctly and in a timely manner.

To my family I would like to thank my parents for all of their gracious guidance through the years. I would like to send my gratitude to my mother and father in law for all of their support and confidence. To my daughters, I would like to thank them for being my inspiration and for helping me keep my eyes on what matters most. And finally, I would like to thank my wife most of all for her constant love and belief in me.

Chapter 1

INTRODUCTION

Fretting wear is an accumulation of damage that occurs at component interfaces that are subjected to high contact stresses coupled with low amplitude oscillation. The distinction between fretting wear and reciprocating wear is best described by Chen et al [1] using volumetric wear rate. During reciprocating wear, for a specified set of loading conditions, the volumetric wear rate will remain constant even if the oscillation displacement is changed. However, if the stroke length is reduced below a critical displacement, the volumetric wear rate will decrease proportional to the stroke length. This critical displacement is the transition point from reciprocating to fretting wear. The transition occurs because of changes in surface interactions and debris formation. In reciprocating wear, most of the debris created at the interface is swept out of the wear track and piles up at the ends of reciprocation, with some debris escaping at the sides. Relatively small amounts of debris get dragged back through the wear track. However, in fretting wear the relative displacements are often so small that the debris never leaves the interface causing a third body effect where the debris grinds into the mating surfaces as explained by Varenberg et al [2].

When dealing with fretting it is important to understand the different underlying wear regimes that have been identified [3-6]. If mating surfaces are subjected to low contact loads and relatively long fretting stroke lengths, gross slip will occur. In gross slip, both surfaces oscillate relative to one another. As the contact load increases and/or the stroke length decreases, “mixed” fretting will occur. The mixed fretting regime is the most complex and involves surface adhesion in metallic interfaces, which causes a mixture of

sticking and slipping throughout the wear track. If one or both of the mating surfaces are rounded geometrically and the load further increases and/or the stroke length is even smaller, then "partial stick" may occur. The idea of partial stick was first described by Mindlin [3] in 1949. The basic premise of partial stick comes from the fact that the force resisting motion is a function of friction and normal load. In order to induce relative motion at the interface, the applied tangential load must overcome the resisting force within the elasticity limits of the bulk material. The Hertzian contact pressure distribution caused by a ball, a cylinder, or an ellipsoid causes maximum resistance at the center of contact that decreases outwards; therefore, causing the center region of the contact to stick while a wear annulus forms around the outside edge, as shown in Fig. 1.1. As the contact load is increased the slip annulus decreases until full stick occurs. In full stick there is no relative motion within the contact.

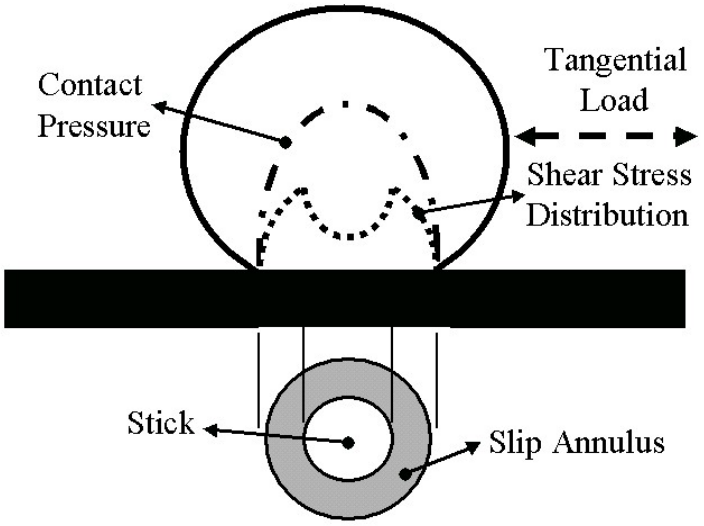

Fig. 1.1. Partial stick fretting wear [7].

Upon the onset of fretting, multiple wear mechanisms such as adhesive, abrasive, fatigue, and oxidative wear can act individually or simultaneously. However, in metallic contacts, surface oxides, adhesion, and material transfer play a primary role in the initial stages of fretting wear degradation. In 1943, Bowden et al wrote a classic paper on ploughing and adhesion of metal surfaces [8]. They showed that in the absence of oxide interaction, nascent metallic surfaces will adhere and cause material transfer from one surface to the other. In 1981, Blau explained that one of the aspects of transitions in friction and wear of metals is the transfer and retransfer of metal from one contacting surface to the next, or galling [9]. Although galling can be considered to be ambiguous by definition, all definitions contain the concepts of localized adhesion and material transfer. The ASM definition of galling likens it to scuffing, which it defines as "localized damage caused by the occurrence of solid-phase welding between sliding surfaces" [10].

In a review of fretting wear mechanisms, Hurricks explains that fretting wear of metallic contacts in most cases can be broken up into 3 major stages: oxide removal, adhesive wear or galling, and finally 3rd body wear [11]. The interfacial wear begins with the removal of the thin oxide layers on the surface of the metals in contact. Once the oxides are disrupted the nascent metallic surfaces come in contact and form adhesive junctions between the surfaces. These adhesive junctions are strained beyond the elastic limit of the bulk material as they accommodate the relative motion between the sliding surfaces. This causes severe plastic deformation to occur, and leads to material transfer as the junctions are eventually ruptured and reformed. The continuous formation and rupture of adhesive junctions, along with the inception of material transfer, creates surface protrusions on both of the contacting surfaces. These surface protrusions then lead to more

plastic deformation of the interface through the act of ploughing. The raised surface regions create localized contact stress concentrations, and get dragged along the contact creating striations or scores on the mated surface. In addition, the surface protrusions can mechanically interlock, like gear teeth, causing shear stress concentrations and more severe surface deformation. Over time, dislocations start to build up in localized regions due to the severe interfacial deformation that has occurred. In these regions, the metallic interface becomes unable to accommodate the imposed displacement and cracks begin to form [12]. In addition to the conventional thought that surface crack formation occurs in the tensile region behind the sliding surface, work by Blau et al and Suh show that these cracks can also nucleate in the compressive zone ahead of the sliding surface and below the surface in the shear zone [13, 14]. Once these cracks become large enough to propagate, loose particles are liberated from the surfaces in contact. Some of the loose particles, also known as 3rd body debris, are swept out of the contact and become passive wear debris. The remaining particles in the contact become active wear debris. As the quantity of active wear debris increases, the interfacial wear mechanisms become dominated by the rheology of the wear debris [15]. In some metallic contacts the active wear debris eventually gets compressed together, as shown in Fig 1.2, and forms a powder bed that separates the contacting surfaces [6]. If the powder bed formation is continuous, then the surface degradation will be concentrated at the edges of the contact and expand the wear track laterally instead of deeper [12].

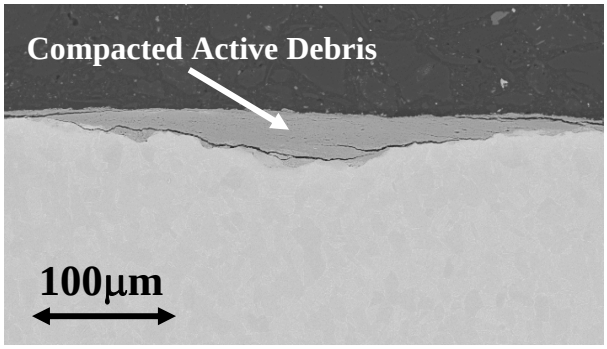

Fig. 1.2. Backscatter SEM image showing the cross-section of an unlubricated Ti6Al4V sample after 100,000 cycles of fretting wear against another Ti6Al4V sample [16].

From the aforementioned mechanisms of fretting wear in metallic contacts, the key to wear reduction is the mitigation of galling at the interface, followed by the control of debris production and the rheology of active wear debris. Once the thin surface species of the metallic interfaces is dispersed, adhesion between the contacting nascent surfaces causes the inception of severe surface deformation and material transfer or removal. This is extremely apparent in the fretting wear of aerospace materials such as titanium alloys. One of the most common occurrences of fretting in a turbine engine is in the compressor section at the blade/disk interface, shown in Fig 1.3. The blade/disk interface, also known as the dovetail joint, is often fabricated from Ti6Al4V (Titanium, 6% Aluminum, 4% Vanadium) because of its high strength to weight ratio and corrosion resistance. Tribologically, mating Ti6Al4V surfaces are especially susceptible to fretting, because titanium alloys have a propensity to gall and can produce hard oxide debris that score the interface [17]. In addition, Sauger et al showed that the debris initially generated in Ti6Al4V contacts comes from a tribologically transformed structure (TTS) that forms at the fretting interface [18]. In this investigation the authors determined that the TTS appeared as a nanocrystalline structure with chemistry corresponding to that of the bulk

material. Sauger et al believed that this layer was generated by deformation induced recrystallization of the microstructure. In addition, it was determined that the TTS layer, formed in Ti6Al4V interfaces, was more than 3 times harder than the bulk material itself. This hardened layer cannot accommodate the imposed fretting displacements and hard titanium particles are released from the wear surfaces. Once detached, these particles can get trapped in the fretting wear interface and cause 3rd body wear. Overtime, the particles breakup and oxidize as shown in the research by Blanchard et al [12].

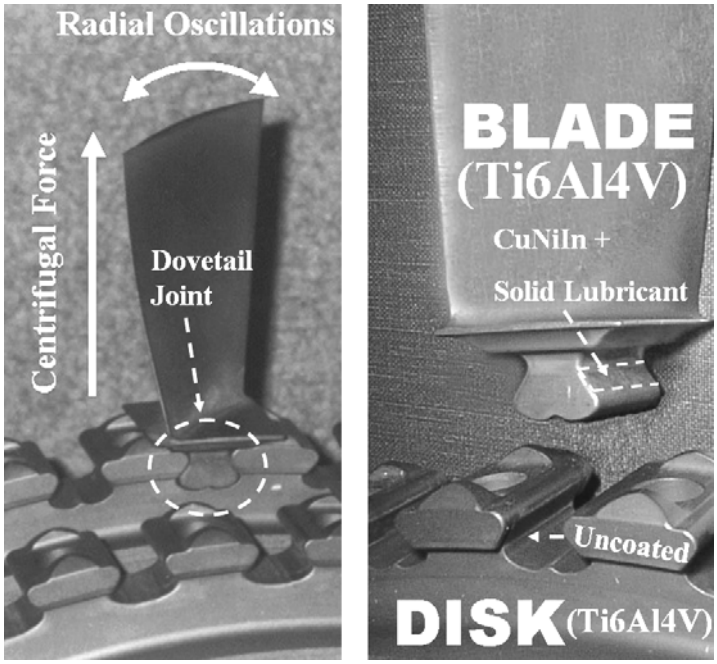

Fig. 1.3. Dovetail joint at the blade/disk interface.

In addition to fretting wear at the interface, the combination of the rotating disk and the airflow through the engine imposes centrifugal forces and radial oscillations on the blades causing bulk cyclic stresses and component fatigue. The combination of the bulk cyclic stresses and fretting surface interactions is often called fretting fatigue. In fatigue, most of the component fatigue life is accommodated by the crack initiation phase. However, component fatigue life is reduced exponentially once critical cracks have been

formed. The imposition of fretting wear at interfaces subjected to bulk cyclic loading can acceleration crack initiation. This is best described by Zhou et al in their fretting wear experiments with aluminum alloys [4]. In this work the authors conducted pure fretting wear tests using a spherical rider loaded normally onto a flat plate. Tests were conducted under various stroke lengths (~20-70 μm) and loads (~100-1200 N) for increased test durations. At the completion of each test, the samples were cross-sectioned and the fretting wear tracks were investigated for cracks. Zhou et al found that during the fretting wear tests, without bulk loading of any kind, cracks were formed in the fretting contact. It was also found that critical cracks (greater than 50 μm) can be formed very quickly when the fretting tests were operated in the mixed fretting regime. The observance of this cracking phenomenon under pure fretting wear conditions (without bulk loading) was also noted within Ti6Al4V contacts in 2004 by Swalla et al [58]. In 2005, Hutson et al conducted extensive fretting fatigue crack analysis in Ti6Al4V contacts, and established that cracks greater than 50 μm can produce a dramatic reduction in fatigue strength [59]. The basic impact of fretting wear on the reduction of fatigue life has been addressed in many publications, and are neatly summarized by Waterhouse in his fretting fatigue review paper in 1992 [19].

Fretting fatigue in dovetail joints can lead to catastrophic blade and/or disk failures by fracture of the blade dovetail or disk edge that holds the blade in place. One common mitigation strategy, or solution, to the fretting wear/fatigue problem is to apply plasma sprayed CuNiIn (Copper-Nickel-Indium) or aluminum bronze coatings and solid lubricants to the dovetails of the Ti6Al4V compressor blades, as shown in Fig 1.3 [20]. In some cases a solid lubricant is also applied to the disk slot; however, the slot geometries are often

too small for the application of a plasma sprayed coating. Therefore, the CuNiIn or aluminum bronze coating and solid lubricant, applied to the blade dovetail, was designed to act as a sacrificial barrier that protects both the blade and disk by preventing the Ti6Al4V surfaces from coming into contact with each other.

The high roughness of the soft plasma sprayed metallic coatings is used as a retainer for the application of a bonded solid lubricant. The implementation of this strategy has increased component life; however, recent studies have shown that unlubricated CuNiIn and aluminum bronze coatings can cause severe damage to mating Ti-alloy counterparts [20]. In fact in 1994 Privet III et al [21] stated that unlubricated CuNiIn coatings caused a slight reduction in high cycle fatigue life as compared to the uncoated Ti 6242 (Titanium, 6% Aluminum, 2% Tin, 4% Zirconium, 2% Molybdenum, 0.1% Silicon) mated baseline tests. In 2000 Freimanis et al conducted a fretting wear analysis of blades and their mated disks after engine operation [22]. In this research it was found that the solid lubricant had worn away and the CuNiIn coated dovetails had caused significant damage to the uncoated disk. Fig 1.4 shows the transfer of titanium to the surface of a CuNiIn coated blade dovetail, via galling with the uncoated disk. This clearly shows that the CuNiIn coatings can have a detrimental impact on the fretting fatigue life of dovetailed components once the applied lubricants wear out.

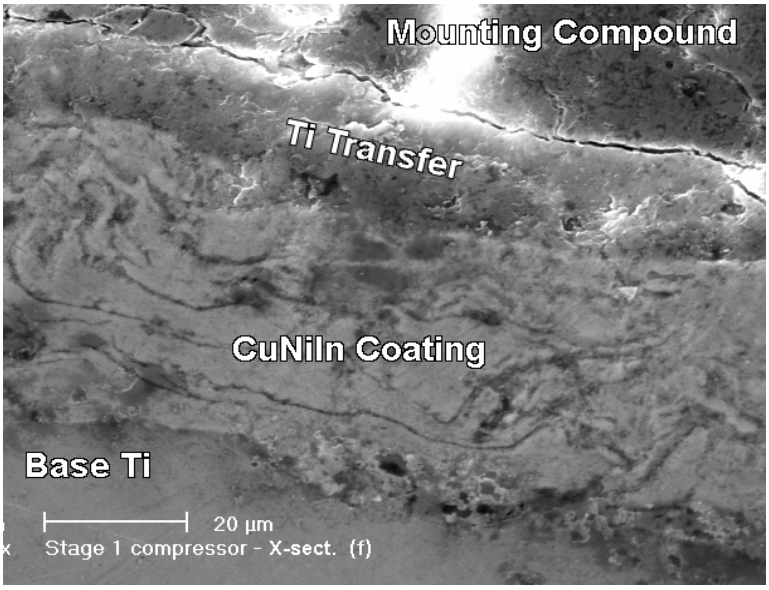

Fig. 1.4. Cross-section of a worn turbine engine compressor blade dovetail [21].

The bonded solid lubricants used for compressor blades typically consist of molybdenum disulfide (MoS_2) or graphite dispersed in an epoxy or acrylic binder. It is important to note that although some of these lubricants claim that they perform well at high temperature, MoS_2 and graphite cannot with stand temperatures above ~400°C and ~500°C respectively. A push by the aerospace industry for high performance aircraft and engines has driven the operational temperatures of engine components higher and higher. Therefore, newer and better coating materials and/or lubricants are needed to improve performance in bladed disk assemblies as well as other areas of aircraft engines that experience fretting wear.

The current approach for the replacement of the standard coatings and coating methodology is by conducting research focused on the performance and wear mechanisms of nickel based coatings and the potential of nickel oxide based solid lubricants. The literature suggests that nickel alloy contacts perform very well in fretting wear contacts at elevated temperatures (in excess of 800°C) due to the formation of what is often called a

'Glaze' oxide layer [23-30]. Although a significant body of work has been accomplished in the study of friction and wear of nickel based materials and coatings, there is an apparent need for better characterization of the tribological properties and deformation mechanisms of nickel oxides and their potential for elevated temperature fretting wear mitigation.

In order to achieve the goal of fretting wear mitigation with nickel based coatings, a knowledge base needed to be established for the fundamental understanding of the fretting wear between self mated Ti6Al4V surfaces and how Ti6Al4V interacts with the current coatings. Therefore, this dissertation can be broken down into two parts. Chapters 2, 3, and 4 cover the fundamental research which developed an understanding of fretting wear regimes and fretting wear mechanisms associated with the degradation of Ti6Al4V surfaces in reference to the current coating systems. Chapter 2 defines the various fretting wear regimes and how they pertain to mated Ti6Al4V surfaces in bench level fretting wear experiments. This work was conducted to map out the regimes so that future testing could focus on gross slip fretting wear. Gross slip fretting was targeted because it yields the highest amount of interfacial wear. Chapters 3 and 4 cover the wear mechanisms associated with the gross slip fretting wear of Ti6Al4V surfaces mated with CuNiIn and aluminum bronze coatings, respectively. This work was conducted to determine how well the current coatings protect the mated Ti6Al4V surfaces, without lubrication.

The second part of this dissertation was focused on the wear mechanisms associated with nickel based coating solutions. This part is lead by a literature review in Chapter 5 which defines the prior art in this area. Then, the subsequent chapters develop an understanding of how nickel based coatings and nickel oxide surfaces can be used to mitigate fretting wear and protect the mated Ti6Al4V surfaces.

Chapter 2

CHARACTERIZATION OF FRETTING WEAR REGIMES AT Ti6Al4V INTERFACES

2.1 Objective

In a study by Zhou et al. [4] it was established that mixed fretting has the most devastating affect on component fatigue. Also known as fretting fatigue, the combination of the bulk cyclic stresses and fretting surface interactions can accelerate crack initiation and cause premature catastrophic failure in many components [19, 31-35]. This is especially apparent in Ti6Al4V compressor blade/disk interfaces of turbine engines where high contact stresses and short oscillations can lead to mixed fretting wear and ultimately component failure. An illustration of this interface is shown in Chapter 1 Fig. 1.3.

Tribologically, Ti6Al4V is especially susceptible to galling and produces hard oxide debris that can score the surface [17, 18, 36]. A common mitigation strategy is to coat the surfaces of the compressor blade roots with plasma sprayed coatings and dry film lubricants [37]. This has lead to many investigations with the purpose of developing and implementing longer lasting coatings and/or new blade/disk materials [21, 38-47]. In order to develop new coatings and materials, it is important to understand the interfacial wear mechanisms and the fretting wear regimes as they pertain to mated Ti6Al4V interfaces.

The work described in this chapter represents fundamental research focused on the transition from mixed to gross slip fretting wear using Ti6Al4V mated surfaces subjected to testing at room temperature and 450°C (842°F). The premise for this work is based on the development of an understanding of the fretting wear transition from mixed to gross slip fretting wear at ambient and 450°C.

2.2. Specimens and Tribological Testing

The contact geometry used in these experiments was an elliptical shaped Ti6Al4V pin pressed against a flat Ti6Al4V disk. The ellipsoid, shown in Fig. 2.1, was designed to eliminate stress concentrations that lead to contact edge effects, and to simplify alignment procedures for reproducible contact areas. The plates were flat circular disks with a diameter of 12.7 mm on the test face and 3.175 mm thick. The surface roughness for all specimens was 0.1 to 0.2 μm Ra.

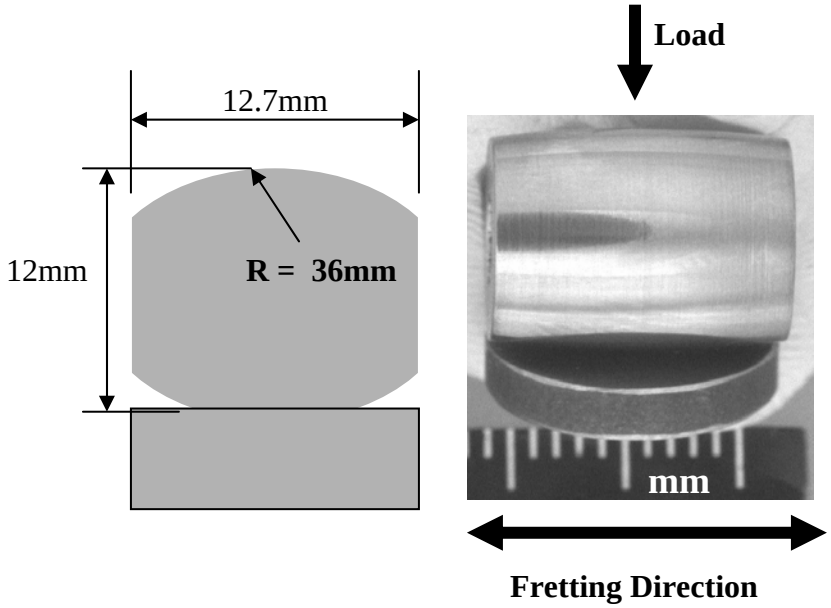

Fig. 2.1. Ellipsoid contact geometry.

The purpose of this study was to experimentally map the critical loads and stroke lengths associated with the transition from mixed to gross slip fretting wear at room temperature and 450°C. The high temperature tests were conducted at 450°C to simulate the upper limit that titanium alloys may experience in a turbine engine compressor. Four repeat tests were performed at various stroke lengths ranging from 45μm up to 230μm with an oscillation speed of 30Hz. During each test a normal load of 200N, yielding a

maximum Hertzian contact pressure of ≈ 1GPa, was initially applied to impose a mixed fretting condition at the interface. The applied normal load was reduced in increments of 10N every 3 minutes (5400 cycles) until it reached 0N. For the duration of each test the root mean square (RMS) of the friction data and the frictional hysteresis was recorded. The frictional hysteresis was obtained using a laser measuring system and a piezo electric transducer. The fretting wear tribometer, shown and illustrated in Fig 2.2 and Fig 2.3, uses the piezo electric transducer to measure friction between the mating specimens. A laser measurement device is then used to continuously track the position of the oscillating specimen during the test. The real time friction and displacement traces are then plotted to produce hysteresis loops as shown in Fig 2.4. These plots show the friction force as a function of position while the oscillating specimen moves through one full cycle of the test (positive friction is forward and negative friction is backward). The shape of these plots indicates the fretting regime the interface is experiencing [7, 41, 48-51]. Elliptical shaped hysteresis loops, Fig 2.4A, depict mixed fretting behavior and quasi-rectangular shaped hysteresis loops, Fig 2.4B, depict gross slip behavior. The area within the hysteresis loop reflects the energy dissipated by the system. The energy loss per cycle was calculated by using a midpoint rectangular approximation to integrate the area of each loop. Once the varied load tests were completed, a number of tests were conducted with constant load to give further insight into the surface interactions and wear mechanisms that occur. Post test analysis was performed using a scanning electron microscope (SEM) and a 3-D contact profilometer.

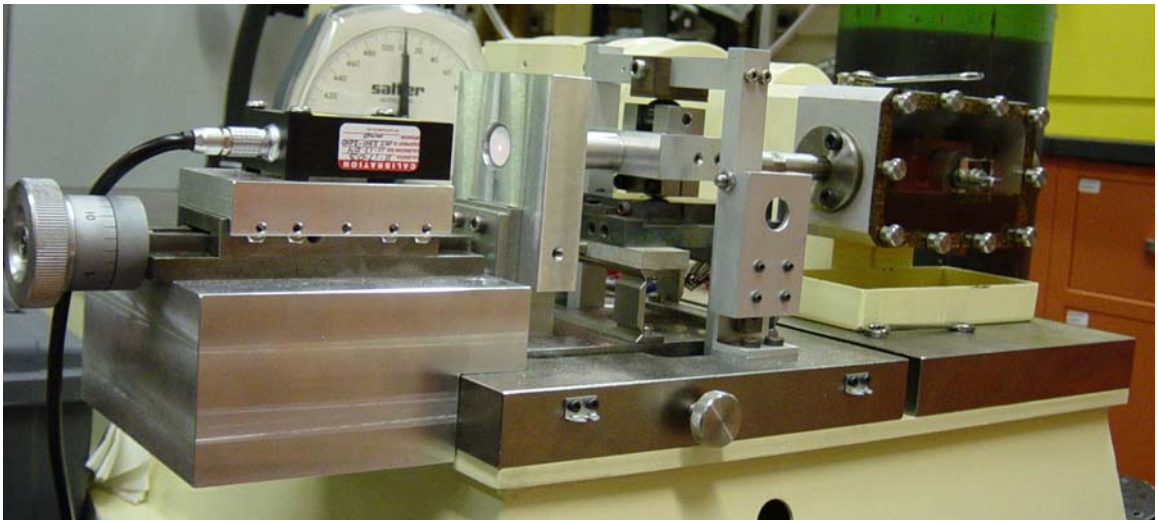

Fig. 2.2. Digital picture of the fretting wear tribometer.

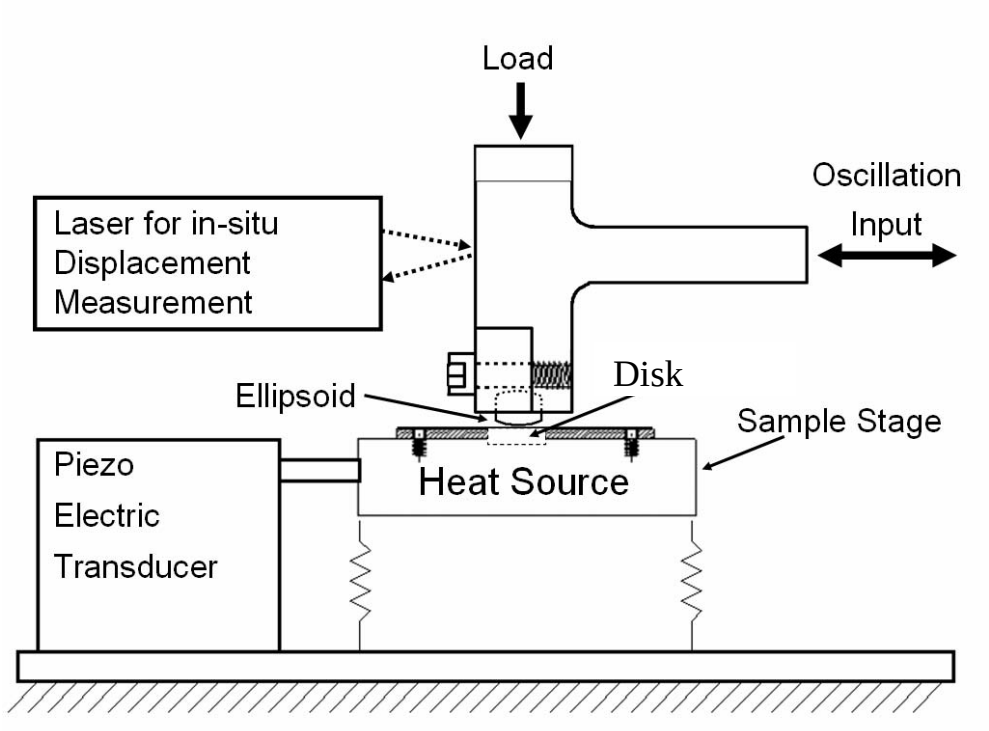

Fig. 2.3. Fretting wear tribometer schematic.

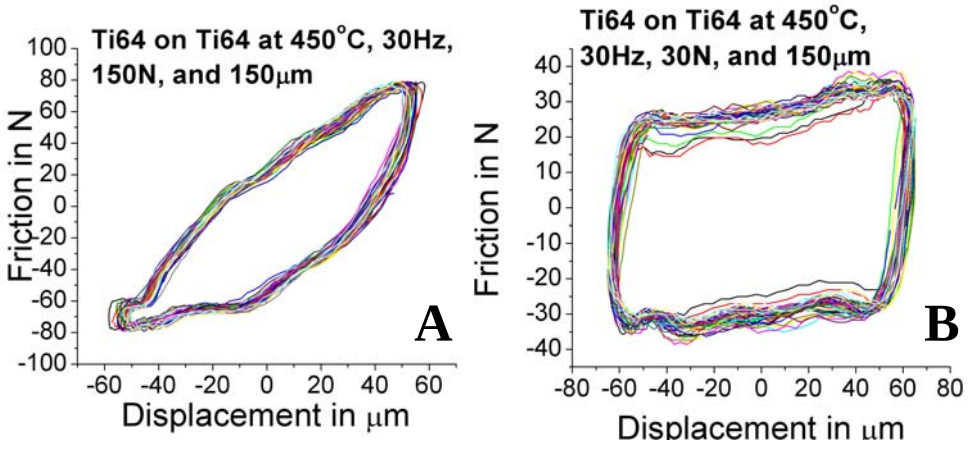

Fig. 2.4. Examples of fretting hysteresis loops. A) Shows mixed fretting and B) Shows gross slip. Full stick would be plotted as a straight line.

2.3 Results

2.3.1 Transition Determination

Varied load tests were first conducted at room temperature. These tests had very distinct transitions from mixed fretting to gross slip. An example of the sharp changes in friction force and hysteresis loops is shown in Fig 2.5, which is one particular test conducted at a 150 μm stroke length. At 60 N the friction drops dramatically and continues to drop with the reduction of the normal load. The hysteresis loops show that loads greater than 60 N; the contacts were operating in the mixed fretting regime. Once the load is reduced to 60 N the hysteresis changes to a quasi-rectangle, signifying the transition to gross slip fretting wear. After validating this test at 150 μm, similar tests were conducted at number of different stroke lengths.

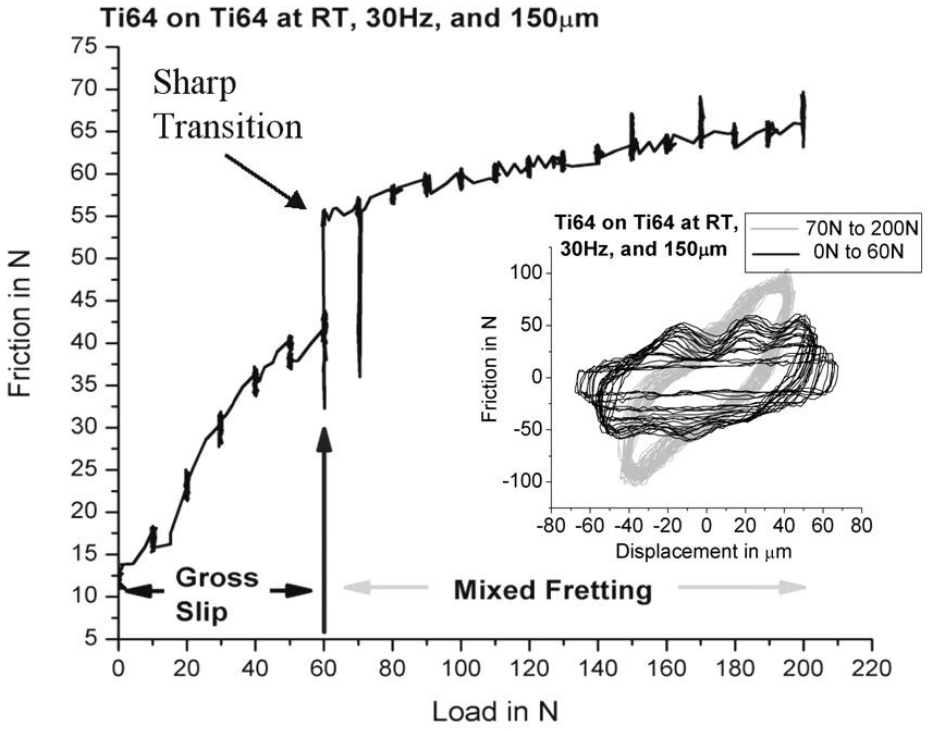

Fig. 2.5. Varied load test showing the normal load at which the transition from mixed to gross slip fretting occurred using friction force. The small graph shows the mixed fretting hysteresis loops in gray and the gross slip loops in black.

Once the room temperature varied load tests were completed the tests were then repeated at 450°C. The data from one of these tests, shown in Fig 2.6, revealed different behavior than the room temperature tests. The sharp transition between regimes, seen in Fig 2.5, was not apparent at 450°C. At this point, it was then decided to plot the energy loss per cycle, the area within the hysteresis loops, with respect to the normal load for both the room temperature and 450°C tests. Fig 2.7 and Fig 2.8 show the energy dissipation plots for the respective low and high temperature examples. It was noticed that the plots for both cases show the same trend. In addition, the sharp transition in all the room temperature tests occurred at a maximum value in the energy loss data. With this in mind a curve was fit to the energy dissipation plots from the high temperature tests. The curve was then differentiated to find the maximum energy loss during the test, and at what load it

occurred. The maximum energy loss in the 450°C tests was then investigated to determine if it occurred at the transition load from mixed to gross slip fretting. For the 200μm example shown in Fig 2.8, the transition load was determined to be 80N. The transition load was validated by conducting tests at various loads using the same 200μm stroke length. Each test was conducted at one constant load. Fig 2.9 shows the hysteresis loops that were recorded during each test. At 80N and 90N, the shape of the loops starts to become rectangular signifying gross slip. Wear mode analysis was also conducted after each test at 200μm to further verify the transition load at 80N. The maximum energy loss per cycle was then used as a transition criterion for all of the subsequent tests conducted.

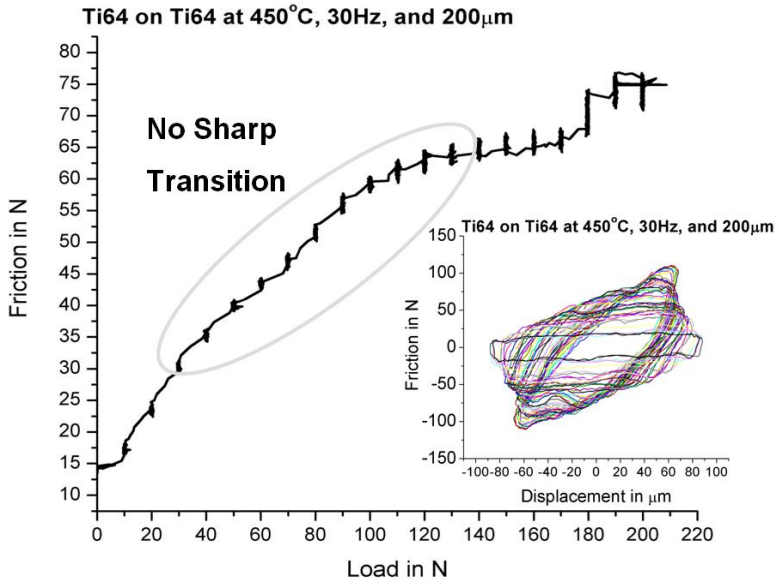

Fig. 2.6. Varied load test showing that the transition from mixed to gross slip fretting appears to be gradual at high temperature. The small graph shows the hysteresis loops that were recorded during the test.

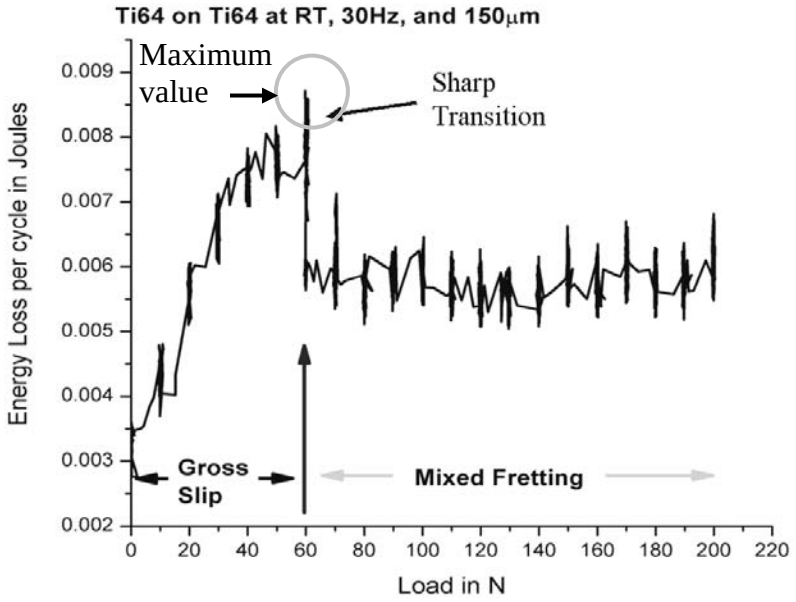

Fig. 2.7. Varied load showing the normal load at which the transition from mixed to gross slip fretting occurred using the energy loss per cycle.

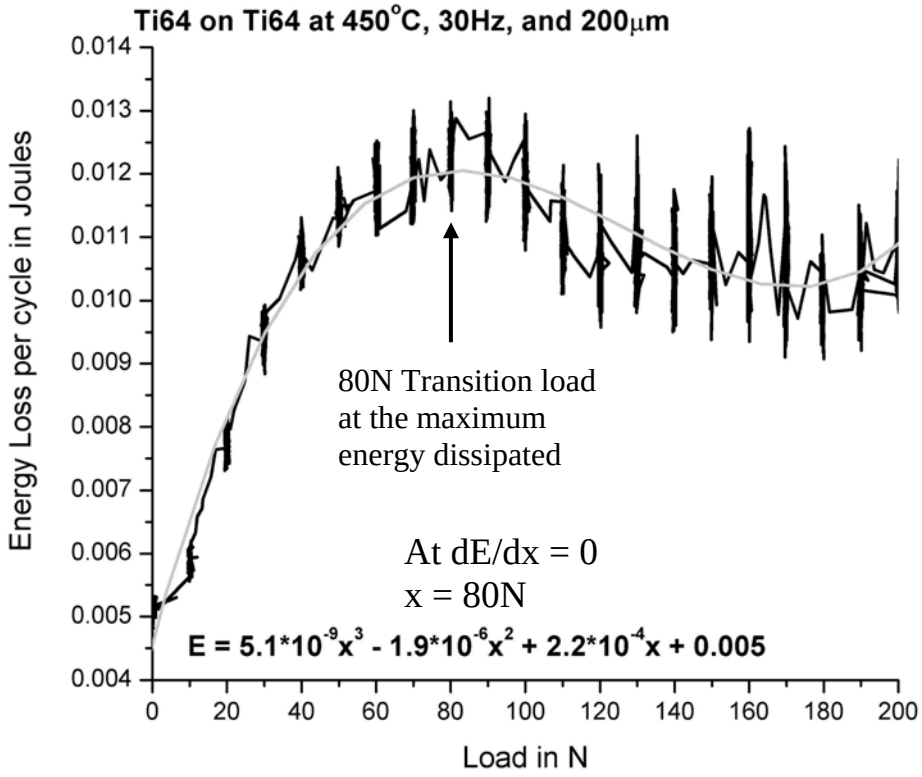

Fig. 2.8. Varied load showing the load at which the energy loss per cycle is plotted versus the normal load applied. The equation displayed is a curve that was fit to the data.

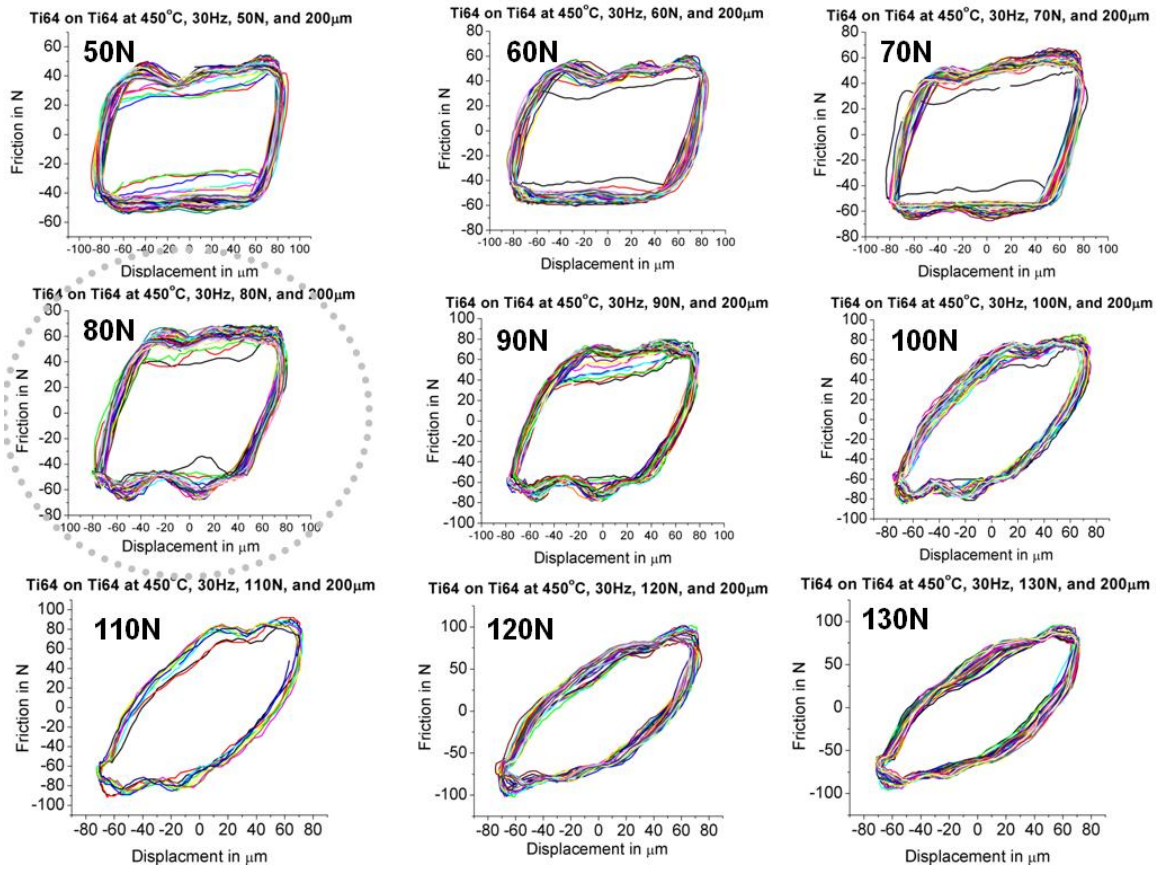

Fig. 2.9. The hysteresis loops plotted as friction vs. displacement for each cycle of the test. Each of the nine plots represents a separate test at the given load.

Upon the completion of all the tests, the transition loads at each stroke length were compiled and plotted in Fig 2.10. The 450°C tests appear to be more susceptible to mixed fretting than the room temperature tests at longer stroke lengths. However, at the short stroke lengths the data converges. There is some scatter in the data at 45μm stroke length that can be attributed to the limitations of the machine.

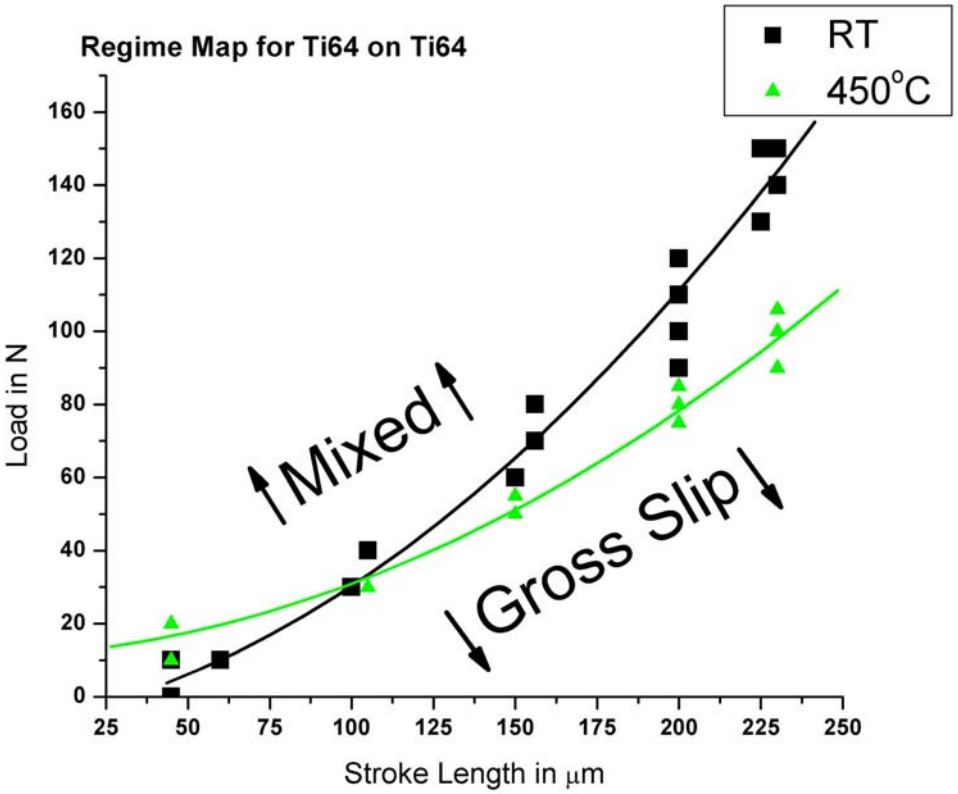

Fig. 2.10. The plot shows the load at which the transition from mixed to gross slip fretting occurred for each stroke length. The area above each line corresponds to the conditions that promote mixed fretting wear.

2.3.2 Coefficient of Friction

Friction coefficient can be complex in fretting wear tests. Tests that are conducted in the mixed and partial stick regime yield friction data that cannot be used to determine the dynamic coefficient of friction. The coefficient of friction data for the tests conducted in this study were determined from the gross slip fretting tests only. Therefore, the friction data from all of the varied load tests were separated and the gross slip coefficient of friction was plotted in Fig 2.11 and 2.12. The scattered data from both temperatures showed that the coefficient of friction varied inversely with the applied normal load. This trend can also be seen in the data from the tests conducted at constant load, as represented by the dark stars and triangles in Fig 2.11 and 2.12.

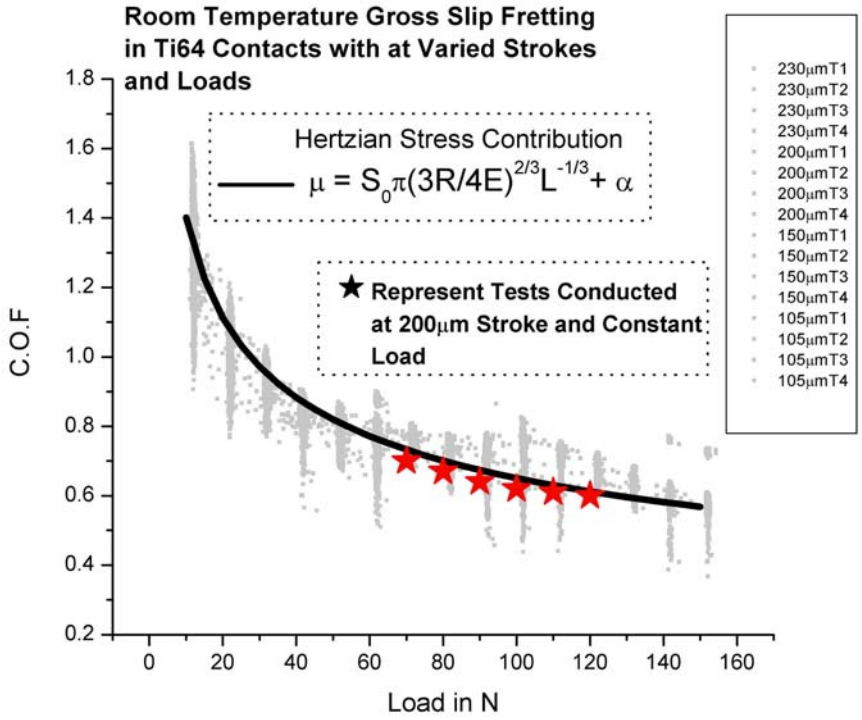

Fig. 2.11. The plot shows the change in coefficient of friction with respect to load. The dark line is a plot of the Hertzian contact model and the dark stars are single tests conducted at each specific load.

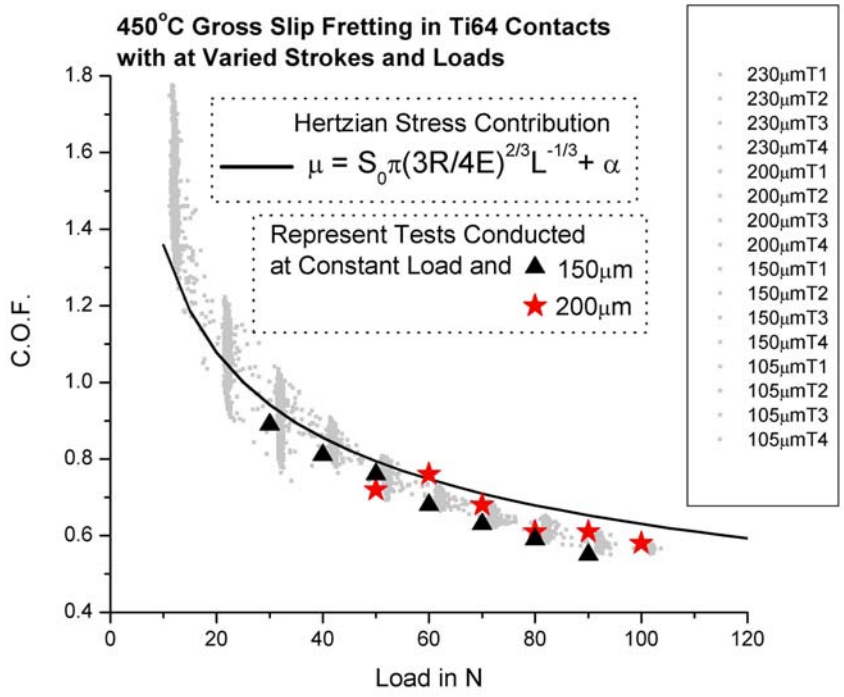

Fig. 2.12. The plot shows the change in coefficient of friction with respect to load. The dark line is a plot of the Hertzian contact model and the dark stars/triangles are single tests conducted at each specific load.

2.3.3 Wear Mode Analysis

At room temperature, the varied load tests exhibited fretting wear from both the mixed and gross slip regimes. In the gross slip regime, all of the wear tracks on both the plate and the ellipsoid contained large quantities of active debris, and displayed evidence of localized galling as shown in Fig. 2.13. The adhered regions appear to have fractured into particles that collected throughout the wear track and abraded the edges of contact.

Because the transitions from mixed fretting wear to gross slip, at 150 μm stroke length, occurred at 60N a definitive mixed fretting wear scar was detected at 80N normal load, in the constant load tests. After these tests, the entire central region of the wear tracks experienced a form of friction weld that adhered the contact region on both the plate and ellipsoid surfaces, at the localized points of contact. This extreme case of adhesive wear can be seen in Fig. 2.14, where the surfaces appear to fit together like a puzzle as shown by the boxed regions in the figure.

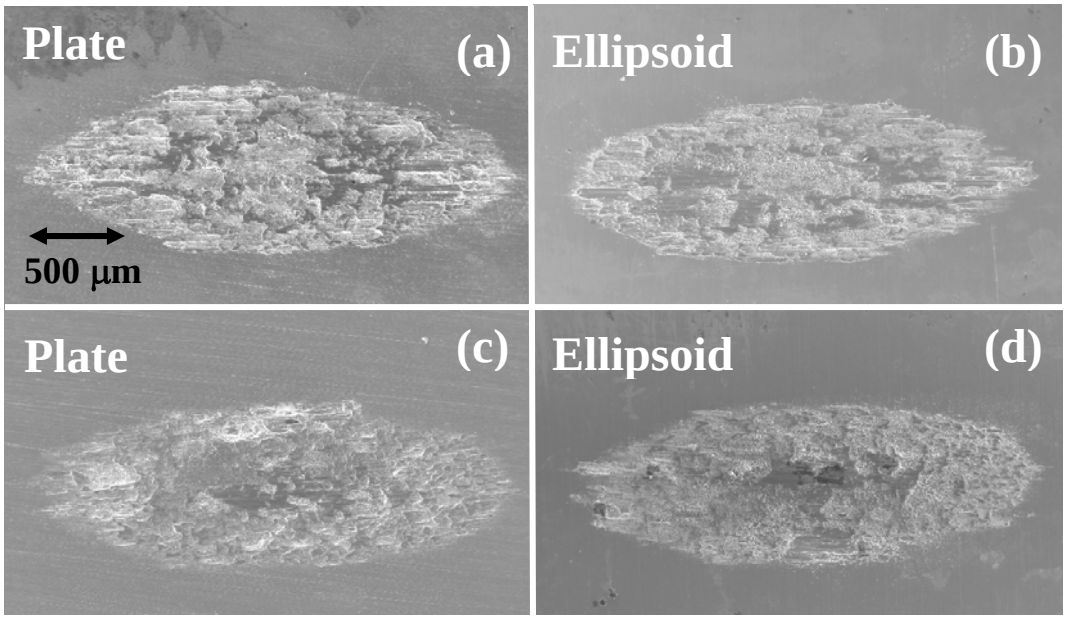

Fig. 2.13. Gross slip fretting wear at 300μm stroke and 50N load, (a) and (b), and at 150μm stroke and 20N load, (c) and (d). The scale for all of the micrographs is the same.

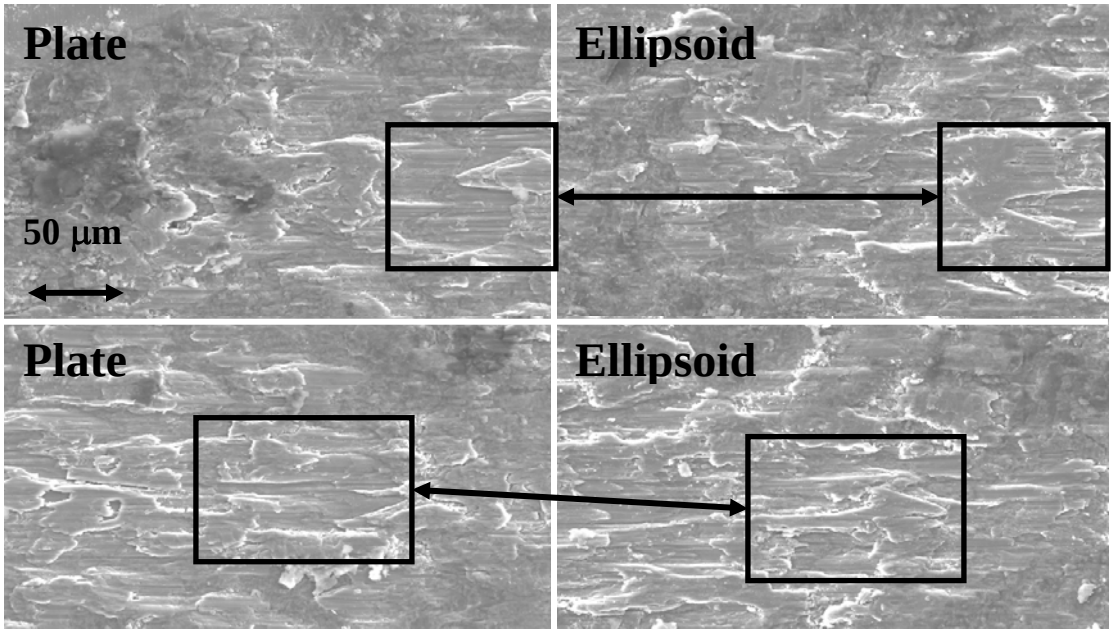

Fig. 2.14. Evidence of severe adhesive wear by way of surfaces fitting together like a puzzle with pieces of one side of the interface adhered to the other. The scale for all the micrographs is the same.

Increasing the load beyond 80N produced localized unworn regions within the center of the wear track. At 140N the localized unworn regions are large enough to suggest partial stick in the central region of the wear track. At loads near 200N the majority of the wear track is unworn and the material at the edges appears mounded up or extruded, as shown in Fig. 2.15. This is clear evidence of partial stick fretting wear.

At 450°C and gross slip fretting conditions, the Ti6Al4V interfaces exhibited severe wear as shown in Fig 2.16. Fig 2.17 shows an SEM micrograph of a typical gross slip fretting wear scar on the surface of the Ti64 specimens tested at 450°C. The wear track is surrounded by an accumulation of loose debris, with pockets of active debris trapped within the contact region. Fig 2.18 indicates that loose debris at the leading and trailing edges of the contact scrape and score the surface as it is evacuated from the wear track. Fig 2.19 shows that at the center of the contact, where the stress was highest, pockets of loose

debris were crushed and ground up into fine particles that polished localized regions of the contact surface.

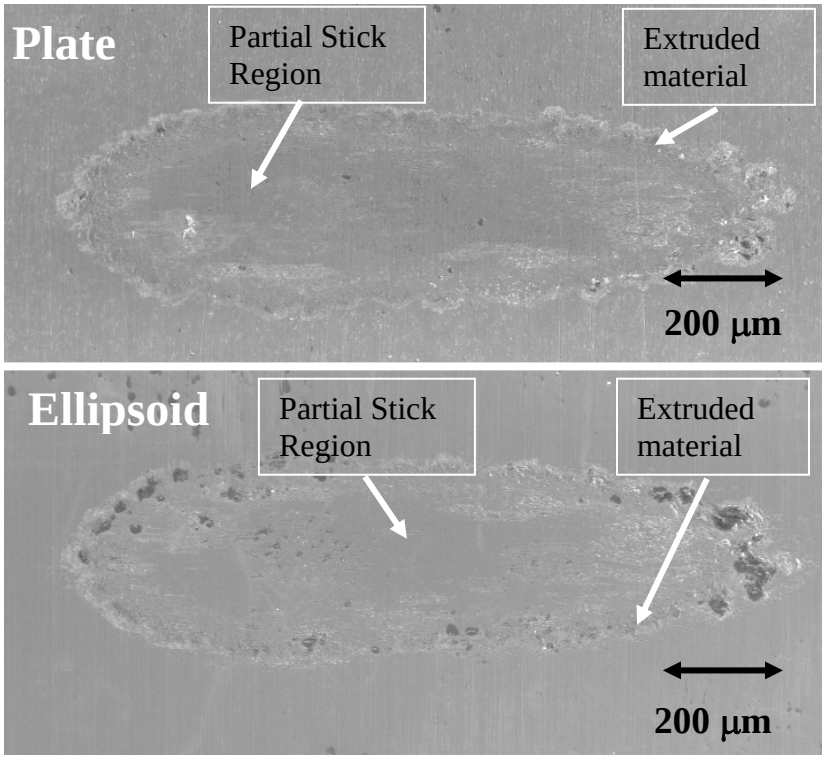

Fig. 2.15. Evidence of partial stick fretting wear at 150μm stroke and 200N load.

Upon the transition into the mixed fretting wear regime, the wear mode changes. Fig 2.20 shows a micrograph of a typical mixed fretting wear scar on Ti6Al4V tested at 450°C. Less debris formation is noted. Instead of the pockets of crushed debris that are seen in gross slip, the center of the contact shows the formation of large transfer particles and a large crater where material has been extracted from the disk surface and adhered to the pin, shown in Fig 2.21. Fig 2.22 is the 3D profile of the flat disk wear track. The profile clearly shows the crater at the center of the wear track, where material has been removed, and the mounds of material that transferred to the disk from the mating Ti6Al4V

surface. At the leading and trailing edges of the wear track, the mating surfaces appear smooth with evidence of plastic flow in the direction of fretting, shown in Fig 2.23.

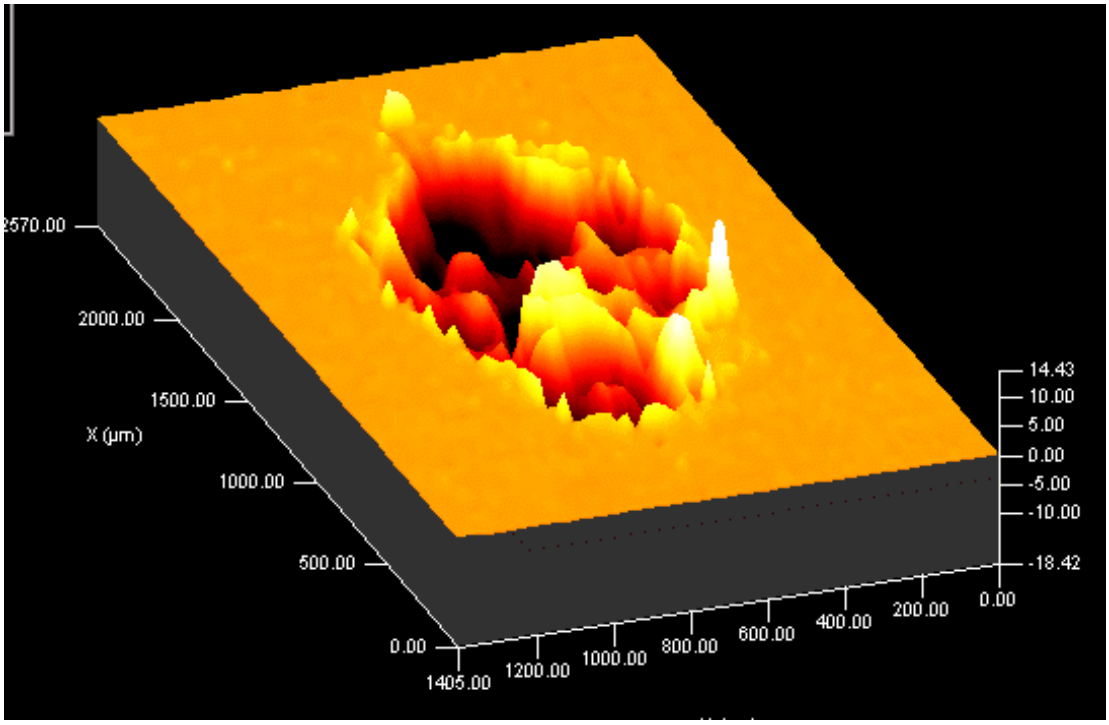

Fig. 2.16. A 3D contact profile of the fretting damage on the surface of the flat disk after a test was conducted at 450°C with a 200µm stroke length and 50N normal load for 7500 cycles. All dimensions shown are in µm.

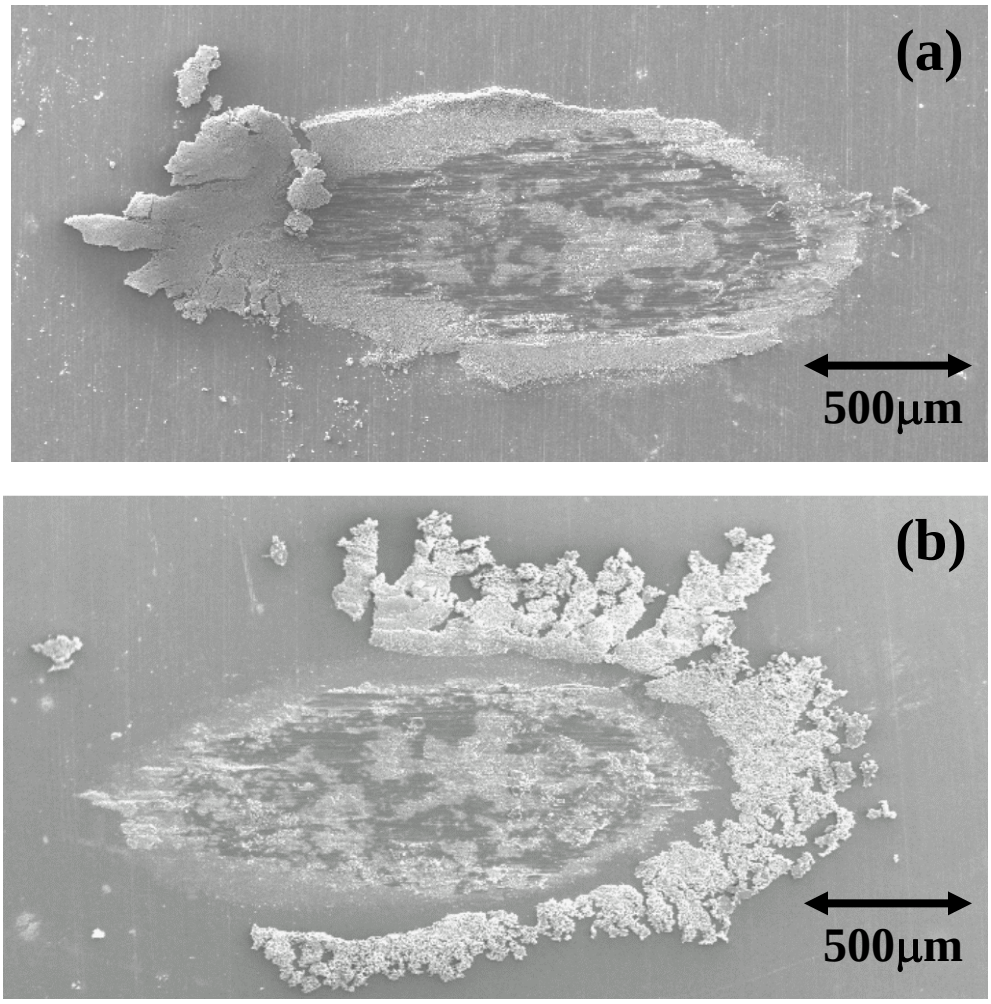

Fig. 2.17. SEM micrographs of gross slip fretting damage on the surface of the (a) flat disk and (b) elliptical pin after a test was conducted at 450°C with a 200μm stroke length and 50N normal load for 7500 cycles.

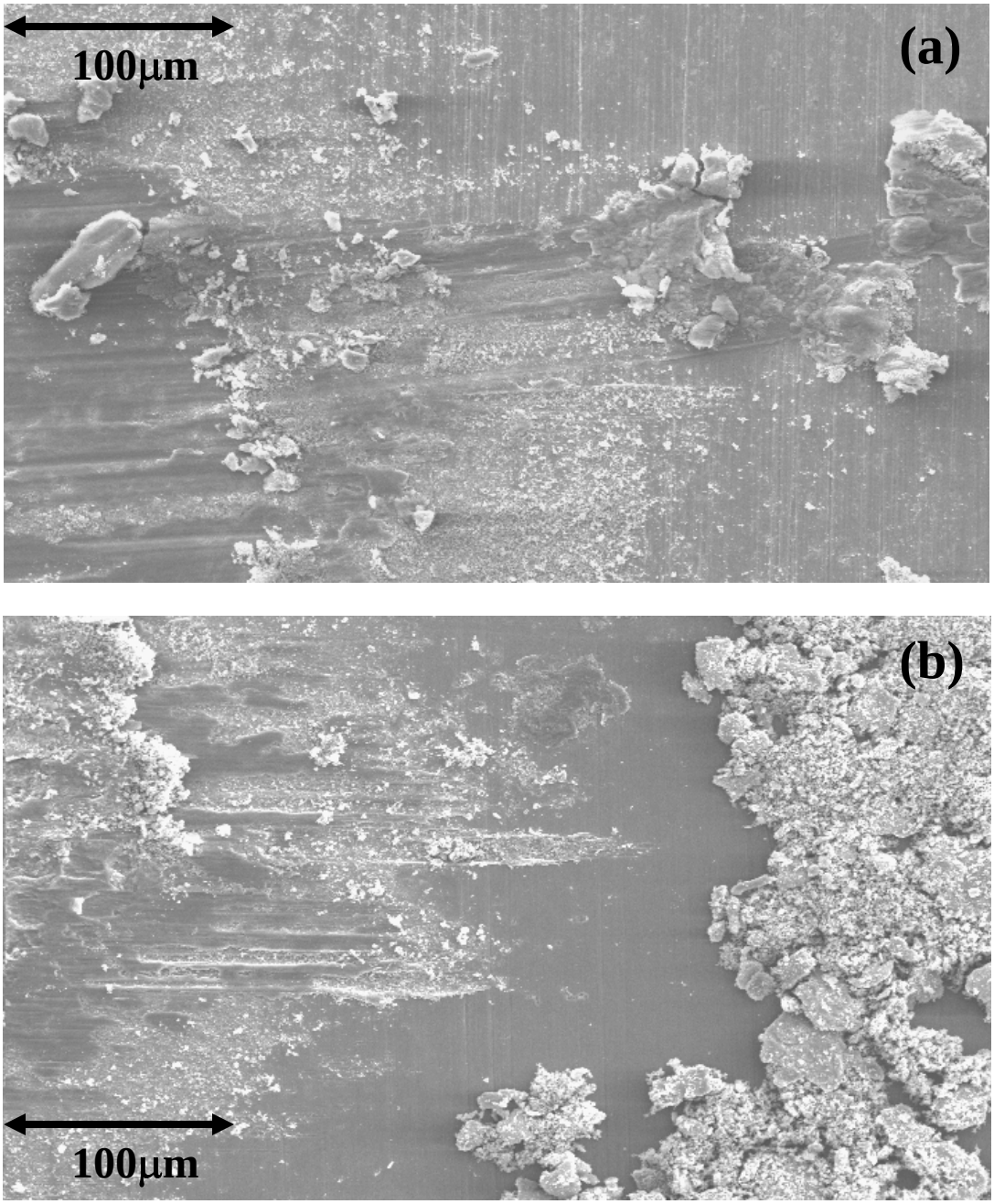

Fig. 2.18. SEM micrographs of the edge of the wear track on the (a) flat disk and (b) elliptical pin after a test was conducted at 450°C with a 200μm stroke length and 50N normal load for 7500 cycles.

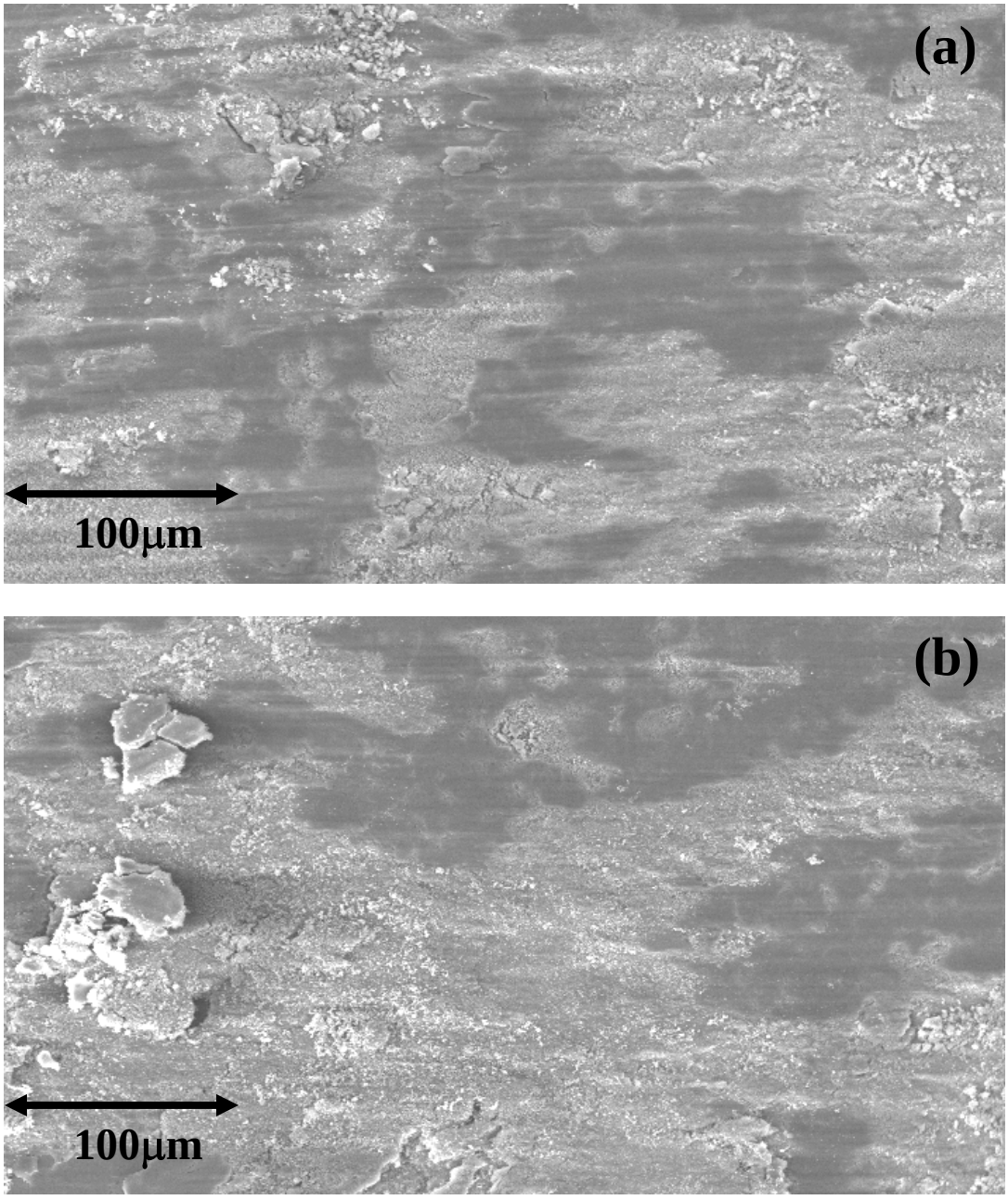

Fig. 2.19. SEM micrograph of the center of the wear track on the (a) flat disk and (b) elliptical pin after a test was conducted at 450°C with a 200μm stroke length and 50N normal load for 7500 cycles.

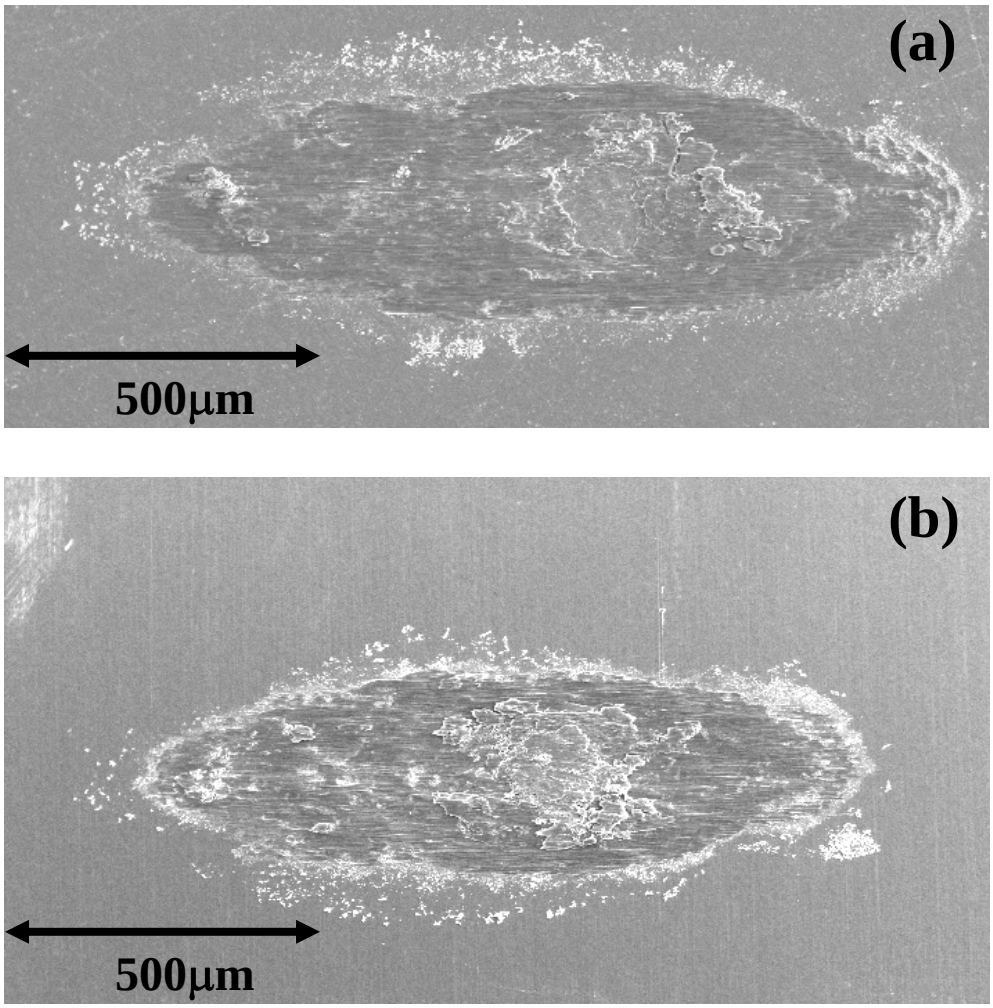

Fig. 2.20. SEM micrographs of mixed fretting damage on the surface of the (a) flat disk and (b) elliptical pin after a test was conducted at 450°C with a 200μm stroke length and 150N normal load for 7500 cycles.

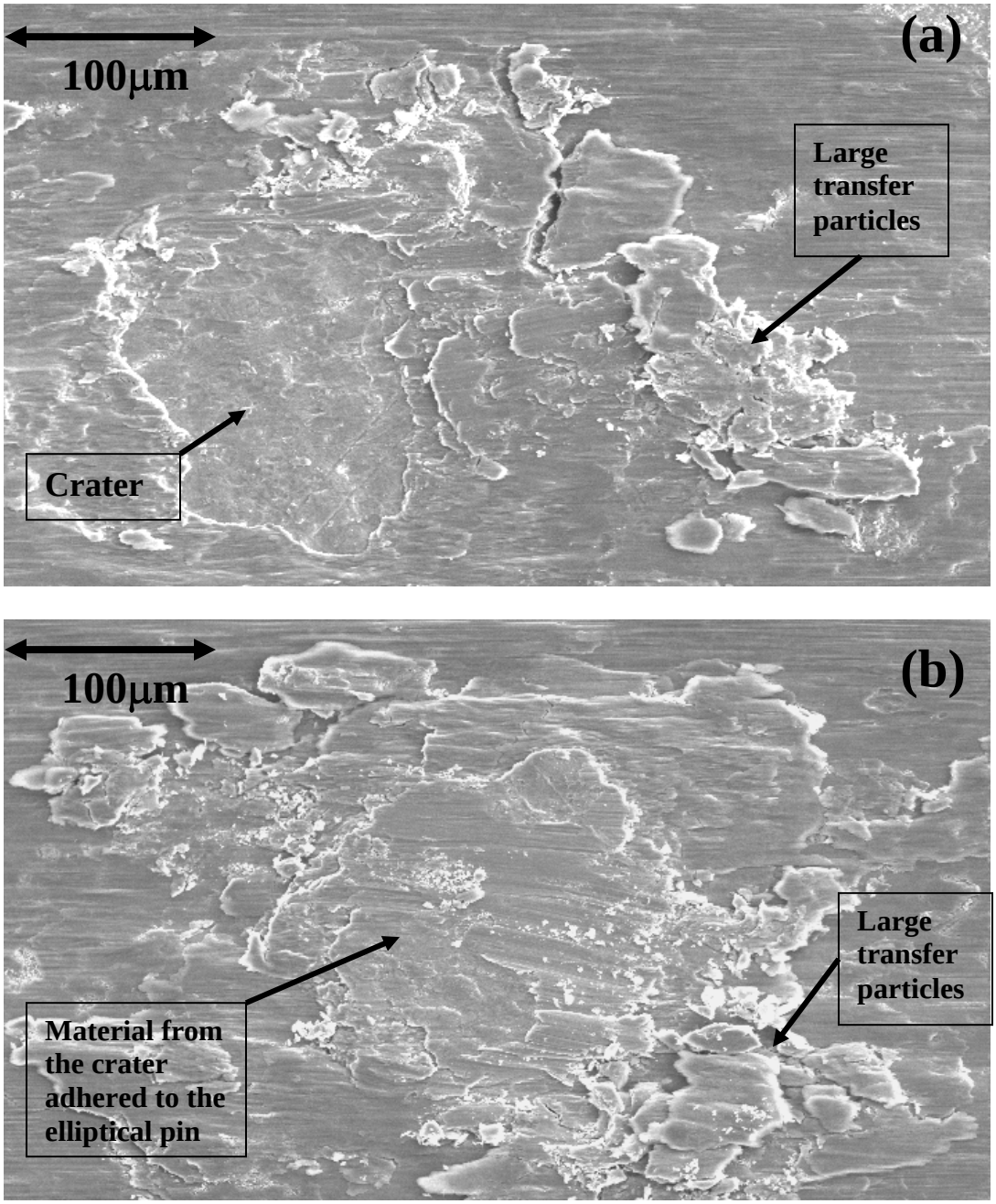

Fig. 2.21. SEM micrographs of the center of the wear track on the (a) flat disk and (b) elliptical pin after a test was conducted at 450°C with a 200μm stroke length and 150N normal load for 7500 cycles.

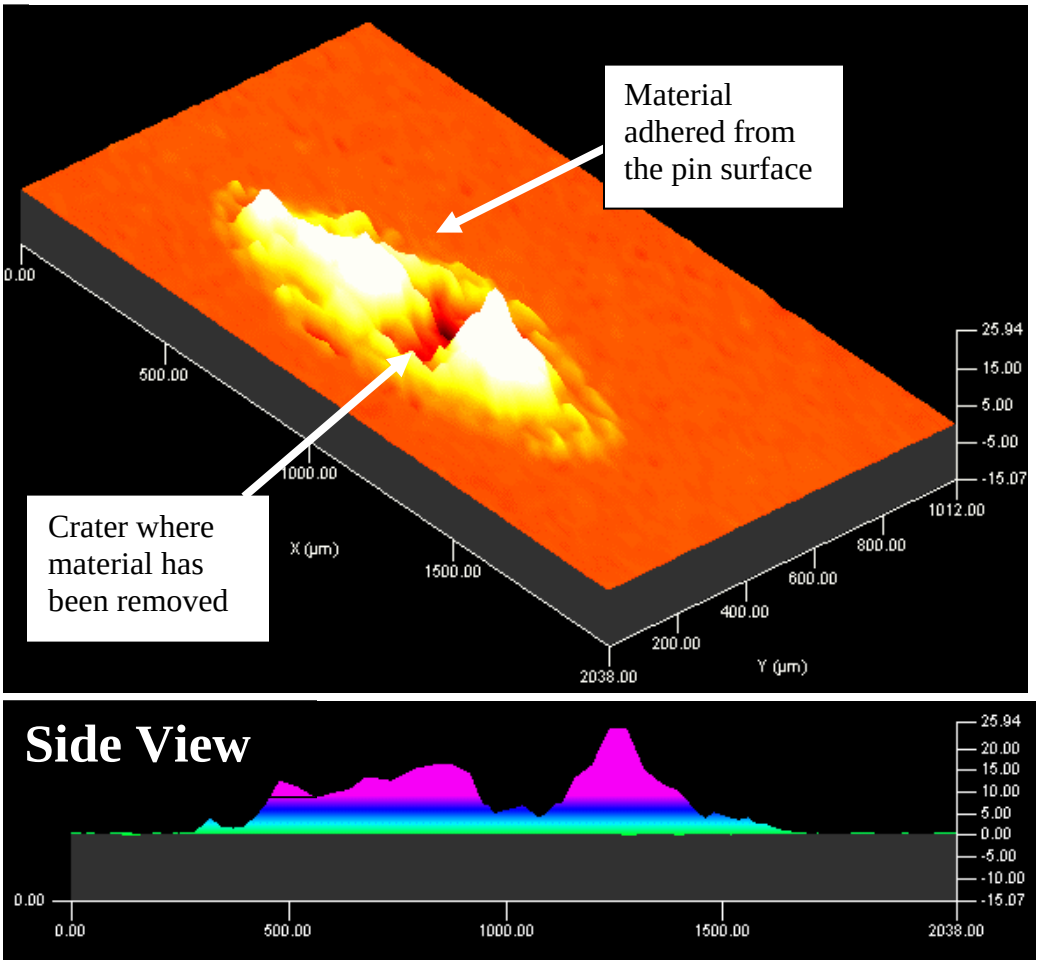

Fig. 2.22. A 3D contact profile with a side view of the fretting damage on the surface of the flat disk after a test was conducted at 450°C with a 200µm stroke length and 150N normal load for 7500 cycles. All dimensions shown are in µm.

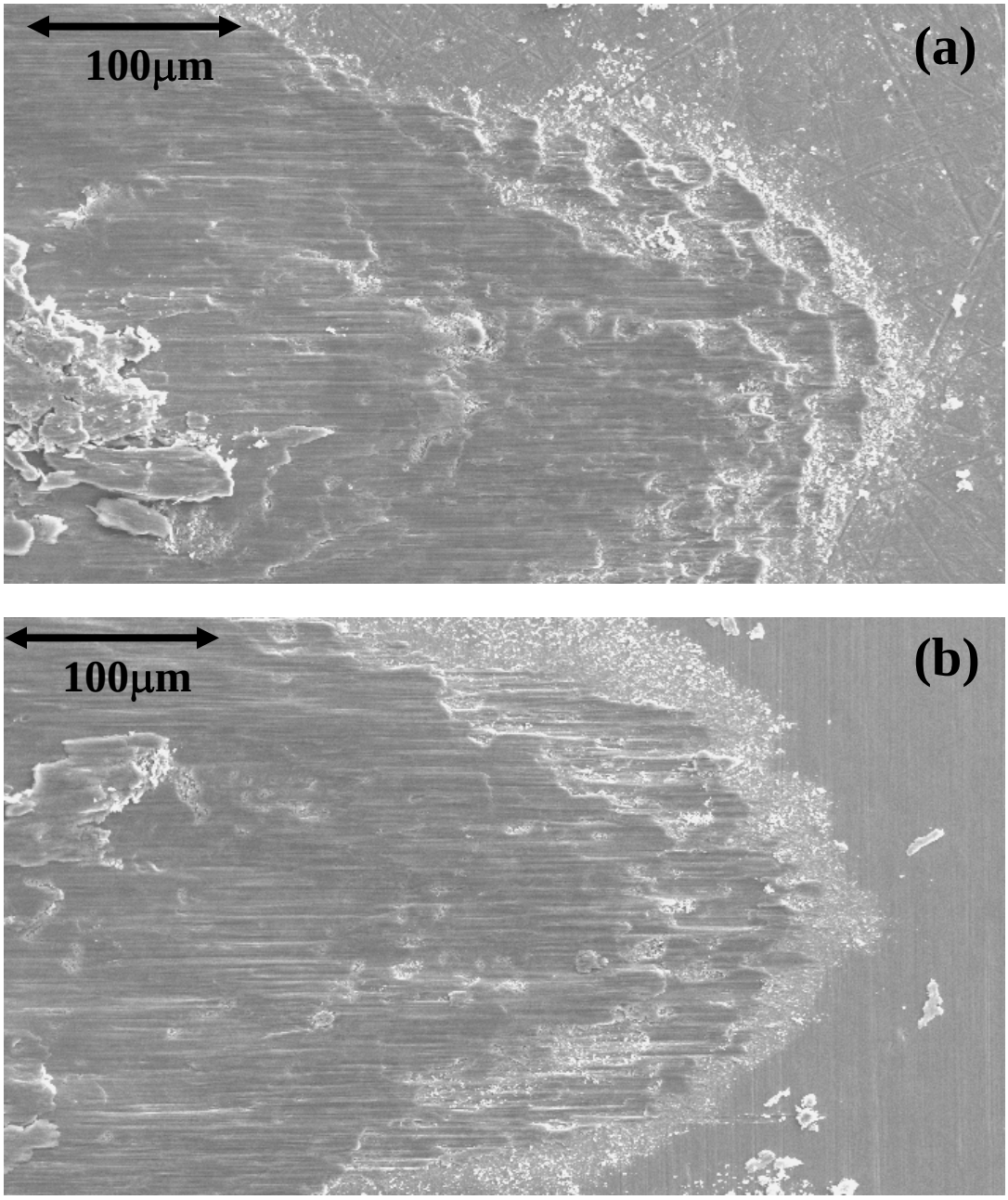

Fig. 2.23. SEM micrographs of the edge of the wear track on the (a) flat disk and (b) elliptical pin after a test was conducted at 450°C with a 200μm stroke length and 150N normal load for 7500 cycles.

At the highest normal loads, the wear mode transitioned from mixed fretting wear to partial stick. Partial stick fretting occurred when the tangential forces could not overcome the contact stresses in the center of the contact. This inhibited gross surface

damage in the center of the contact and promoted gross slip and/or mixed fretting wear at the edges of the contact. Fig 2.24 shows a micrograph of a typical partial stick fretting wear scar on the surface of the Ti6Al4V specimens tested at 450°C. The 3D contact profile, illustrated in Fig 2.25, shows that galling occurred at the edges of the stick region and promoted material transfer between the contact surfaces. In this particular case, the material has adhered to one of the leading edges of the stick region. Depicted in Fig 2.26, the galled region on the leading edge of contact showed that material had been removed and transferred from one surface to the other. Evidence of gross slip wear just beyond the galled region was also observed.

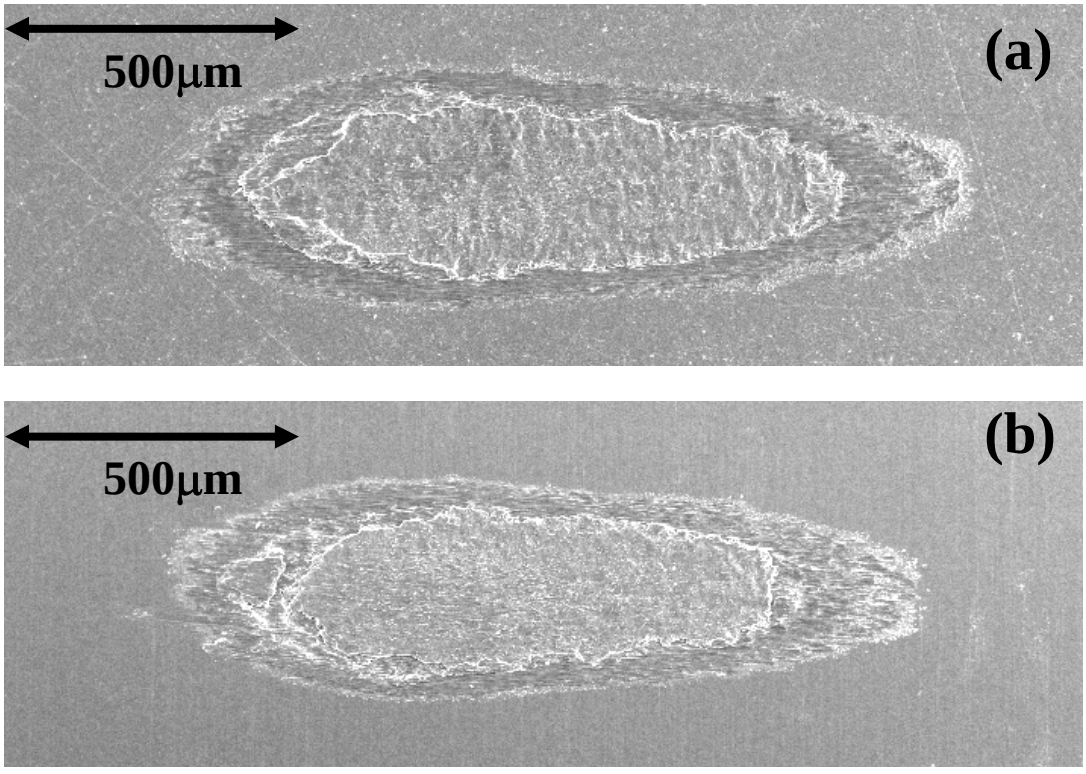

Fig. 2.24. SEM micrographs of partial stick fretting damage on the surface of the (a) flat disk and (b) elliptical pin after a test was conducted at 450°C with a 200μm stroke length and 180N normal load for 7500 cycles.

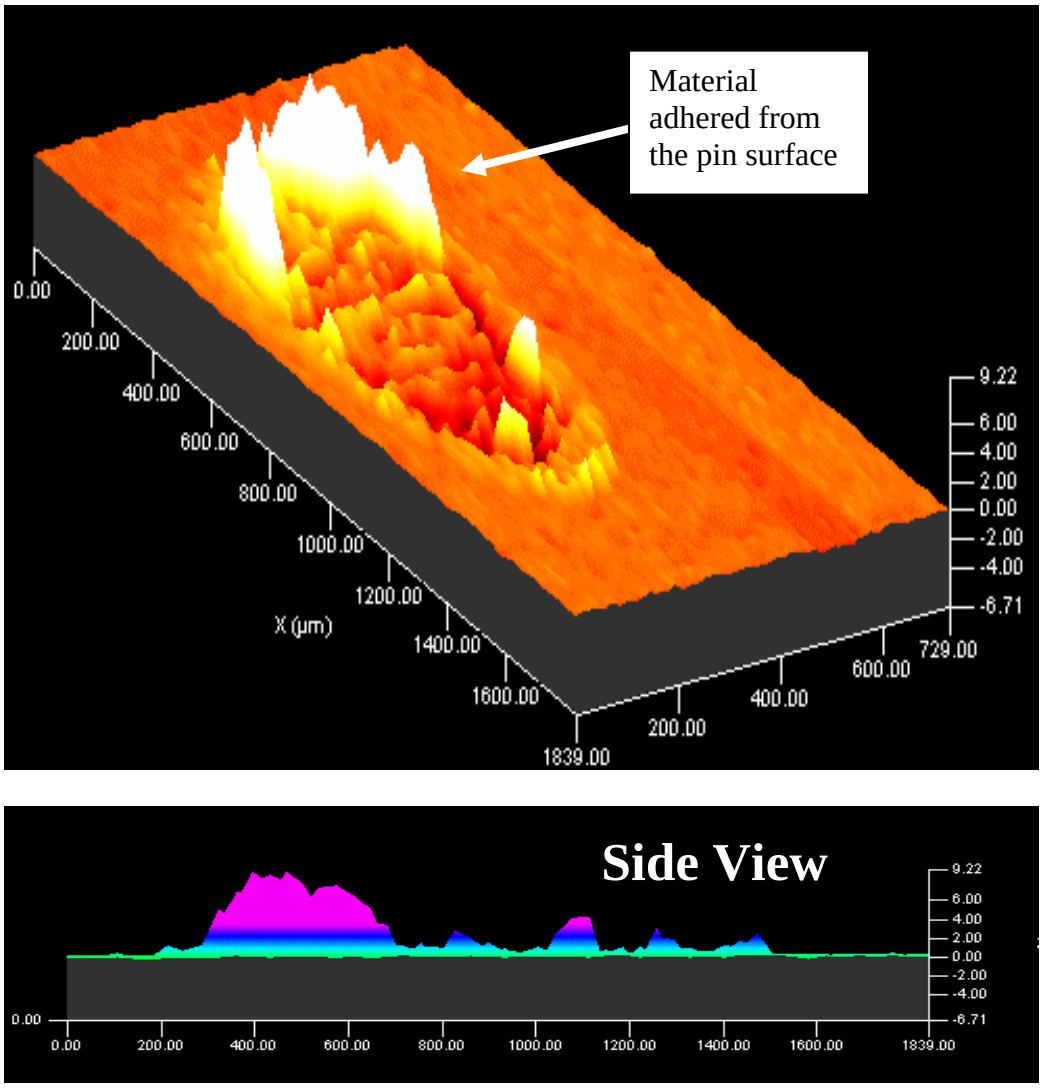

Fig. 2.25. A 3D contact profile with a side view of the partial stick fretting damage on the surface of the flat disk after a test was conducted at 450°C with a 200µm stroke length and 180N normal load for 7500 cycles. All dimensions shown are in µm.

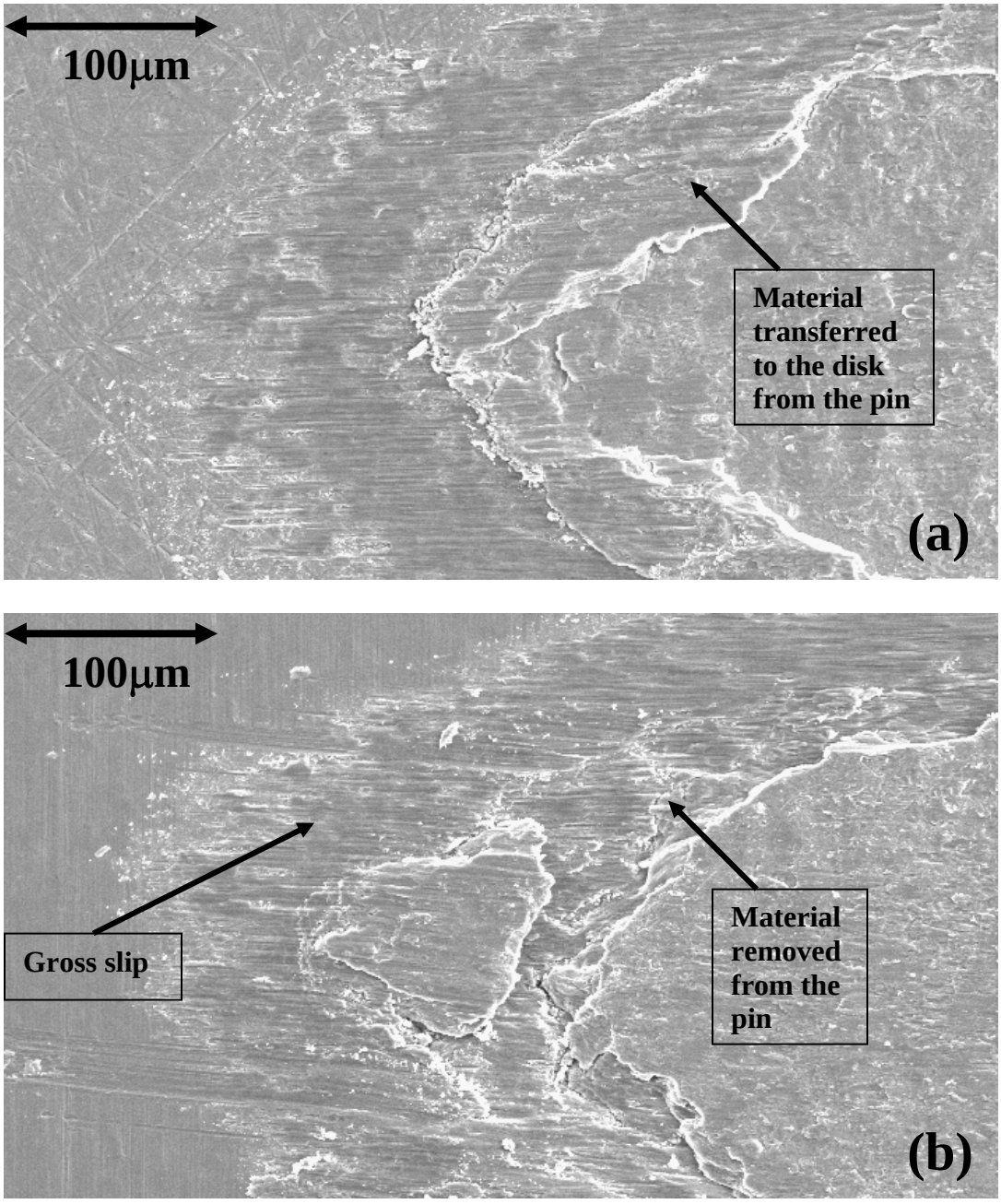

Fig. 2.26. SEM micrographs of the edge of the wear track on the (a) flat disk and (b) elliptical pin after a test was conducted at 450°C with a 200μm stroke length and 180N normal load for 7500 cycles.

2.4 Discussion

The varied load tests conducted were designed to determine the amount of load required to impose mixed fretting between mating Ti6Al4V surfaces at various stroke lengths. In the room temperature tests, the transition from mixed to gross slip fretting is abrupt and dramatic. The transition can even be seen in friction data as a sharp drop. This can be explained using the work by Sauger [18] and Zhou [52] et al on the formation of a tribologically transformed structure (TTS) induced by fretting wear of titanium contacts. TTS is formed by a critical accumulation of plastic deformation, or strain hardening, between mating titanium surfaces and can have as much as twice the hardness of the bulk titanium. Based on the work by Sauger and Zhou, it is believed that strain hardening occurs at the Ti6Al4V interface during the mixed fretting portion of the room temperature varied load tests. Once formed, the hardened TTS layer is very brittle and fractures instantly during the transition from mixed to gross slip fretting [7]. This causes the surfaces to be separated by a layer of metal and metal oxide debris, which can reduce friction [53] and impede surface adhesion.

At elevated temperatures, the transition from mixed to gross slip fretting is gradual and can be determined by the critical load at which the maximum energy loss per cycle occurred. At room temperature, strain hardening (TTS) at the interface is believed to be the primary cause of the acute transition from mixed to gross slip fretting. This sharp transition was not seen at 450°C because more slip systems may be active making it more difficult to build up a network of dislocations that will develop into strain hardening. Therefore, the surfaces do not experience the brittle fracture observed at room temperature.

In addition to the impedance of strain hardening, the hot titanium specimens undergo accelerated surface oxidation and substantial softening. Initially it was believed that the accelerated surface oxidation would favor gross slip wear because of the potential lubricity of the TiO_2 formed at the interface [53]. However, the experimental results indicated that the elevated temperature tests favored mixed fretting and increased the propensity for the contacts to gall. This suggests that the softening of the surface becomes the most influential factor governing the transition from mixed to gross slip fretting at high temperatures in Ti6Al4V contacts. At 450°C the Ti6Al4V specimens experience approximately a 50% reduction in tensile strength, a 40% reduction in compressive and shear strength, and a 20% reduction in elastic modulus [54]. The reduction in tensile strength, shear strength and elastic modulus, caused by the heating of the specimens, allows the surface to deform readily without strain hardening. This allows the interface to accommodate longer stroke lengths and/or lower loads while fretting occurs within the mixed regime.

During the varied load tests, it was observed that the dynamic coefficient of friction (COF) varied inversely with applied normal load at room temperature and 450°C, Fig 2.11 and 2.12. This is a phenomenon that was studied extensively by Bowers et al [55-56] in the late 1960's and early 1970's for polymers and thin solid films and then again by Singer et al [57] in the early 1990's for MoS_2 coatings. A Hertzian contact model was used to explain why the friction decreased with increased load, and to predict what the friction would be at a given load. The model is derived from an equation that relates the coefficient of friction to the material and mechanical properties of the contact. The basic form of the equation is:

$$\mu = S/P$$

Where S is the shear strength of the interface and P is the contact pressure. The shear strength can then be approximated as:

$$S = S_o + \alpha P$$

Which then gives the expression:

$$\mu = (S_o/P) + \alpha$$

In this equation S_o and α represent constants derived from the material properties controlling friction. P is the Hertzian contact pressure for smooth balls and flat substrates loaded below the elastic limit, yielding the following equation in final form:

$$\mu = S_o\pi(3R/4E)^{2/3}L^{-1/3} + \alpha$$

Where E is the elastic modulus of the couples, R is the effective contact radius, and L is the normal load.

Using this equation and modifying it to fit the elliptical contact, a curve was fit to all of the room temperature and high temperature gross slip coefficient of friction measurements, Fig 2.11 and 2.12. For the room temperature tests, the curve displays a good correlation with the Hertzian contact model. However, the model does not provide a good fit to the 450°C data. Instead, the high temperature friction data appears to fit a function of $L^{-1/2}$ instead of the $L^{-1/3}$, as described by the Hertzian model. It is believe that this discrepancy is due to the accelerated surface oxidation that occurred at high temperature, which affects the interfacial properties and surface chemistry in a way that the model does not account for.

2.5 Conclusions

Using the combination of RMS friction, hysteresis loops, energy loss, surface profilometry, and scanning electron microscopy, the stroke length and loading conditions that induce mixed fretting wear for Ti6Al4V mating surfaces were characterized at room temperature and 450°C. This work revealed that the transition from mixed to gross slip fretting occurs at higher loads in the room temperature fretting tests. This indicated that elevated temperature promoted mixed fretting wear. At room temperature, the transition from mixed to gross slip fretting wear is abrupt. This is caused by TTS formation (or the strain hardening of the surface), which lead to the brittle fracture of the surface and created large amounts of active debris at the interface. A sharp transition was not seen at 450°C, because more slip systems were likely active which would have impeded the build up of a network of dislocations that were required to develop strain hardening. At 450°C, the maximum energy loss per cycle was needed to determine the critical load at which the interface changed from mixed to gross slip fretting. This methodology was then confirmed with wear analysis and surface morphology investigations.

The variance in the coefficient of friction with respect to the applied normal load showed a good correlation with the Hertzian contact model at room temperature. At high temperature, the Hertzian model fits the trend, but does not correlate as well as it does at room temperature. This may be due to the accelerated surface oxidation that occurred at high temperature.

Chapter 3

UNLUBRICATED GROSS SLIP FRETTING WEAR OF PLASMA SPRAYED CuNiIn COATINGS

3.1 Objective

The common mitigation strategy, or solution, to the fretting wear/fatigue problem in titanium alloy compressor blades is to apply plasma sprayed CuNiIn (Copper-Nickel-Indium) or Al-bronze (aluminum bronze) plasma sprayed coatings and solid lubricants to the dovetails of the Ti6Al4V compressor blades, as shown in Chapter 1 Fig 1.3 [22, 37]. In some cases a solid lubricant is also applied to the disk slot; however, the slot geometries are often too small for the application of a plasma sprayed coating. Therefore, the CuNiIn or Al-bronze coating and solid lubricant, applied to the blade dovetail, were designed to act as a sacrificial barrier that protects both the blade and disk by preventing the Ti6Al4V surfaces from coming in contact with each other.

The roughness of the soft plasma sprayed metallic coatings is used as a retainer for the application of the bonded solid lubricant. The implementation of this strategy has increased component life; however, recent studies have shown that unlubricated CuNiIn and aluminum bronze coatings can cause severe damage to mating Ti-alloy counterparts [22, 60]. In 2000, Freimanis et al conducted a fretting wear analysis of Ti-alloy blades and their mated disks after engine operation [22]. In this research it was found that the solid lubricant had worn away and the CuNiIn coated dovetails had caused significant damage to the uncoated disk. Fig 1.4 in Chapter 1 shows the transfer of titanium to the surface of a CuNiIn coated blade dovetail, via galling with the uncoated disk. This clearly shows that

the CuNiIn coatings can have a detrimental impact on the fretting fatigue life of uncoated titanium alloy disks (via galling at the interface) once the applied lubricants wear out.

Although the implementation of these thermal spray coatings capped with solid lubricants has increased component life, there is a tremendous cost associated with schedule based maintenance of these systems. Therefore, the development of new coatings, coating processes, and lubricants that are able to reduce fretting damage and withstand the hostile engine environment will provide significant reductions in maintenance costs. In order to develop these coatings, it is important to characterize the Ti6Al4V surface interactions with current coatings and compare them with potential replacement materials.

In this work, an in depth wear analysis was conducted on the gross slip fretting wear of Ti6Al4V worn against plasma sprayed copper-nickel-indium (CuNiIn) coatings. CuNiIn was chosen because it is one of the two most prominent thermal sprayed coatings for titanium compressor bladed disk assemblies. In addition, Hutson et al. and Conner et al both determined that plasma sprayed CuNi and Al-Bronze coatings, respectively, extended the fretting fatigue limit and provided resistance to crack initiation of Ti6Al4V samples in bench level experiments [61-62].

Although CuNi and CuNiIn coatings have been analyzed in previous fretting wear and fretting fatigue studies, the focus has been on experiments conducted under predominantly mixed or partial stick fretting conditions. However, Freimanis et al conducted wear analysis of actual compressor blades and disks and discovered that the resultant wear was defined by a mixture of gross slip and mixed fretting wear conditions [22]. In fact, Freimanis et al were not able to mimic the fretting wear conditions of the

engine without a two phase fretting wear test that combined an initial phase of gross slip fretting, followed by a primary phase of mixed fretting. They believed that this was due to the fact that the blades experience a significant amount of gross slip fretting wear during the startup and shutdown of the engine. Because gross slip fretting wear is defined by a higher wear rate than mixed fretting, as shown in Fig 3.1, the authors of this work believe that it is pertinent to understand the wear mechanisms associated with this phase of the coating degradation. Therefore, gross slip fretting wear experiments and post test analysis were designed to analyze the interfacial wear mechanisms associated with the Ti6Al4V/CuNiIn worn interfaces tested at room temperature and 450°C. Room temperature was chosen for these experiments, because all turbine engines must go through a cold startup. Therefore, there will be some gross slip fretting wear cycles at the ambient temperature of the engine. 450°C was chosen as the highest steady state operational temperature that titanium alloys may be expected to survive.

Upon the completion of the bench level fretting wear experiments, special attention was paid to the wear of the uncoated Ti6Al4V surfaces mated with the plasma sprayed coatings. This is due to the fact that these coatings are typically used as a sacrificial interface that prevents the intimate contact between the Ti6Al4V component surfaces, while reducing the damage to both the coated and uncoated surface.

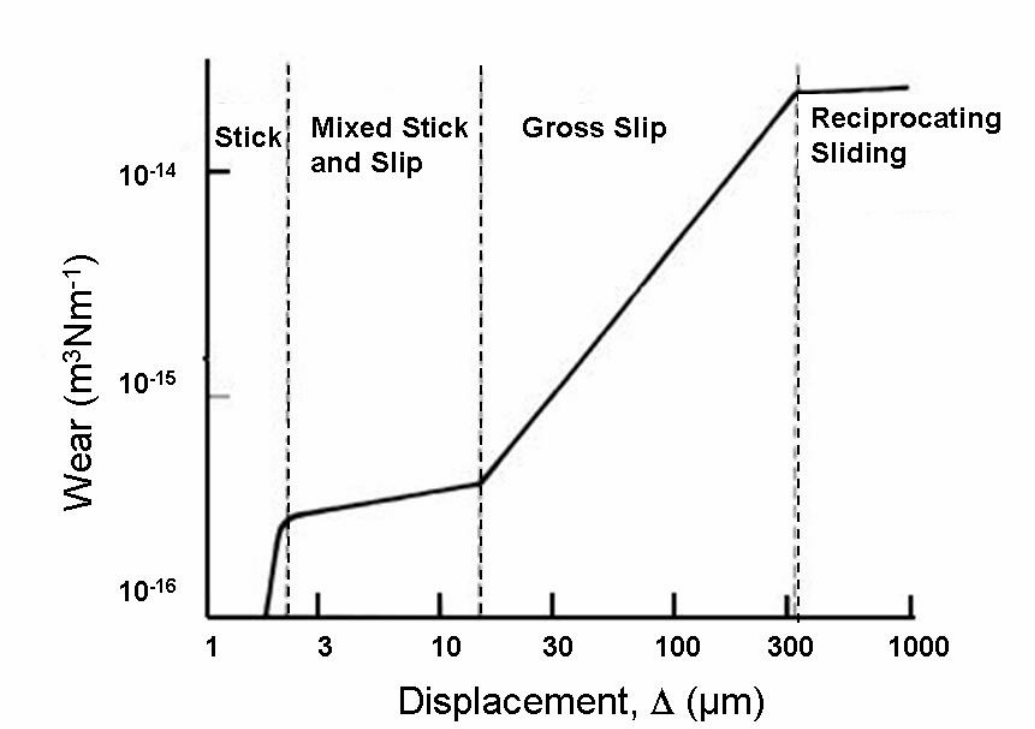

Fig 3.1. Wear regime example plot using steel on steel with a fixed geometry, constant load, and varied stroke length from I.M. Hutchings, Tribology [6].

3.2. Specimens and Tribological Testing

The fretting wear experiments in this chapter were conducted using Ti6Al4V ellipsoids and disks of the same geometry and finish as the ones described in Chapter 2 section 2.2.1. Prior to testing, the Ti6Al4V disks were commercially grit blasted and then plasma sprayed with approximately 100 μm thick CuNiIn coatings. The CuNiIn coating weight % composition was 64% Cu, 35% Ni, and 1% In (as-sprayed). Coating hardness was measured to be ≈138 HV with a Vicker's microhardness tester, and ≈2.4 GPa with an MTS nanohardness tester. Along with hardness, the MTS nanoindenter was also used to determine that the Young's modulus of the CuNiIn coatings was ≈90 GPa. In comparison, the Ti6Al4V ellipsoids and disk substrates were measured to have micro and nanohardness values of ≈284 HV and 4.1 GPa, respectively. The Young's modulus of the Ti6Al4V

samples was measured to be ≈143 GPa. Therefore, the Ti6Al4V uncoated ellipsoids have approximately twice the hardness and almost twice the stiffness of the mated CuNiIn coatings.

The purpose of this work was to develop an understanding of the wear mechanisms associated with the degradation of uncoated Ti6Al4V surfaces coupled with CuNiIn coatings and subjected to gross slip fretting wear at room temperature and 450°C. The room temperature tests were designed to simulate cold engine startup. The 450°C experiments were designed to simulate the highest temperature that titanium alloys and CuNiIn coatings are expected to survive in a turbine engine compressor. The experimental setup, shown in Fig 3.2, uses an uncoated ellipsoid to simulate an uncoated disk slot and a coated disk to simulate a coated dovetail. In this configuration, the coatings were tested as-sprayed. The surface of the coatings had a measured roughness average of approximately 9 μm Ra, as compared to the 0.1 μm Ra finish on the mated Ti6Al4V ellipsoid. Three to four repeat tests were conducted on each coating and on a set of uncoated Ti6Al4V disks. The uncoated disks were used to compare the fretting wear evolution and wear mechanisms of the Ti6Al4V/CuNiIn coating system to the mated Ti6Al4V contacts.

The Fretting wear tests were conducted using a 200 μm stroke length, 30 Hz oscillation speed, and a 50 N normal load for 100,000 cycles. The applied 50 N normal load yields a maximum Hertzian contact stress of approximately 650 MPa, which is based on the design loads of the dovetail joints during engine operation. In addition, shorter duration tests were conducted at 2 Hz oscillation speed, to supplement the longer tests for wear analysis. All of these experiments were conducted using the fretting wear tribometer that is described in detail in Chapter 2 section 2.2.2.

Once the fretting wear tests were completed, post test analysis was performed using scanning electron microscopy (SEM) and 3-D contact profilometery for morphology, along with energy dispersive spectroscopy (EDS) for chemical analysis. All cross-sections were cut perpendicular to the fretting wear direction using a low speed diamond saw. The coating cross-sections were mounted using an air cured epoxy mount, and the uncoated ellipses were mounted using a hard carbon filled conductive hot compression mount. The hot compression mounts were used on the ellipse cross-sections because they have a higher hardness and better edge retention, which is needed to keep the worn regions intact during the polishing process. Once mounted, all cross-sectioned samples were polished prior to microstructure and EDS analysis.

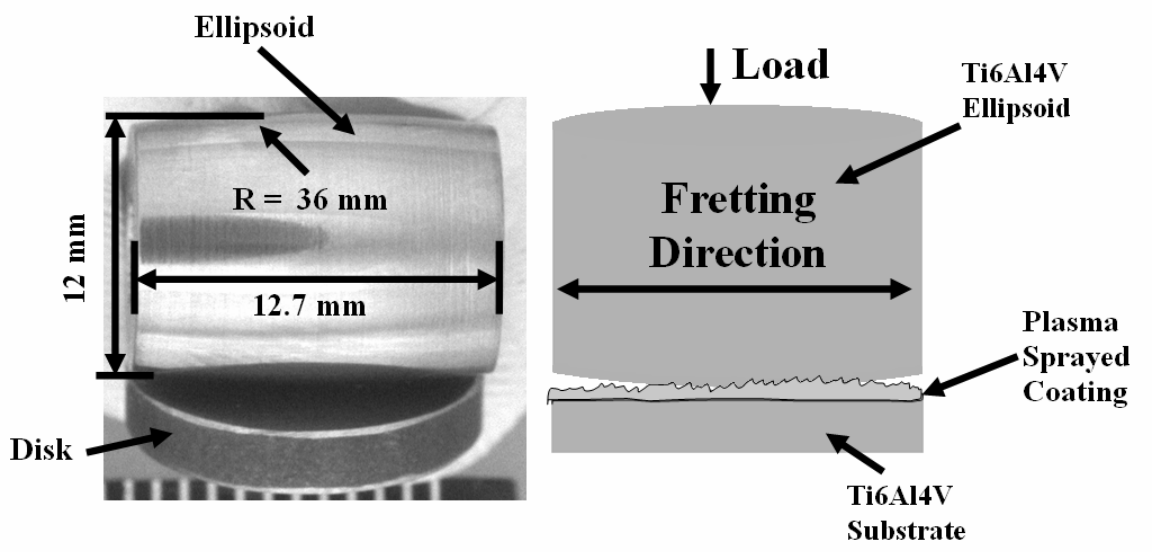

Fig. 3.2. Experimental setup and contact geometry.

3.3 Results

3.3.1 Friction and Wear

The coefficients of friction for all the tests ranged from approximately 0.75 at room temperature to approximately 0.8 at 450°C. This is in the same range as the friction measured in uncoated Ti6Al4 mated contacts, which ranged from 0.8 at room temperature to 0.7 at 450°C. Therefore, the CuNiIn coating does not provide any advantage based on friction reduction.

In addition to measuring the friction, the coating wear was assessed by approximating the wear volume of each fretting wear track using a 3-D contact profilometer. Although there is evidence of compacted debris and material transfer in the wear tracks, as discussed in the next section, the contact profilometer yielded a sufficient approximation of the overall size and depth of the wear track. Prior to scanning, the normal load on the profiler stylus can be adjusted. The surface scans were conducted with high enough load that the stylus was able to plow through most of the debris within the wear track.

The room temperature fretting wear tracks on the CuNiIn coated surfaces exhibited a ~44% reduction in coating thickness, which accounted for a wear volume of ~0.09 mm^3. In comparison, the uncoated Ti6Al4V disks yielded a wear volume of ~0.06 mm^3. The coated surfaces that were tested at 450°C had a large mound of transferred material in the center of the wear track, which made it virtually impossible to determine the wear volume or the depth of the wear track. The origin of this mound of material required further analysis, and is explained in the next section by cross-sectional wear analysis of the fretting wear tracks.

3.3.2 Wear Mode Analysis

Initially the Ti6Al4V mated surfaces, tested at room temperature, are damaged primarily by galling, and then by 3rd body wear as the large adhered particles deform and start to break apart. After 10 cycles, with 2 Hz oscillation speed, the gross slip fretting wear at the Ti6Al4V interface of the test specimens is composed of adhesive wear and ploughing, as shown in Fig 3.3A. The mated surfaces exhibited severe plastic deformation with large wear particles, on the order of 100 μm long and 50 μm wide, adhered to the wear track. After 100 cycles the continued deformation of the large wear particles in the contact cause them to break up into smaller wear debris, as shown in Fig 3.3B. The majority of the debris gathers around the edges of the contact, with some of the debris getting trapped inside the wear track. After 1,000 cycles almost the entire wear track is filled with wear debris, as shown in Fig 3.3C. Some large wear particles can be seen near the center and the edges of the wear track. Some of these larger particles are produced in local regions throughout the wear track where the Ti6Al4V surfaces make contact in the absence of the trapped wear debris. In addition, some of the particles may have survived from the adhesive wear that was predominant during the initial stages of the test. After 100,000 cycles, with 30 Hz oscillation speed, the wear track is completely filled with wear debris, as shown in Fig 3.3D. This exact wear mode has been described in detail in a fretting wear review paper by Hurricks [11], and by Blau [9] in his work with wear mechanisms in metallic interfaces.

Fig 3.4A and 3.4B shows cross-sectional micrographs of a typical 100,000 cycle Ti6Al4V mated fretting wear test. The cross-sections of the ellipsoid wear tracks were cut perpendicular to the fretting direction as shown by the arrows in Fig 3.3D. In the center of

the wear track, the wear scar is approximately 30 to 40 µm deep. The dark region is a compacted powder bed of fine titanium and oxide wear debris. Using Raman Spectroscopy, Hager et al [7] determined that the accumulation of gross slip fretting wear debris in the contact of Ti6Al4V mated surfaces contained significant amounts of rutile TiO_2. Fig 3.4B shows the plastically deformed surface layers, or highly deformed layer (HDL) as defined by Rigney et al [63], near the edge of the wear scar and beneath the trapped wear debris. In these contact regions the accumulation of plastic deformation occurs until the surface material becomes unable to accommodate the imposed strain, a similar phenomenon has also been seen in titanium contacts by Blanchard et al [12]. This type of deformation eventually leads to the breakup of surface regions and the formation of large wear particles, as shown in Fig 3.4B.

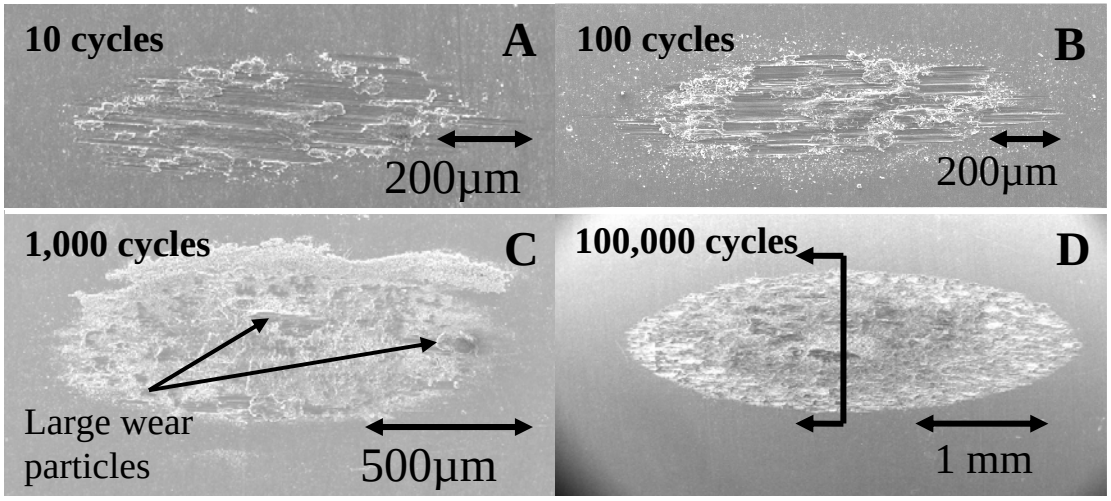

Fig. 3.3. SEM micrographs of the fretting wear on the surface of the ellipsoid after being worn against a Ti6Al4V uncoated disk for A) 10 cycles at 2 Hz, B) 100 cycles at 2 Hz, C) 1,000 cycles at 2 Hz, and D) 100,000 cycles at 30 Hz.

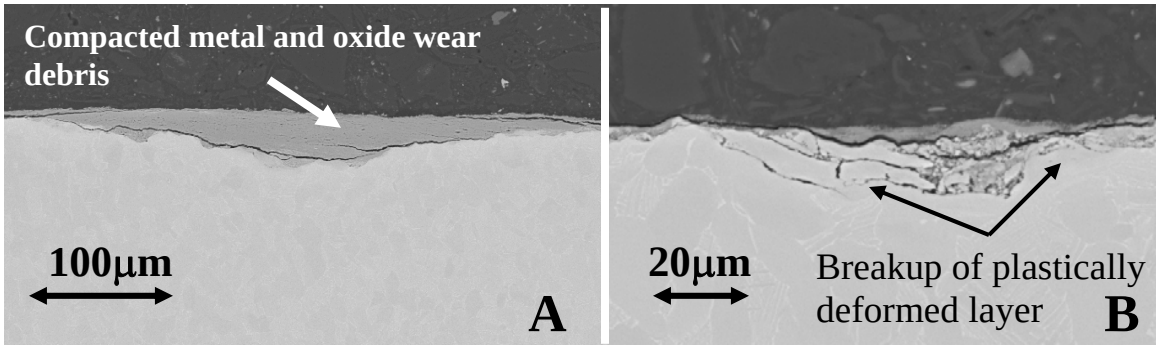

Fig. 3.4. Images A and B are back scatter (BSE) SEM images showing the cross-section of a Ti6Al4V ellipsoid worn against uncoated Ti6Al4V at room temperature for 100,000 cycles, at the center and edge of the wear track respectively.

The uncoated Ti6Al4V surfaces tested at 450°C exhibited severe galling. In all of these tests there was very little or no debris detected, but there were thick transfer layers in the fretting contact region of both mating surfaces, an example is shown in Fig 3.5. At this temperature there wasn't any cracking observed in the contact regions, except for cracking that appeared to originate within the layers of adhered material that transferred between the worn surfaces. Although the cracking occurred within the transferred material, some of these cracks did propagate into the bulk material, as seen in Fig 3.5. Inside the contact region there was some evidence of fretting corrosion, which appeared predominantly in the regions where material was removed. Fretting corrosion is the precursor to the severe adhesion that occurs between the surfaces. At 450°C, the surfaces oxidize forming TiO_2. The TiO_2 is harder than the underlying Ti6Al4V, which at this temperature has been significantly softened. Mismatch between the hard layer and the soft bulk material make the oxide easy to remove during the fretting cycles. Once the oxide layers are removed the underlying nascent Ti6Al4V is revealed and able to come into contact with nascent

material on the counter-face, causing the two surfaces to adhere and the fretting contacts to gall.

The wear mode analysis conducted on the uncoated Ti6Al4V ellipsoids, worn against the plasma sprayed CuNiIn coatings, determined that the wear evolution and damage mechanisms are same as those exhibited by mated Ti6Al4V surfaces. Fig 3.6 shows SEM micrographs of the ellipsoid surface damage caused by room temperature gross slip fretting against the CuNiIn plasma sprayed coatings. Wear against the CuNiIn coating for 100 cycles produced large adhered coating particles, on the order of 20 to 100μm in size. In addition, 100 cycles of fretting was enough to cause galling throughout most of the contact area and create large amounts of trapped oxide debris, the tiny white particles that are dispersed throughout the wear track as shown in Fig 3.6A. EDS analysis and X-ray mapping of the magnified regions showed that the large adhered particles are adhered metallic particles from the mated CuNiIn surfaces. These large adhered particles plowed large channels in the form of striations on the surface of the Ti6Al4V ellipsoids. In addition, the micrographs from these tests also indicated a significant amount of tiny wear debris trapped within the wear track.

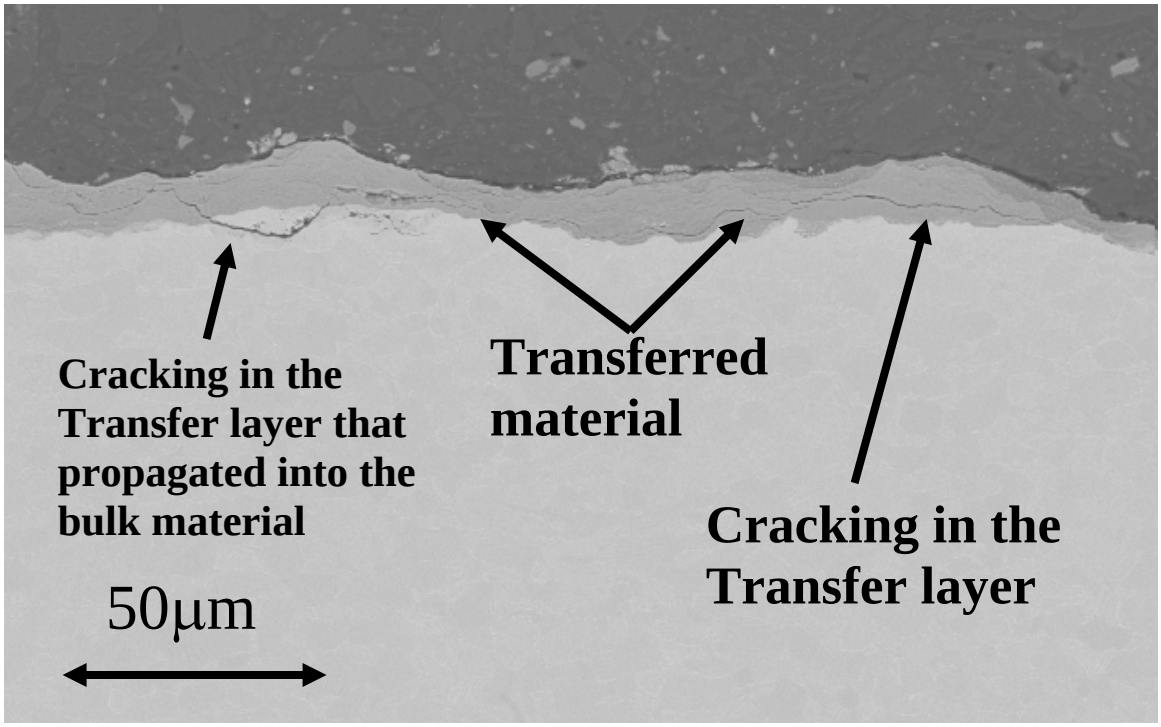

Fig. 3.5. This is a BSE SEM image showing the cross section of a Ti6Al4V ellipsoid worn against uncoated Ti6Al4V at 450°C.

After 100 cycles, a separate set of room temperature fretting wear experiments were conducted against the CuNiIn coatings for 1,000 and 100,000 cycles. After the 1,000 cycle fretting tests, the wear tracks exhibited an increased amount of fine oxide debris trapped within the wear track, and the absence of the large transfer particles that were seen in the 100 cycle tests. However, some of the wear scars, created by the CuNiIn coatings, exhibited large regions near the center of the contact where evidence of localized adhesive wear (or galling) was still apparent, as shown in Fig 3.7. After 100,000 wear cycles, all surfaces of the Ti6Al4V ellipsoid wear tracks worn against CuNiIn were completely covered with a powder bed of compacted wear debris. This debris was composed of mostly oxidized Ti6Al4V and coating particles along with some larger metallic particles,

typically from the coating surfaces. Micrographs of the ellipsoid wear tracks after 100,000 cycles are shown in Fig 3.7.

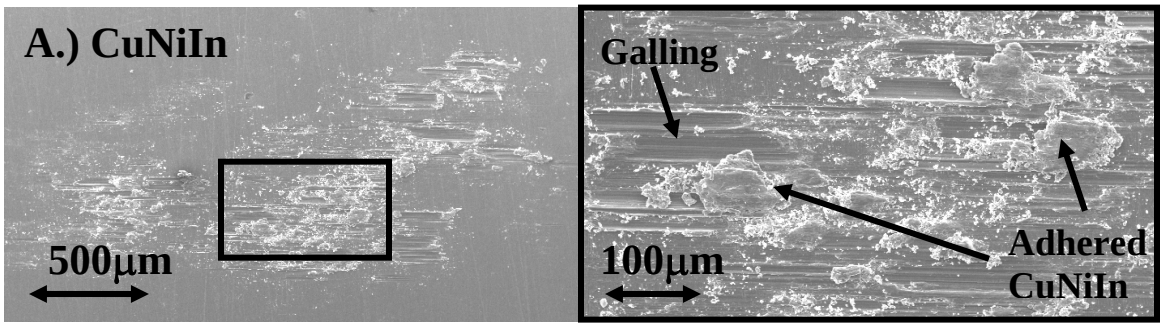

Fig. 3.6. SEM micrographs of the fretting wear on the surface of the Ti6Al4V ellipsoid after being worn against CuNiIn at room temperature for 100 cycles at 2Hz. The images outlined in black on the right are zoomed images of what is contained in the black squares on the left.

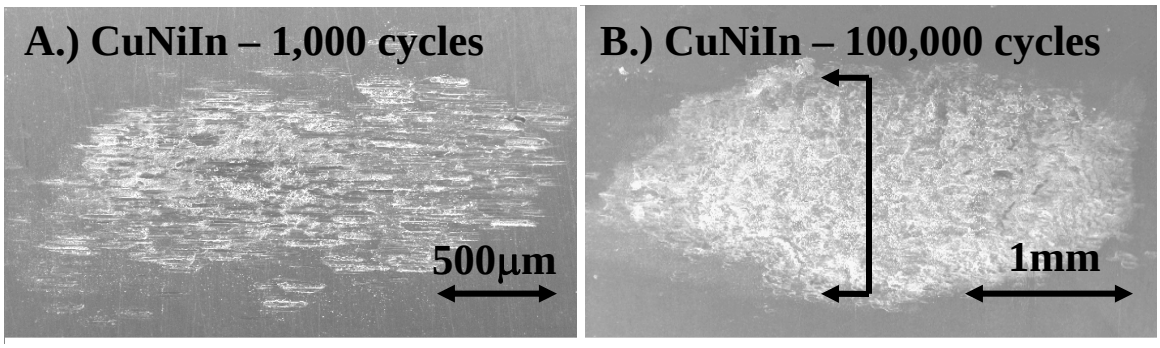

Fig. 3.7. SEM micrographs of the fretting wear on the surface of the Ti6Al4V ellipsoid after being worn against CuNiIn at room temperature for 1,000 and 100,000 cycles respectively.

In addition to the wear scar surface analysis, all of the Ti6Al4V ellipsoids worn for 100,000 cycles were cross-sectioned perpendicular to the fretting direction, as shown by the black arrows in Fig 3.7B. Analysis of the back scatter (BSE) SEM micrographs of the ellipsoid cross-sections, shown in Fig 3.8, further verifies the similarities in the fretting wear mechanisms that damage these Ti6Al4V surfaces when self mated or worn against the CuNiIn plasma sprayed coatings. Fretting wear of Ti6Al4V ellipsoid surfaces mated with

the CuNiIn coatings produced virtually identical wear to that of the mated Ti6Al4V surfaces, as seen by comparing Fig 3.8 with Fig 3.4. The only differences being that the mixture of the metal and oxide debris compacted into the worn ellipsoid surfaces have different chemistries.

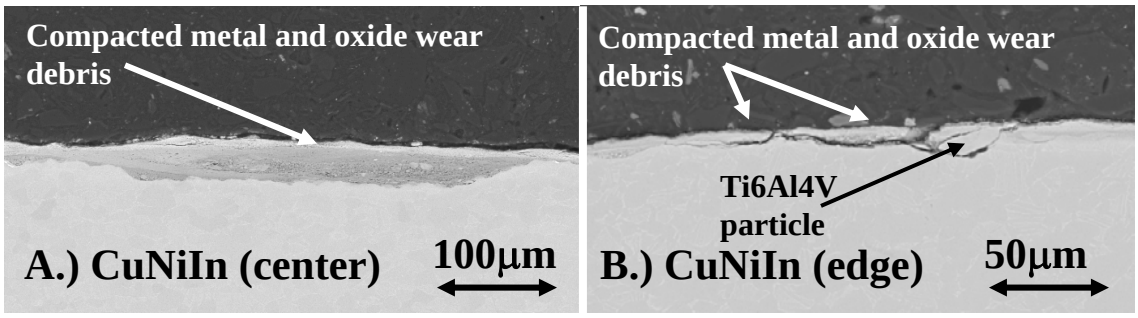

Fig. 3.8. Back scatter (BSE) SEM image showing the cross-section of a Ti6Al4V ellipsoid worn against CuNiIn at room temperature for 100,000 cycles. Images on the left are from the center of the wear track, and images on the right are from a region near the edge of the respective wear track.

The CuNiIn coatings tested at 450°C proved to be very wear resistant. However, the coatings caused severe galling to occur at the interface, similar to that seen in the uncoated tests. Fig 3.9 shows the wear that occurred on the coating and Ti6Al4V counter face. Looking closely at Fig 3.9A, it can be seen that a thick layer of titanium has adhered to the surface of the coating in the center of the wear track. This extreme galling produced titanium transfer layers approximately 30μm thick on the coating surface in every test conducted at this temperature. This thick layer of titanium that adhered to the surface of the coating is in complete agreement with the findings in a study that analyzed worn CuNiIn coated compressor blades (Fig 3.10 shows a scaled comparison of the bench test cross-section to a cross-section from a worn CuNiIn coated dovetail) [22]. Fig 3.9B shows the crater region on the Ti6Al4V ellipsoid, where the material has been removed.

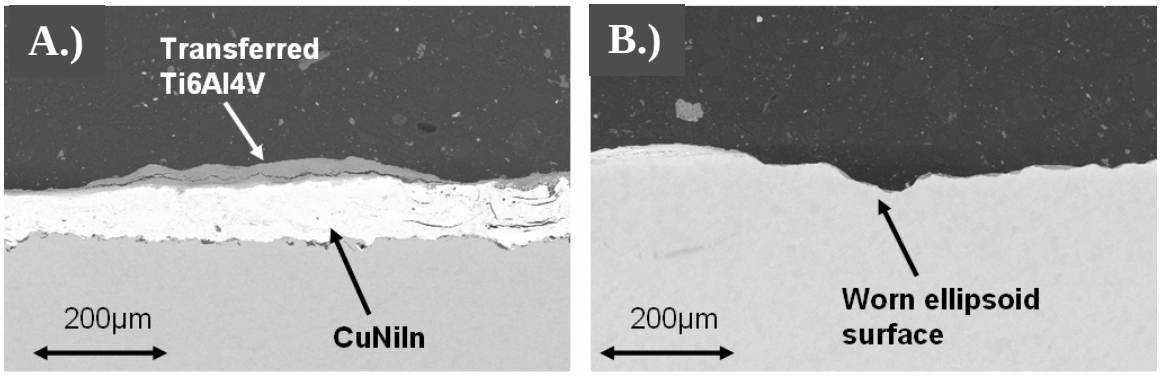

Fig. 3.9. (A and B) are BSE SEM images showing the cross sections of (A) CuNiIn coated disk and (B) Ti6Al4V ellipsoid tested at 450°C.

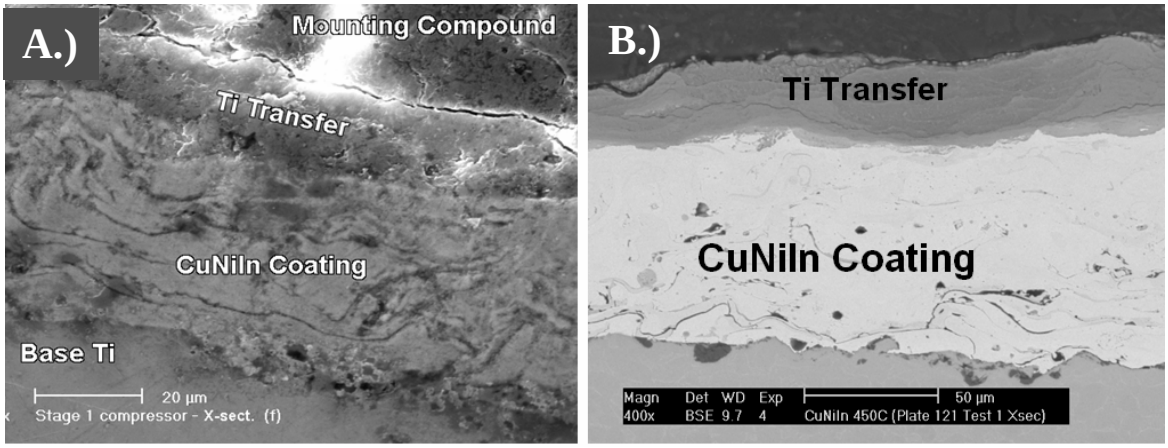

Fig 3.10. A scaled comparison of the cross-section of (A) a worn CuNiIn coated compressor blade dovetail [22], and (B) a bench level tested CuNiIn coated disk.

3.4. Summary and Discussion

In overview, this work was conducted to assess the interfacial wear mechanisms associated with gross slip fretting of Ti6Al4V in contact with CuNiIn plasma sprayed coatings at room temperature and 450°C. These tests were conducted without lubrication and caused metallic wear at the fretting contact. All metallic engineering surfaces are covered by thin oxide layers that are typically angstroms or nanometers in thickness [11, 64]. This contaminant layer initially protects the underlying metal from interfacial

adhesion. However, these surface species were dispersed during the first few cycles of the fretting wear process and allowed the intimate contact of the Ti6Al4V ellipsoid surfaces with the metallic CuNiIn coated surfaces. When this happened the contacting nascent metallic surfaces caused adhesive wear and ultimately galling. The galling of the Ti6Al4V ellipsoid surface coincided with the shearing of the coating surface asperities, and the simultaneous transfer metallic material between the contacting surfaces. Fig 3.11 shows the transfer of titanium from the Ti6Al4V ellipsoids to the CuNiIn coated disks during the first 100 fretting wear cycles at room temperature.

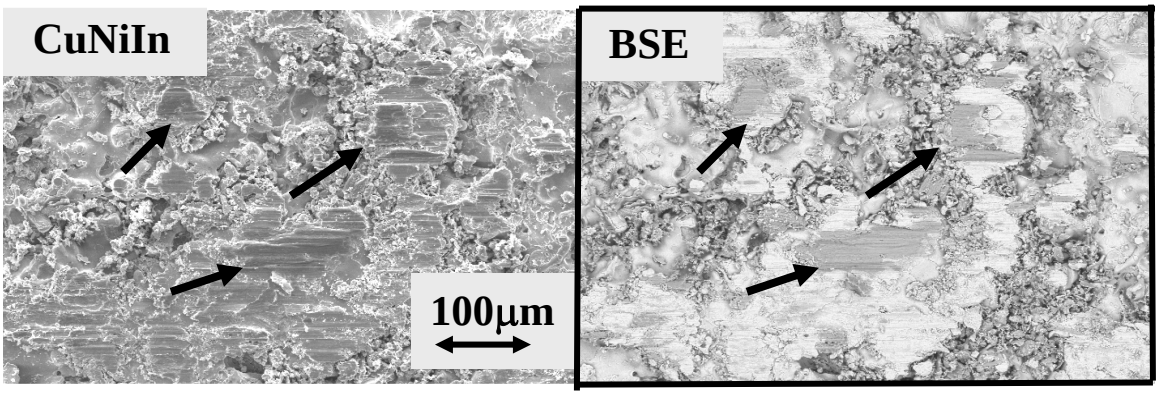

Fig. 3.11. SEM micrographs of a wear track on the CuNiIn surface after 100 cycles at room temperature. On the left is a secondary electron (SE) image and on the right is the same image using a back scatter (BSE) detector. The black arrows in all of the images point to titanium that is adhered to the coating wear surface.

The plasma sprayed CuNiIn coatings tested were approximately half as hard as the Ti6Al4V contact surface. This would lead one to believe that material transfer at the fretting interface would consist of the softer coating surfaces transferring to the harder Ti6Al4V surface, and in fact this is what predominantly occurs. However, there are localized regions where large Ti6Al4V particles, on the order of 50 to 100μm, were adhered to the CuNiIn coated surfaces, as shown in Fig 3.11. Bowden et al [8] also

witnessed a similar phenomenon when they observed the transfer of small fragments of mild steel to the surface of copper during sliding wear experiments. This is an extremely devastating phenomenon that accelerates the ellipsoid wear as the adhered Ti6Al4V particles form raised plateaus on the coating surface. These titanium plateaus promote further galling by creating titanium on titanium contact within the fretting interface.

Galling and material transfer, along with the shearing of coating asperities typically occurs within the first 100 gross slip fretting wear cycles at room temperature. Between 100 and 1,000 cycles of wear, the highly deformed surface layer of the Ti6Al4V ellipsoid becomes unable to accommodate the imposed fretting displacement and begins to crack and break, as shown in Fig 3.4B. In addition, the continued deformation of the transferred material plateaus causes them to breakup as well [7]. This creates an abundance of wear debris within the contact. The wear debris represents a wear mechanism shift from adhesive driven wear to wear that is mostly controlled by the rheology of the 3rd body debris.

As the room temperature fretting wear progresses from 1,000 cycles to 100,000 cycles, some of the wear debris is swept out of the wear track, and some of the wear debris remains. The trapped or active wear debris continuously gets crushed into fine particles and oxidizes. As the active wear debris builds up in the wear track, it gets compressed together and forms a powder bed that separates the contacting surfaces. If the powder bed formation is continuous, as shown in Fig 3.4 and 3.8, then the surface degradation will be concentrated at the edges of the contact and expand the wear track laterally instead of deeper.

Ultimately, the unlubricated CuNIn coatings did not change the associated wear mechanisms or reduce the apparent wear damage imposed on the Ti6Al4V ellipsoid surface. At room temperature, this wear similarity is driven by adhesive wear followed by the formation of a debris powder bed. The rheology of the 3rd body debris, primarily the titanium oxide debris which is constant to all of the tests, controls the extent of the fretting wear damage to the Ti6Al4V ellipsoid after 1,000 cycles, or once enough debris has been established in the contact. In addition, the CuNiIn coatings sustained severe wear during each of the room temperature fretting wear tests (where 40% of the coating thickness had been worn away after 100,000 cycles of fretting). At 450°C, both the CuNiIn coatings and the uncoated Ti6Al4V disks exhibited galling throughout the entire 100,000 cycle test. Although the CuNiIn coatings did not sustain significant damage during these tests, the formation of a ~30 μm titanium transfer layer created a titanium on titanium mated contact. This effectively damaged the uncoated Ti6Al4V ellipsoid in the same manner as the uncoated disk had done, during the same tests.

The wear analysis from this work supports the need for a different coating system. Although the actual compressor blades are coated with thermal sprayed coatings and then with solid lubricants, this study shows the dangers of what can happen if/or when the lubricants fail or are completely worn away. In gross slip fretting, these soft CuNiIn coatings do not effectively protect the mating Ti6Al4V surfaces without solid lubrication.

3.5. Conclusions

This work was conducted to examine the wear mechanisms associated with the comparison of Ti6Al4V/Ti6Al4V and Ti6Al4V/CuNiIn mated fretting contacts, under gross slip. It was found that the measured coefficient of friction in all of the tests was very

high, from 0.7 to 0.8. In addition, all of the wear mechanisms that governed the surface damage accumulation were the same in the coated and uncoated test configurations. This ultimately lead to similar amounts of Ti6Al4V ellipsoid wear against the CuNiIn coatings and in the Ti6Al4V mated tests. Therefore, the CuNiIn coatings were unable to adequately protect the mated Ti6Al4V ellipsoids at room temperature or at 450°C without lubrication.

Chapter 4

UNLUBRICATED GROSS SLIP FRETTING WEAR OF Al-BRONZE COATINGS

4.1 Objective

As explained in Chapter 3, fretting wear at titanium alloy compressor blade/disk interfaces is often mitigated with the use of CuNiIn and Al-Bronze coatings on the blade root. Chapter 3 summarized the degradation of Ti6Al4V surfaces worn against CuNiIn coatings, without lubrication. This chapter will be focused on the unlubricated fretting wear of Ti6Al4V worn against three Al-Bronze coatings, two plasma sprayed coatings of different copper to aluminum (Cu/Al) ratios and one cathodic arc coating. Bench level gross slip fretting wear experiments and post test analysis were used to determine the wear mechanisms and damage associated with unlubricated Al-bronze coatings worn against uncoated Ti6Al4V surfaces at room temperature, 163°C, and 450°C. Similar to the design of CuNiIn coatings, Al-Bronze coatings are applied as a sacrificial layer to protect the wear of both the coated and uncoated titanium surfaces. Therefore, special attention was paid to the wear of the uncoated Ti6Al4V surfaces mated with the plasma sprayed coatings, in the post test analysis.

4.2. Specimens and Tribological Testing

The fretting wear experiments in this chapter were conducted using Ti6Al4V ellipsoids and disks of the same geometry and finish as the ones described in section 2.2.1. Prior to testing, some of the Ti6Al4V disks were commercially grit blasted and then plasma sprayed with Al-bronze coatings 1 and 2 (which had different Cu/Al ratios). The remaining Ti6Al4V disks were also coated with Al-bronze; however, these disks were coated using cathodic arc PVD (physical vapor deposition). Cathodic arc is a vacuum PVD technique

that typically yields high adhesion, high density, and minimal oxygen in the coatings. The coating compositions (as measured with EDS prior to testing), surface roughness, hardness, modulus, and thickness measurements are listed in Table 4.1. The properties of the Ti6Al4V ellipsoids and disks are listed in Table 4.2. Metallography showed that both plasma sprayed coatings were dense, but the cathodic arc coatings had a clearly visible interlayer from the two coating cycles required to obtain the 100 μm coating thickness.

.

	Deposition	Cu/Al in At%	Roughness Ra (μm)	Nano Hardness (GPa)	Modulus (GPa)	Thickness (μm)
1	Plasma	≈ 6	≈ 12	≈ 1.8	≈ 89.6	≈ 300
2	Plasma	≈ 4	≈ 6.7	≈ 2.9	≈ 107.7	≈ 100
3	Cathodic Arc	≈ 6	≈ 4.2	≈ 2.2	≈ 83.7	≈ 100

Table 4.1. Coating properties.

.

Materials	Composition Weight %	Roughness Ra (μm)	Nano Hardness (GPa)	Modulus (GPa)
Ti6Al4V	90% Ti 6% Al 4% V	≈ 0.1	≈ 4.1	≈ 143

Table 4.2. Ti6Al4V properties.

The purpose of this work was to provide an understanding of how plasma sprayed and cathodic arc Al-Br coatings perform when coupled with Ti6Al4V, and subjected to gross slip fretting wear at temperatures ranging from ambient up to 450°C. The two different plasma sprayed coatings and the cathodic arc coating were used in the investigation to demonstrate the effect that aluminum and oxygen content in the coatings had on their fretting wear performance.

Three test temperatures were chosen for the bench level gross slip fretting wear experiments conducted, in order to sufficiently mimic real world conditions. Room

temperature tests were conducted to simulate cold startup of a turbine engine. 163°C was chosen as a moderate temperature to simulate a steady state temperature in the outer stages of a jet engine compressor and fan. 450°C was chosen to simulate an extreme upper limit that titanium alloys and Al-bronze coatings are expected to survive in the hot sections of the compressor. Three to four repeat tests were conducted on each coating at every temperature. The tests were conducted using a 200 μm stroke length, 30Hz oscillation speed, and a 50N normal load for 100,000 cycles (similar to the experiments conducted in Chapter 3). The 50N normal load yielded a maximum Hertzian contact stress of approximately 650MPa, which was based on the design loads of the dovetail joints during engine operation. All of these experiments were conducted using the fretting wear tribometer that is described in detail in section 2.2.2.

Once the fretting wear tests were completed, post test analysis was performed using scanning electron microscopy (SEM) and 3-D contact profilometery for morphology, along with energy dispersive spectroscopy (EDS) for chemical analysis.

4.3. Coating Wear and Analysis

In the fan and compressor sections of a turbine engine the wear analysis is two fold. As shown in Fig 4.1, the blade/disk interface has a coated surface (blade root) worn against an uncoated surface (disk slot). The damage on the worn coatings is presented in this section.

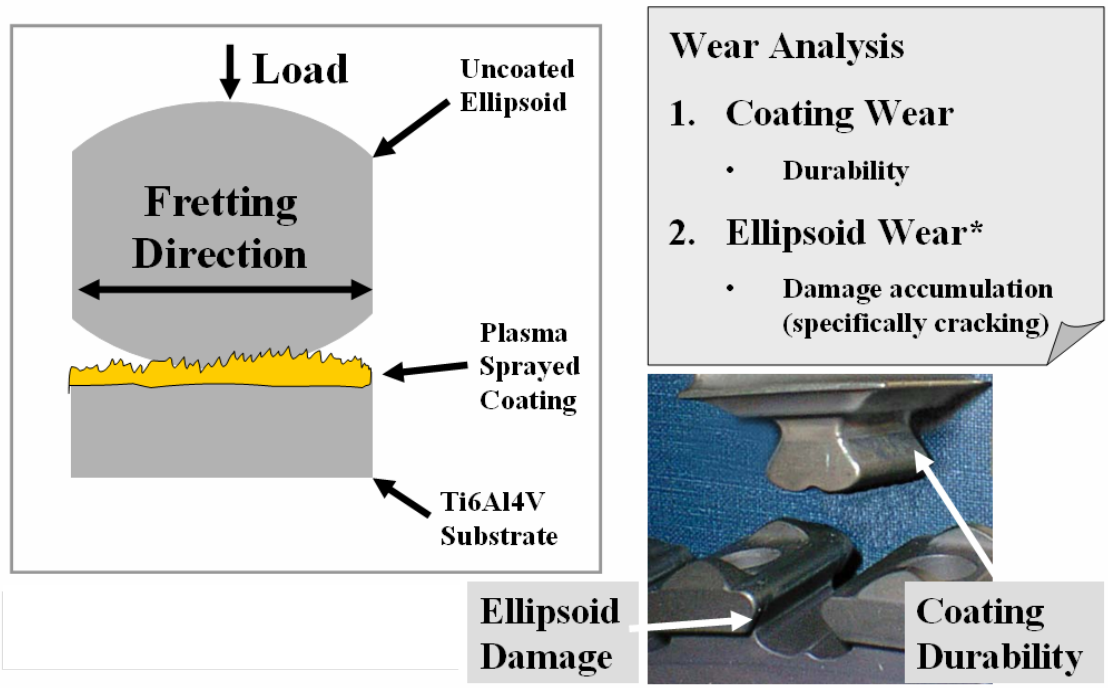

Fig. 4.1. Experimental contact and its relationship to the actual engine components.

The friction measurements from the experimental fretting wear tests and the estimated coating wear are shown in Fig 4.2 and Fig 4.3. The measured coefficient of friction was determined using the applied normal load and the measured RMS friction data. The estimated coating wear was determined by multiplying the area of the formed elliptical wear track by the maximum depth measured in the wear track. The area of the elliptical wear scars were calculated using the major and minor radii from the wear geometry, as measured using the SEM. The maximum depth in the wear track was determined from a 3-D profile of the wear that was constructed using a contact stylus profilometer.

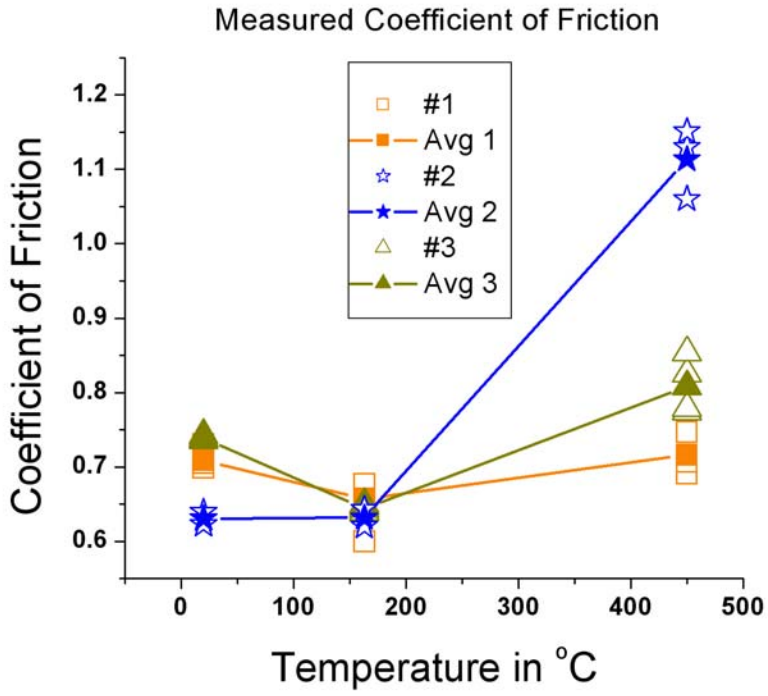

Fig. 4.2. Measured coefficient of friction.

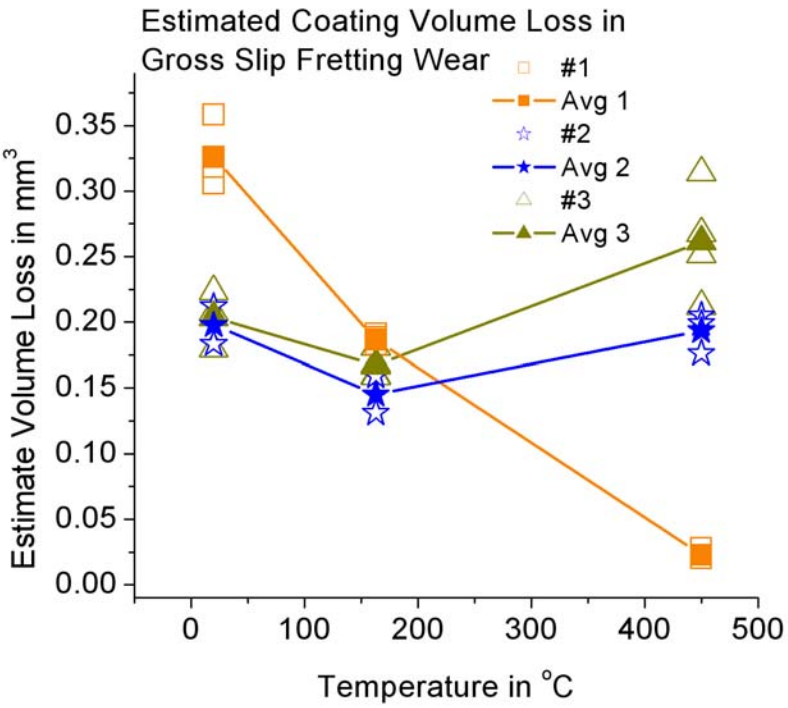

Fig. 4.3. Estimated coating volume loss.

The experimental test results show that the metal/metal contact between the Al-bronze coatings and the Ti6Al4V ellipsoids exhibit high friction at all of the temperatures tested. At room temperature coating 2 had the lowest friction, while coatings 1 and 3 had the highest, refer to Fig 4.2. Coating 2 is the second of the two plasma sprayed coatings, and has the highest aluminum content of all three coatings, as determined by EDS prior to testing. However, the EDS scans that were conducted in the wear scar on the coated and ellipsoid surface, plotted in Fig 4.4 and Fig 4.5, indicate that after fretting the contact surfaces of coatings 2 and 3 (plasma and cathodic arc) have similar chemistry. Due to the coating process, coating 2 has a large amount of oxidized material through the coating thickness, in contrast to coating 3 which was applied to the titanium substrate in a vacuum. Since copper oxides can be lubricious, the increased oxide content of coating 2 could explain why it exhibited a lower coefficient of friction than coating 3 even though the chemistry in the wear track was similar. In addition, Fig 4.6 shows that coating 3 had a lot of titanium transfer in the wear track. The worn and oxidized titanium debris would also contribute to the higher levels of friction experienced in the contact of the fretting tests on coating 3. Fig 4.4 shows that both of the plasma sprayed coatings had increased copper content in the coating wear track, with coating 1 having an increase of more than two times the levels measured on the unworn surface. Coating 1 also had a higher coefficient of friction and higher wear than coating 2. This suggests that the aluminum helps the performance of coating 2 significantly, at room temperature.

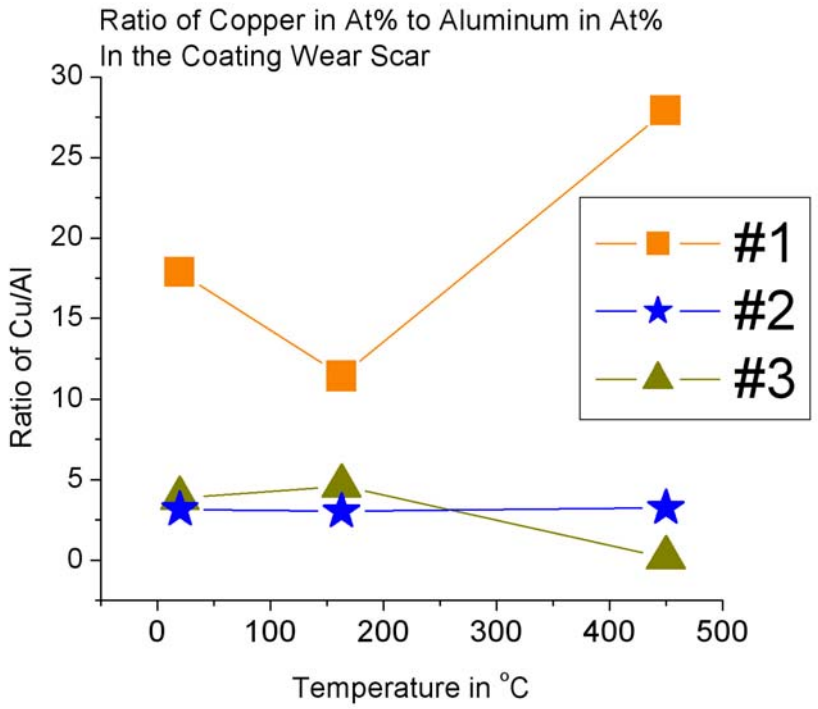

Fig. 4.4. Cu/Al ratio in the coating wear scar measured with EDS.

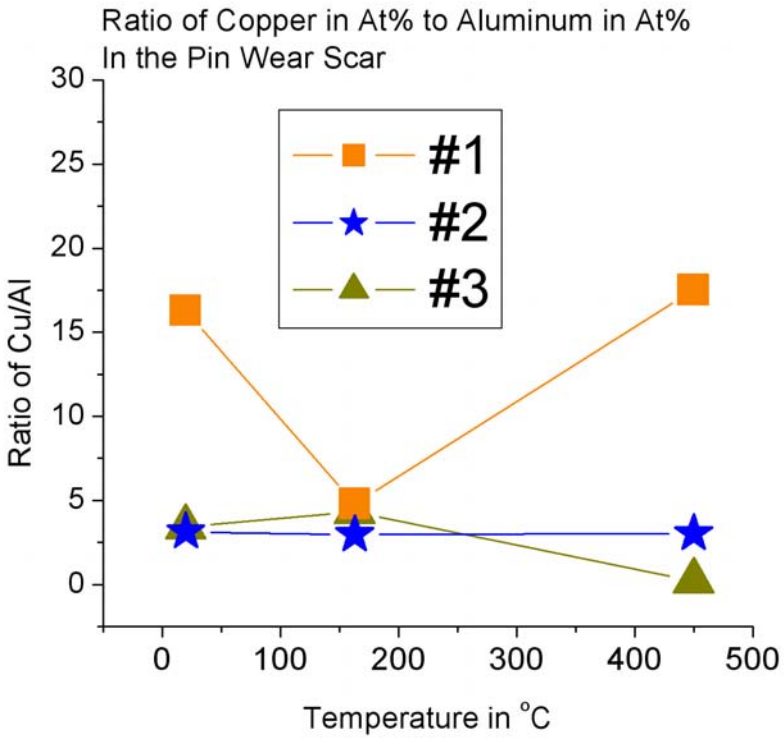

Fig. 4.5. Cu/Al ratio in the ellipsoid wear scar measured with EDS.

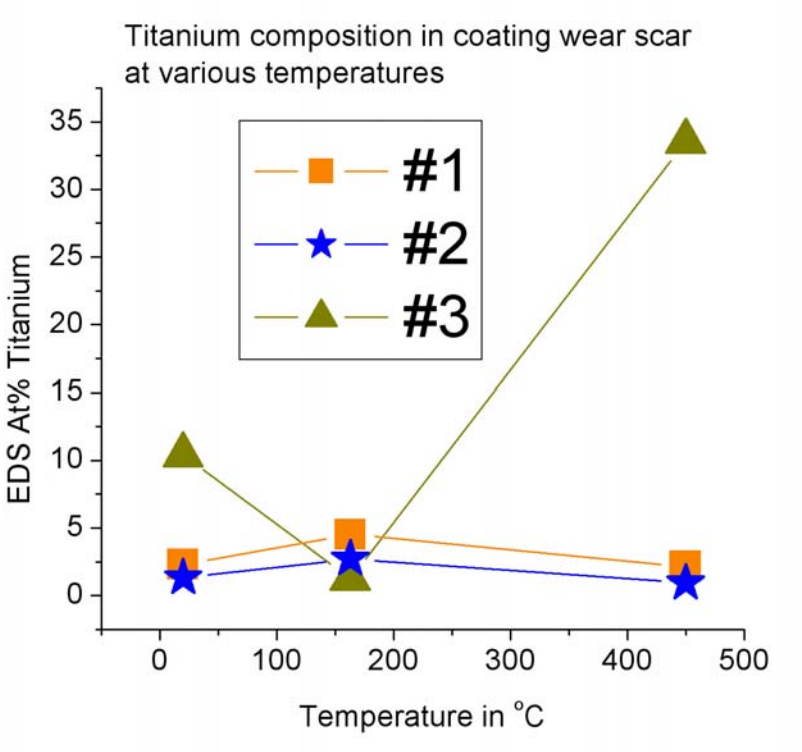

Fig. 4.6. Titanium content in the coating wear scar measured with EDS.

At 163°C all of the coatings exhibited approximately the same coefficient of friction, which was the lowest for all of the temperatures tested. The coatings also exhibited similar amounts of wear. This phenomenon is best described by Fig 4.5, which indicates that at 163°C the transfer layer on the ellipsoid surfaces of all the experiments were similar in chemistry. Therefore, the aluminum and copper content of the fretting wear tracks over time were similar and yielded similar friction and wear results.

At 450°C the coatings exhibited nearly the opposite performance that they displayed at room temperature. Coating 1, which has the lowest aluminum content in both the coating and pin wear tracks, had the lowest coefficient of friction and the lowest wear. Coating 3 did not have any copper in the wear track on the coating or the ellipsoid. This

was because the coatings had worn completely through. The coating failure was due to a combination of increased friction, wear rate, and the impact of increased temperature on the cohesion between the two layers in which the coating was applied. Earlier it was stated that the metallographic cross sections of the cathodic arc coating showed a clear interface between the two layers in which the coating was applied in order to get the desired 100 μm thickness. Coating 2 consistently had the same chemistry in the wear track at every temperature, including 450°C. However, at 450°C the coefficient of friction for coating 2 increased dramatically. In comparison to coating 1, coating 2 had a lot more aluminum in the wear track. However, coating 1 exhibited a much better performance at 450°C than coating 2. This suggests that the higher aluminum content in the interface is detrimental to the coating performance at 450°C.

4.4 Ellipsoid Wear and Analysis

Fig 4.1, shows that the blade/disk interface consists of a coated blade coupled with an uncoated disk. Therefore, fretting damage sustained by the disk is equally detrimental to the fatigue life of the compressor system. These coatings were designed to act as sacrificial layers to protect the uncoated Ti6Al4V counter surface as well. This section will present the microscopy and analysis of the damage accumulated on the contact surface of the uncoated ellipsoids used in the previously described fretting wear experiments.

The fretting wear tracks on the uncoated ellipsoids were analyzed by back scatter scanning electron microscopy of cross-sections cut through the worn regions. All cross-sections were cut perpendicular to the fretting direction as depicted in Fig 4.7 by the dashed line. EDS was also conducted on the cross-sections for all chemical analysis.

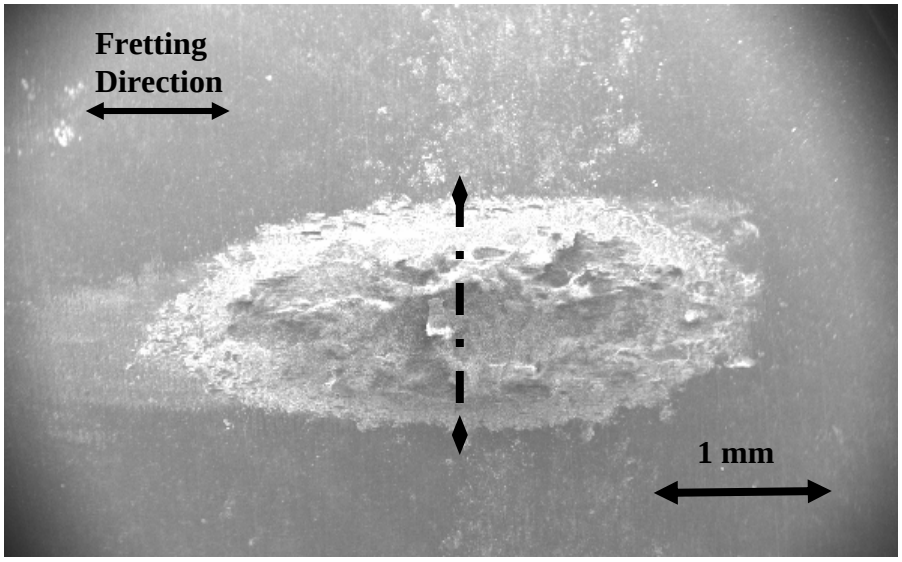

Fig. 4.7. SEM image of an ellipsoid wear scar. The dashed line indicates the orientation of the cross-sections to the fretting wear scars.

The microscopy showed that the titanium surface, worn against these coatings at room temperature, experienced galling and surface plasticity which over time caused cracks and fractures of the surface, as shown in Fig 4.8. Some of these particles were on the order of 20-50μm in size. During the beginning of the fretting test these fractured particles were released into the contact and got broken up and eventually oxidized. Some of these particles were found imbedded in the coating surface. While this occurred, the roughened Ti6Al4V surface and third bodies damaged the coating and created Al-bronze debris in the contact. Evidence of the Al-bronze debris mixed with broken up Ti6Al4V particles can be seen pressed into the worn ellipsoid surface in Fig 4.9. As the tests progressed the fine Al-bronze and Ti6Al4V debris filled in the worn craters on the ellipsoid surface, as shown in Fig 4.10. In some cases this compacted transfer layer covered over large fractured Ti6Al4V particles and trapped them underneath. Evidence of this phenomenon is also shown in Fig 4.10.

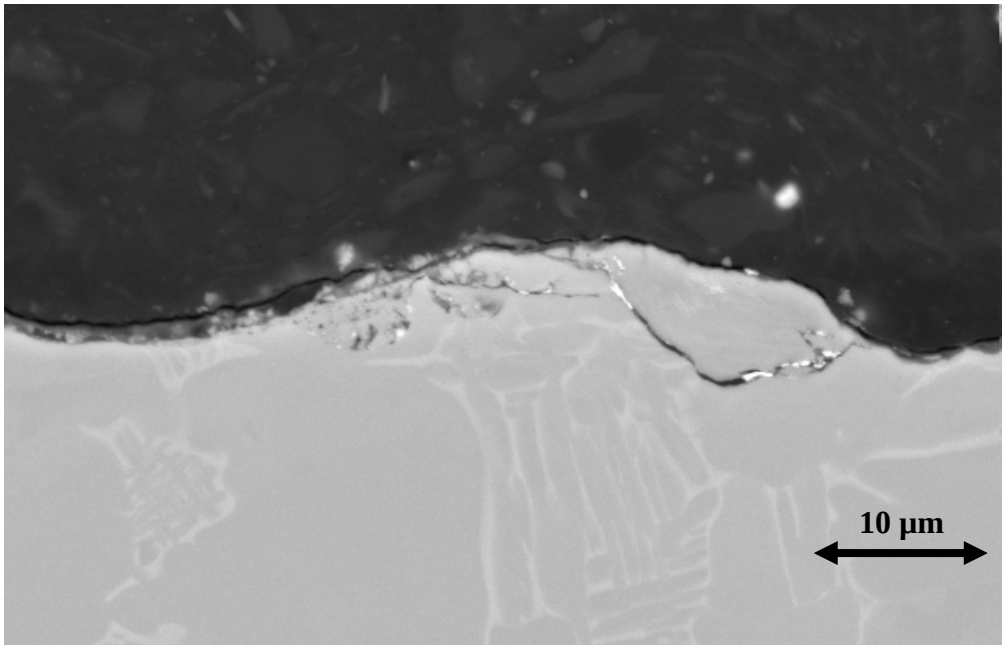

Fig. 4.8. SEM image of the fractured surface of a Ti6Al4V ellipsoid worn against coating 3 at RT.

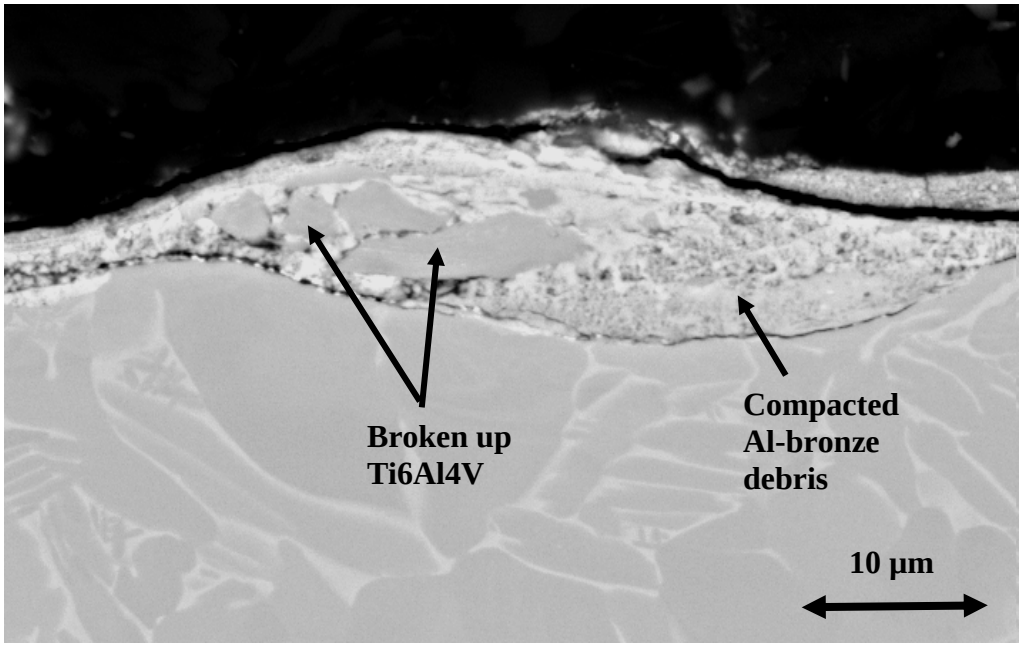

Fig. 4.9. SEM image of the surface of a Ti6Al4V ellipsoid worn against coating 1 at RT.

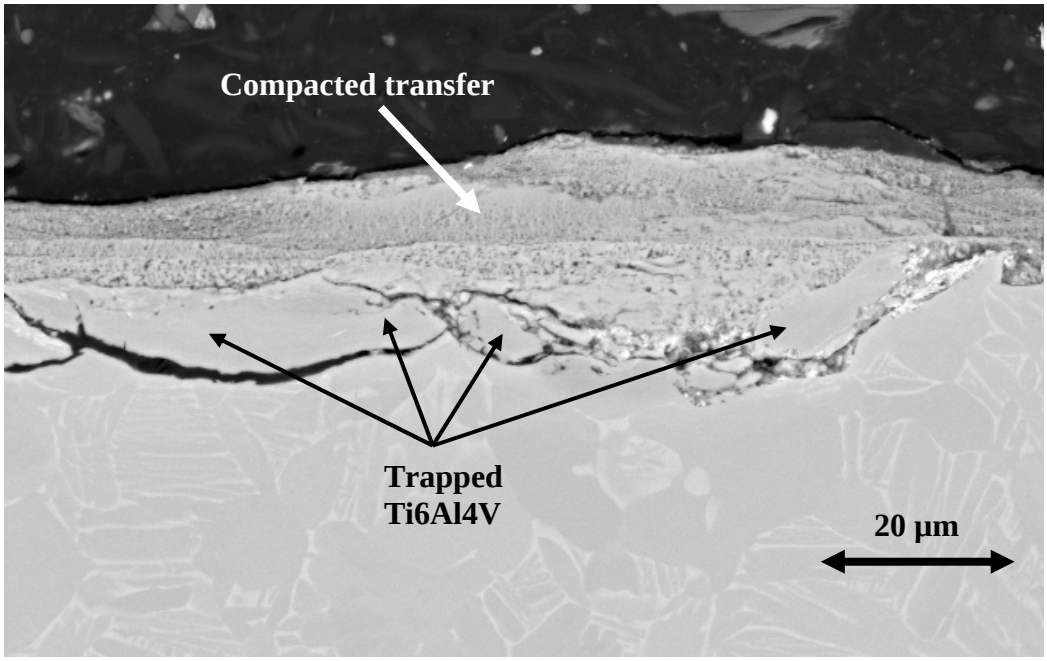

Fig. 4.10. SEM image of the surface of a Ti6Al4V ellipsoid worn against coating 3 at RT.

As expected at the room temperature, the Ti6Al4V surfaces worn against coating 3 exhibited the most damage, while coating 2 caused the least damage. Both coating 1 and coating 3 had higher friction and the mated ellipsoid surfaces had the most large fracture particles and craters evident. Coating 2 caused some initial damage, but had the thickest layer of transferred coating debris. This debris was then covered with a transfer layer of the Al-bronze coating, shown in Fig 4.11. The transfer layer helped to reduce the friction and the damage to the ellipsoid surface.

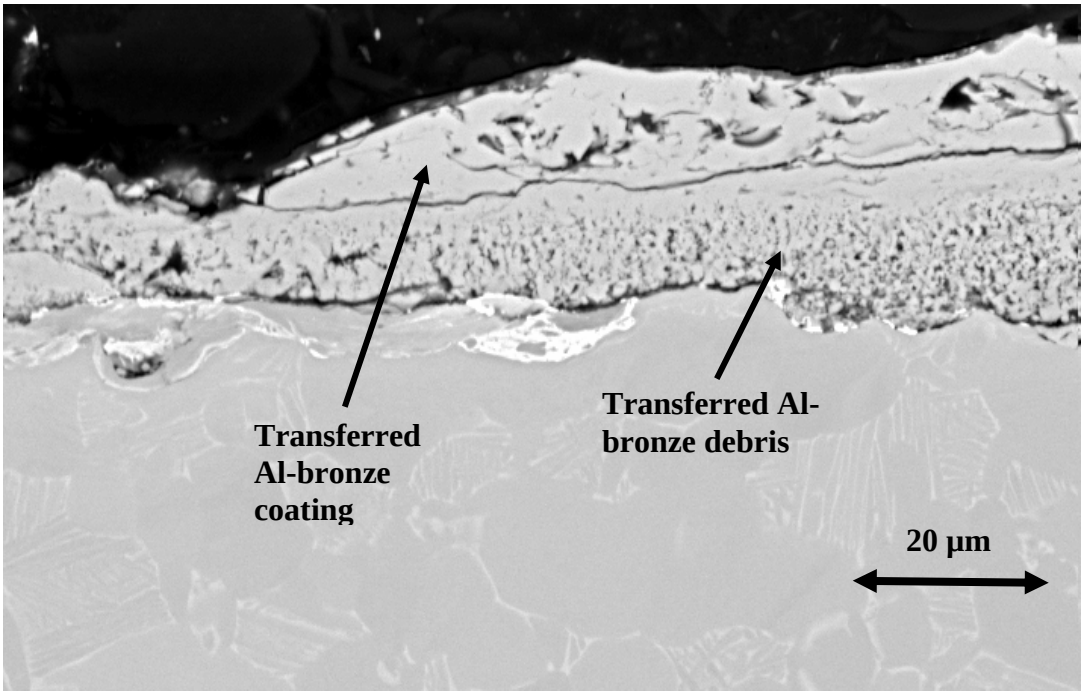

Fig. 4.11. SEM image of the surface of a Ti6Al4V ellipsoid worn against coating 2 at RT.

At 163°C the surfaces of all the ellipsoids exhibited a reduction in wear, in comparison to the room temperature experiments. At this temperature all of the wear mechanisms were the same as at room temperature. However, all the ellipsoid surfaces had much less cracking, fracturing, and crater formation. The craters and particles were also much smaller and shallower. In addition, the coating transfer to the Ti6Al4V surfaces was significantly reduced, except in the surfaces worn against coating 2.

At 450°C the wear mechanisms detected on coatings 1 and 3 changed, while the mechanisms remained unchanged on coating 2. Fig 4.12 shows the typical cross-section of an ellipsoid worn against coating 2 at 450°C. This micrograph shows fractured Ti6Al4V surface particles, worn titanium rich material that has adhered to the ellipsoid surface, and transferred Al-bronze. These are all characteristics that were detected in the ellipsoid wear

scars at the cooler test temperatures. However, at 450°C the damage was significantly more severe. This is most likely due to the sharp increase in friction as the ellipsoids were worn against coating 2 at this temperature. Coating 1 caused the least amount of damage to the surface of the mating ellipsoid. Fig 4.13 shows that at this temperature coating 1 caused some galling, but mostly formed a thin layer of transferred Al-bronze. From the previous section, it is known that coating 3 failed at 450°C and the coating was completely worn through in the contact region. Fig 4.14 shows the typical damage that this failure imposed on the ellipsoid contact surfaces. It can be clearly seen that the worn coating adhered to the uncoated ellipsoid counter surface. However, the worn Al-bronze that adhered to the ellipsoid eventually started to gall severely against the Ti6Al4V substrate that has emerged from underneath the coating. This formed a thick layer of titanium on top of the transferred coating layer, as shown in Fig 4.14.

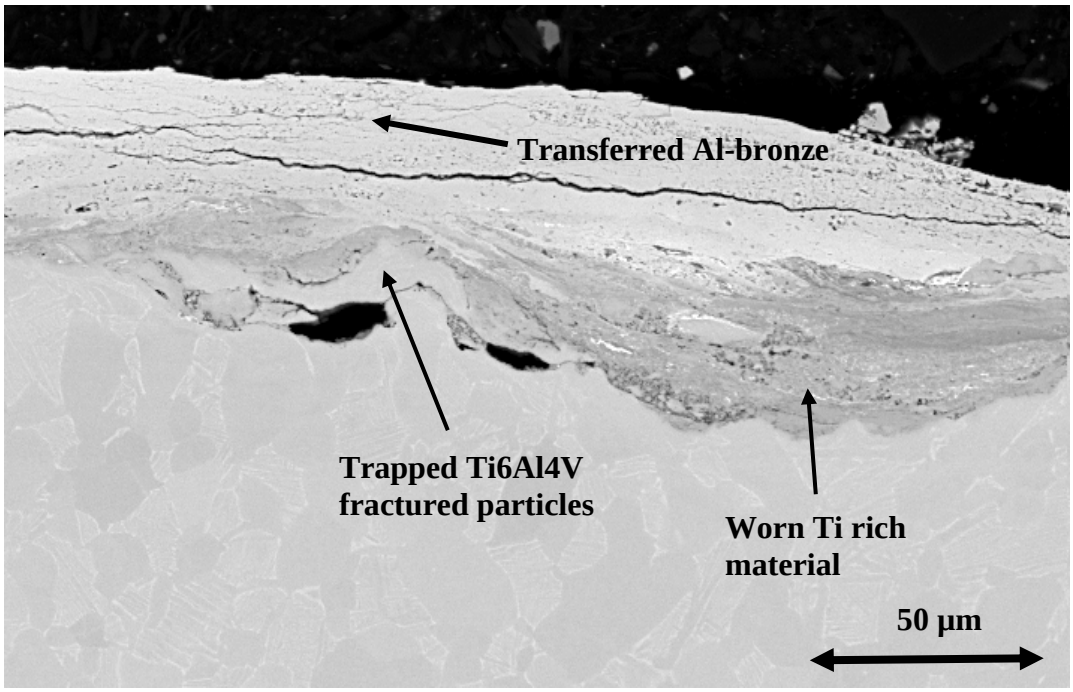

Fig. 4.12. SEM image of the surface of a Ti6Al4V ellipsoid worn against coating 2 at 450°C.

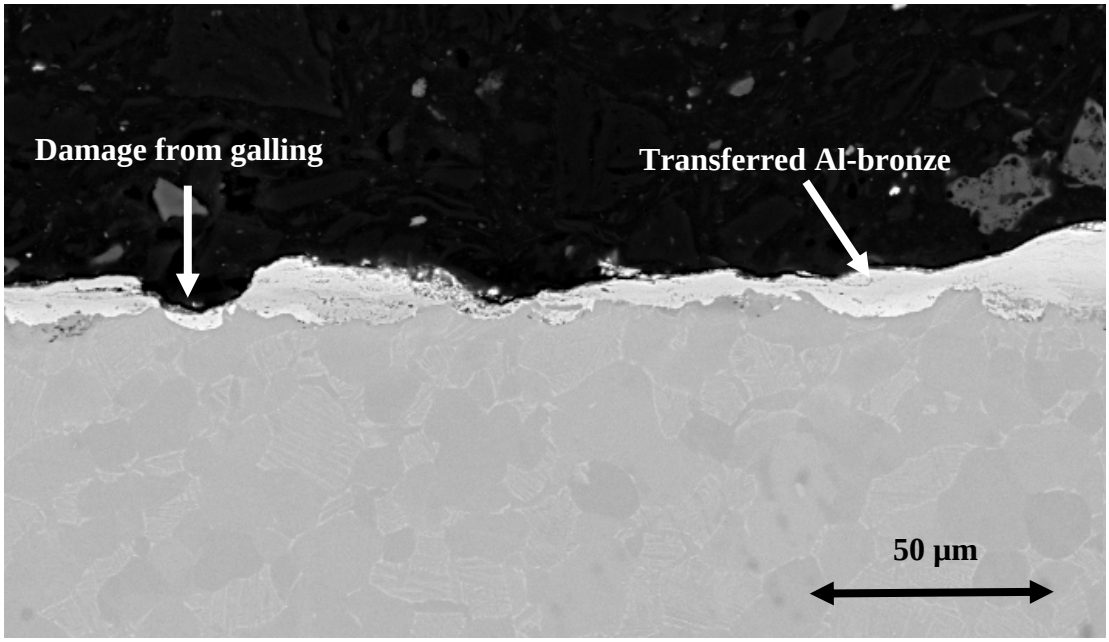

Fig. 4.13. SEM image of the surface of a Ti6Al4V ellipsoid worn against coating 1 at 450°C.

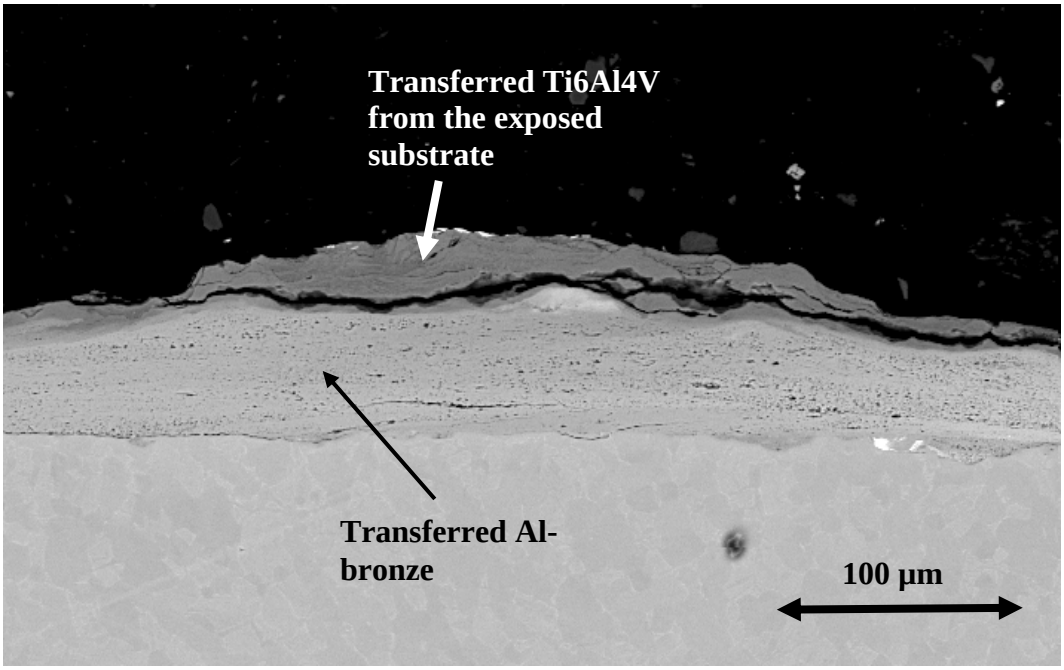

Fig. 4.14. SEM image of the surface of a Ti6Al4V ellipsoid worn against coating 3 at 450°C.

4.5 Summary and Conclusions

In overview, the tests conducted in this work were designed to evaluate the performance of three different Al-bronze coatings, and the damage mechanisms associated with the degradation of the mated Ti6Al4V surfaces, under gross slip fretting conditions at room temperature, 163°C, and 450°C.

At room temperature the performance of the two plasma sprayed coatings indicated that the aluminum content in the applied coating and wear track enhanced the performance of the coating. This is attributed to the good performance of coating 2 and the poor performance of coating 1, which had virtually all copper in the wear track. At this temperature it was also found that the cathodic arc coatings did not perform as well as the plasma sprayed coatings, even though there were increased levels of aluminum detected in the wear track after the test. This is believed to be attributed to the lack of available oxide within the coating, in comparison to the plasma sprayed coatings. The mated ellipsoid surfaces were all damaged significantly during the room temperature tests, and the wear scars all exhibited similar wear characteristics. All of the coatings had formed transfer layers on the ellipsoid surfaces, but the adhered material just seemed to mask the damage underneath. Each of the wear scars had medium to large craters that formed when particles fractured off of the surfaces of the ellipsoids.

The phenomenon of large particle detachment has been widely researched [9,12-14,17,18,31,65-68]. All of the explanations are derived from the formation of a highly plastically deformed layer near the surface that forms with a fine microstructure, and in the case of Ti6Al4V is always measured to be harder and more brittle than the bulk material. Once the accumulation of strain or stress reaches a critical level cracks form. Depending

on the material, contact geometry and loading conditions, these cracks can form at the surface or just below the surface. Over time these cracks propagate relieving the built up stresses and releasing pieces of the surface into the contact.

At 163°C the friction and wear on all of the coatings was very similar. This was due to the fact that all three coatings formed a transfer layer, with the same chemistry, on uncoated ellipsoid surface. In addition, all three coatings also exhibited the lowest coefficient of friction at this temperature. This suggests that there is an optimal chemistry and temperature in which these coatings perform the best. In this study that was at approximately 163°C with a Cu/Al ratio of 5/1 in atomic percent in the wear track.

At 450°C the performance of the two plasma sprayed coatings indicated that more aluminum within the interface was a performance inhibitor at this temperature. Coating 1, which was almost all copper in the wear track after the fretting tests, exhibited the lowest friction, the least amount of coating wear, and the least damage on the mated Ti6Al4V ellipsoid. Coating 2, which had significantly more aluminum in the wear track, exhibited very high friction and severe damage to the mated surface. In addition, the fretting wear experiments at this temperature wore completely through coating 3. The coating failure was due to the combination of increased friction, wear rate, and the impact of increased temperature on the cohesion between the two layers in which the coating was applied to get the desired 100 μm thickness.

Chapter 5

LITERATURE REVIEW AND NICKEL BASED COATINGS RESEARCH SCOPE

Nickel and nickel based surfaces are of interest as a replacement for the current CuNiIn and Al-Bronze coatings used for fretting wear mitigation at titanium alloy aerospace component interfaces. Nickel was considered as a candidate material, due to the lubricious oxides that nickel and nickel alloys produce at elevated temperatures. This chapter outlines the reviewed body of literature grouped under 4 major categories: wear of nickel based alloys, wear of pure nickel, wear of nickel and/or nickel oxide based surfaces, and XPS surface chemistry of nickel oxides. The literature in each of these categories will be chronologically summarized herein.

5.1 Wear of Nickel Based Alloys

In depth tribological studies on nickel based alloys began in the early 1970's with high temperature pin on disk and reciprocating wear tests on Nimonic 75, Nimonic C263, Nimonic 108, and Incoloy 901, compositions are shown in Table 5.1. In 1972 Earles et al. conducted experiments on Nimonic 75 as well as two steel alloys [69]. In their studies it was shown that the wear rates of the tested materials increased with elevated temperature (up to 300°C) and sliding speed (up to 100 m/s), using pin on disk experiments. Then in 1973, Stott et al. and Lin et al. published papers based on the formation of 'Glaze' oxide layers on nickel base alloys at high temperatures and the wear behavior of nickel based alloys at room temperatures, respectively [23, 24]. Stott and his colleagues conducted reciprocating wear experiments at temperatures in excess of 800°C on all of the materials listed in Table 5.1. This was the first study that attempted to characterize the formation of a glaze layer on nickel alloys during high temperature sliding. Prior to this work, it was

known that there is a dramatic reduction in the friction and wear of nickel base alloys at high temperatures, between 600 and 800°C [70]. However, there isn't any evidence that the surfaces had been characterized as to what surface chemistry or material properties caused the phenomenon. Using scanning electron microscopy (SEM) and electron diffraction analysis of the worn surfaces, Stott et al described the morphology and surface chemistry of the wear scars from their experiments. At temperatures from 150°C up to 400°C, the glaze layers formed on all of the samples contained simple nickel, cobalt and iron oxides (NiO, CoO, FeO, or Fe_2O_3) based on the alloy composition. At higher temperatures all of the surfaces exhibited evidence of chrome oxide (Cr_2O_3) and/or a complex oxide described as $NiCr_2O_4$. Stott et al. believed that the glaze layers of these compositions reduced the friction and wear of these materials at elevated temperatures. In addition, a follow up study by Lin et al showed that at room temperature the oxide films formed on the contact areas had no significant effect on the interfacial wear behavior of the very same alloys [24].

Alloy	C	Si	Cu	Fe	Mn	Cr	Ti	Al	Co	Mo	B	Zr	Pb	S	Ni
Nimonic 75	0.08 0.15	1.0 max	0.5 max	5.0 max	1.0 max	18.0 21.0	0.2 0.6								bal
Nimonic C263	0.03	0.25	0.20 max	0.75 max	0.4	20.0	2.15	0.45	20.0	5.9	0.001 max	0.02 max		0.007 max	bal
Nimonic 108	0.20 max	1.0 max	0.5 max	2.0 max	1.0 max	13.5 15.75	0.9 1.5	4.5 4.9	18.0 22.0	4.5 5.5			0.005 max		bal
Incoloy 901	0.1 max	0.6 max	0.5 max	bal	2.0 max	11.0 14.0	2.35 3.00	0.35 max		7.0 5.0	0.01 0.02				40.0 45.0

Table 5.1. Composition of nickel based alloys in weight % from Stott et al [23].

In 1976, Stott et al. studied the effect of temperature on the tribological behavior of binary Ni-Cr alloys [25]. Once again reciprocating wear experiments were conducted at temperatures ranging from ambient up to 800°C. In addition, the Ni-Cr alloy compositions were varied from 0% to 40% Cr. In this study it was found that the glaze layers formed on

the wear surfaces at elevated temperatures of the 5% to 40% Cr alloys had similar morphology and chemistry as compared to the wear surfaces of the Nimonic alloy experiments conducted in the 1973 publication. Stott et al. believed that this correlation indicated that the trace elements in the Nimonic alloys play a very minor role in the wear behavior and glaze formation of the aforementioned nickel based alloys.

Stott et al followed the conclusion of their Ni-Cr alloy work with a 1978 short analysis or review paper on "The influence of oxides on the friction and wear of alloys" [26]. This publication outlined the current understandings of metal oxide formation. It began with extensive explanations of oxide growth in the absence of sliding, through transient and steady state oxidation. Then it discussed the effects of reduced oxygen pressures, or vacuum, and the effects of elevated temperatures on the wear of iron and nickel based alloys. In this publication, Stott et al. concluded that glaze layers consist of fine crystalline oxide particles that compacted or compressed into a continuous oxide layer during interfacial sliding at elevated temperatures. They went further to state that there is nothing unusual about the composition of glazes, since they can be formed from most oxides or other crystalline materials.

In 1981, Hamdy and Waterhouse began studying high temperature fretting wear of titanium alloy Ti6Al4V, nickel alloy Inconel 718, and austenitic stainless steel type 321 [71, 72]. The composition of Inconel 718 is approximately 53% Ni, 19% Cr, 17% Fe, 5% Nb, 3% Mo, 1% Co, and 1% Ti (with all other constituents less than 1%). In these two studies it was once again determined that elevated temperatures, in excess of 300°C or 500°C, lead to the formation of a glaze layer on all three materials. The glaze layers formed were determined to be a compaction of surface oxides; however, Hamdy and

Waterhouse did not conduct any chemical analysis of their wear surfaces. They attributed all of the surface chemistry to work by Hurricks [73] on the fretting wear of mild steel at high temperature and the aforementioned body of work by Stott et al.

In 1985, Iwabuchi conducted high temperature fretting wear experiments on Inconel 625 in air and in vacuum [74]. Inconel 625 is composed of approximately 61.5% Ni, 20.9% Cr, 9% Mo, and 3.6% Fe (with all other constituents less than 1%). In these fretting wear experiments, Iwabuchi found that in vacuum the interfacial wear mechanisms were governed solely by high friction and adhesive wear. This produced wear that was more severe at higher temperatures. However, the coefficient of friction was unaffected by temperature in vacuum. In atmosphere, fretting wear experiments conducted at temperatures in excess of 300°C produced a glaze surface layer that reduced friction and wear. Just as Hamby and Waterhouse, Iwabuchi did not conduct any surface chemistry analysis on his wear tracks. Instead, he too attributed all of this explanation to the aforementioned work by Stott et al.

From the mid 1980's till the early 1990's the literature does not reflect any significant work in the high temperature wear of nickel based alloys. This is likely because the authors (such as Stott et al.) that had built the current understanding of glaze oxide formation on nickel alloys had refocused most of their work and publications on the glaze layers formed on Fe based alloys and/or Fe-Cr based alloys.

In 1994, Jiang et al. published a study on the sliding wear of nickel based alloy Nimonic 80A at temperatures up to 250°C [75]. Nimonic 80A is composed of approximately 68% Ni, 21% Cr, 3% Fe, 2.7% Ti, 1.8% Al, 1% Si, 1% Co, and 1% Mn

(with all other constituents less than 1%). In these experiments, Jiang et al. measured friction and contact resistance at the interface. At all temperatures they found that the contact resistance quickly increased from almost zero initially up to positive values throughout all of the tests. This was attributed to the formation of oxides that separated the nascent metallic surfaces. At room temperature, the wear track was filled with loose compacted debris. At 250°C, the wear track had formed a smooth glaze layer that was continuous throughout the entire contact area. However, the wear track exhibited an intermediate structure at 150°C. The wear track had some localized regions that appeared to form a glaze layer, while other localized regions had loose debris compressed into the voids of the surface. This surface structure caused a reduction in friction coefficient when the experiments were heated to 150°C. However, the friction at 250°C, where a continuous glaze layer had formed, did not change much from the values measured at 150°C. The composition of the glaze layer and debris in this study was determined to be NiO, with the use of wavelength-dispersive x-ray microanalysis of the wear tracks and x-ray diffraction of the loose wear debris that was collected. In addition to the data presented, Jiang et al. developed a model in which they believed that a phenomenon called tribo-sintering lead to the development of the lubricious glaze layers. They believed that the pressure and temperature at the contact actually sintered the produced oxide debris, seen at lower temperatures, into a solid oxide layer or glaze.

Jiang et al. followed up their model for tribo-sintering with the development of a mathematical model for the prediction of sliding wear of metals at elevated temperatures [76]. This model was developed based on the theory that a certain distribution of small wear debris would be trapped within the contact, during the friction and wear process.

The agglomeration of the smaller debris particles would inhibit the wear of the metallic contacts. In addition, an increase in temperature would increase the probability and/or distribution of the particles that would sinter together into a protective glaze layer. This model proved an important point, that the size of the active wear particles and the sintering properties of the trapped media do have a significant impact on the reduction of wear at the metallic interface. However, the model only seemed to mimic the performance of nickel alloy N75, not N108 or Nimonic 80A. Therefore, the model is only fitting one data set, not adequately predicting the outcome of the other materials tested.

In 1995, Ikeno et al. studied the wear properties of nickel alloys and oxide dispersed nickel alloys at room temperature [77]. This study concluded that the addition of small amounts of fine alumina to the nickel matrix deteriorated the wear properties of the nickel at room temperature. Ikeno et al attributed this to the wettability of the alumina particles with the nickel matrix. The alumina particles lead to the development of dislocation tangles that were formed by cross-slip or climb dislocation interactions. These tangles then grew into cell structures, which ultimately lead to the enhanced formation of wear particles. In contrast, the nickel based alloy MA6000 had yttoria particles which prevented the cross-slip or climb dislocations at the particle locations. This prevented the formation of cell structures and reduced wear particle formations, therefore, enhancing the wear performance of MA6000.

In 1997, Chaudhuri et al. studied the correlation of deformation and sliding wear resistance of Ni-Co and Ni-Cu single phase solid solution alloys with their stacking fault

energy (SFE) [78]. The wear experiments were conducted by reciprocating wear tests of diamond balls against the selected alloys in ambient air. The Ni-Co alloys tested had a composition that varied from 10% to 60% cobalt. The Ni-Cu alloys had a varied composition of 10%, 48%, and 90% copper. Upon the conclusion of these wear experiments, Chaudhuri et al. conducted x-ray photoelectric spectroscopy (XPS) on the wear scars and wear debris. They found that all of the wear tracks and debris from all of the materials tested had significant amounts of Ni_2O_3. In fact, all of the wear products had equal amounts or more Ni_2O_3 than NiO. This is significant, because this is the first time that Ni_2O_3 within the wear track of worn nickel alloy surfaces at low temperatures is mentioned in the literature. However, Chaudhuri et al. did not comment on the significance of the formation of Ni_2O_3. They just presented it within the XPS surface chemistry analysis, and concluded that stacking fault energy plays a significant role in the wear resistance of Ni-Co and Ni-Cu alloys. They also concluded that Ni-Cu alloys containing more than 50% Cu formed a soft thick Cu_2O layer that acted as a lubricant and minimized friction and wear.

In 1997, Jiang et al. published a paper based on the effects of partial pressure of oxygen on the wear of nickel alloy Nimonic 80A [79]. In this work pin on disk reciprocating wear tests were conducted under a controlled oxygen/argon environment. Experiments were conducted at temperatures up to 600°C. The authors found that the variations in friction and wear were controlled solely by the temperature of the tests, as long as the partial pressure of oxygen was greater than or equal to 0.1 atm.

In 1998, Jiang et al. wrote a follow up paper to the work that they published in

1997 on wear testing of Nimonic 80A [80]. In this work, they conducted experiments at room temperature, 150°C, and 250°C. They also conducted experiments that started at 20°C and were increased up to 250°C after a sample wear in time, and tests that started at 250°C and were decreased to 20°C after a wear in time. Interestingly, the experiments that were started at low temperature and increased up to 250°C did not exhibit a glaze layer after the test. This showed that the oxidized wear particles do not form together to make the glaze layer. In addition, the tests that were started at high temperature and reduced to 20°C exhibited a mixed surface structure that had some glaze layer apparent as well as some compacted debris. This showed that the glaze layer is fairly robust and does not get worn away immediately at low temperature. The surface chemistry analysis in this work was some electron probe micro-analysis (EPMA), which was used to see where the oxygen was concentrated in the wear track, and some XRD of the wear debris, which showed a composition of mostly Ni with some NiO content. This paper also continues with the development of the theory of tribo-sintering, saying that the compacted wear debris with in the wear scars were sintered together. This theory is based on the fact that a large amount of the compacted surface debris appeared to be load bearing and wasn't easily removed from the worn surface. An ultrasonic cleaner was needed to release the wear particles from the wear track for analysis.

A second paper of significance in 1998 was published by Lawen et al. [81]. This paper provided a compilation of results from an extensive sliding wear study of 5 nickel based alloys, 4 cobalt based alloys, and 6 types of stainless steel that are commonly used in ground based gas turbines and aircraft engines. These materials were tested under reciprocating sliding wear conditions from temperatures of 290°C up to a maximum of

815°C. Various combinations of the alloys were worn against themselves and each other. The authors then measured the wear rates from all of these combinations. They concluded that the self mated cobalt based alloys gave the lowest wear, and a nickel alloy with 7% Cr, 6% Al, and 7.5% Co exhibited the lowest wear in the mixed alloy combinations.

In 1999, Berns et al. compared the wear rates of metal matrix composites made from a nickel based alloy using powder metallurgy [82]. These composites incorporated the use of WC/W_2C and Cr_3C_2 hard particles within the metal matrix for improved wear performance. The fabrication of these materials was followed by sliding abrasion experiments conducted against crushed flint (SiO_2), corundum (Al_2O_3), and silicon carbide (SiC) in a ring-on-disc device at temperatures ranging from ambient up to 900°C. In addition, each of the experiments was conducted in air and in argon. From these experiments, the authors concluded that above 600°C, in air, the oxidation of WC/W_2C rapidly increased with temperature in comparison to the Cr_3C_2 particles. The Cr_3C_2 had lower hardness, but higher resistance to oxidation. At high temperatures, the porous WC/W_2C oxides did not provide any abrasion resistance. In addition, it was found that a self-protecting particle layer consisting of debris and small abrasive particles formed at the interface during sliding abrasion. At 800°C in air, the debris layer oxidized and formed a glaze layer of high density. X-ray diffraction of the built up layer determined its composition to be NiO, $NiWO_4$, WO_3, $CrWO_4$, and Cr_2O_3.

In 2001, Kim et al. conducted block on block type reciprocating sliding wear tests on Ni-base Deloro 50 hard-facing alloy [83]. These experiments were conducted with

contact stresses ranging from 55 to 207 MPa and with temperatures ranging from ambient up to 350°C. From these experiments, Kim et al. found that at low temperatures the Deloro 50 exhibited severe adhesive wear. However, at temperatures above 100°C the wear mode changed and the wear rate decreased significantly. This wear transition was attributed to the formation of protective oxide layers within the wear track. This conclusion was based on some wavelength dispersive spectroscopy analysis of the wear tracks. In addition, the authors found that wear transition temperature increased as they increased the contact stress during the wear experiments. This phenomenon was attributed to the need for more active oxide debris/particles within the wear track under higher contact stress.

In 2002, Xu et al. characterized the wear of the wheel/work piece interface during the grinding of the nickel based superalloy K417, using an SEM and XPS [84]. The interfacial temperature and loads during the grinding process are measured using a grindable foil-work piece thermocouple and a dynamometer. At grinding temperatures above 990°C, the surface of the nickel alloy turned color and adhesion started to occur between the abrasive grits and the alloy surface. This interfacial adhesion created a severely deformed surface with high roughness. XPS of these ground surfaces yielded a chemical composition of Ni_2O_3, Cr_2O_3, Al_2O_3, and TiO_2. The formation of Ni_2O_3 at temperatures above 990°C is very unusual and the authors do not offer an explanation of this phenomenon. They just state that NiO and/or $NiCrO_4$ are the oxidative states that are for the static oxidation of K417 at 900°C.

In 2002, Stott also published a second paper based on the wear model that was

published by Jiang et al. in 1995 [85,76]. This paper used only the Nimonic 80A to demonstrate the accuracy of the model. Unfortunately, there is no clear evidence that this journal article further enhances the model as compared to the previously published work.

In 2003, Inman et al. analyzed the glaze layers formed during high temperature sliding of Stellite 6 (a cobalt based alloy) and Nimonic 80A (a nickel based alloy) at 750°C [86]. Energy dispersive spectroscopy confirmed that the glaze layers had a composition of 34.2% Co, 36.2% Cr, 16.7% Ni, 3.8% Si, and 1.3% Fe (in at%), with the dominant phases identified as $CoCr_2O_4$ and $Ni_{2.9}Cr_{0.7}Fe_{0.36}$ (by x-ray diffraction). Transmission electron microscopy (TEM) and scanning tunneling microscopy (STM) were used to determine that the grain sizes of the glaze layers varied from 5 to 10nm, and the thickness of the grains were approximately 10nm. From all these analyses, the authors hypothesized that the process for glaze layer formation involved: (1) deformation of the alloy surface, (2) the intermixing of debris from both of the mated surfaces, (3) oxidation, (4) further mixing, (5) repeated welding and fracture. They added that these processes were then aided by high temperature oxidation and diffusion. In addition, they concluded that a process called “fragmentation” was responsible for the formation of the nano-structured grains. Fragmentation involved material deformation, the generation of dislocations, and the formation of sub-grains. This structure was then continuously refined, which increased misorientation.

In 2004, Xie et al. characterized the microstructure and wear performance of Ni-20 wt% Pb hypomonotectic alloys [87]. Xei et al. found that the undercooling temperature, by which the alloy is fabricated, controls the microstructure of the alloy. At

low undercooling temperatures (85K), the structure was defined by large clumps of Pb rich material surrounded by nickel rich dendrites. At higher undercooling temperatures (390K), the structure was defined by anomalous grains and fine Pb particles. Reciprocating sliding wear tests were conducted on these various microstructures at different load conditions and sliding speeds, against GCr15 steel. It was found that at all of the test conditions, the 390K undercooled samples exhibited the lowest wear rate. The second best was always the 85K undercooled samples, with all of the rest yielding higher wear rates. XPS of the wear scars found the presence of a lubricious Ni_2O_3 and lead oxide layer. The amount of lead oxide within this layer was believed to control the wear reduction between of Ni-20Pb alloy surfaces. In this work it is significant that once again the use of XPS has revealed the presence of Ni_2O_3 in the wear track after room temperature tests were conducted.

In 2005, Inman et al. followed up their 2003 work by increasing the sliding speed from 0.314 m/s to 0.905 m/s, in Stellite 6 and Nimonic 80A mated contacts [88]. At the slower sliding speed, the authors found that a nano-structured glaze layer formed at the interface with a composition of $CoCr_2O_4$, NiO, and some Cr_2O_3. At 0.905 m/s sliding speed, there was no evidence of $CoCr_2O_4$. Inman et al. believed that the increased presence of Cr_2O_3, combined with the absence of $CoCr_2O_4$, resulted in a loose oxide that increased wear at the interface through abrasion. Since it was known that NiO could form a glaze layer by itself and with $CoCr_2O_4$, the authors believed that the increased presence of Cr_2O_3 prevented the sintering formation of a glaze layer. EDS, XRD, and STM were used to analyze the chemistry of the worn interfaces.

In 2006, Inman et al. wrote a follow on publication to their 2005 work by studying Stellite 6 mated with Incoloy MA956 with the same experimental test conditions [89]. Incoloy is an iron chrome alloy, instead of a nickel based alloy. At low temperatures and 0.314 m/s sliding speed, the wear mechanisms were similar to that of the Stellite 6 and Nimonic 80A. Up to 450°C the interface was filled with loose Co-Cr based wear debris which separated the surfaces and caused mild wear. Between 510°C and 750°C, the chemistry of the wear debris did not change. However, the wear debris began to sinter together and form a protective glaze layer. At 0.905 m/s sliding speed, mild wear with loose Co-Cr based wear debris governed the wear up to 270°C. Between 390°C and 450°C, the absence of oxide debris allowed the nascent metallic surfaces to come in contact and caused severe adhesive wear. This severe wear regime was also observed from 510°C up to 630°C. Above 630°C, a glaze layer of Fe-Cr composition began to form. This protective layer reduced the friction and wear up to 750°C. This is different from the Nimonic 80A, which formed abrasive Ni-Cr based oxides at these temperatures.

In addition to Inman et al's continuance publication, Hejwowski studied the impact sliding and pure sliding wear of Fe, Co, and Ni base alloys at ambient and 600°C [90]. The Co based alloys performed best in the impact sliding tests, and the Ni based alloys performed best in the pure sliding tests. The Fe alloys were the worst materials in both sets of experiments. EDS of the wear tracks showed the presence of adhesive wear and material transfer after the low temperature experiments, and oxide formation after the high temperature experiments. The oxide layers were believed to prevent direct metal to

metal contact, and prevent interfacial adhesion and material transfer at high temperatures.

5.2 Wear of Pure Nickel

In 1964, Alison and Wilman studied the difference in wear behavior of hexagonal (Cd, Mg, Zn, Zr, Ti) and cubic (Pb, Ca, Al, Cu, Pt, Fe, Ni, Mo, Cr) metals [91]. The authors discovered that for a given hardness, the volumetric wear rate for the hexagonal metal was approximately half the wear rate of the cubic metals. This is believed to be directly related to the ease of slip, the number of slip systems, and their orientation. The hexagonal metals can displace a larger portion of material by plastic flow (slip) from the groove along a single slip plane. The cubic materials require multiple slip planes to move the same amount of material and often experience work hardening, which often leads to the removal of material instead of deformation. In addition, Alison and Wilman found that the coefficient of friction of cubic metals decreased with increasing hardness. This is in contrast to the hexagonal metals which had a virtually constant coefficient independent of hardness.

In 1985, Goto and Buckley studied the influence of water vapor on the coefficient of friction between pure Fe, Al, Cu, Ag, Cr, Ti, and Ni, during fretting wear experiments [92]. For this work, fretting wear experiments were conducted at room temperature with relative humidity that ranged from 0 to 50%. At very low humidity, up to about 2%, the Ni mated samples exhibited very high friction and high wear. From 2% to 5% there was a sharp decrease in coefficient of friction and wear. As the relative humidity was increased, the coefficient of friction decreased at a slow linear rate. The wear also decreased at a high rate until it reached a minimum at approximately 15%. Then the

wear increased at a high rate with higher humidity. The authors did not study the surface chemistry, or elaborate as to why there was minimum wear at 15% relative humidity.

In 1992, Takadoum and Roques-Carmes studied the room temperature sliding wear and friction of Al_2O_3 against polycrystalline Al, Ti, Ni, and Cu [93]. From these experiments, the authors found that the coefficient of friction of these metals were ranked from lowest to highest as Cu, Ni, Ti, and Al. Electron microprobe analysis of the Al_2O_3 counter-surface revealed large amounts of Al and Ti transfer, with little transfer of Ni and no transfer of Cu. The transfer of the Al and Ti to the Al_2O_3 surface indicates that the bonds between the metal and ceramic surfaces are stronger than the cohesive bonds within the metals themselves. This phenomenon was attributed to the affinity for oxygen of the metallic surfaces. Metals, such as Ti and Al, that have a high affinity for oxygen form interfacial oxides through which the metal adheres to the Al_2O_3. In order to prove this claim, the author reduced the affinity for oxygen of the Ni surface by ion implantation of boron. This slightly lowered the friction coefficient of the Ni surfaces. However, it may have formed an amorphous Ni_3B, on the surface, which may also have contributed to the reduction in friction.

5.3 Wear of Nickel and/or Nickel Oxide Based Surfaces

In 1974, Moore and Flitter evaluated the friction and wear properties of NiO/CaF_2 and NiO/SrF_2 plasma sprayed coatings on Incomel 601 substrates at elevated temperatures [94]. The counter-surface for these experiments was a lithia alumina silicate ceramic. In this study, the authors varied the amount of CaF_2 from 0 to 40%. The increased amount of CaF_2 decreased the coefficient of friction from approximately

0.5 down to approximately 0.28 for the 40% mixture, for tests at 760°C. Although the friction coefficient was reduced, the wear rate of the coating increased substantially. Therefore, it was found that the optimum mixture was 85% NiO and 15% CaF_2. Then the lubricant additive was changed to 20% and 15% SrF_2, instead of CaF_2. The substitution SrF_2 for CaF_2 gave no improvement in wear and friction behavior of the coatings at 760°C. Therefore, the authors decided to test both mixtures at 590°C. At lower temperature, both coatings exhibited a reduction in friction coefficient from approximately 0.5 at 760°C to approximately 0.3 at 590°C. However, the coatings containing SrF_2 exhibited a significantly higher wear rate at 590°C.

In 1985, Harris et al. studied the fretting wear performance of arc sprayed chrome steels, arc sprayed Ni-Al-Mn, and electroless nickel containing 11% phosphorous [95]. At 475°C, the arc sprayed chrome steels exhibited the formation of a glaze layer that reduced the friction and wear of the coatings. The Ni-Al-Mn coatings did not form a wear protective glaze until 700°C. However, a composite arc sprayed coating was made that mixed the chrome steel and the Ni-Al-Mn and formed a wear protective glaze layer at 475°C. The composite coatings exhibited the good friction and wear performance of the chrome steel at temperatures lower than 475°C, and exhibited the performance of the Ni-Al-Mn at high temperature. The electroless nickel coatings exhibited high friction and poor wear performance at 350°C. However, at 600°C the friction and wear were reduced by the formation of a glaze layer. The authors believed that this improved performance at 600°C was caused by phosphorous pentoxide formation and sublimation, which allowed for nickel oxide to form in the wear track.

In 1987, Lankford et al. studied the sliding friction coefficients and wear rates of carbide, oxide, and nitride materials for use as sliding seals in diesel engines [96]. From all of the various ceramic combinations tested, the lowest coefficient of friction that was attained in diesel exhaust was 0.24. This was attained at 800°C with TiC-Ni-Mo against silicon nitride (Si_3N_4). However, this wear couple had a coefficient of friction of 0.75 at room temperature. In addition to the testing of standard ceramic materials, the authors modified the surfaces of silicon nitride and partially stabilized zirconia (PSZ) by ion mixing with TiNi, Ni, Co, and Cr. Ion mixing is a technique that involved the vapor deposition of a thin metallic layer on the surface of the ceramic, followed by the bombardment of argon ions. The ion bombardment drives the deposited metal atoms into the ceramic substrate surface. In the case of the TiNi implant, a layer of nickel was deposited, followed by a layer of titanium. Then, both layers were simultaneously mixed. After testing again at 800°C, it was found that Cr ion mixing was not beneficial to friction and wear reduction. However, the ion mixing of TiNi and Co into a zirconia surface worn against TiC-Ni-Mo yielded a friction coefficient of 0.09 and 0.06 respectively. In addition, TiC worn against Si_3N_4 implanted with TiNi exhibited a friction coefficient of 0.09. When Si_3N_4 was implanted with just Ni, the same wear couple yielded a friction coefficient of 0.14. The low friction from the ion mixed surfaces was attributed to the formation of lubricious Ti and Ni oxides. However, the exact surface chemistry was not analyzed.

In addition to the work by Lankford et al. in 1987, Gawne and Ma conducted a study on the wear mechanisms of electroless nickel coatings containing 8.5% and 12% phosphorous [97]. The electroless nickel coatings, of both compositions, exhibited

severed adhesive wear against plain carbon steel. However, heat treatment of the coatings eliminated the adhesive wear by creating a Ni_3P surface layer that was incompatible with the steel interface. In addition, chrome plating of the steel counter-surface also alleviated the severe adhesive wear. However, the use of stainless steel did not mitigate the problem. This was due to the single phase microstructure and low durability of its surface oxide film.

In 1991, Ahmed et al. studied the room temperature wear resistance of plasma sprayed Ni-%5Al and tungsten carbide cobalt (WC-15%Co) coatings on mild steel, subjected to different aqueous environments [98]. Both coatings exhibited high wear resistance in various NaCl and sand containing solutions. The Ni-5%Al coatings exhibited enhanced wear performance after heat treatment at 900°C. The authors believed that the improved performance was due to the growth of NiO on the coating surfaces, although this theory was not confirmed by chemical analysis. In addition, the Ni-5%Al samples also exhibited better performance when they were aged for 4 hours at 700°C. From the literature, the authors believed that this was due to the precipitation hardening of the coatings.

In 1993, Sue and Chang conducted a short study of titanium nitride (TiN), zirconium nitride (ZrN), and chromium nitride (CrN) worn against the nickel alloy Inconel 718 at 500°C and 600°C [99]. At 500°C, the TiN and ZrN coatings exhibited a coefficient of friction of approximately 0.4. This was similar to that of the mated Inconel 718. However, CrN yielded a lower coefficient of friction of approximately 0.3. All of the coatings also caused significantly more wear to the Inconel counter-surface, than the

uncoated Inconel 718 samples. The total wear was ranked from highest to lowest as exhibited by the TiN, ZrN, and CrN coatings respectively. The ZrN and CrN coatings were both tested at 700°C, and both exhibited a friction coefficient of approximately 0.3. The CrN coating yielded very low wear to the Inconel 718 surface at 700°C. In fact, the wear was even lower than the wear exhibited by the baseline Inconel mated surfaces. The ZrN only experienced a slight reduction in wear at 700°C.

In 1999, Taylor et al. examined the friction and wear properties of sol-gel derived NiO, TiO_2, and SiO_2 based coatings [100]. From this study, the authors concluded that the best friction and wear performance came from the coatings that were derived from NiO and TiO_2. These coatings yielded low coefficient of friction values of approximately 0.2 at room temperature, and moderate coefficient of friction values of approximately 0.5 at 500°C. XRD analysis of the coated surfaces found the presence of nickel titanate ($NiTiO_3$) within all of the NiO and TiO_2 derived coatings. The authors believed that the nickel titanate may have enhanced the friction and wear performance of these coatings.

In 2000, Jun et al. studied the microstructure and wear properties of composite nickel and partially stabilized zirconia (Ni-PSZ) electro-formed coatings [101]. Optical and transmission electron microscopy (TEM), of the microstructure, showed that the electroformed coatings contained uniformly distributed PSZ particles within a Ni matrix. XPS analysis of the coatings showed the presence of $Ni(OH)_2$ within the deposited coatings. In addition, it was found that the amount of $Ni(OH)_2$ within the deposited coatings increased as the amount of PSZ within the Ni matrix was increased.

Reciprocating wear tests, with a GCr-15 steel counter-surface, were conducted to determine the wear rates of the as deposited coatings. The authors found that the addition of PSZ to the Ni matrix decreased the coating wear rate to a maximum at approximately 25% PSZ. At approximately 37.5% PSZ the integrity of the Ni matrix was compromised, and the coating exhibited a higher wear rate than the Ni matrix itself. The 37.5% PSZ were then vacuum annealed at 250°C, 500°C, 750°C, and 1000°C. As the annealing temperature was increased the wear rate of the 37.5% PSZ coating decreased. At 1000°C the wear performance of the 37.5% PSZ was lower than that of the best as deposited sample, approximately 25% PSZ. XPS analysis of the 1000°C annealed samples, showed that the $Ni(OH)_2$ had reduced to NiO and Ni_2O_3. The enhanced performance of the annealed coatings was then attributed to the process by which the formed NiO wetted the PSZ particles and increased the bond strength between the particles and the metal matrix.

In 2002, Taylor et al. characterized the frictional properties of a range of titanium and nickel oxide sol-gel derived coatings [102]. Coated samples were made of various ratios of TiO_2 and NiO, varying from 25% NiO to 75% NiO. 50/50 TiO_2 to NiO ratio samples were heated to temperatures ranging from 400°C to 1400°C, after the coatings had been cured. It was found that the samples heat treated above 600°C started to form significant amounts of nickel titanate ($NiTiO_3$), with more nickel titanate forming at higher temperatures. At 1400°C, the coating was virtually all nickel titanate, as confirmed by XRD. Although some $NiTiO_3$ was found within all of the constructed coating chemistries, the substrates used of for the reciprocating wear tests could not be heated to 1400°C. Therefore, the room temperature friction and wear tests were not conducted on pure $NiTiO_3$ films. The results from the friction and wear tests showed that

all of the coatings made exhibited friction coefficients below 0.45. The 50/50 composition coating yielded the highest friction, and the 75% TiO_2 coating yielded the lowest friction. With these findings the authors concluded that $NiTiO_3$ is a good solid lubricant that is stable over a wide temperature range, even though they did not test any pure $NiTiO_3$ films and the 75% TiO_2 coating had the lowest friction.

In 2004, Chao and Liang studied the microstructure and wear properties of TiO_2 doped nickel based laser-clad coatings [103]. These coatings were made by mixing a nickel G112 powder with TiO_2 powder, to make mixtures that ranged from 0 to 4 wt% TiO_2. G112 is a nickel alloy powder that contains 16.5% Cr, 14% Fe, 0.7% C, 4% B, and 3.5 % Si. The powder mixtures were then adhered to the substrate surfaces with cellulose acetate prior to the laser-clad process. Adding the TiO_2 powder to the coatings reduced the nominal G112 microhardess of approximately 950 HV (Vickers) down to a minimum of 700 HV, with 4 wt% TiO_2. Although the 4 wt% TiO_2 coatings exhibited the lowest microhardness, they yielded the lowest friction coefficient (0.2) and the lowest wear (3.3 mg mass lost) during and after the room temperature sliding wear experiments. EDS and XRD suggested the formation of new phases such as TiB_2 and TiC in the TiO_2 doped coatings.

In 2004, Kumar et al. electro deposited Ni and Co coatings in an electrolytic suspension containing Cr_2O_3 [104]. This process produced both Ni and Co coatings containing 12 vol% Cr_2O_3. After the coatings were deposited, the coated surfaces were heat treated at various temperatures up to 600°C. Both coatings were found to exhibit increased microhardness with increased heat treatment temperature, with the Co coatings

being slightly harder at higher temperatures. Using a Taber Wear Index, the abrasive wear resistance was measured for the heat treated coating surfaces. The Ni coatings exhibited good wear resistance with little change in performance from the heat treatments. The Co coatings yielded similar results to the Ni coatings heat treated up to 250°C. At heat treatment temperatures above 250°C, the wear on the Co coatings was reduced significantly with increased treatment temperature up to 600°C.

5.4 XPS Surface Chemistry of Nickel Oxides

In 1972, Kim and Davis published the first XPS analysis of nickel-oxygen surfaces [105]. In this paper the authors reported the binding energies of the Ni $2p_{3/2}$ and O 1s peaks corresponding to NiO and Ni_2O_3. They found that when Ni is oxidized in air at room temperature or 250°C the XPS spectra has two Ni $2p_{3/2}$ bands and one O 1s peak, which suggested that the nickel ion was in a higher oxidation state than that of NiO. Although NiO was generally considered the only stable oxide formed in air, there have been earlier studies that proposed that Ni_2O_3 may exist at low temperature [106].

In 1974, a follow up paper was published by Kim and Winograd which used XPS to study nickel-oxygen surfaces subjected to temperature changes as well as oxygen and argon ion-bombarded [107]. The authors found that Ni_2O_3 was present on most nickel-oxygen surfaces, except those exposed to air for many hours at temperatures above 600°C. This work identified that the stability of Ni_2O_3 was decreased as the temperature was increased. In addition, the exposure of Ni_2O_3 to argon ions caused a reduction that produced both NiO and Ni products. This phenomenon also holds true for NiO, which was reduced to Ni when exposed to argon ions. In contrast, NiO and Ni_2O_3 were formed

when Ni was exposed to oxygen ions.

In 1992, Uhlenbrock et al. used XPS to study NiO single crystals [108]. Just as Kim and Winograd had shown, Uhlenbrock et al. found that ion bombardment of cleaved NiO single crystals causes a reduction to Ni. Uhlenbrock et al. also found that there are no Ni^{3+} defects on freshly cleaved or epitaxially grown NiO surfaces. The Ni^{3+} defects are only produced by sputtering these prepared surfaces.

In 2007, Payne et al. used XPS to study the structure and growth of oxides on polycrystalline nickel surfaces [109]. In this work the authors analyzed the oxide chemistry on the surface of polycrystalline nickel samples after exposure to oxygen gas at 25°C and 300°C at pressures near 130 Pa. At room temperature, the surface chemistry was analyzed after exposure for 10, 25, 50, and 100 minutes. Interestingly, the surfaces showed evidence of Ni_2O_3 in both the Ni 2p and the O 1s peaks at every time interval. The O 1s peak suggests that at 10 min, the surface oxide consisted of mostly Ni_2O_3. As time progressed, more and more NiO became present. However, there was always a significant amount of Ni_2O_3. At 300°C, there was evidence of a large amount of Ni_2O_3 present after 1 min exposure. As the oxidation continued, the relative amount of Ni_2O_3 was reduced as more NiO was formed. After 60 min, the surface chemistry indicated that the oxide was mostly NiO.

5.5 Nickel Based Coatings Research Scope

Throughout the literature (outlined in the previous sections) there has been a significant body of research focused on the friction and wear of nickel based alloys and

materials. Most of these investigations have concentrated on the transition from severe to mild wear and the reduction of friction at elevated temperatures. This phenomenon has often been attributed to the formation of a 'glaze' layer. In addition, these tribological investigations have primarily used electron diffraction, energy dispersive spectroscopy, electron probe micro-analysis, and/or x-ray diffraction to diagnose the surface chemistry of the worn surfaces. Using these techniques, the surface species (or glaze layer) has been described as being composed of nickel oxide (NiO). Interestingly, there were only four papers, in all of the friction and wear studies of nickel based materials, that used x-ray photoelectron spectroscopy (XPS) for surface chemistry analysis [78, 84, 87, 101]. All four of these papers report the presence of Ni_2O_3 at the interface of the wear experiments conducted at relatively low temperatures. In addition, the presence of Ni_2O_3 was also noted in the major XPS studies conducted on nickel-oxygen surfaces [105-109]. In these fundamental studies of pure nickel surfaces, it was determined that Ni_2O_3 was always present within the oxide layer at temperatures below 250°C. This could be one of the major keys to the friction and wear performance of nickel based surfaces that have been overlooked.

Friction and wear of NiO based coatings were published in three summarized papers [94, 100, 102]. However, the coatings used in these papers were NiO/CaF_2 and NiO/SrF_2 thermal sprayed coatings and various mixtures of TiO_2/NiO sol-gel derived coatings. There were no published friction and wear studies of pure NiO films. The only published tribological studies on pure NiO films were erosion studies [110, 111]. In these studies thick NiO films were grown by oxidizing commercially pure nickel (alloy Ni200) at 1,000°C. Examination of the microhardness and microstructure, along with

erosion wear testing, were the techniques used to characterize these films.

Based on the literature presented, nickel based materials have the potential to exhibit low friction and wear at elevated temperatures. This performance is governed by the formation of a glaze layer that is typically defined as NiO. It has also been demonstrated that there is always a critical temperature at which the surfaces must exceed before this lubricious layer is formed. However, there have not been friction and wear studies (or more importantly no fretting wear studies) on pure NiO films. In addition, the lack of XPS analysis in the bulk of the published work, has overlooked the potential influence that Ni_2O_3 may or may not have on the tribological performance of the NiO glaze layer.

The foundation for this research was based on the effect of temperature on the fretting wear and tribochemical mechanisms of nickel coating and nickel oxide surfaces mated with Ti6Al4V (for potential dovetail joint coating replacement). This goal was met through a three phase research plan, which will be presented within the following chapters. Phase one was based on the temperature effects on the fretting wear performance of commercially pure Ni coatings. These coatings were applied on the Ti6Al4V substrates by cold gas dynamic spraying. This is a high energy process that utilizes an inert carrier gas and low temperature to minimize the oxidation of the metallic powder during the coating process. These coatings were experimentally analyzed through fretting wear experiments that ranged from room temperature up to 450°C.

Phase two consisted of similar fretting wear experiments conducted on NiO films. As the oxidation temperature of nickel is increased the oxidation rate and total thickness

of the oxide film are also increased. Work by Gulbransen and Andrew showed that nickel has a transition temperature at which the oxidation mechanism changes from a slow protective oxidation to a more rapid non-protective type of oxide formation [112]. For this phase of the research, commercially pure nickel alloy Ni200 (99.5% Ni) was polished to a finish of 5 to 10 nm Ra, and oxidized at 1,000°C for 100 hours to form a thick nickel oxide film [113]. Oxidation of the Ni200 research samples at 1,000°C maximized the oxide thickness and minimized the Ni_2O_3 content. This is because Ni_2O_3 is reduced to NiO at temperatures above 600°C [114]. XRD, Raman Spectroscopy, and XPS were then used to verify the state of the oxide film, while micro and nanohardness measurements were used to identify the mechanical properties of the oxidized films.

The overall scope of phase two was focused on answering four fundamental questions about the fretting wear and tribochemical mechanisms of nickel oxide films. Generally, it is known that oxide formation and tribological performance is governed by the diffusion rate and thickness of the oxide relative to the removal rate of the oxidized surface. On Ni based materials, the diffusion rate and oxide thickness increase with temperature, while the Ni_2O_3 content of the oxide decreases. Is the critical temperature governed solely by the oxide thickness? Or, is Ni_2O_3 preventing the formation of a stable NiO glaze layer? Or, is a certain temperature required to get the lubricious properties of the NiO glaze layer (via oxide softening or debris sintering as suggested in the literature)?

Following the analysis of the cold sprayed Ni coatings, the NiO surfaces yielded similar results that were not bound by some of the cold sprayed coating uncertainties

such as compressive stress and coating roughness. The compressive stress may have affected the performance of the Ni coatings at elevated temperatures due to annealing. Annealing of the coating could increase the amount of plowing at the interface. This increase in coating deformation would increase the wear rate as well as increase the friction. In addition, Iwabuchi et al wrote three separate articles based on their work with the role of oxide debris and its effect on the friction and wear of steels [115-117]. In this work, the authors found that rough surfaces often performed better than smoother surfaces because of the inherent ability of the surface roughness to trap debris below the surface of the interface. This prevented the inception of abrasive wear that was typically caused by the active oxide debris trapped within the wear track. The cold sprayed coatings were tested as-sprayed. Therefore, they had very high surface roughness, and there were slight differences in surface roughness from sample to sample. In addition, the high level of surface roughness of the coatings may have improved the fretting wear performance of the coatings, due to debris trapping.

The knowledge base developed from the tribological and tribochemical performance of nickel oxides were then utilized in Phase three of this research, the development of self-lubricating nickel based composite coatings. As stated in Chapter 1, the dovetail joints in compressor blade systems for aircraft turbine engines are often coated with a thermal sprayed CuNiIn or Al-bronze coating and then capped with a bound solid lubricant. Typically, the lubricants are MoS_2 or graphite based in an epoxy or silicate based binder. A Ni based composite coating would alleviate the need for a bound lubricant and mitigate the degradation that can occur when the solid lubricants are worn away. In addition, a Ni based coating would be able to utilize the low friction and

low wear that is exhibited by nickel oxides at elevated temperatures. This would make the coating very versatile for use in many elevated Ti-alloy fretting contacts.

The self-lubricating Ni based composite coatings, in Phase three, utilized imbedded graphite particles for solid lubrication at low temperatures, and were applied to Ti6Al4V substrates via plasma spray. For proof of concept, initial experimentation was conducted on Ni-graphite abradable coatings (NiG-A). NiG-A coatings are currently used as an abradable seal within aircraft turbine engines to prevent airflow from passing the tips of the compressor blades. The coatings have approximately 50% graphite by volume in the pre-sprayed powder mixture, and were flame sprayed on to the component surfaces. Typically, NiG-A coatings are very porous so that the blades can cut a groove in the coatings during the initial rotation of the engine shaft, without damaging the blade tips.

Along with NiG-A coatings, denser plasma sprayed coatings were applied to Ti6Al4V samples with pre-spray powder mixtures of 5% (NiG-5), 10% (NiG-10), and 20% (NiG-20) graphite by volume. These coatings were made to be denser and have a higher wear resistance than the NiG-A coatings. The variance in graphite content aided in the determination of how much graphite was needed to attain low friction at the interface. Extended experimentation and surface analysis was conducted on the selected candidate from the 5%, 10%, and 20% nickel graphite mixtures, and proved the viability of these coatings for fretting wear mitigation at low and elevated temperatures in Ti-alloy aircraft components.

Chapter 6

EFFECT OF TEMPERATURE ON COLD SPRAYED NICKEL COATINGS

6.1 Objective

The objective of this research was to determine the effect of temperature on inter-metallic fretting wear between Ti6Al4V (Titanium, 6% Aluminum, 4% Vanadium) and cold sprayed commercially pure nickel coatings. Nickel coatings were chosen because of the potential to produce what is often called a "glaze" oxide layer at high temperature, which has been shown in the previous chapter to reduce friction and wear in nickel-based alloys. The formation of nickel oxide and the evolution of the inter-metallic fretting wear mechanisms, between nickel and Ti6Al4V at elevated temperatures, were investigated to determine the potential of nickel based coatings for high temperature fretting wear mitigation in titanium alloy contacts.

6.2 Cold Spray Coating Process

The cold-spray method, as shown in Fig 6.1, is the process of applying coatings by exposing a metallic substrate to a high velocity (300-1000 m/s) gas jet loaded with small (1-50 μm) solid particles [118, 119]. In this process, the coating material is introduced as a solid powder into a compressed (1 to 3 MPa) gas stream that expands through a converging-diverging nozzle. A heater is then used to raise the temperature of the gas and solid particles as they enter the converging section of the nozzle. The increased temperature causes the hot pressurized gas to expand through the converging section of the nozzle, which serves to increase the gas and particle velocities as they are accelerated and forced out the diverging end. Using the supersonic gas jet as a carrier, solid coating particles are accelerated and propelled towards the substrate at very high velocities. Upon

impact, the particles deform or “splat” and bond to the surface of the substrate. As more and more particles impact the surface, the “splats” buildup and form a uniform coating with relatively low porosity.

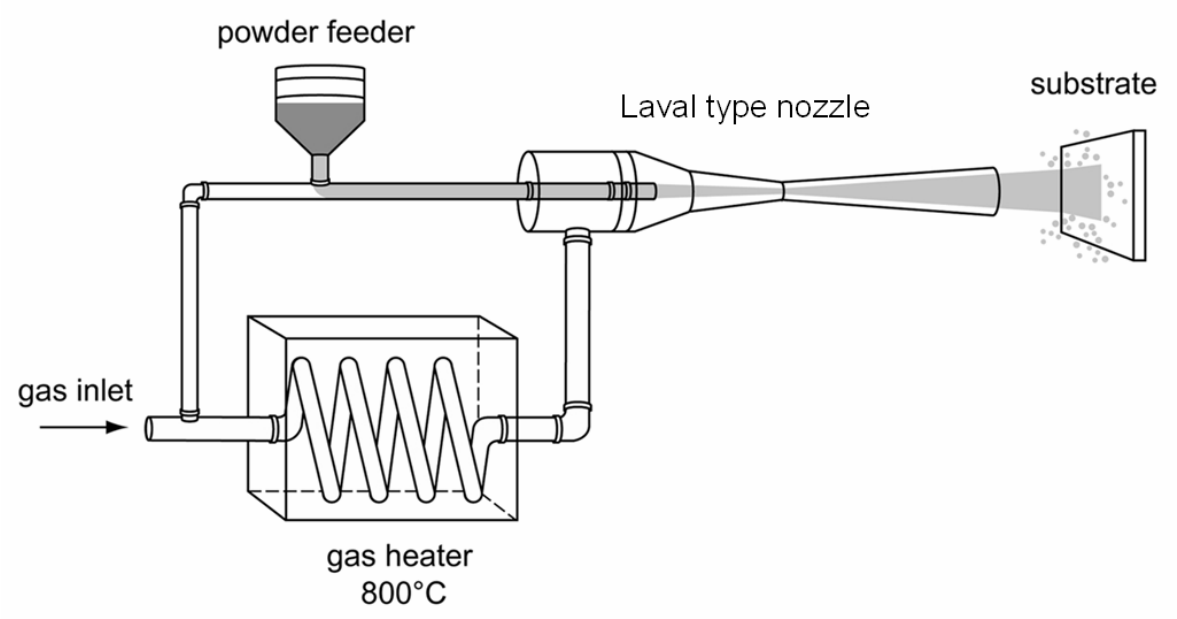

Fig. 6.1. Cold spray coating process.

Conventional thermal spray processes, such as plasma spray and high-velocity oxygen-fuel (HVOF), use superheated gas to preheat the coating particles to a molten or semi-molten state as they are propelled toward the substrate. The “soft” particles then “splat” on the surface as the coating is built up. As the hot “splats” cool they contract and solidify, creating residual stress and/or flaws at the interface. In addition to the residual stresses caused by thermal expansion mismatch between the cooling “splats” and the substrate, the superheated coating particles are also partially oxidized as they are deposited on the substrate surface.

The cold spray process is conducted at temperatures much lower than other more conventional thermal spray processes, as shown in Fig 6.2 [119]. The low temperatures

allow for the deposition of solid particles that retain their microstructure as they are propelled to the substrate, as well as the deposition of particles on substrates with relatively low melting points. Therefore, cold sprayed coatings exhibit minimal thermal stress effects or oxidation of the coating particles. This is shown in Fig 6.3, where x-ray diffraction (XRD) was used to analyze plasma sprayed and cold sprayed commercially pure nickel coatings on Ti6Al4V substrates. The XRD results show that the cold sprayed nickel coating has the same structure as the plasma sprayed coating, without the presence of nickel oxide (NiO).

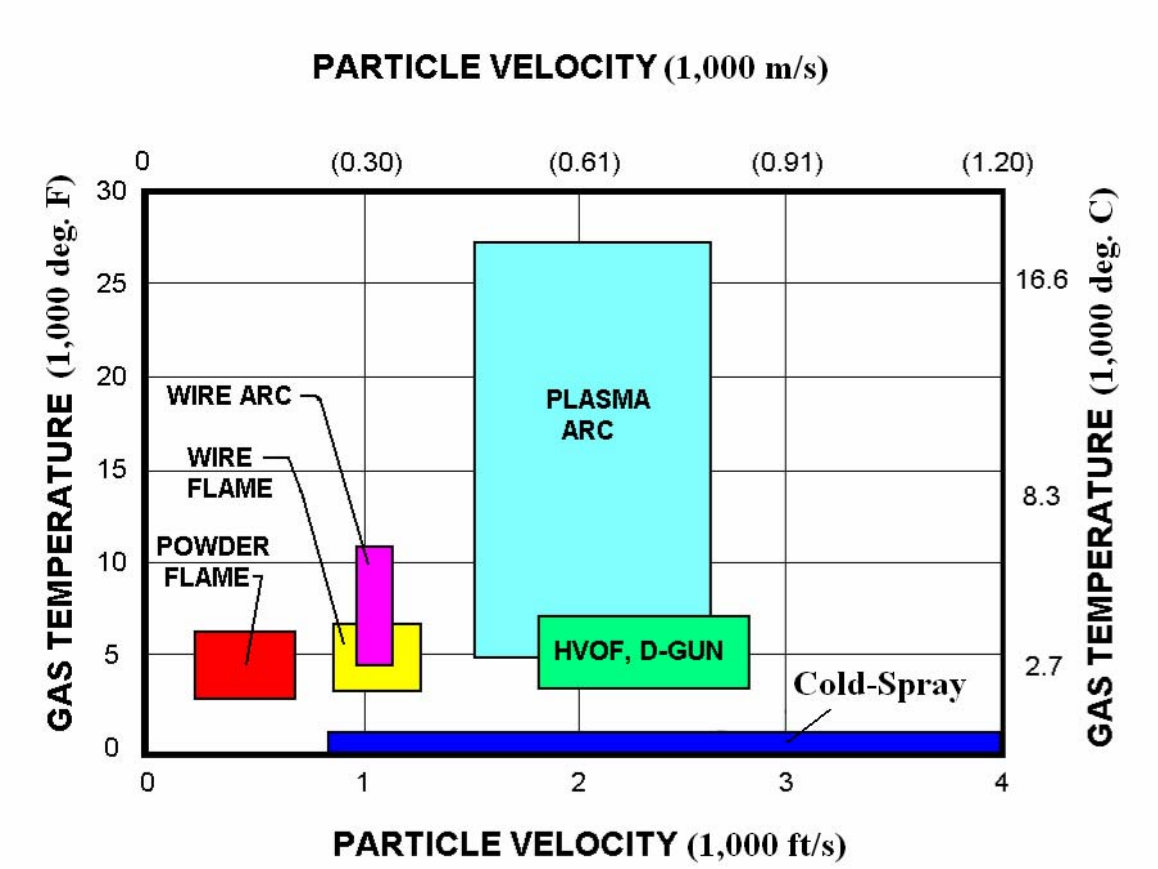

Fig. 6.2. Temperature comparisons between conventional thermal spray methods [119].

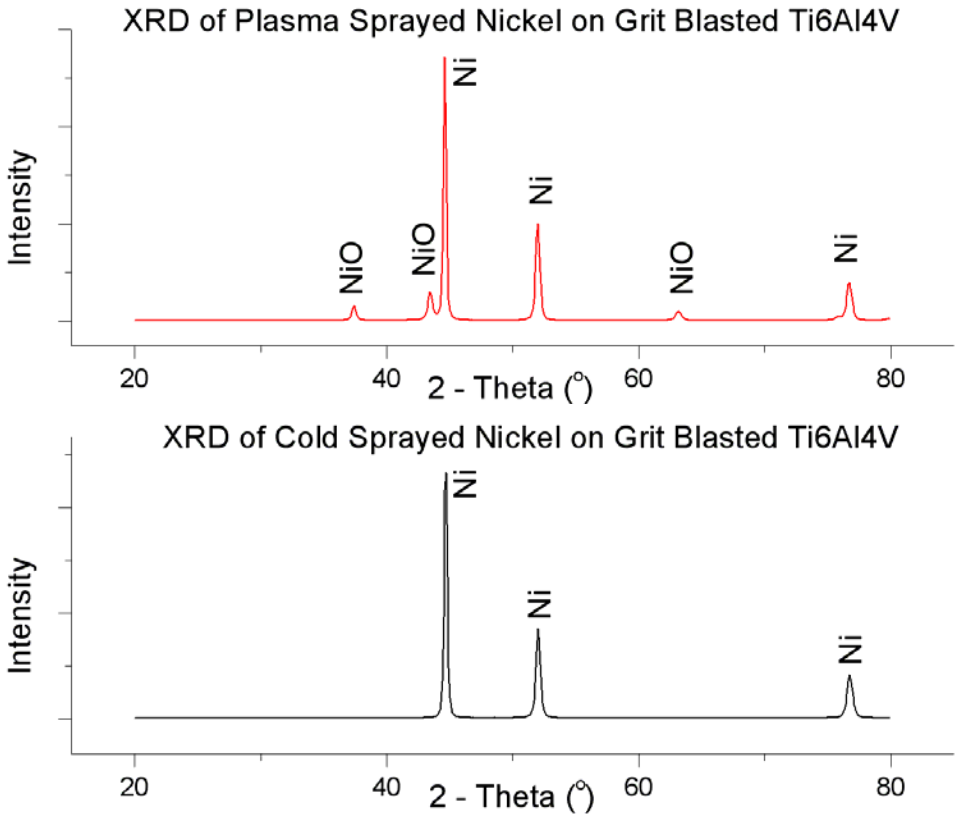

Fig. 6.3. XRD analysis of (top) plasma sprayed nickel on Ti6Al4V and (bottom) cold sprayed nickel on Ti6Al4V.

6.3 Experimental Work

The purpose of this study was to provide an understanding of how temperature affects the gross slip fretting wear performance of cold sprayed nickel coatings coupled with Ti6Al4V. This study consisted of two to six repeat tests conducted with a 200 μm stroke length, 30 Hz oscillation speed, and a 50 N normal load for 100,000 cycles. The 200 μm stroke length was chosen as a displacement that was determined to induce gross slip in Ti6Al4V contacts under the applied loading condition, as described in Chapter 2. The applied 50 N normal load yields a maximum Hertzian contact stress of approximately 650

MPa. In addition, some shorter duration tests (e.g. 10, 100, and 1000 cycles) were conducted at 2 Hz oscillation speed, to supplement the longer tests for wear analysis

The specimens used for this investigation were Ti6Al4V, and the test geometry was an ellipsoid on a flat plate, shown in Fig. 6.4 and further explained in Chapter 2. Prior to testing, the Ti6Al4V disks were grit blasted, and cold spray was used to apply approximately 100 μm thick nickel coatings. Substrate and coating properties are listed in Table 6.1. The micro and nano-hardness were measured on the polished cross-sections of the nickel coatings. Nano-indents were made using a Berkovic indenter to a depth of 2 μm into the coating. Vicker's micro-indents were made using 100 gf.

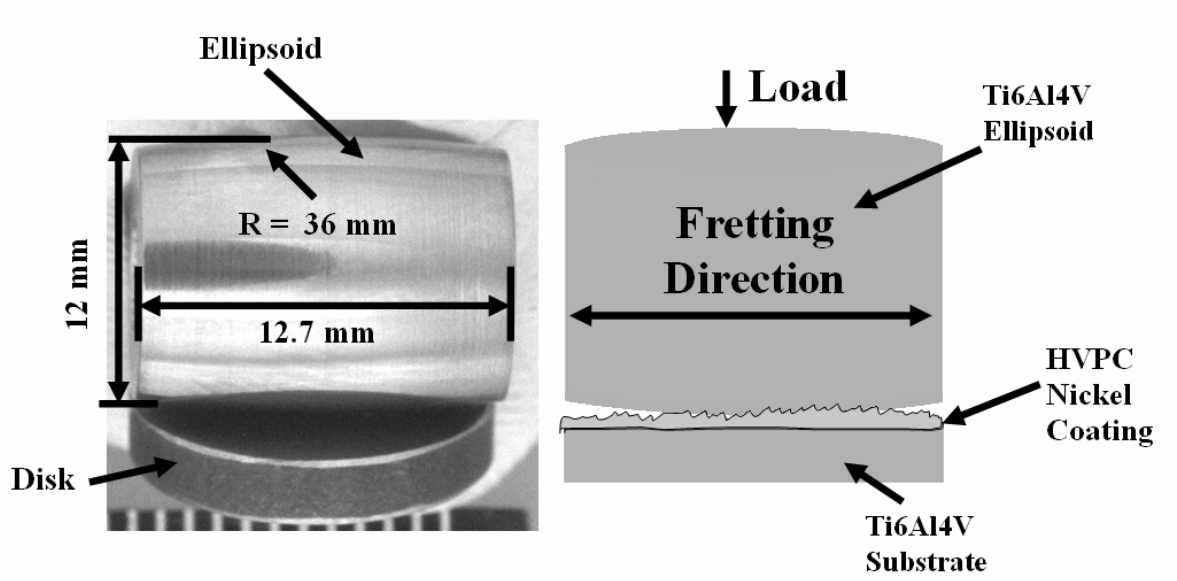

Fig. 6.4. Ellipsoid contact geometry and test setup.

Materials	Composition Weight %	Roughness Ra (μm)	Modulus (GPa)	Nano Hardness (GPa)	Micro Hardness (HV)
Substrate and Counterface	90% Ti 6% Al 4% V	0.1	128	4.2	265
Nickel Coating	Commercially Pure	18.7	158	3.2	211

Table 6.1. Titanium alloy and cold spray nickel coating properties.

6.4. Results

6.4.1 Friction Analysis

Initially experiments were conducted at room temperature (RT), 165°C, and 450°C for 100,000 cycles. These three target temperatures were chosen based on the applicability of this coating system to aircraft compressor blade fretting wear mitigation. In a turbine engine fretting wear occurs during cold engine startup (RT), during steady state operation in the fan and lower temperature stages of the compressor (≈165°C), and in high temperature stages of the compressor (≈ 450°C). The friction dropped significantly in the 165°C experiments compared to the room temperature tests. The friction decreased further and became more stable in the 450°C experiments.

The initial friction results prompted more extensive experimentation at the temperatures between the three initial target points. Fig 6.5 is a plot of the RMS friction per cycle of typical tests at the listed temperatures. The RMS coefficient of friction over the duration of each test was then averaged and plotted in Fig 6.6.

In conjunction, Fig 6.5 and Fig 6.6 show that the coefficient of friction in the aforementioned experiments decreases from 0.8 (at room temperature) down to 0.3 (at

300°C). Then above 300°C the coefficient of friction slightly rises with temperature up to 0.4, at 450°C. This suggests that cold sprayed nickel coatings may produce desirable fretting wear and frictional properties at certain temperatures, with an apparent optimum (at 30 Hz oscillation speed with ≈ 650MPa contact stress) at approximately 300°C. In addition, the friction from the experiments conducted at 2 Hz oscillation speed for shorter durations yielded a similar trend in friction with temperature at RT, 165°C, and 450°C. The only difference that was noted is that the friction at 165°C was significantly lower in the 2 Hz tests. At 2 Hz, the coefficient of friction at 165°C was approximately 0.45.

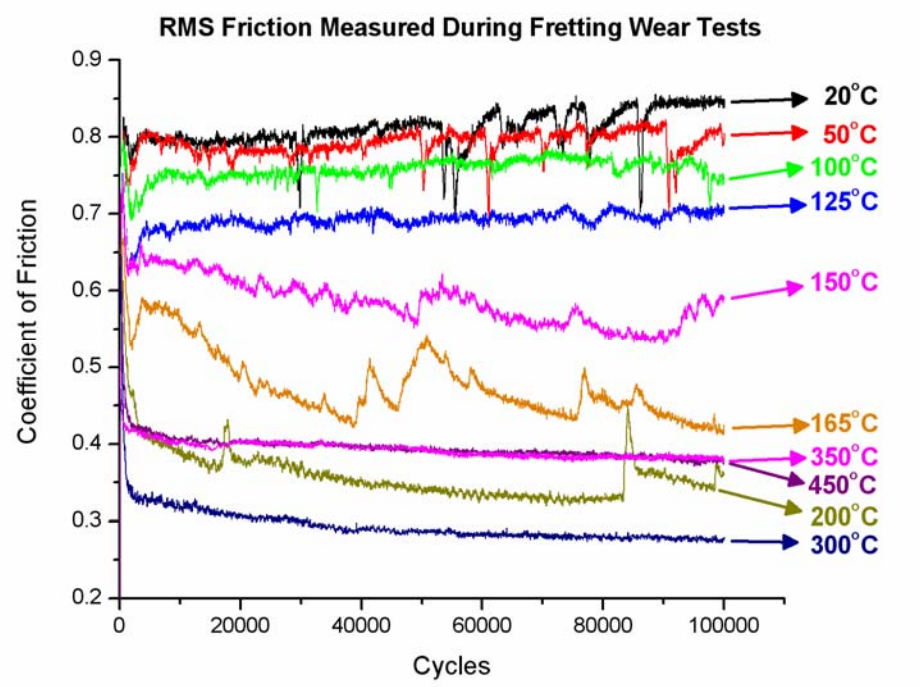

Fig. 6.5. RMS friction measured during fretting wear tests at elevated temperatures.

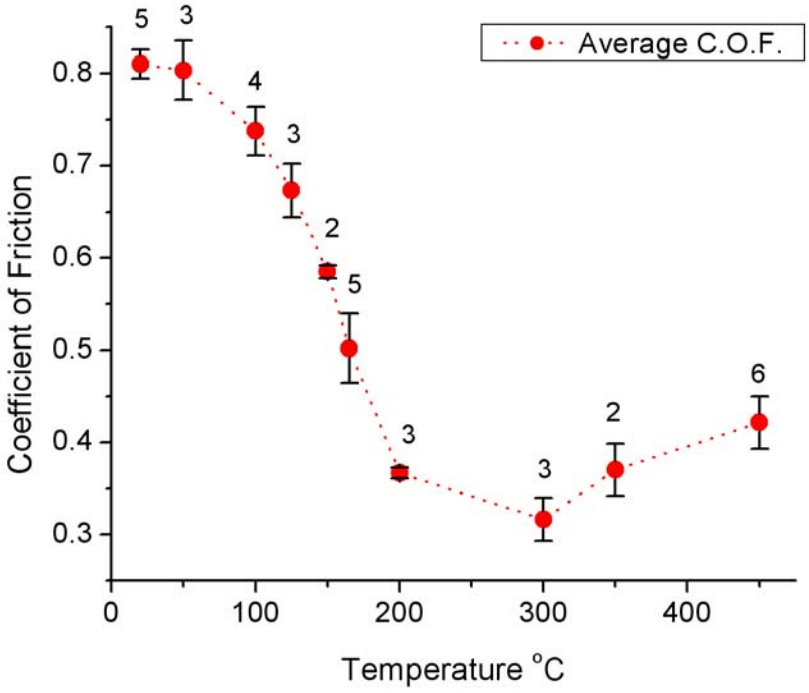

Fig. 6.6. Averaged coefficient of friction measured during fretting wear tests at elevated temperatures. The numbers above each plotted data point describe the number of experiments conducted at that temperature.

6.4.2 Wear Analysis

The progression of fretting wear at room temperature, 165°C, and 450°C exhibited by the Ti6Al4V ellipsoids and cold sprayed nickel coated surfaces was analyzed after conducting experiments for test durations of 10, 100, and 1,000 cycles at 2 Hz oscillation speed, and after 100,000 cycles at 30 Hz oscillation speed.

After 10 cycles, the gross slip fretting wear at the interface of the test specimens was composed of adhesive wear and ploughing. Fig 6.7 shows secondary electron images of the mated titanium and nickel surfaces, where it can be seen that material from the titanium surface has transferred to the opposing nickel surface at all three temperatures. Further evidence of this is shown in Fig 6.8, with the use of backscatter imaging and x-ray mapping. In the backscatter images, the dark gray regions show where titanium has

transferred to the nickel coating surfaces. At room temperature and 165°C, the wear after 10 cycles is practically identical. The large transferred titanium particles are on the order of 100 μm to 200μm in size. At 450°C, the transferred titanium particles were approximately half the size of the particles observed in the lower temperature experiments. In addition, there was also significant nickel transfer to the titanium surfaces, as shown by the white regions in Fig 6.7E. There was little to no nickel transfer to the titanium ellipsoid surface in the room temperature and 165°C experiments.

Further fretting wear progression was analyzed after 100 cycles of gross slip fretting wear. The similarities in wear of the room temperature and 165°C experiments were still apparent. There was still significant titanium transfer to the nickel coating surface, as shown in Fig 6.9 and Fig 6.10. However, the adhered titanium particles decreased in size between 10 and 100 cycles. In addition, material from the nickel coated surface started to transfer to the titanium ellipsoid surface as shown by the white regions around the surface scuffing in Fig 6.9A and 6.9C.

At 450°C the contact surface of the Ti6Al4V ellipsoid was almost completely covered with a nickel and nickel oxide transfer layer, with some intermixed titanium wear particles. As with the room temperature tests, the 450°C ellipsoid surfaces had some localized gouges from metallic contact with the nickel coating. However, unlike the lower temperature tests, the transferred material formed a smooth tribo-layer on the Ti6Al4V ellipsoid surface. Fig 6.9E shows an image of this tribologically transferred layer on the titanium surface. In addition, the wear on the nickel coating, as shown in Fig 6.9F, has become completely smooth with the transferred titanium smeared onto the fretting wear contact. This phenomenon can also be seen in Fig 6.10C. The backscatter electron image

and x-ray map, show the dispersed titanium on the smoothed nickel coating contact surface. The smoothed contact layer on the nickel surface had an RMS roughness of approximately 0.9 µm.

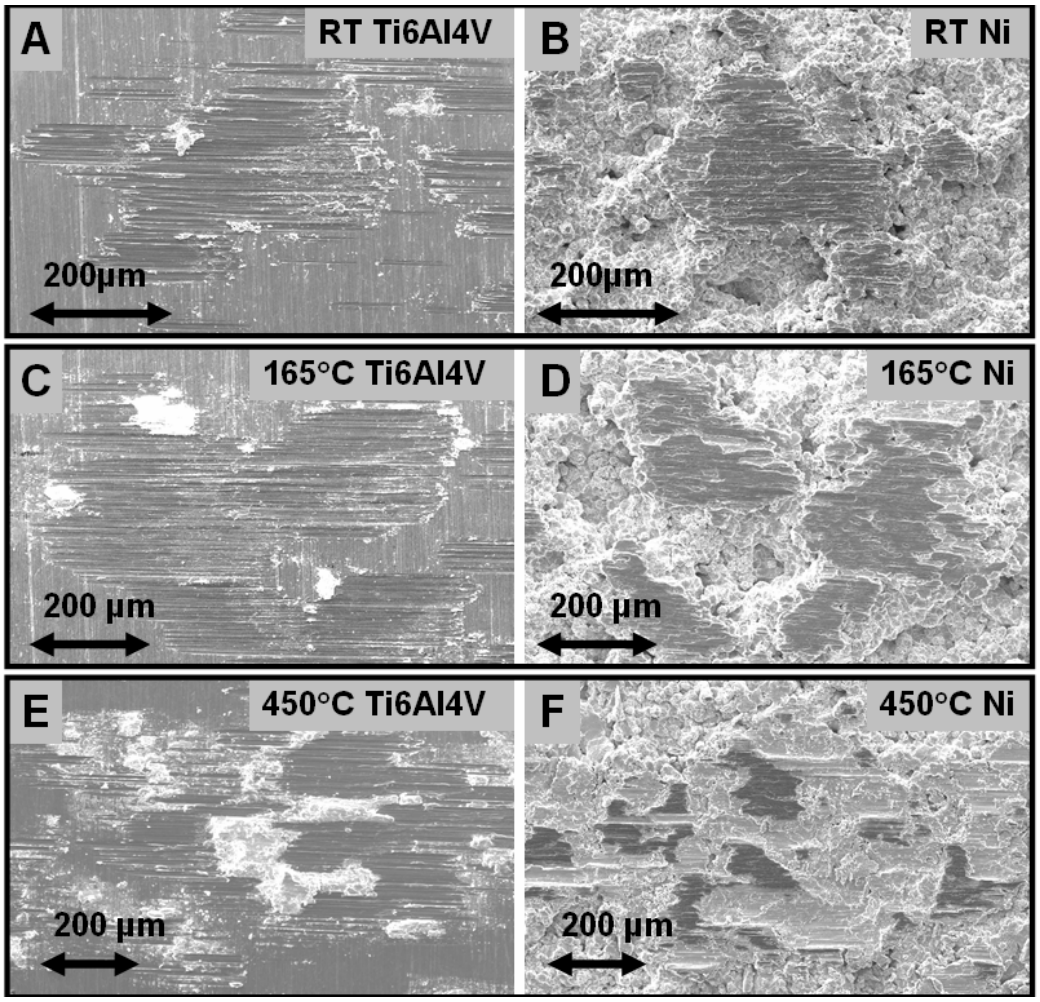

Fig. 6.7. Scanning electron microscope images of the wear on the surface of the Ti6Al4V ellipsoids and nickel cold sprayed coatings tested at RT, 165°C, and 450°C for 10 cycles.

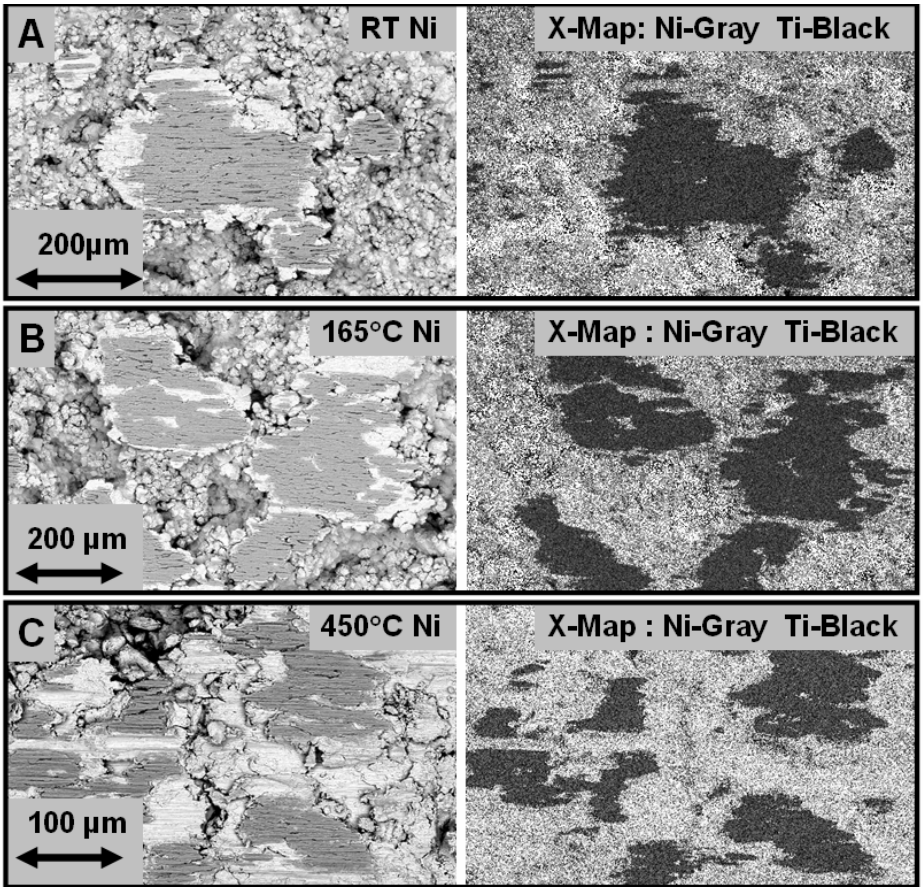

Fig. 6.8. Back scatter scanning electron microscope images and associated x-ray maps of the wear on the surface of the nickel cold sprayed coatings tested at RT, 165°C, and 450°C for 10 cycles.

After 1,000 cycles of gross slip fretting wear, the entire contact area of the Ti6Al4V ellipsoid in each test was covered with transferred nickel and wear debris from the mated surface. However, the room temperature Ti6Al4V ellipsoid interface still had evidence of localized galling where large gouges in the surface existed even after 1,000 cycles, as shown in Fig 6.11A. The 165°C titanium surface, shown in Fig 6.11C, still exhibited wear characteristics similar to those observed on the room temperature ellipsoid wear surface, with large amounts of loose wear debris adhered to the ellipsoid surface. However, the 165°C ellipsoid wear tracks had a more stable or continuous layer adhered to the ellipsoid

wear track, and did not exhibit the large localized gouges that were observed in the room temperature wear tracks. The 450°C titanium surfaces had a relatively smooth and continuous nickel transfer layer, shown in Fig 6.11E. The transfer layer filled in the initial wear on the Ti6Al4V ellipsoid surface, as seen in the 10 and 100 cycle tests, and appeared to protect the center of the wear track from further fretting wear damage.

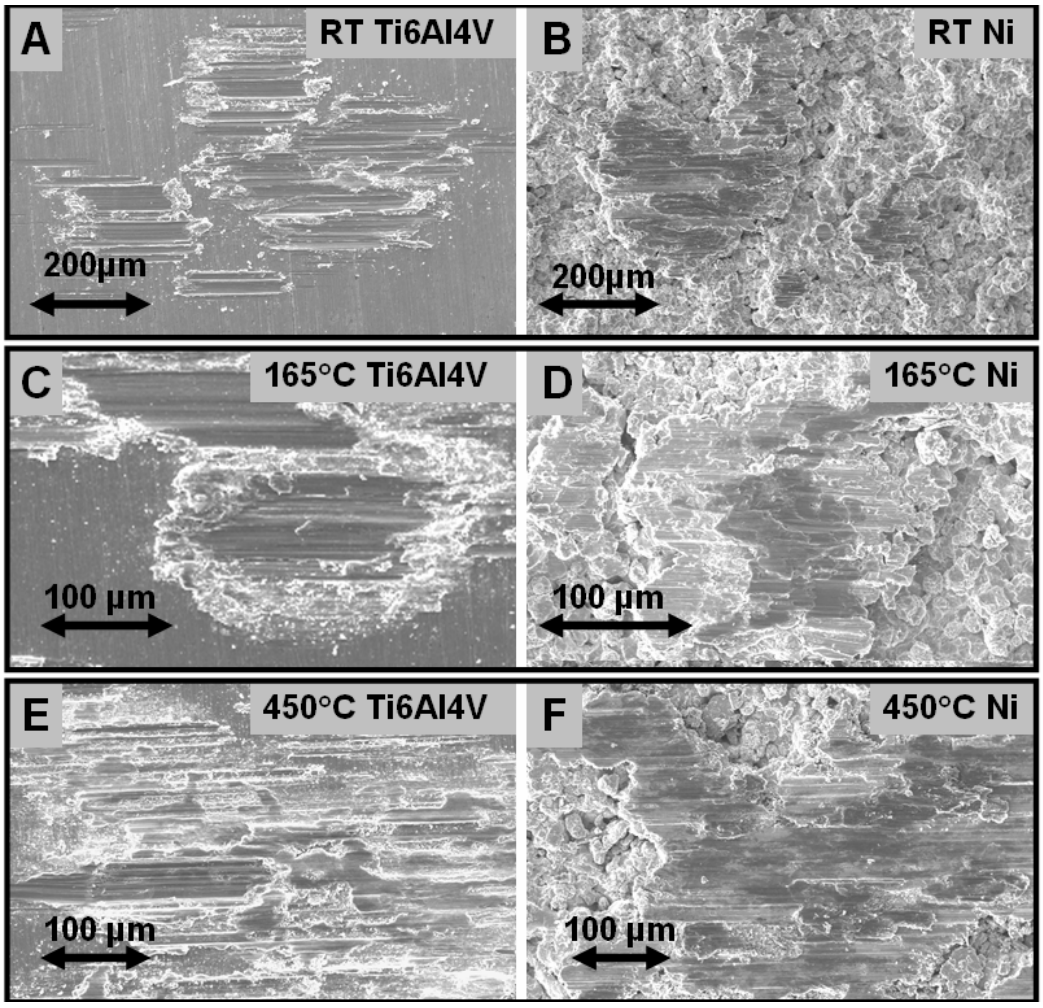

Fig. 6.9. Scanning electron microscope images of the wear on the surface of the Ti6Al4V ellipsoids and nickel cold sprayed coatings tested at RT, 165°C, and 450°C for 100 cycles.

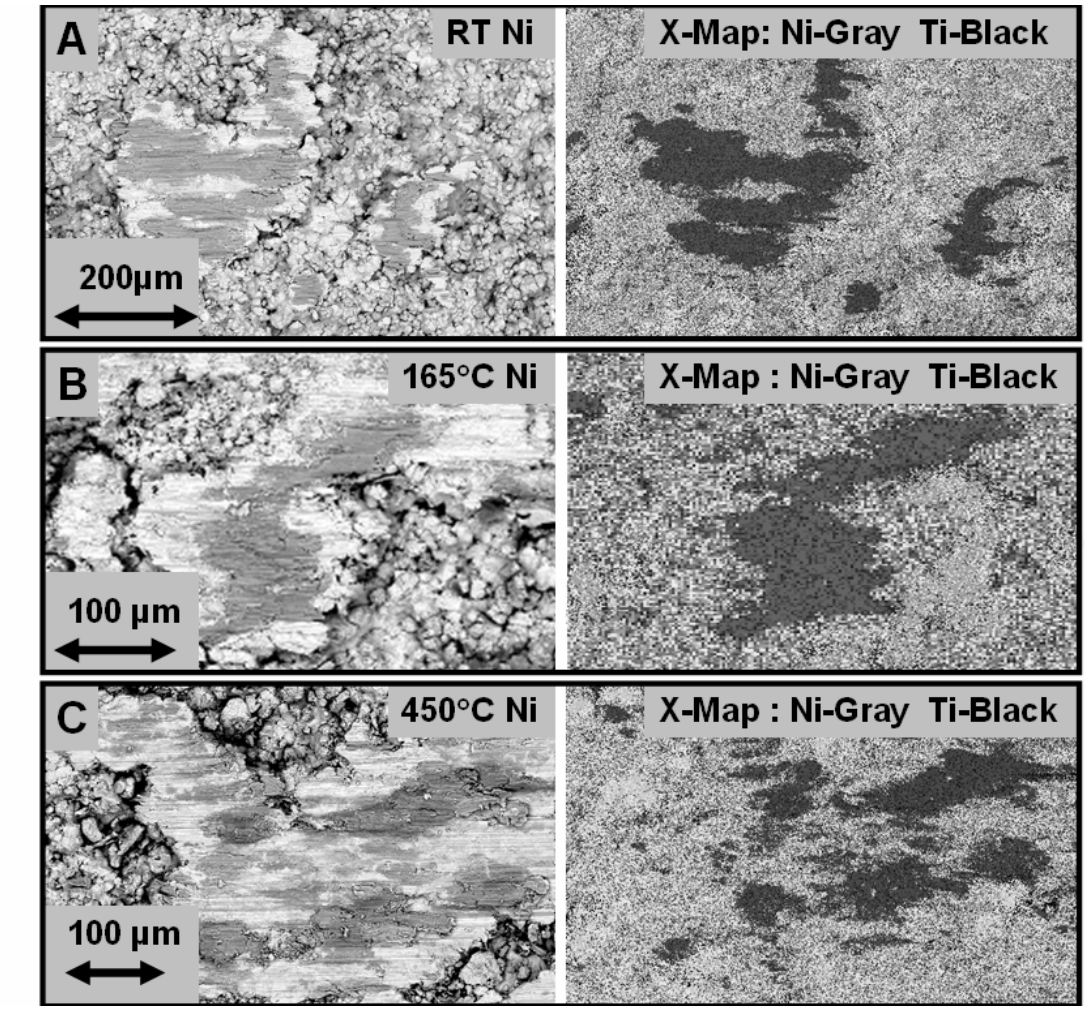

Fig. 6.10. Back scatter scanning electron microscope images and associated x-ray maps of the wear on the surface of the nickel cold sprayed coatings tested at RT, 165°C, and 450°C for 100 cycles.

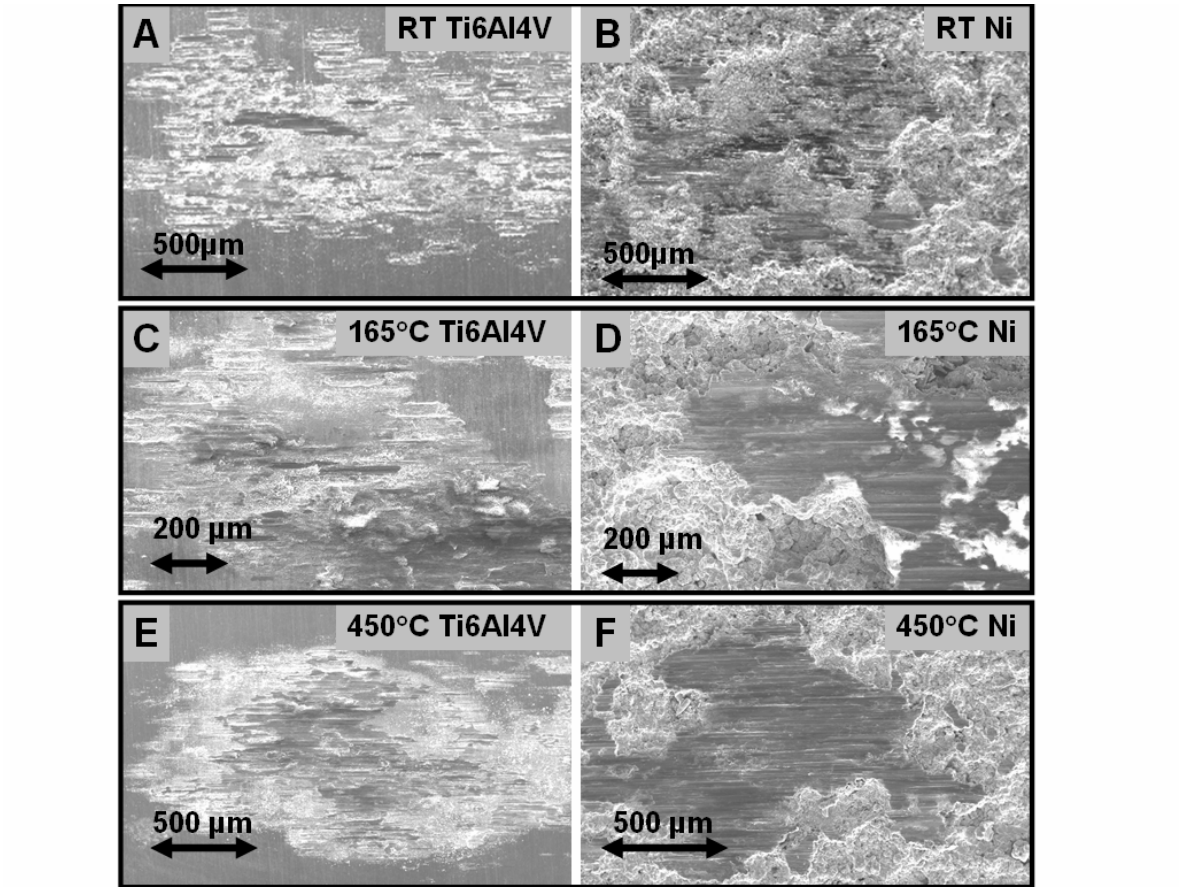

Fig. 6.11. Scanning electron microscope images of the wear on the surface of the Ti6Al4V ellipsoids and nickel cold sprayed coatings tested at RT, 165°C, and 450°C for 1000 cycles.

The gross slip fretting wear on the cold sprayed nickel coatings was significantly different at the tested temperatures after 1,000 cycles. The room temperature tests exhibited a rough wear track filled with large amounts of loose and compacted wear debris, as shown in Fig 6.11B. In addition, the room temperature wear tracks also had some large titanium transfer particles (often on the order of 100 µm in size), as seen in the shorter duration tests. The 165°C nickel wear tracks were smooth, with an RMS roughness of approximately 1µm in the worn regions. Loose and compacted wear debris were also observed on top of the smoothed wear track. This wear debris is shown as the white

regions in Fig 6.11D, because of charging, and as the powdery regions in the backscatter image shown in Fig 6.12B. The 450°C nickel wear tracks were smooth like the 165°C nickel wear tracks, with an RMS roughness of approximately 0.8 µm. However, the 450°C wear tracks did not exhibit evidence of loose wear debris within the wear track, as shown in Fig 6.11F and Fig 6.12C. There was still some evidence of transferred titanium and titanium oxide, from the initial wear at 10 cycles, in the wear track, but it was intermixed into the smooth contact surface.

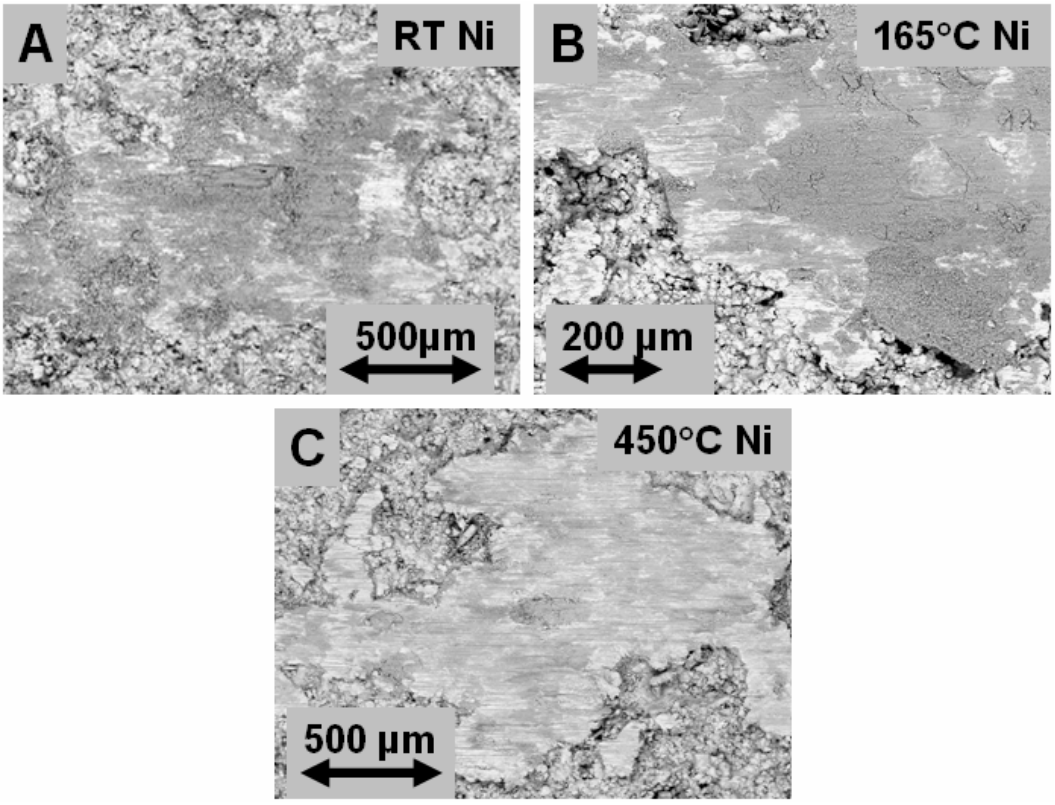

Fig. 6.12. Back scatter scanning electron microscope images of the wear on the surface of the nickel cold sprayed coatings tested at RT, 165°C, and 450°C for 1000 cycles.

At the conclusion of the short duration experiments, a final set of tests were conducted for 100,000 cycles at 30 Hz oscillation speed. At room temperature the fretting wear showed a transition from an adhesively driven interfacial damage mechanism towards

a wear mechanism that is controlled by the rheology of the active third body debris trapped in the interface. The 1,000 cycle wear tracks still had some evidence of localized galling on the Ti6Al4V ellipsoid surface. However, after 100,000 cycles there is virtually no evidence of galling at the interface. Instead, the entire wear track on the ellipsoid surface is covered with compacted wear debris that was trapped in the interface, as shown in Fig 6.13A. The wear on the mated nickel surface was smooth with similar wear debris compacted into the surface, as shown in Fig 6.13B. The wear on both the Ti6Al4V ellipsoid and the nickel coating at 165°C, after 100,000 cycles, was similar to what was exhibited by the room temperature experiments, as shown by Fig 6.13C and 6.13D. This is curious because the experiments conducted at 165°C had a coefficient of friction of approximately 0.5, as opposed to the room temperature experiments that had a coefficient of friction of approximately 0.8. Although the room temperature and 165°C tests yielded similar wear characteristics after 100,000 cycles, the 450°C tests were quite different. At 450°C, both the ellipsoid and nickel coating had a smooth tribologically formed layer in the wear track, as shown in Fig 6.13E, 6.13F, and 6.14. Fig 6.15 is a cross-section of the 3 μm transfer layer on the ellipsoid wear surface, which was cut perpendicular to the wear track. This smooth layer on the ellipsoid surface, combined with the smooth surface of the nickel coating, reduced the interfacial friction and wear once it formed on both surfaces after about 100 cycles of fretting wear. Fig 6.16 shows the wear progression on the nickel coating surface at 450°C from 1,000 up to 100,000 cycles. From this figure it can be concluded that there is a minimal increase in coating wear after approximately 1,000 cycles of fretting wear.

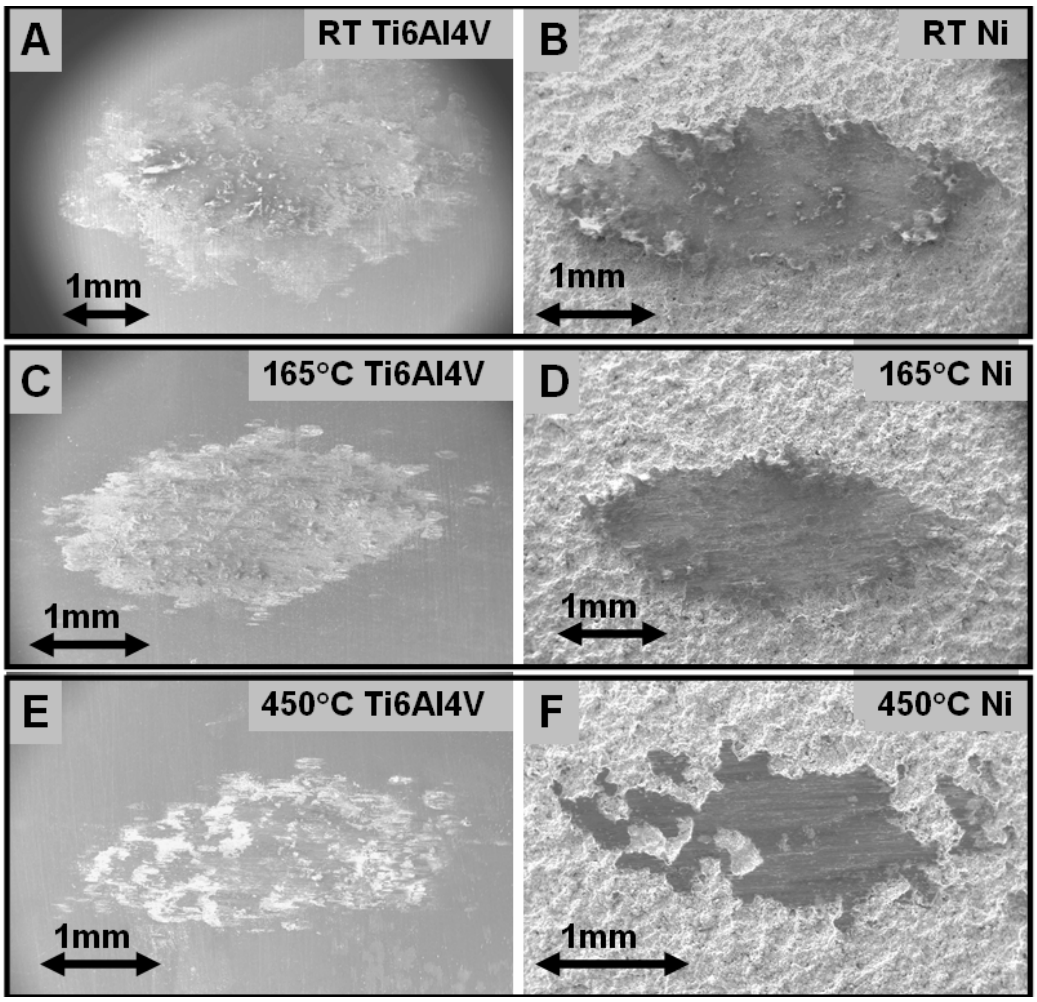

Fig. 6.13. Scanning electron microscope images of the wear on the surface of the Ti6Al4V ellipsoids and nickel cold sprayed coatings tested at RT, 165°C, and 450°C for 100,000 cycles.

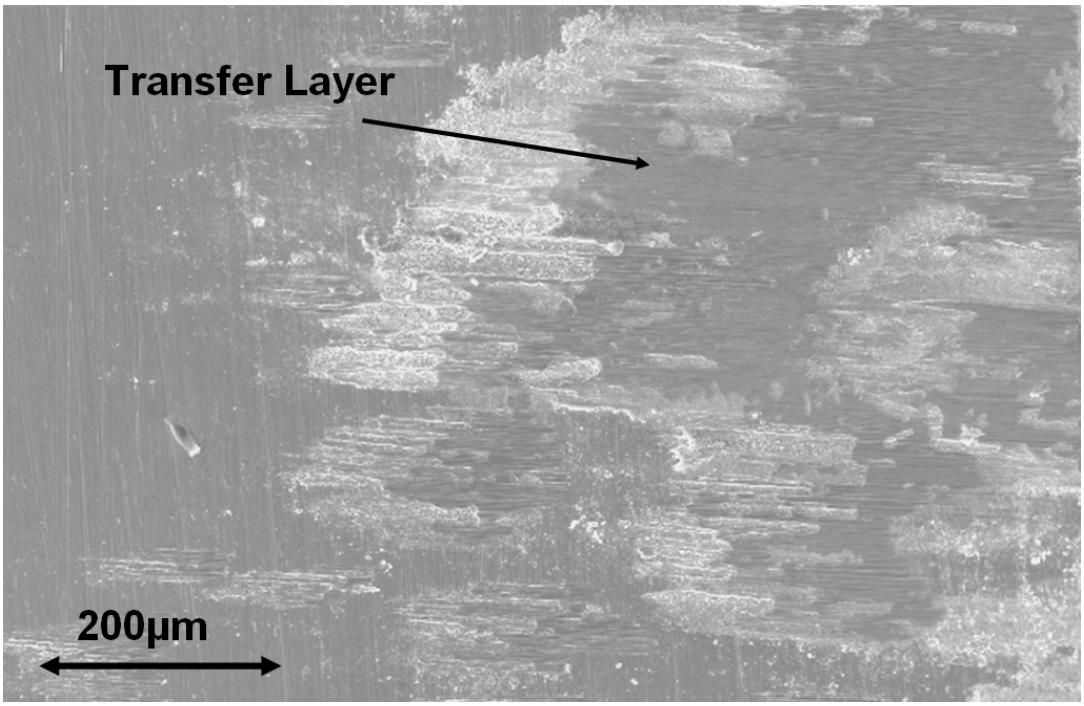

Fig. 6.14. A magnified SEM image of the wear shown in Fig 6.13E.

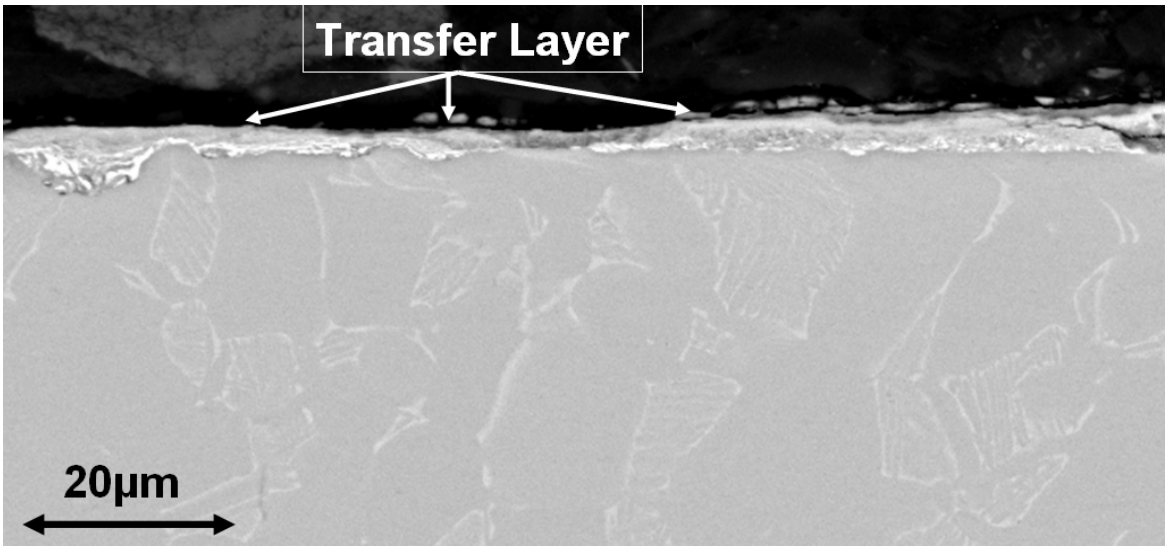

Fig. 6.15. A magnified back scatter SEM image of the cross-section of the wear surface shown in Fig 6.14.

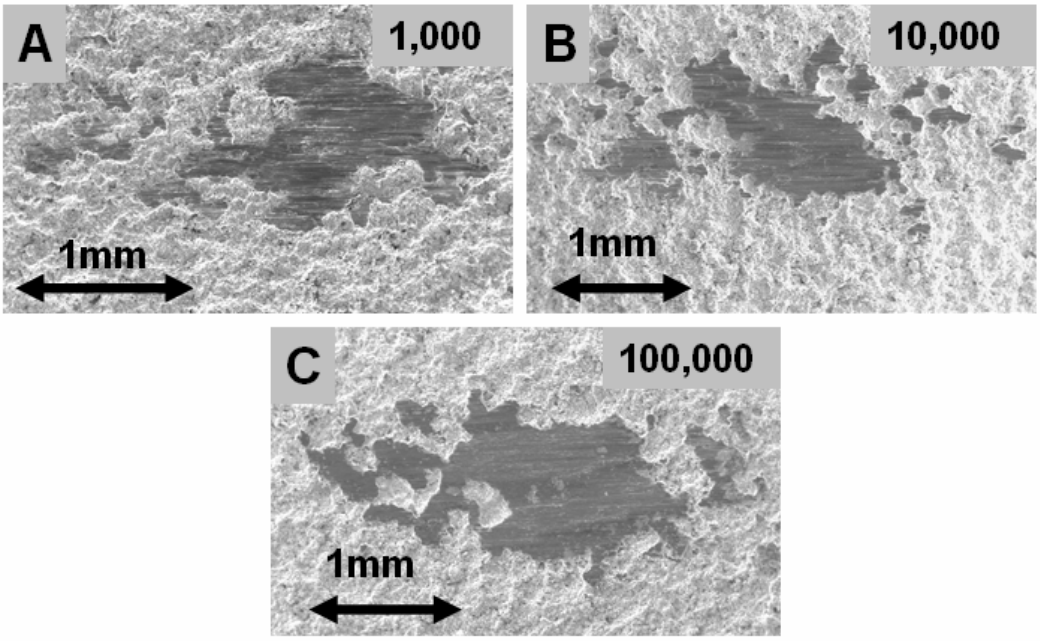

Fig. 6.16. SEM of the wear on the surface of the nickel coatings tested 450°C for various test durations.

6.4.3 Surface Chemistry

At the conclusion of the fretting wear experiments, x-ray photoelectron spectroscopy (XPS) of the worn nickel coatings was performed to determine the effect that the combination of fretting and increased bulk temperature had on the surface chemistry in the wear track. The room temperature tests had a significant amount of wear debris in the wear track, which in combination with adsorbed carbon made the nickel oxide spectra hard to capture. Therefore, all of the samples were sputtered with Ar+ for 1 min prior to obtaining the XPS scans. Although this can obscure the chemistry, the fact is that sputtering will make the NiO and Ni peaks more prominent (see literature review in Chapter 5 for more detail). Therefore, any evidence of Ni_2O_3 is still very significant.

Fig 6.17A shows the progression of the Ni 2p peaks in the wear tracks on the nickel coatings after the 100,000 cycle experiments at various temperatures. The nickel surface chemistry is defined by the relative heights of the Ni $2p_{3/2}$ peaks that are located near 852.5

eV for Ni, 854 eV for NiO, and near 855.5 eV for Ni_2O_3. The wear tracks from the experiments above 165°C exhibit Ni 2p spectra that are similar. However, the room temperature experiments yielded a spectrum that is shifted towards higher energy, which suggests an increased presence of Ni_2O_3 with respect to the other experimental temperatures. Evidence of Ni_2O_3 presence in the wear tracks of low temperature wear tests was also noted in the literature [78, 84, 87, 101].

A simple explanation for the presence of Ni_2O_3 maybe in the chemistry of the reactions:

$$4Ni + 3O_2 \rightarrow 2Ni_2O_3$$

$$2Ni + O_2 \rightarrow 2NiO$$

In these reactions two Ni_2O_3 or NiO molecules can be formed by breaking only one oxygen bond. This means that you need to break only one oxygen bond per every four atoms of nickel to form two Ni_2O_3 molecules. In contrast, you need to break one oxygen bond per every two atoms of nickel to form two NiO molecules. This suggests that it may take less energy to form Ni_2O_3 at the interface, while the bulk temperatures are low enough for the oxide to be thermally stable.

Fig 6.17B shows the variation of the O1s peaks in the nickel coating wear tracks after fretting wear experiments at the defined temperatures. The vertical dotted lines are drawn at 529.9 eV and 531.7 eV, which are the locations that typically define the presence of NiO and Ni_2O_3 respectively (in addition to the associated Ni 2p peaks). The figure also shows the curve fits for the NiO and Ni_2O_3 peaks. The relative quantity of these oxide phases are defined by the relative areas under each of the curve fits, and are plotted in Fig

6.18 as the percentage of the total peak area that is from the Ni_2O_3 curve fit. Fig 6.18 shows a clear decay of the quantity of Ni_2O_3 with increased temperature.

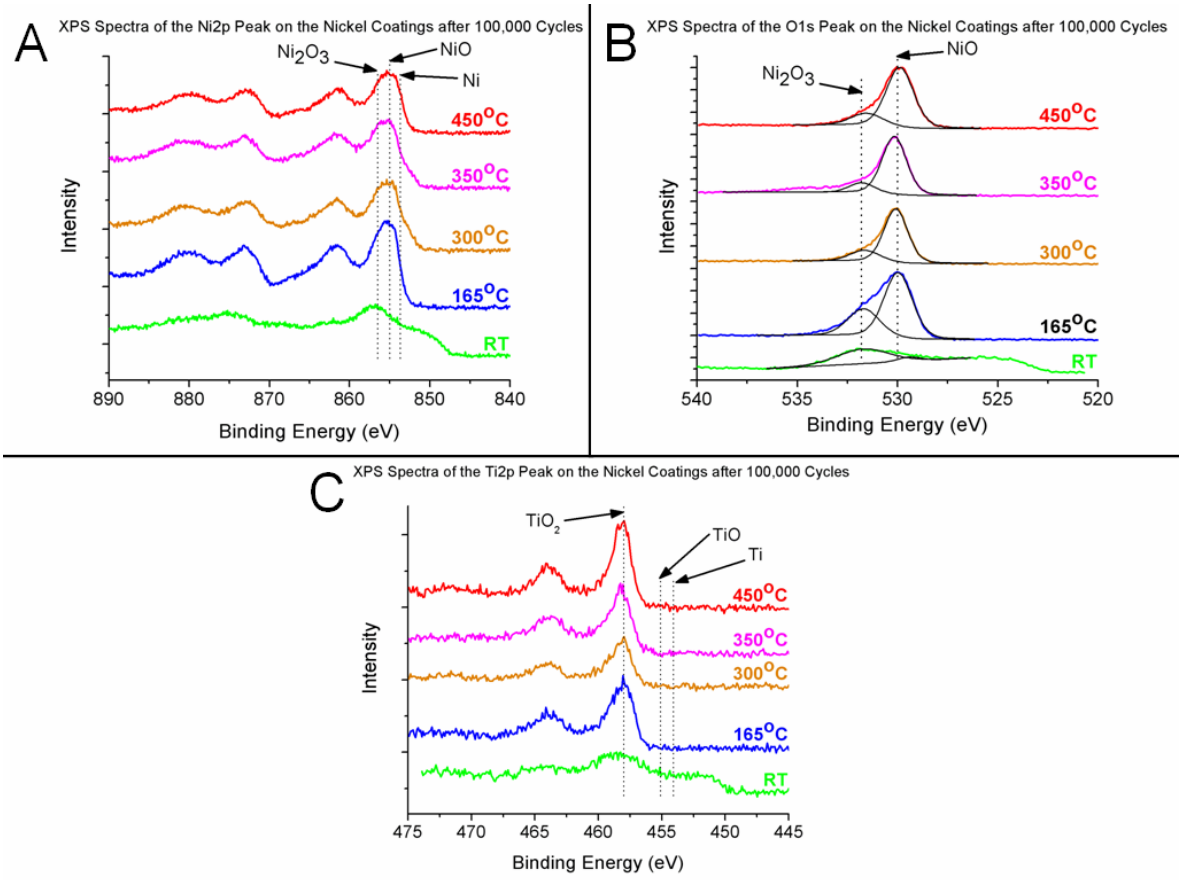

Fig. 6.17. High resolution XPS spectra of the wear track on the nickel coatings after 100,000 cycles at increasing temperature near the A) Ni 2p peaks, B) O1s peaks, and C) Ti 2p peaks.

Fig 6.17C shows the Ti 2p peaks as measured in the wear tracks on the nickel coatings after fretting wear experiments at various temperatures. This plot shows that there is no apparent shift in the Ti $2p_{3/2}$ peak location throughout all but one of the experiments. In addition, the location of the peak (which is marked with a dotted line) defines the surface chemistry as TiO_2. The only noticeable differences in the spectra with varied temperature is that the 450°C wear tracks clearly have more TiO_2 present, and the room temperature

spectrum flattens and shifts slightly. This change in the room temperature spectrum is likely due to the large amount of loose debris that remained in the wear track after the experiment.

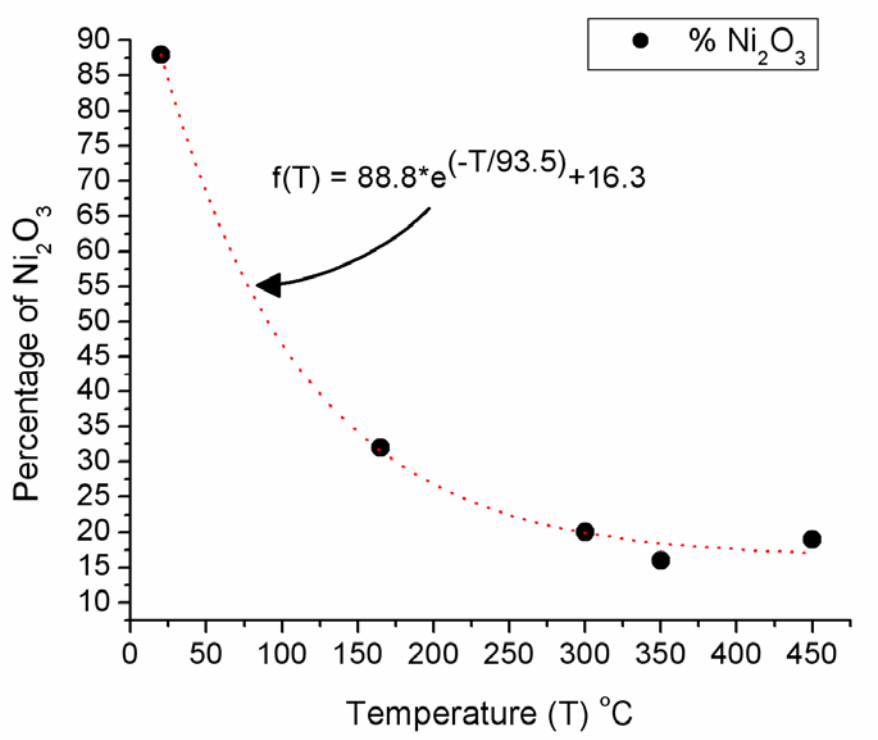

Fig. 6.18. The percentage of the total peak area under the O 1s peaks in Fig 6.17B that is from the Ni_2O_3 curve fit.

6.5 Discussion

The gross slip fretting wear experiments presented in this research show that increased temperature, up to 300°C, reduces the friction and wear between Ti6Al4V and the protective cold sprayed nickel coating. Fig 6.6 shows that the coefficient of friction between the mated surfaces reduces from 0.8 at room temperature down to a minimum of 0.3 at approximately 300°C. The fretting wear mode exhibited galling and titanium transfer to the nickel coating during the initial fretting cycles. Then, at room temperature

the galling products reduced to particulate debris and filled the wear track progressively over time. This caused a transition from an adhesive driven wear mechanism towards an interface where the surface damage was predominantly governed by the rheology of the trapped wear debris. Increased temperature promoted the formation of a smooth lubricious interface between the mated surfaces. XPS of the nickel coating wear tracks (Fig 6.19) showed that after 100 fretting cycles there was still a strong presence of nickel from room temperature up to 165°C. On the other hand, the 450°C experiments had a uniform oxide layer present in the wear track. It took at least 1,000 cycles to form a uniform oxide layer in the wear contact of the 165°C experiments, and at least 10,000 cycles in the room temperature experiments. In addition, Fig 6.18 shows that there is a decreased presence of Ni_2O_3 in the wear track at elevated temperatures. This could be the reason that the friction decreases with increased temperature. The presence of Ni_2O_3 in the wear track may act as gross surface defect in the structure of the formed NiO layer, which may inhibit the friction reduction capability of the more stable NiO film. From 165°C to 300°C, there is a significant reduction in the presence of Ni_2O_3 in the wear track. Above 300°C the surface chemistry in the contact does not change much. This clearly shows that the lowest friction is obtained at the point when a uniform NiO film is formed at the interface, with the least amount of Ni_2O_3 present.

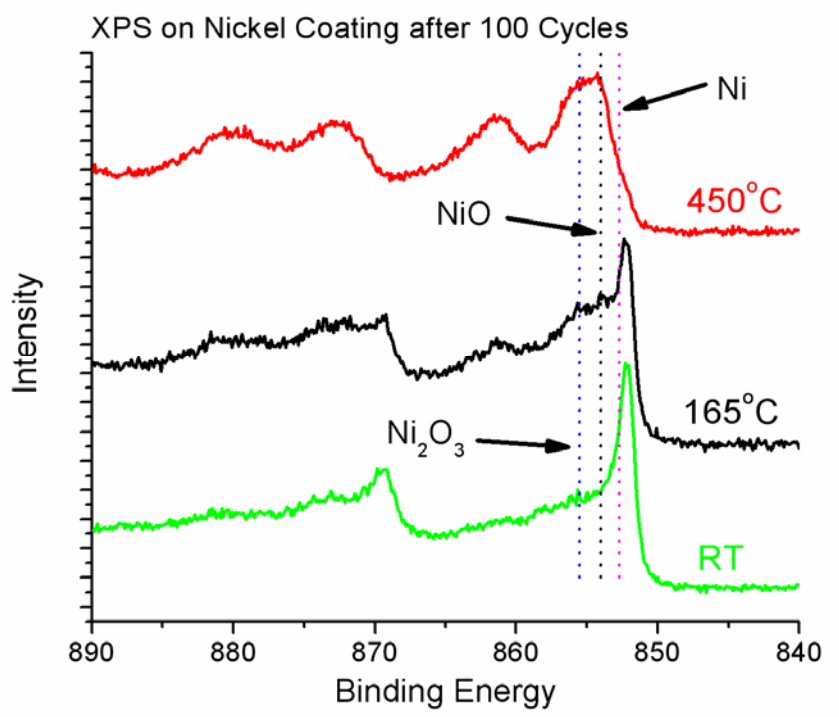

Fig. 6.19. High resolution XPS spectra of the wear track on the nickel coatings after 100 cycles at increasing temperature near the Ni 2p peaks.

Above 300°C the coefficient of friction steadily increased up to approximately 0.4, where the trend appears to be tapering off to a steady state value near 450°C. Fig 6.17 and 6.18 show that there was very little change in surface chemistry between 300°C and 450°C. However, micro and nano-indentation of the samples after the 450°C experiments yielded hardness values of 104 HV and 1.6 GPa respectively. This is approximately half the hardness of the as-sprayed coatings, as shown in Table 6.1. Because the cold spray process utilizes a high velocity particle jet, the coatings have a large amount of built up compressive stress. Above 300°C, the increased temperature begins to anneal these coatings and reduces the hardness to about half the initial as-sprayed value (at 450°C). It is

this reduction of hardness that likely increases the coefficient of friction, by promoting more surface deformation and potential ploughing within the fretting wear track.

In the literature, reviewed in Chapter 5, there is mention of a binary or double oxide that may form in the mixture of titanium and nickel oxides [100, 102]. This complex oxide is not well characterized and is defined as $NiTiO_3$ or nickel titanate. However, one XPS study of this complex oxide suggested that it has a Ni^{2+} peak at (854.8 eV) and a Ti^{3+} peak at (457 eV) [121]. The 854.8 eV peak would be located between the broad Ni $2p_{3/2}$ peaks that describe NiO and Ni_2O_3, and would be hard to identify in the presented spectra. However, the Ti $2p_{3/2}$ peak at 457 eV would be easy to see, but it is clearly not present in any of the spectra from the nickel surfaces. Therefore, there is no current evidence of the formation of this complex oxide in the XPS data obtained in this research.

6.6 Conclusions

This research was conducted to examine the effect of increased temperature on the wear mechanisms and interfacial chemistry associated with the gross slip fretting wear of Ti6Al4V mated with cold sprayed nickel wear protective coatings. It was found that increased temperature promoted the formation of NiO in the wear track, while decreasing the amount of Ni_2O_3. At elevated temperatures, the lowest friction occurred when a uniform film of NiO was formed in the wear track, with a minimal presence of Ni_2O_3.

At elevated temperature there was an apparent optimum friction and wear performance at approximately 300°C. Above 300°C, the compressive stresses built into the cold-sprayed nickel coatings began to anneal and soften the coating to half of its original hardness. This reduction in hardness likely caused the coefficient of friction to rise slightly at temperatures above 300°C.

For all temperatures tested, the wear mode during the initial fretting cycles was defined by adhesive wear and titanium transfer to the nickel coating. After the initial cycles, the temperature had a significant effect on the progression of the wear. At room temperature, debris formation and 3rd body wear dominated the surface degradation over time. As the temperature of the experiment was increased, the formation of a smooth NiO layer was observed. The oxide layer formation reduced the production of wear debris, and change the wear mode from an active 3rd body wear mode to one with the formation of a lubricious nickel and NiO based transfer film.

Chapter 7

THE MECHANISMS OF GROSS SLIP FRETTING WEAR ON NICKEL OXIDE/Ti6Al4V MATED SURFACES

7.1 Objective

The focus of this research was to determine the interfacial wear mechanisms associated with the fretting wear of Ti6Al4V and nickel oxide mated surfaces. Based on the formation of lubricious 'Glaze' layers, as described in the literature, the author of this work previously conducted gross slip fretting wear experiments using Ti6Al4V mated with commercially pure nickel cold sprayed coatings (as described in Chapter 6). It was found that the coefficient of friction was decreased at elevated temperatures, and that a protective nickel oxide transfer film had formed on the mated Ti6Al4V surfaces. In addition, x-ray photoelectron spectroscopy (XPS) analysis of the tribofilms suggested that a significant amount of Ni_2O_3 formed within the wear track at low temperatures. However, as the temperature was increased the Ni_2O_3 reduced to NiO until there was only ~15-20% present within the wear track. Interestingly, the friction reduction followed the reduction of Ni_2O_3 to NiO within the tribofilm.

In order to determine the significance of the reduction reaction (Ni_2O_3 to NiO) and to prove the tribo-sintering theory, nickel oxide films were grown with similar surface chemistry to that of the lubricious tribofilms formed on the cold sprayed nickel coatings at elevated temperatures, as described in Chapter 6. These thick nickel oxide surfaces were then tested under gross slip fretting wear conditions at room temperature (RT), 150°C, 300°C, and 450°C. The wear mechanisms and surface chemistry from this research are presented here in.

7.2. Tribological Testing

Gross slip fretting wear tests were conducted using Ti6Al4V ellipsoids mated with oxidized commercially pure nickel (Ni200) disks. A detailed description of the ellipsoid samples and the fretting wear test machine is given in Chapter 2. The Ni200 disks had a 25.4 mm diameter and were 3 mm thick. Prior to testing the surfaces of the disks were polished to a 5-10 nm Ra surface finish. The polished samples were then oxidized in an open air furnace for 100 hours at 1,000°C. This yielded a ~1 μm Ra oxide scale that was ~70 μm thick, and had a microhardness of ~420 HV. Cross-section and surface morphology of the nickel oxide scale are shown in Fig 7.1.

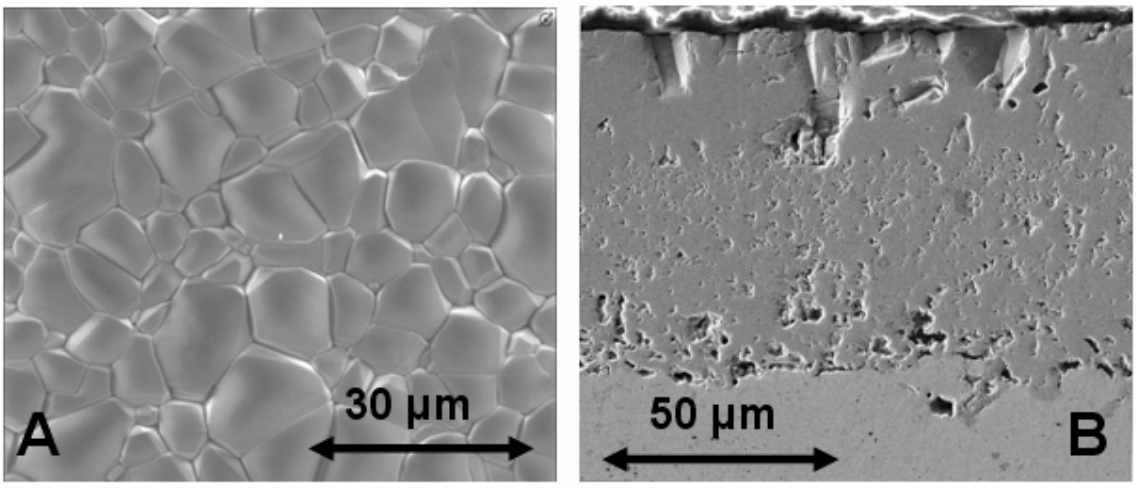

Fig. 7.1. Secondary electron SEM images of A) the surface of the oxide, and B) the cross-section of the oxide on the Ni200 sample.

The fretting wear experiments were conducted at room temperature, 150°C, 300°C, and 450°C with a 50 N normal load and a 250 μm stroke length. The 50 N load was chosen because it yields an approximate maximum Hertzian contact stress of 650 MPa, which is a typical contact stress in the dovetail bladed disk assemblies of interest. The 250 μm stroke length was chosen to induce gross slip fretting wear at the interface, and the

temperatures were chosen to determine the temperature effects on nickel oxide tribofilm formation and performance. In addition, short duration tests (e.g. 10, 100, 1000, and 10,000 cycles) were conducted at 2 Hz oscillation speed, and longer duration tests (100,000 cycles) were conducted at 30 Hz oscillation speed.

7.3. Surface Chemistry

Prior to tribological testing, the surface chemistry of the grown nickel oxide films was analyzed extensively using XPS, x-ray diffraction (XRD), and Raman spectroscopy. The coupled and decoupled XRD spectra are shown in Fig 7.2, both describe the surface as a crystalline NiO structure. Following the fretting wear tests, the unworn nickel oxide surfaces were analyzed using Raman spectroscopy and XPS. Fig 7.3 shows Raman data collected using a 514 nm laser source. The Raman data shows that the elevated temperature testing did not alter the surface chemistry or structure of the oxidized Ni200 surfaces. In addition, Fig 7.4 shows the Ni2p and O1s XPS peaks from high resolution scans on the unworn oxide surfaces after the elevated temperature tests as well. The XPS data shows that there is some Ni_2O_3 present in the surface oxide. The amount of Ni_2O_3 present was quantified by curve fitting the O1s peaks and recording the ratio of the area under the Ni_2O_3 peak, to the total area under both O1s peaks. This data is plotted in Fig 7.5, along with the same data that was measured within the wear tracks of fretting wear tests on the commercially pure cold sprayed Ni coatings that were tested in the previous Chapter. The XPS data shows that the surface chemistry of the oxide surfaces did not change while held at the fretting test temperatures, and that the oxide surfaces have the same chemistry as the lubricious oxide tribofilms that formed on the cold sprayed Ni coating surfaces at temperatures above 300°C (where the friction was the lowest).

Therefore, the author has grown an oxide of similar chemistry to the naturally forming nickel oxide tribofilms (as formed on the Ni coated surfaces), and maintained that chemistry at the tested temperatures.

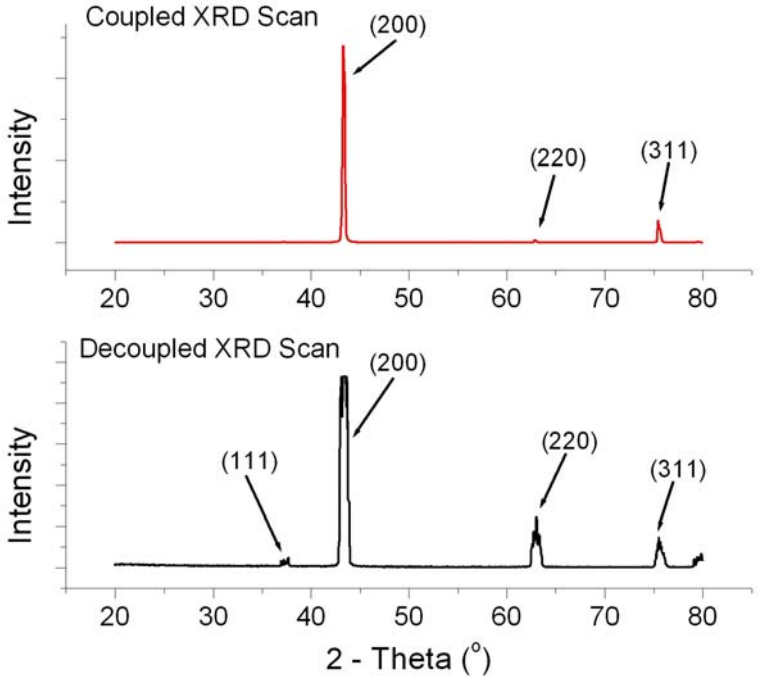

Fig. 7.2. Coupled and decoupled XRD scans of the oxidized surface prior to testing.

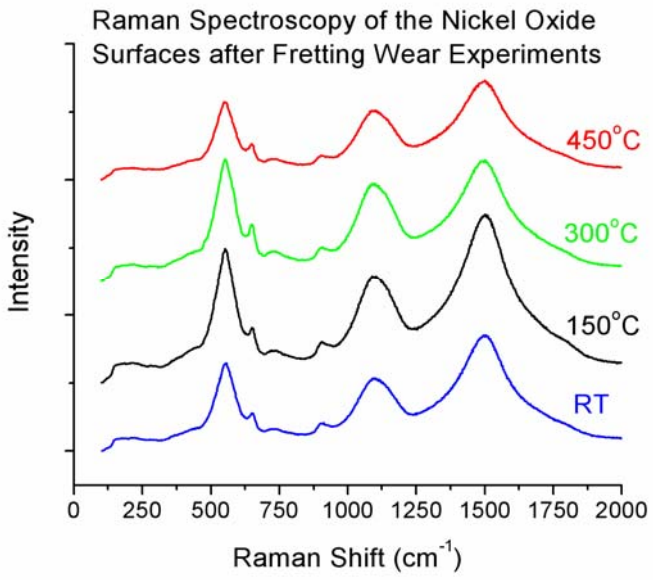

Fig. 7.3. Raman spectroscopy of the untested regions (outside the wear tracks) after the tests were conducted at the listed temperatures.

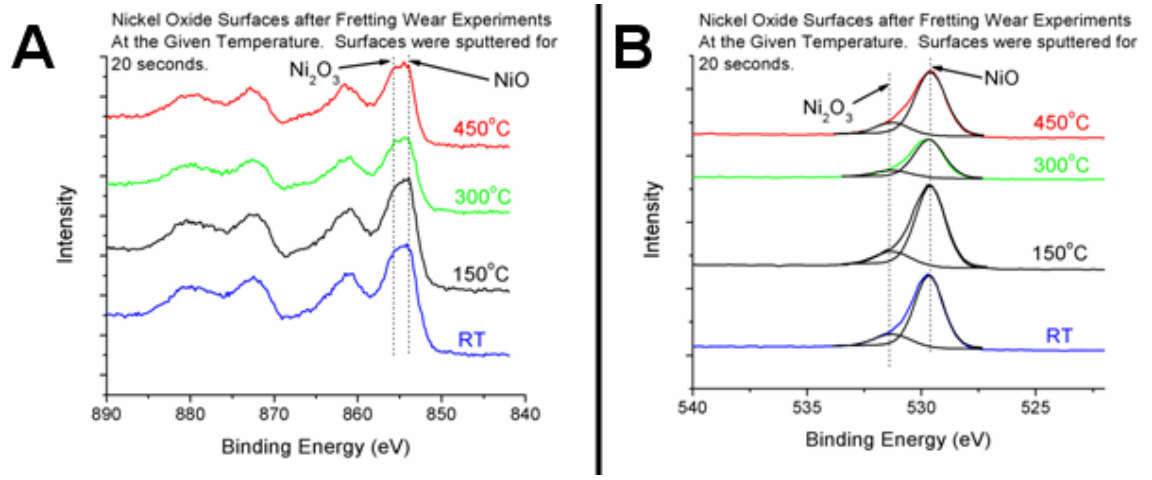

Fig. 7.4. XPS of the oxidized nickel surfaces (outside of the wear tracks), A) is the Ni2p peaks and B) is the O1s peaks with curve fits for the NiO and Ni_2O_3 binding energies.

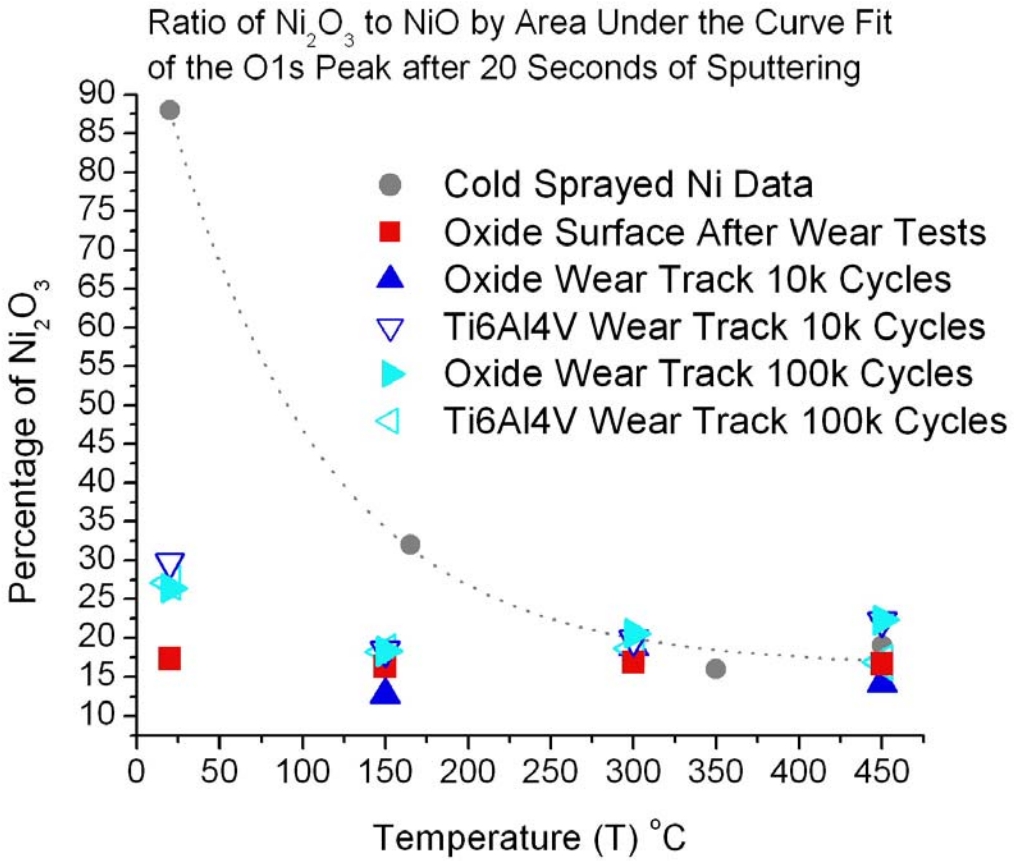

Fig. 7.5. Percentage of Ni_2O_3 as determined from XPS O1s curve fits.

Along with the analysis of the unworn oxide surface, XPS was also used to analyze the chemistry within the fretting wear tracks. Fig 7.6 shows the XPS scans from the wear tracks on the mated Ti6Al4V ellipsoid surfaces, after 100,000 fretting wear cycles. In these scans, and in all of the XPS scans within the fretting wear tracks, the O1s peaks were fit for NiO, TiO_2, and Ni_2O_3. This was done because there was some TiO_2 present within all of the wear tracks. The ratio of the areas under the Ni_2O_3 O1s peaks relative to the areas under the NiO O1s peaks were added to the plot in Fig 7.5. The compilation of all of this surface chemistry data (inside and outside of the wear tracks) shows that at elevated temperatures the chemistry of the oxide within the interface remains virtually unchanged. However, the room temperature fretting wear tests were the exception. The room temperature wear tracks had an increased presence of Ni_2O_3, which is a trend similar to what was seen in on the fretting wear of the Ni coating surfaces as well.

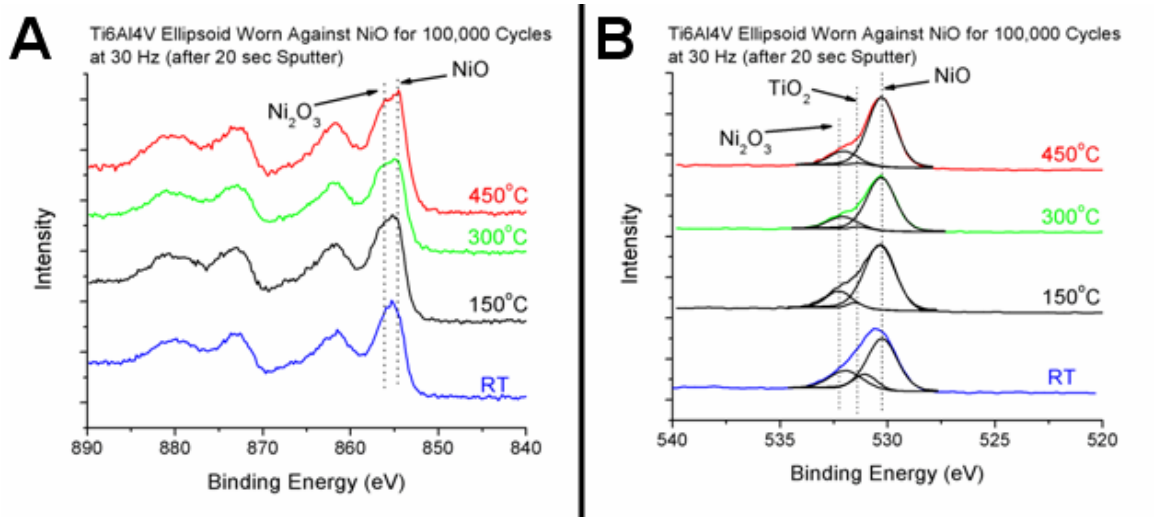

Fig. 7.6. XPS of the Ti6Al4V wear tracks that were worn against the oxidized nickel surfaces for 100,000 cycles, A) is the Ni2p peaks and B) is the O1s peaks with curve fits for the NiO, TiO_2, and Ni_2O_3 binding energies.

7.4. Friction and Wear Analysis

Upon the completion of all of the fretting wear tests, both the friction and the wear were analyzed. Fig 7.7 shows a plot of the typical root mean square (RMS) friction data that was recorded during the course of the fretting wear tests. Since the friction data reached a steady state value early in the test, the friction data from each test was averaged and then plotted in Fig 7.8. In addition, Fig 7.8 also shows the averaged friction data from similar experiments conducted on the commercially pure Ni cold sprayed coatings.

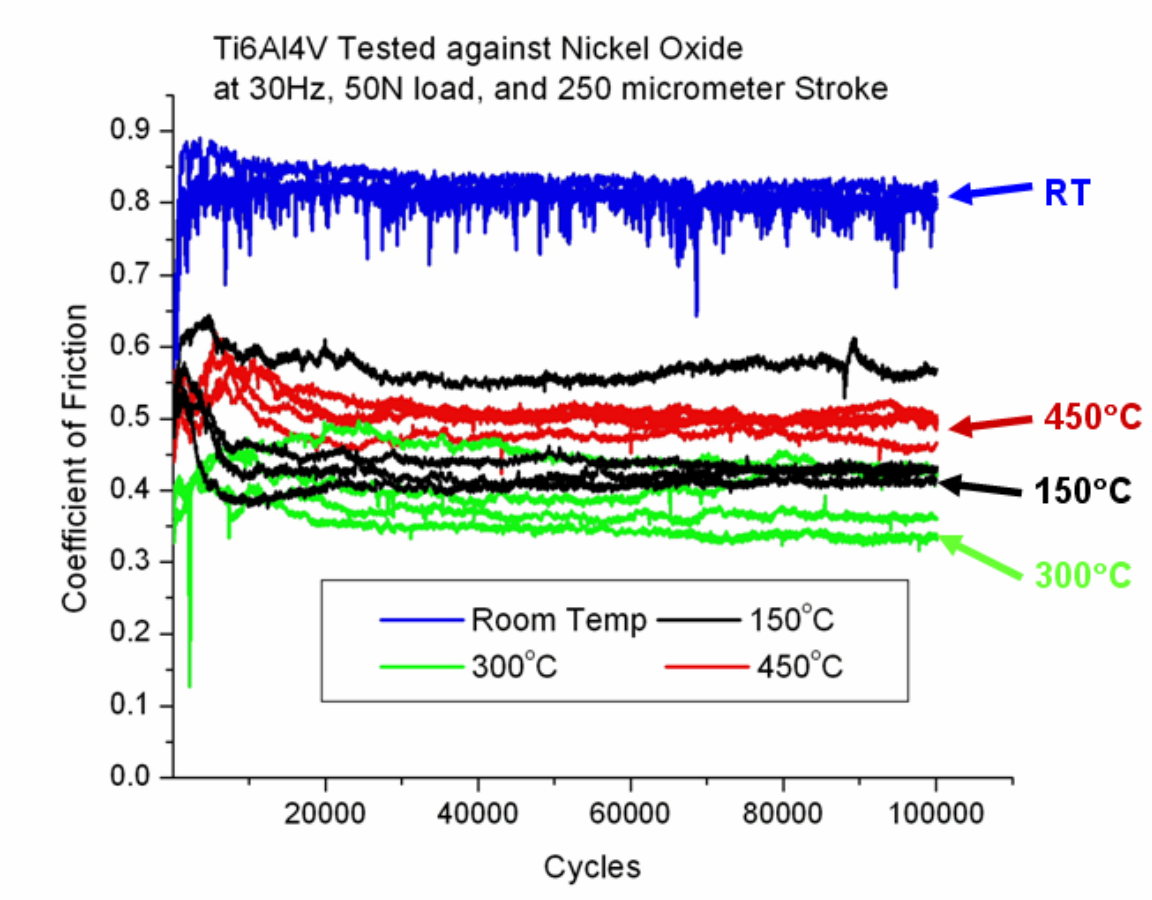

Fig. 7.7. RMS friction plots from the 100,000 cycles fretting wear tests.

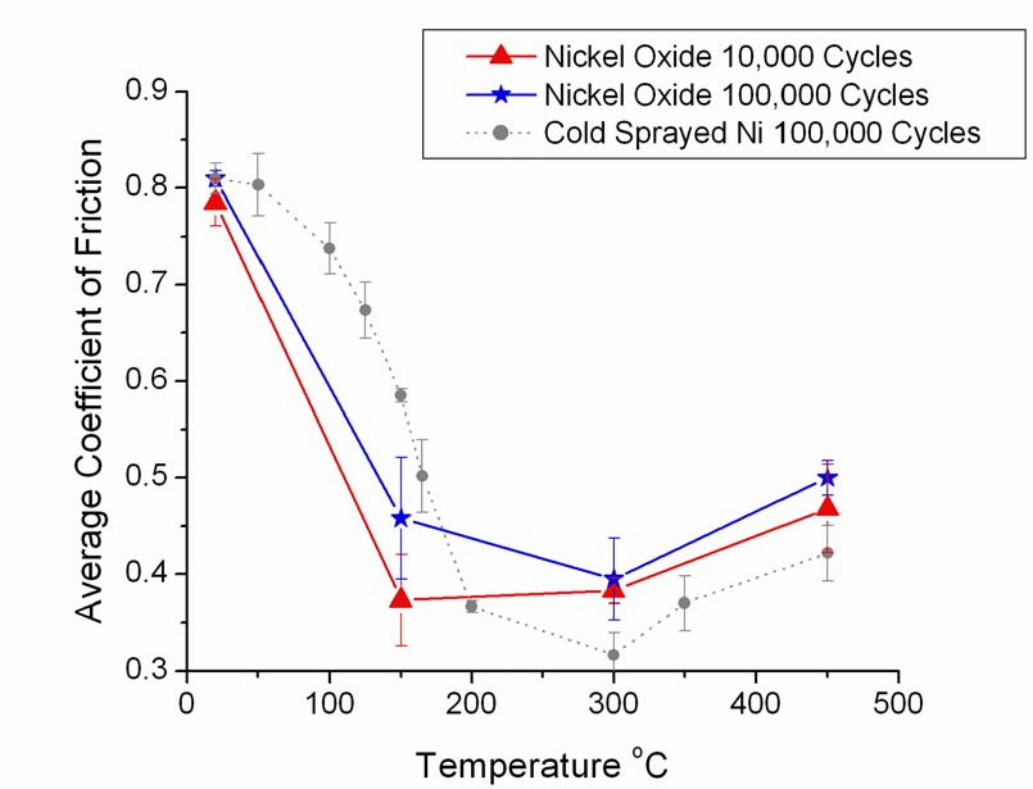

Fig. 7.8. Plot of the average RMS friction as measured during the 100,000 and 10,000 cycle tests.

The friction from the nickel oxide surfaces, tested at 30 Hz and 100,000 cycles, exhibited the same trend as the friction from the Ni coated surfaces. However, the friction at 150°C was significantly lower on the nickel oxide surface. In addition, it was found that at 150°C the friction was significantly lower in the tests conducted at 2 Hz for 10,000 cycles, in comparison to the tests conducted at 30 Hz for 100,000 cycles. At room temperature, 300°C, and 450°C, the coefficient of friction measured on the nickel oxide surfaces did not vary with oscillation speed.

Fretting wear tests at 2 Hz oscillation speed were conducted for durations of 10, 100, 1000, and 10000 cycles to facilitate wear evolution analysis of the Ti6Al4V and oxide surfaces. At room temperature 10 cycles of wear caused abrasive and adhesive

wear between the Ti6Al4V ellipsoid and the nickel oxide surfaces. In these wear tracks, large particles were removed from the Ti6Al4V ellipsoid surface and adhered to the nickel oxide surface. This caused adhesive wear to occur in the localized regions where titanium on titanium contact was facilitated by the adhered metallic particles. As the fretting wear continued from 10 to 100 cycles, the wear evolution continued via the same wear mechanisms. However, the continuous breakdown of the large titanium wear debris began to produce large quantities of trapped TiO_2 debris. The evolution of the oxidized wear debris particles caused a polishing type wear to occur on the nickel oxide surface. This polishing wear began to liberate fine debris particles from the nickel oxide surface. Due to the nature of fretting wear, large quantities of TiO_2 debris and nickel oxide debris were trapped within the interface. After 100 cycles, the wear track was almost completely filled with active oxide debris particles from both surfaces. Therefore, the interfacial damage that occurred between 100 cycles and 10,000 cycles, was controlled by the rheology of the trapped wear debris. The evolution of the fretting wear damage on the mated Ti6Al4V surfaces is shown in Fig 7.9.

At 150°C, the wear evolution on both the Ti6Al4V surface and the nickel oxide surface had a significant deviation from the mechanisms described at room temperature. The wear morphology on the Ti6Al4V surface at 150°C is shown in Fig 7.10. After 10 and 100 cycles of fretting wear at 150°C, the wear on both the Ti6Al4V and the nickel oxide surface were similar to what was seen at room temperature. However, the wear similarities began to differ as the fretting wear tests progressed. Between 100 and 1000 cycles, the fine nickel oxide debris (that remained trapped at the interface) began to sinter together into localized smooth pads throughout the wear track. Shown in Fig 7.10C, the

smooth tribofilm is the dark regions between the loose compacted debris that are shown as bright areas (due to charging). This sintering mechanism continuously occurred throughout the duration of the test. After a total of 10,000 cycles, the fretting wear track on the Ti6Al4V surface (as shown in Fig 7.10D) was covered with large smooth platelets of sintered nickel oxide. The continuous formation and deformation/degradation of these platelets created a nickel oxide tribofilm on the mated Ti6Al4V surface, and reduced the friction and wear at the interface by shear accommodation. The tribofilm formation on the mated Ti6Al4V surface completely covered the contact area, and filled in regions where damage had previously occurred. This prevented the continued progression of wear on the Ti6Al4V surface.

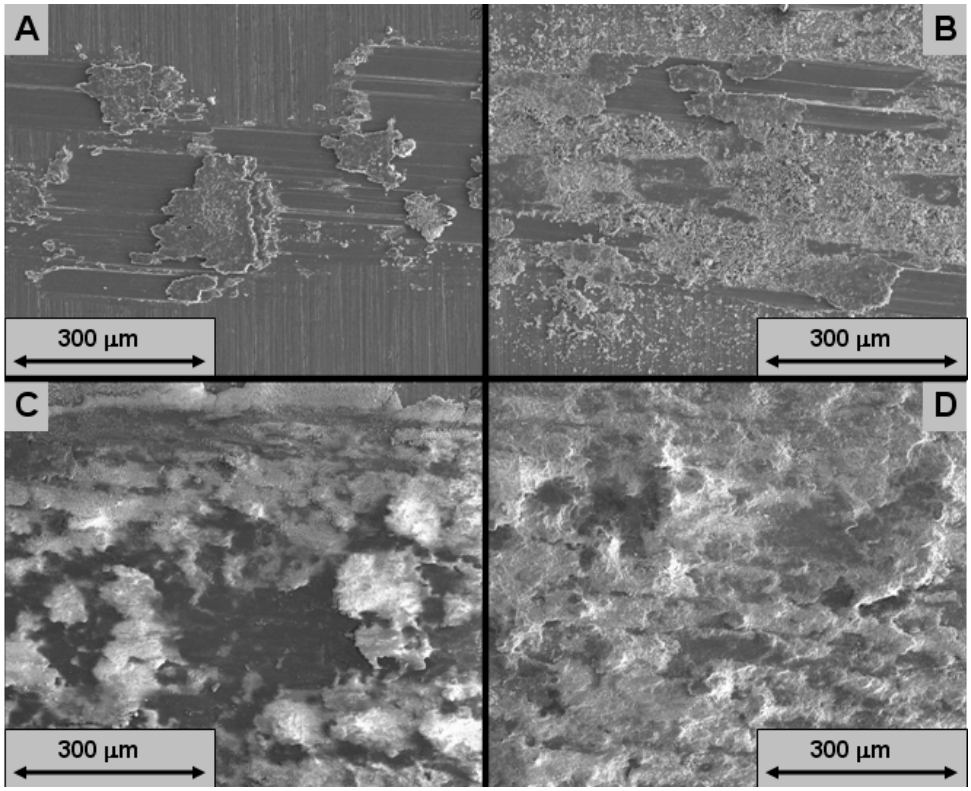

Fig 7.9. Wear progression on the Ti6Al4V surface after A) 10, B) 100, C) 1,000, and D) 10,000 fretting wear cycles at RT.

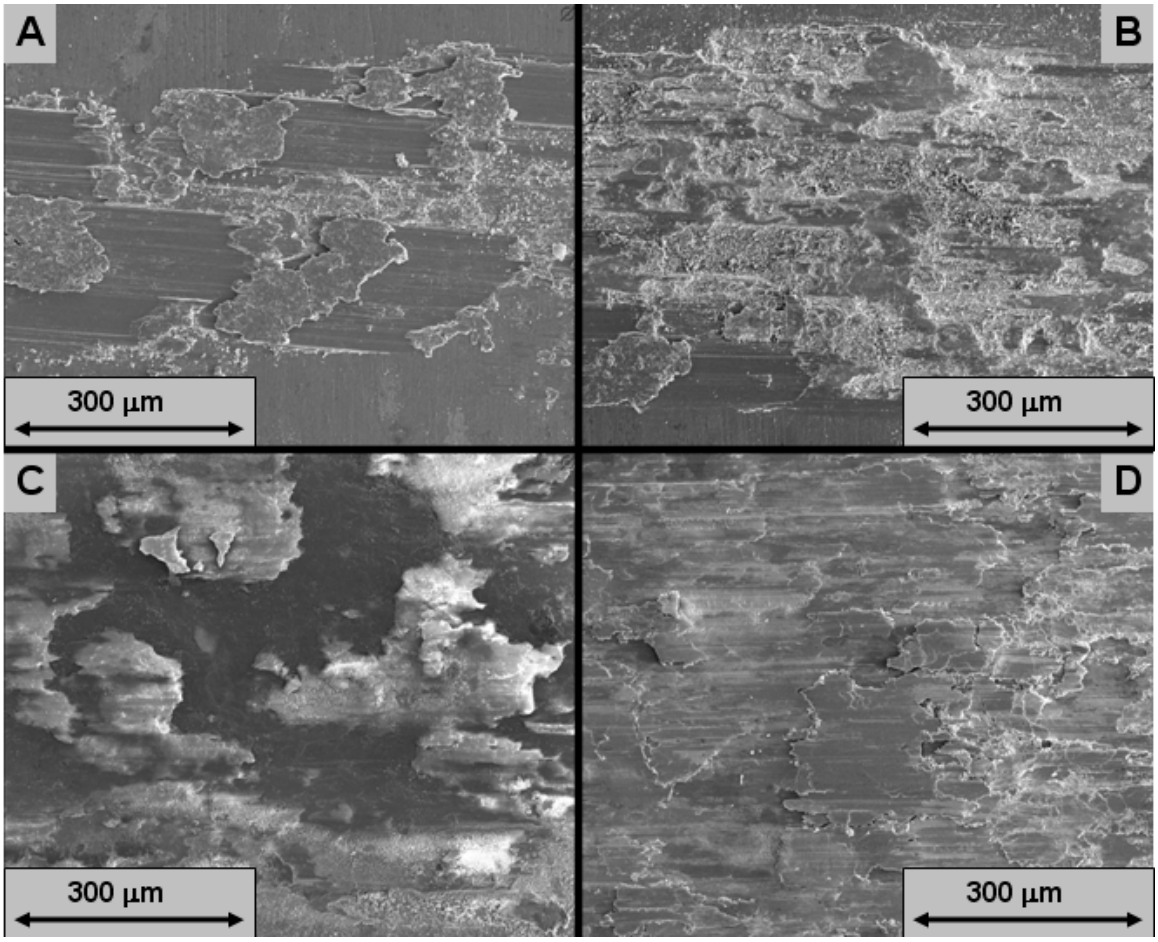

Fig 7.10. Wear progression on the Ti6Al4V surface after A) 10, B) 100, C) 1,000, and D) 10,000 fretting wear cycles at 150°C.

Although the coefficient of friction increases slightly at 300°C and 450°C, in comparison to 150°C at 2 Hz, the wear morphology of the interface was similar. The wear on the Ti6Al4V surface went through the exact same wear progression after 10 and 100 cycles, and then evolved as the nickel oxide particles sintered into lubricious platelets at the interface. In addition, increased temperature created thicker tribofilms on the mated Ti6Al4V surfaces. This enhanced the wear protection on the Ti6Al4V surface, even though the measured friction was slightly increased. Fig 7.11 shows the similarity of the smooth nickel oxide tribofilm platelets formed on the mated Ti6Al4V surfaces

after 10,000 fretting wear cycles at 150°C and 450°C.

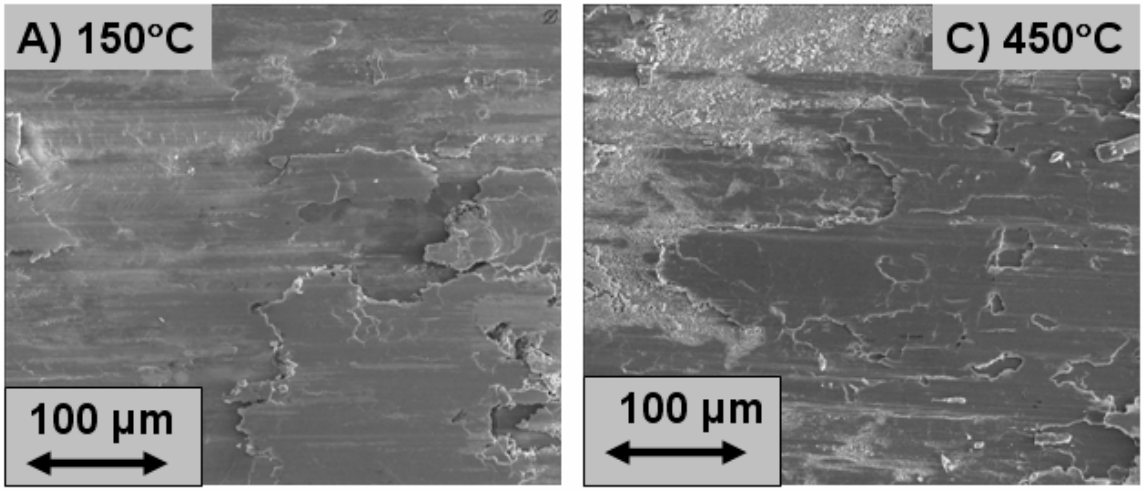

Fig 7.11. Wear on the Ti6Al4V surface after 10,000 fretting wear cycles at the 150°C and 450°C.

Once the wear evolution was identified, extended fretting wear tests were conducted at 30 Hz for 100,000 cycles. These tests yielded similar friction and wear evolution as compared to the slower 2 Hz fretting tests, with the exception of 150°C. At 150°C, the increased oscillation speed increased the shear rate such that stable tribofilms were not maintained throughout the wear track. However, there was evidence of small localized patchy tribofilms, surrounded by large quantities of loose wear debris. This follows directly with the sintering process in that the densification rate is dependant on time, pressure, temperature, particle size, and grain size. If all else is held constant, the order of magnitude speed increase at 30 Hz, reduced the amount of time that the particles are compacted in a given shear direction. In addition, the higher speed also aids in the breakdown of any partially sintered tribofilms that may have formed within the contact.

7.5. Tribofilm Structure

The tribofilms that formed on the mated Ti6Al4V surfaces were analyzed with XPS, SEM, and high resolution transmission electron microscopy (HRTEM). The surface chemistry of the tribofilms was described by XPS as being composed of mostly NiO with some Ni_2O_3 and TiO_2. From the XPS survey scans, the TiO_2 composition of the tribofilms on the mated Ti6Al4V wear tracks were plotted in Fig 7.12. The TiO_2 composition shows that at elevated temperature, the tribofilms were protecting the Ti6Al4V surfaces more effectively by covering the wear track and accommodating the interfacial shear. If further damage was accumulated on the Ti6Al4V surfaces, more titanium oxide would be present within the chemistry of the worn surface. There was no evidence of metallic titanium within the wear tracks.

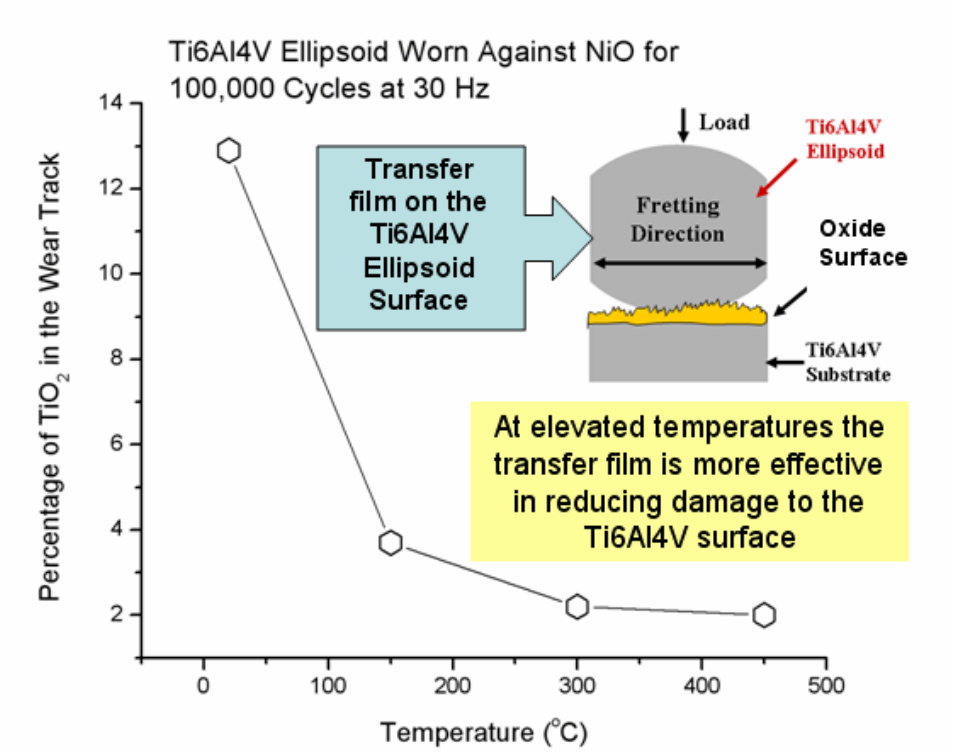

Fig. 7.12. Plot of the TiO_2 composition of the tribofilms formed on the Ti6Al4V worn surfaces.

In addition to the XPS analysis, a focused ion beam (FIB) microscope was used to make a thin TEM sample of the tribofilm for HRTEM analysis. Fig 7.13 shows the surface of a 2 μm thick tribofilm formed on the Ti6Al4V surface after 100,000 cycles of fretting at 450°C. In addition to the generation of the sample with the FIB, nano ion milling (with 900 V and 200 μA per micron size area) was used to clean the sample prior to HRTEM imaging. Fig 7.14 shows the HRTEM images of the nanocrystalline tribofilm structure. The images show that the nanocrystalline grain size is in the range of 5-20 nm, which is in agreement with the structure that has been identified by Inman et al for tribofilms formed on nickel alloy Nimonic 80A at 750°C [86,88]. Selected area diffraction, shown in Fig 7.15, exhibited rings that define the oxide structure as face centered cubic (fcc).

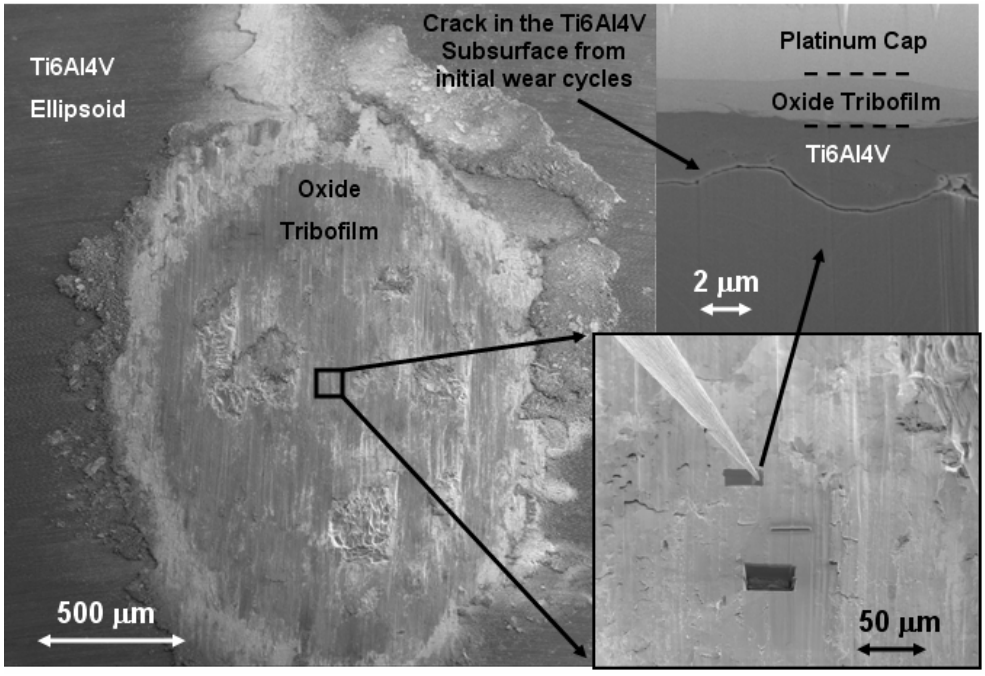

Fig. 7.13. SEM images of the tribofilm formed on the Ti6Al4V surface after 100,000 cycles of fretting at 450°C. The side images show the FIB cross-section that was ion milled out of the wear track.

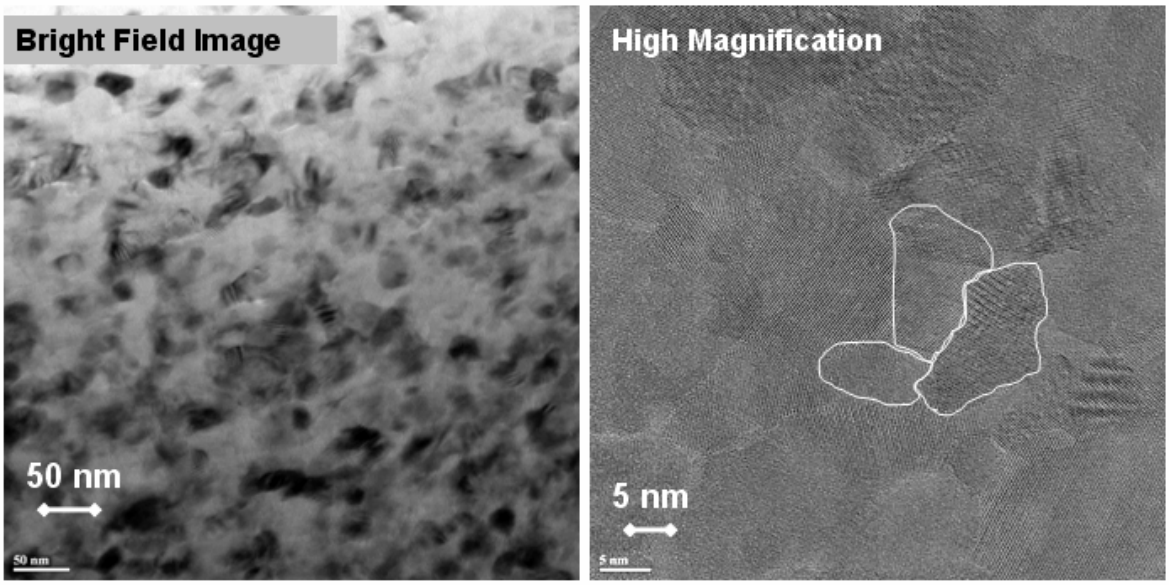

Fig. 7.14. HRTEM images of the tribofilm formed on the Ti6Al4V surface after 100,000 cycles of fretting at 450°C.

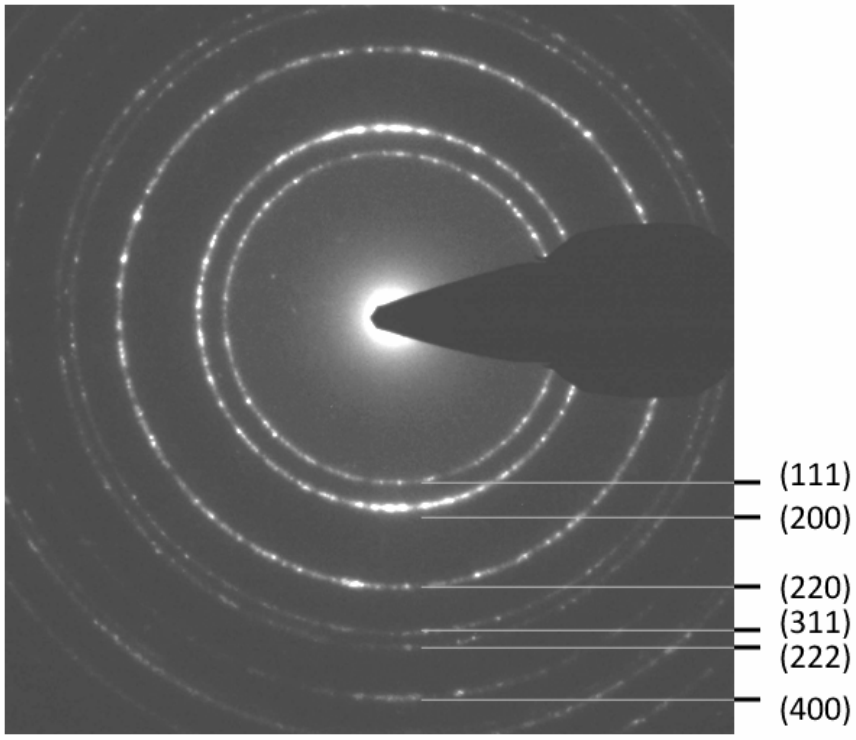

Fig. 7.15. Selected area diffraction of the tribofilm formed on the Ti6Al4V surface after 100,000 cycles of fretting at 450°C. This shows the rings for the nickel oxide structure.

7.6. Discussion

Tribo-sintering is a recent term that has been used to describe the formation of many tribofilms within the wear tracks of elevated temperature experiments. Adachi et al observed a pressure and temperature dependence with tribofilm formation (via tribo-sintering) on worn alumina surfaces [122]. In addition, Kato et al found that for various oxides and particles sizes from 30 nm up to 1 μm, tribo-sintering can occur over extended sliding distances, even at room temperature [123]. Kato et al noted that for smaller particle sizes, tribo-sintering occurred over shorter sliding distances and with less applied normal load. Fig 7.16 shows the friction and wear morphology of the nickel oxide surface after 10,000 cycles of fretting at room temperature. Once the 10,000 cycles were completed, the test was stopped and unloaded. The samples were left in contact (unloaded) while they were heated to 450°C. Once the temperature of 450°C was achieved, the normal load was reapplied and the fretting wear test was continued for another 10,000 cycles. This test demonstrated that once the surfaces had formed fine nickel oxide debris within the contact, the combination of temperature and pressure can sinter these particles together into lubricious tribofilms. Fig 7.17 shows high magnification images of the tribofilm morphology. It is important to note that the debris that made up the compacted film is shown as submicron particles. Interestingly, the tribofilm formed in the debris bed at 450°C exhibited a coefficient of friction of 0.4. This friction is much lower than the friction coefficients measured in the previous 450°C experiments, and is within the error of the minimum friction that was measured in the low speed 150°C experiments.

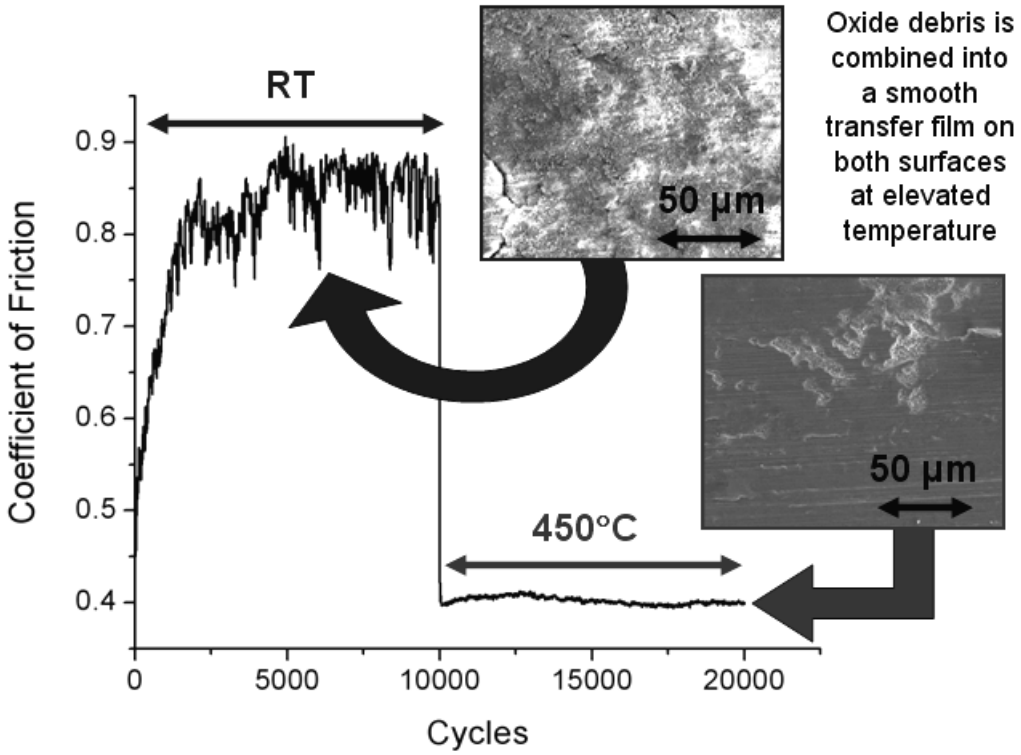

Fig 7.16. Friction and wear track morphology from room temperature debris formation and 450°C tribo-sintered nanocrystalline tribofilm.

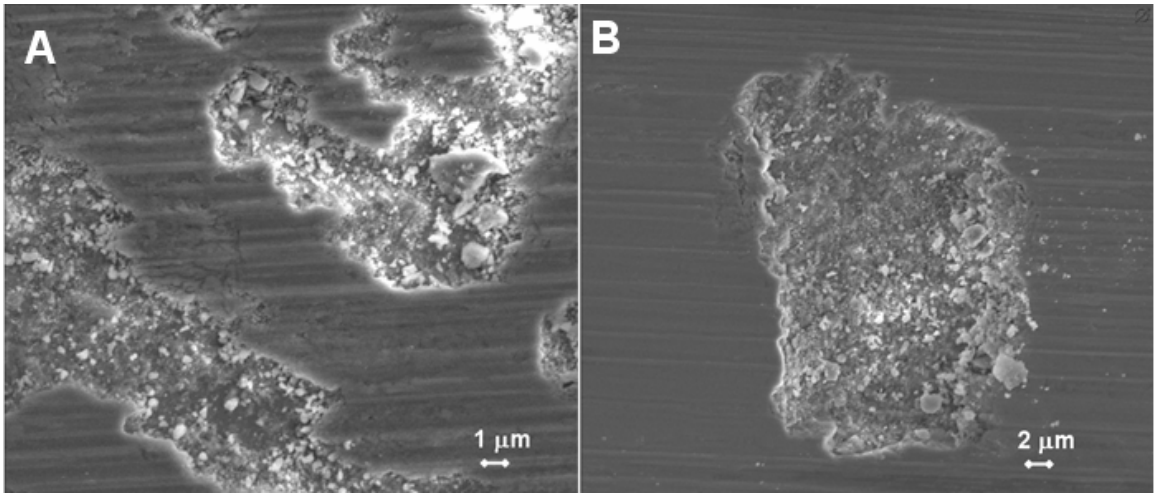

Fig 7.17. SEM images of the tribofilms formed on A) the oxide surface and B) the ellipsoid surface after the test conducted in Fig 7.16.

The low friction and wear exhibited in the aforementioned two phase test can be explained by the structure of the thick oxide films, and the wear morphology of the oxide

surfaces. Rhines et al studied the growth of nickel oxide on pure nickel (Ni270) at 1,000°C [124]. From there work it was determined that nickel oxide grows as large columnar void free grains. These grains stretch from the metal/oxide interface to the gas/oxide interface. After approximately 16 hours, the oxidation rate decreases and a new equiaxed fine grain structure begins to grow adjacent to the metal/oxide interface. This growth is typically called 'undergrowth', and has been documented in a number of nickel oxidation studies. Continued oxidation extends the fine 'undergrowth', while leaving a ~20 μm thick coarse grained columnar surface structure. The columnar layer in the oxide samples for this work had grains that were approximately 20 μm tall and approximately 10 to 20 μm in width. Many polycrystalline oxides do not have enough primary slip systems to accommodate large deformations, and the amount of stress required to activate secondary slip systems is often more than the amount of stress required to initiate a crack (below transition temperatures) [125]. It is this reason that the columnar micro-grained nickel oxide structure is unable to accommodate the deformation imposed by the fretting wear of the mated Ti6Al4V and the trapped wear debris at low temperatures. Therefore, fine wear particles are easily liberated from the nickel oxide surfaces through a polishing type wear mechanism with the trapped TiO_2 and nickel oxide debris. For a given speed: elevated temperature, pressure, particle size, and grain size facilitate the formation of the nanocrystalline tribofilm via tribo-sintering. Once formed, the nanocrystalline tribofilms have an increased plasticity due to the evolution from an intragranular dislocation-based deformation to a grain boundary sliding and/or grain rotation based deformation [126].

Nanocrystalline oxides have been shown to exhibit high plasticity and low

friction, even at low temperature. Work by Prasad and Zabinski et al showed that nanocrystalline ZnO films yield friction coefficients lower than 0.2 at room temperature, with little wear [127-130]. Bulk ZnO surfaces that were hot pressed, had limited plasticity and exhibited friction coefficients of 0.6 to 0.7. Romanes et al more recently showed that nanocrystalline columnar ZnO oxide structures deform in the wear track, and yield very low friction with minimal wear [131].

Once the nanocrystalline tribofilms were formed (at 150°C for 2 Hz oscillation and 300°C for 30 Hz oscillation), the coefficient of friction increased slightly with temperature, as shown in Fig 7.8. This increase in friction was followed by an increase in wear of the nickel oxide surface, as shown in Fig 7.18. The proposed mechanism for the increased coefficient of friction and wear is based on an increased plasticity of the columnar exterior of the grown oxide scale. Fig 7.19 and Fig 7.20 show the morphology of the nickel oxide wear tracks after 100 cycles of fretting wear at 150°C and 450°C, at 2 Hz oscillation speed. At 150°C, the wear morphology of the oxide surface exhibited a smooth wear track with minimal oxide deformation. The interface appeared to have experienced a form of polishing wear, combined with the inception of tribofilm formation. At 450°C, the wear morphology is much different. In contrast, the oxide wear track shows severe plastic deformation and wear. Fig 7.21 shows the Ti6Al4V wear tracks that were mated with the worn oxide surfaces shown in Fig 7.19 and Fig 7.20. At 150°C, there was a large quantity of very fine wear debris, on the order of 1 to 2 μm in size, adhered to the mated Ti6Al4V surface. In addition, there were patches of localized tribofilm formation (shown as smooth islands in Fig 7.21A). At 450°C, the

mated Ti6Al4V surface yielded very large wear debris particles, approximately 10 to 20 μm in size, which surrounded localized patches of smooth tribofilm formation. Since the formation of the tribofilm is governed by the size of the debris particles, the large wear debris exhibited at 450°C would need to be broken down further before the sintered tribofilm can form in the wear track.

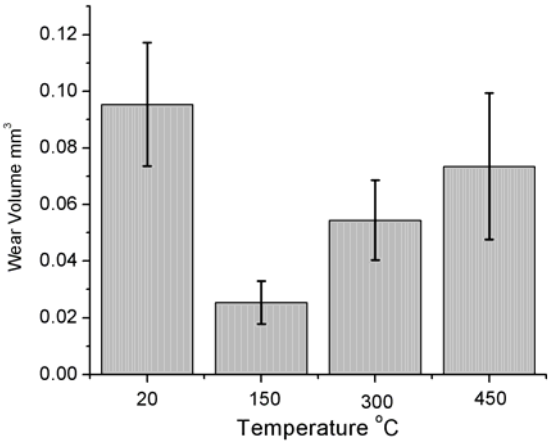

Fig 7.18. Wear volume measured on the nickel oxide surfaces after 100,000 fretting wear cycles.

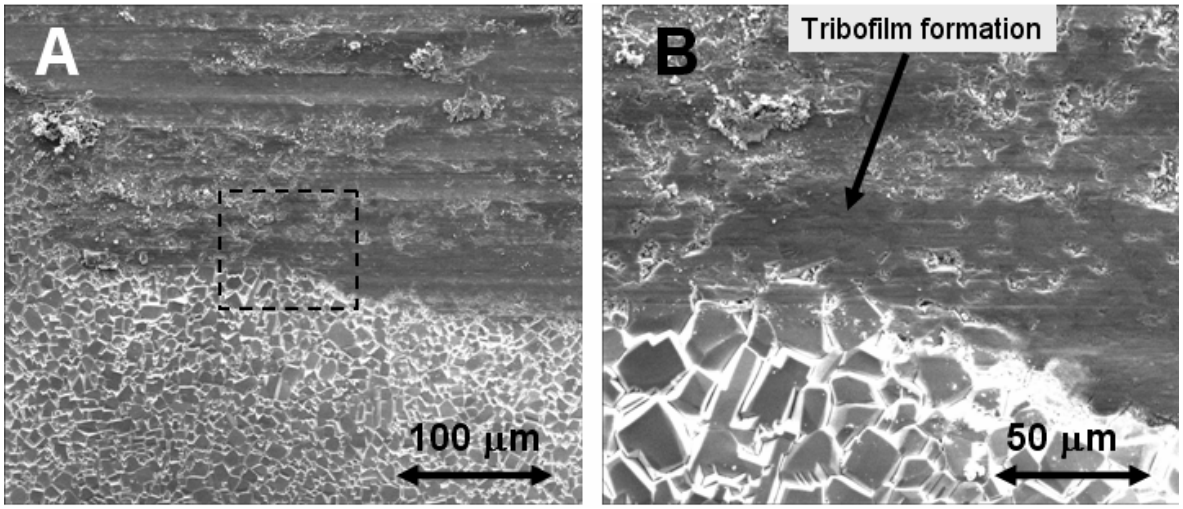

Fig. 7.19. Wear morphology of fretting wear on the nickel oxide surface after 100 cycles at 150°C. B) is the zoomed image of the area outlined by the box in A).

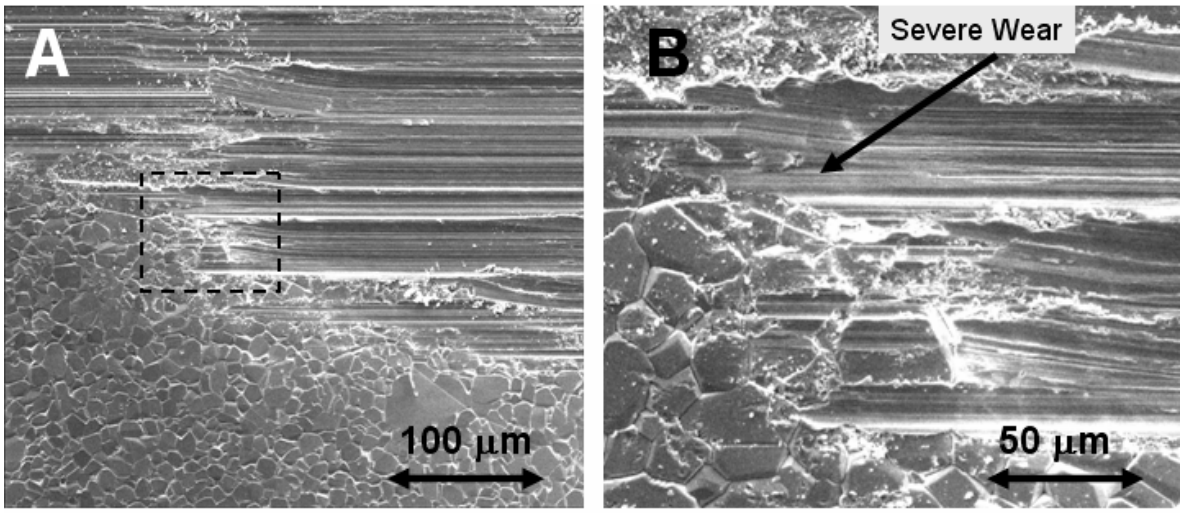

Fig. 7.20. Wear morphology of fretting wear on the nickel oxide surface after 100 cycles at 450°C. B) is the zoomed image of the area outlined by the box in A).

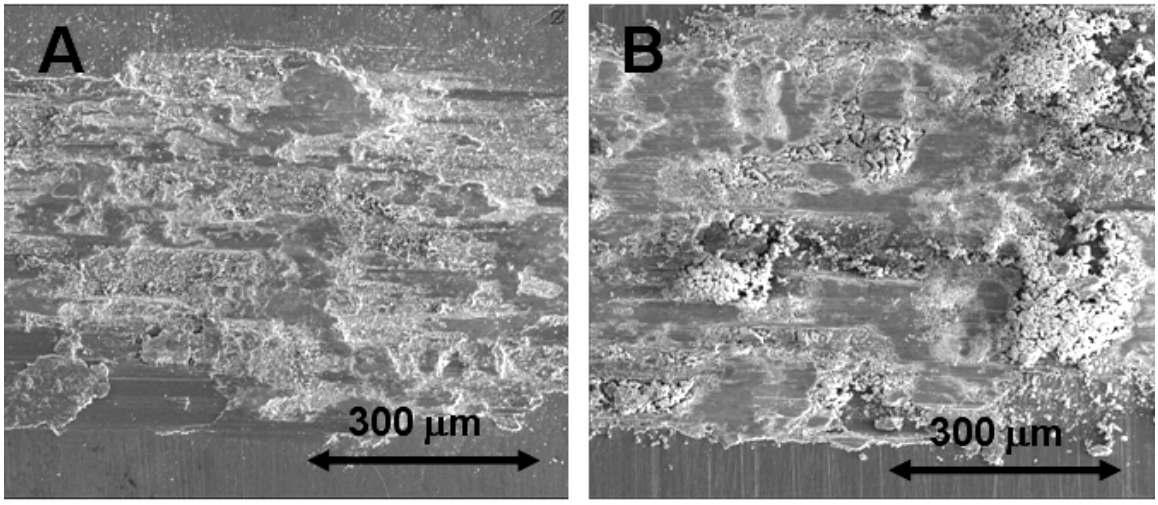

Fig. 7.21. Wear morphology of fretting wear on the Ti6Al4V surface after 100 cycles at A) 150°C. and B) 450°C.

The increased friction and wear at elevated temperatures was caused by a competition between the wear and plastic deformation of the oxide surface, and the refinement of the wear debris into a lubricious nanocrystalline tribofilm. Nickel oxide is a soft transitional metal oxide. In this work the microhardness was measured to be approximately 420 HV. However, the indents were made on the cross-section of the

thick fine grained equiaxed structure. Zambelli et al conducted room temperature erosion studies of nickel oxides grown Ni200 surfaces after 72 hours of oxidation at 1,000°C in air [110]. They concluded that the erosion of the columnar surface layer yielded plastic deformation with some cracking, where as the equiaxed sub layer yielded only elastic deformation followed by brittle fracture. This suggests that the columnar layer is softer than the equiaxed sub layer. In addition, Evans et al showed that there is a brittle to ductile transition on bulk nickel oxide surfaces above 400°C (as shown in Fig 7.22) [138]. Therefore, the softer columnar structure exhibited enhanced plasticity at 450°C. This lead to the increased wear of the oxide surface (at elevated temperatures), and the production of large nickel oxide wear particles. Once formed, the large wear particles must be broken down into finer debris before they can be sintered into a lubricious tribofilm. This is why the friction and wear was much lower at 450°C in the test conducted in the debris bed formed by 10,000 cycles of fretting at room temperature. In this test, there was a ready supply of submicron particles to be sintered into a nanocrystalline tribofilm. In addition, the rheology of the debris bed was such that a flat continuous contact was made while the tribofilm was formed. This allowed for the formation of a smooth continuous tribofilm. Once a continuous film was formed, the friction and wear was similar to that of the 2 Hz tests conducted at 150°C. Therefore, the increased friction and wear at elevated temperatures was created by the wear of the bulk nickel oxide and the formation of the tribofilm, not from the tribofilm itself.

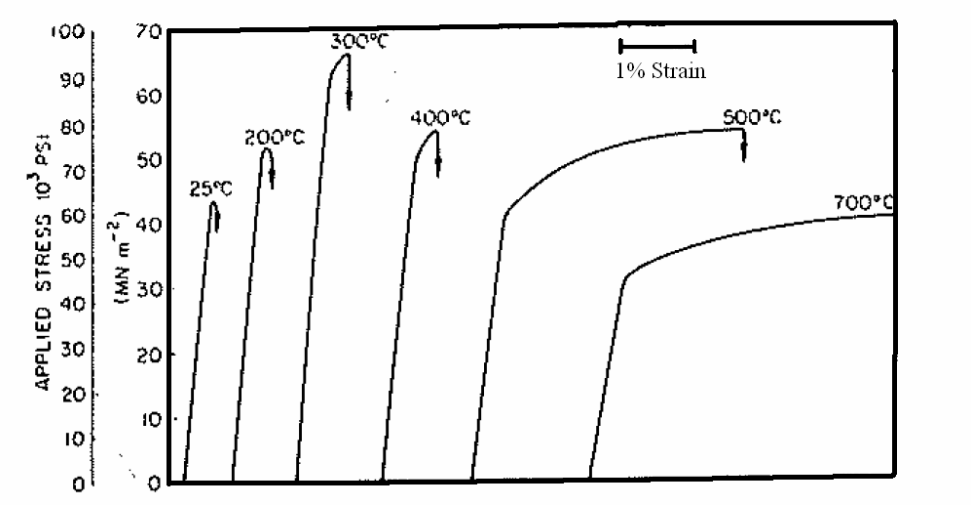

Fig. 7.22. The stress-strain characteristics of 99.5% dense nickel oxide, for a range of temperatures [138].

Tribofilm formation via tribo-sintering of fine oxide wear particles, as described in this work, also helps to shed light on the conclusions of Sullivan et al from their work with the severe to mild wear transition of steel surfaces at elevated temperatures [132]. In their work, Sullivan et al concluded that the transition to mild wear was facilitated by the formation of a smooth iron oxide tribofilm. However, there was no observed benefit from preoxidizing the steel prior to testing. This was because the natural oxide does not form with grains small enough to facilitate grain boundary sliding and grain rotation. Therefore, the micrograined structure will be worn away and broken up into fine submicron particles. These particles are then reformed into a nanocrystalline tribofilm that can reduce friction through the inception of grain mobility.

7.7. **Summary and Conclusions**

The objective of this work was to determine the mechanisms of tribofilm formation during the gross slip fretting wear of Ti6Al4V and a thick nickel oxide film. It has been shown that lubricious nanocrystalline tribofilms were formed in the fretting

wear contact via a tribo-sintering mechanism. At all temperatures the wear primarily occurred on the mated Ti6Al4V surface during the first few fretting wear cycles. At low temperatures, the Ti6Al4V wear debris facilitates a polishing type wear on the nickel oxide surface, which created and trapped fine nickel oxide debris within the contact. A speed dependence on tribo-sintering allowed for tribofilm formation at 150°C with 2 Hz oscillation speed. At 30 Hz oscillation speed, 150°C was not hot enough to facilitate the formation of a continuous tribofilm with in the fretting wear contact. At elevated temperatures the tribofilm formation continued to protect the mated Ti6Al4V surfaces. However, the friction and wear of the nickel oxide surface increased with temperature. The increase in friction was due to the enhanced plasticity of the nickel oxide surface at elevated temperatures, which created larger wear particles within the fretting wear interface. These large particles impeded tribofilm formation, while the interfacial shear was accommodated by the competition between the deformation/wear of the soft oxide surface and the localized formation of lubricious nanocrystalline tribofilms. In addition, the surface chemistry showed that the fretting wear tracks maintained the same amount of Ni_2O_3 at all temperatures, except room temperature. At room temperature, there was a 10% increase in the Ni_2O_3 content. However, the room temperature tests did not yield lower friction than the room temperature tests on the cold sprayed Ni coatings, even though the Ni_2O_3 content was much lower. Therefore, these experiments suggest that the temperature and speed at which the fretting wear experiments were conducted, have more influence on the tribofilm formation than the Ni_2O_3 content.

Chapter 8

THE USE OF NICKEL GRAPHITE COMPOSITE COATINGS FOR THE MITIGATION OF GROSS SLIP FRETTING WEAR ON Ti6Al4V INTERFACES

8.1 Objective

Chapter 6 focused on the fretting wear of commercially pure nickel coatings, and Chapter 7 focused on the fretting wear of thick nickel oxide films. From the work in these two chapters, it has been concluded that nickel oxide tribofilms can form thick transfer layers on the surfaces of the mated Ti6Al4V surfaces. Even at 30 Hz oscillation speed, nickel oxide tribofilms can provide low friction and protect the mated Ti6Al4V surfaces from wear at and above 300°C. However, Ti6Al4V compressor blade dovetail joints must be able to survive cold start up. This means that the coatings applied to the dovetail surfaces, must provide wear protection at low temperatures as well as at high temperatures.

Using the knowledge base that has been developed, a new mitigation strategy for the amelioration of fretting wear in Ti6Al4V dovetail joints was developed. This new strategy was based on the high temperature potential of nickel coatings to produce lubricious oxide tribofilms and the low temperature use of graphitic solid lubrication to prevent galling at the metallic interface over a broad temperature range. Graphite based solid lubricants are often bound using a silicate and applied to the surface of the plasma sprayed CuNiIn or Al-bronze coatings that are currently used to mitigate fretting wear of Ti6Al4V compressor bladed disk assemblies. In this work, the graphite was imbedded within thermal sprayed nickel coatings to create a self lubricating composite surface. This composite would then negate the need for a bonded solid lubricant on the surface of the coating, while providing wear protection of the Ti6Al4V surfaces at elevated temperatures.

8.2 Tribological Testing and Analysis

The specimens used for this research were Ti6Al4V, and the test geometry was an ellipsoid on a flat plate, as explained in detail in Chapter 2. The plates were flat circular disks with a diameter of 12.7 mm on the test face and 3.2 mm thick. Average surface roughness (Ra) was 0.1 μm on both the disk and the ellipsoid. Prior to testing, the Ti6Al4V disks were commercially grit blasted and then plasma sprayed with the Ni based coatings. For proof of concept, nickel graphite abradable coatings were also applied to a few Ti6Al4V substrates. Abradable coatings are designed for low friction and high wear. Therefore, they are flame sprayed porously and have approximately 50% graphite powder in the pre-spray mixture. In addition to the abradable nickel graphite (NiG-A) coatings and the commercially pure thermal sprayed Ni coatings, a set of plasma sprayed coatings were made with approximately 5%, 10%, and 20% (by volume) of graphite powder in the pre-spray coating mixture. These coatings were made to determine the graphite concentration required to get low friction and low wear, as compared to the NiG-A and Ni coatings.

The flat disks and thermal sprayed Ni based coatings were used to simulate the surface of the blade dovetail, and the uncoated Ti6Al4V ellipsoids were used to simulated the surface of the slotted disk the in bench level fretting wear experiments. The properties of the Ti6Al4V substrates and the commercially pure thermal sprayed Ni coatings are listed in Table 8.1.

The purpose of this work was to analyze the fretting wear of Ti6Al4V coupled with nickel graphite composite thermal spray coatings, and subjected to gross slip fretting wear at room temperature and 450°C. The room temperature tests were conducted to simulate cold engine startup, and the 450°C experiments were conducted to mimic the highest

temperature that Ti6Al4V might be subjected to within an aircraft engine. Three to four repeat tests were conducted on each coating. The tests were conducted using a 200 μm stroke length, 30 Hz oscillation speed, and a 50 N normal load for 100,000 cycles. In addition, shorter duration tests were conducted at 2 Hz oscillation speed, to supplement the longer tests for interfacial wear analysis.

Once the fretting wear tests were completed, post test analysis was performed using scanning electron microscopy (SEM) and 3-D contact profilometery for morphology, along with energy dispersive spectroscopy (EDS), x-ray photoelectron spectroscopy (XPS), and Raman spectroscopy for chemical analysis

Materials	**Composition Weight %**	**Roughness Ra (μm)**	**Nano Hardness (GPa)**	**Micro Hardness (HV)**	**Modulus (GPa)**
Titanium Substrates	90% Ti, 6% Al, 4% V	0.1	4.1	284	143
Copper Nickel Indium	64% Cu, 35% Ni, 1% In	9	2.4	138	90
Nickel	Commercially Pure	7	2.1	133	82

Table 8.1. Substrate and coating properties.

8.3 Friction Comparison

Fretting wear experiments were initially conducted on the commercially pure Ni coatings. The coefficients of friction for the Ni mated with Ti6Al4V fretting wear experiments were approximately 0.8 and 0.55 at room temperature and 450°C respectively. The NiG-A coatings yielded coefficients of friction that were approximately 0.25 and 0.35 at room temperature and 450°C respectively, when mated with the Ti6Al4V ellipsoids.

However, the high graphite content and high porosity of the NiG-A coatings caused an increase in wear of more that six times that of the commercially pure Ni coatings (at both room temperature and 450°C). Therefore experiments were conducted on nickel graphite thermally sprayed composite coatings with initial volumetric powder loadings of 5% (NiG-5), 10% (NiG-10), and 20% (NiG-20) graphite. Fig 8.1 shows the measured coefficients of friction from each of the nickel graphite composite coating mixtures tested at room temperature. The lowest coefficient of friction (at just under 0.35) was exhibited between 5% and 20% graphite content in the pre-spray mixture. Therefore, the 10% graphite pre-spray mixture was considered to be the best choice for further experimentation.

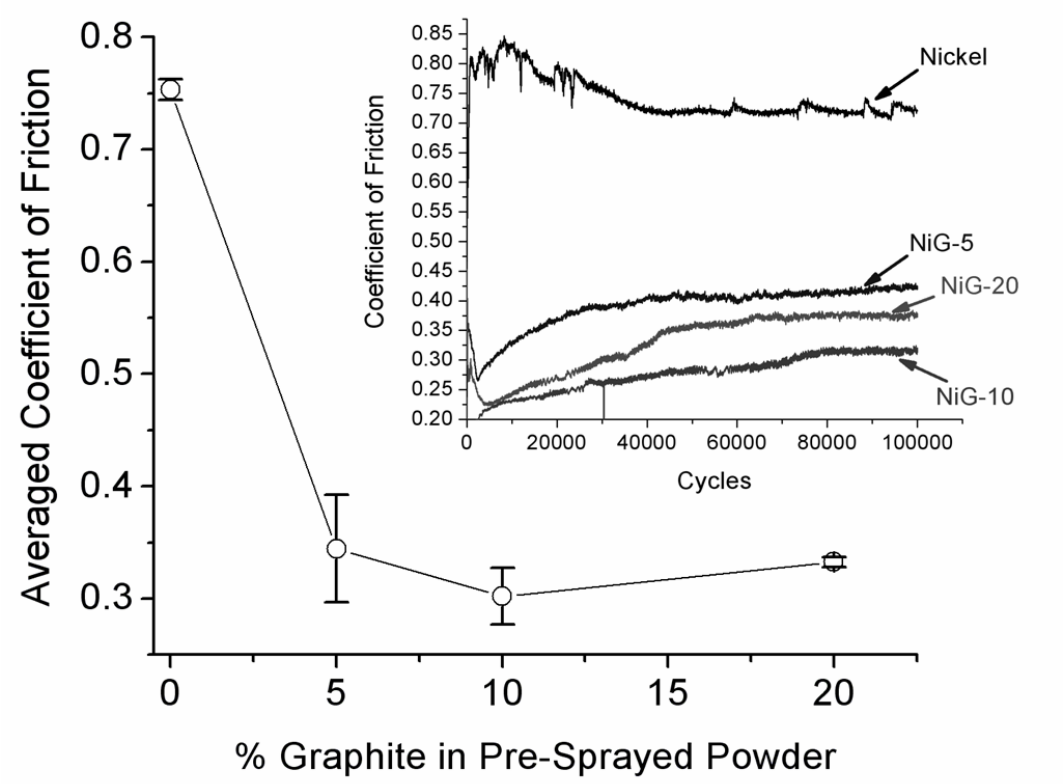

Fig. 8.1. Typical RMS friction data from 30 Hz fretting wear experiments on the thermally sprayed nickel graphite composite coatings with varied graphite composition in the pre-sprayed powder mixtures. The small plot (upper right) is a plot of the typical RMS friction data recorded during any single test. The large plot is the average of 4 experiments conducted on each coating composition.

Further experimentation was conducted on the selected NiG-10 coatings at 450°C. The friction and wear results from these experiments, in comparison to the results from the room temperature and 450°C tests on the NiG-A coatings and the commercially pure Ni coatings, are plotted in both Fig 8.2 and Fig 8.3 respectively. Although the measured coefficient of friction in the NiG-10 experiments were 0.1 and 0.05 higher than the values exhibited by the NiG-A coatings at room temperature and 450°C respectively, the NiG-10 coating wear was one sixth that of the NiG-A coating wear at room temperature and an order of magnitude lower at 450°C.

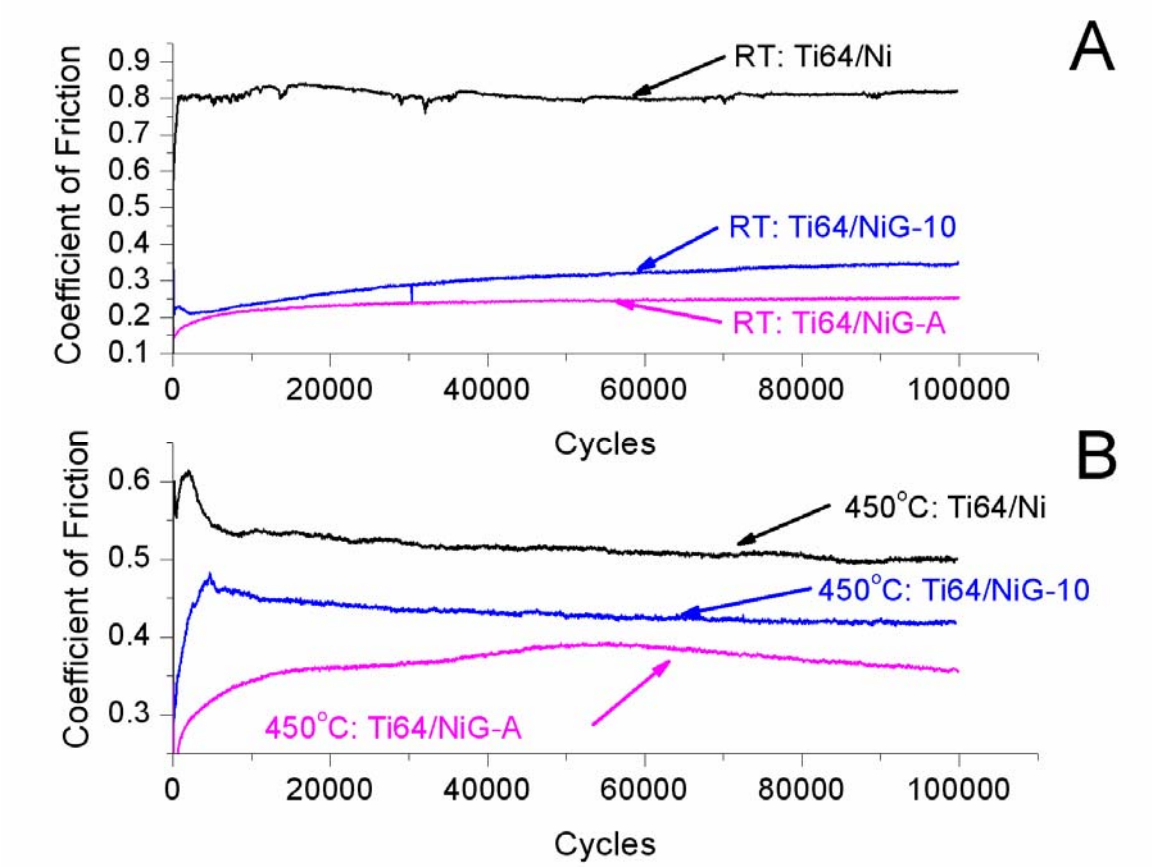

Fig. 8.2. Typical RMS friction data from 30 Hz fretting wear experiments. Data in (A) is from experiments conducted at room temperature, and data in (B) is from experiments conducted at 450°C.

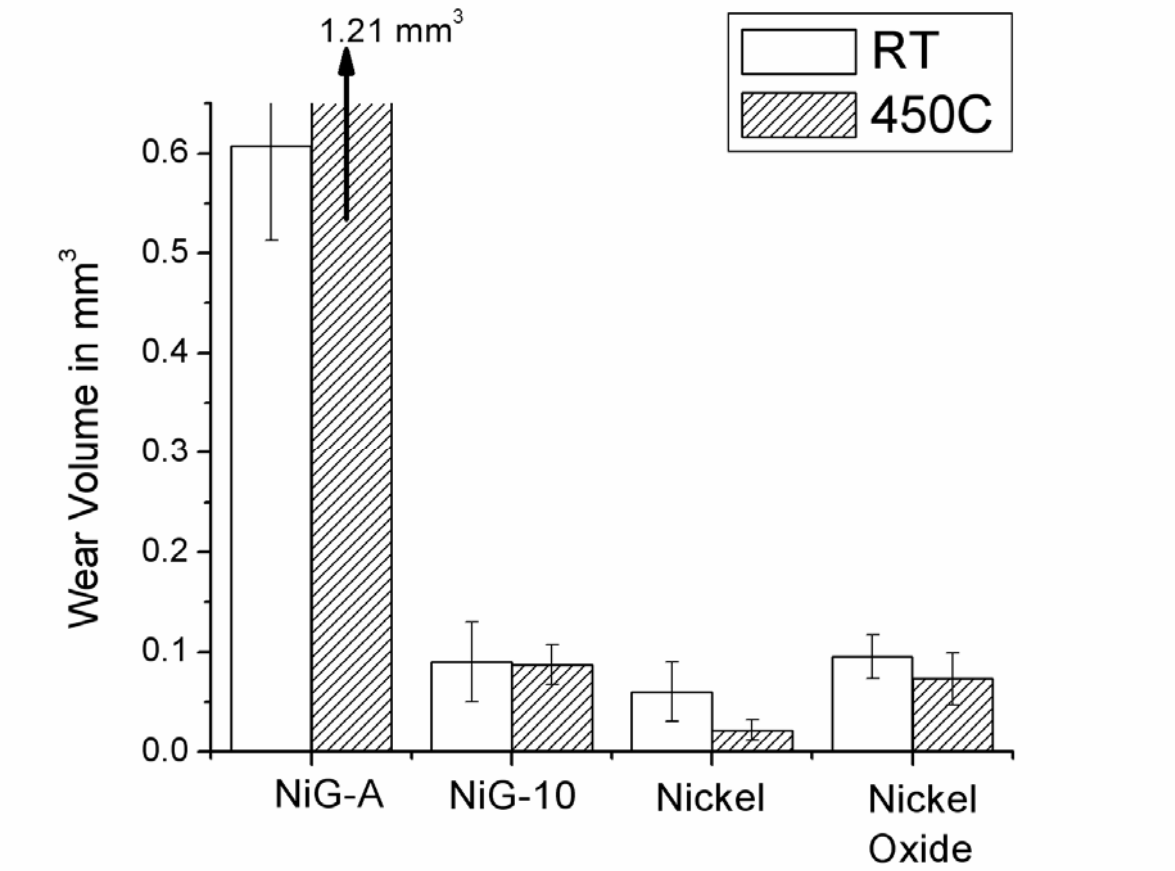

Fig. 8.3. Average wear volume in the fretting wear tracks on the thermal sprayed coatings after experiments conducted at room temperature and 450°C (Nickel Oxide is the wear of the nickel oxide samples from Chapter 7).

8.4 Wear Analysis

Initially, adhesive wear was the primary wear mechanism that caused interfacial damage in Ti6Al4V and Ni coated interfaces during unlubricated gross slip fretting wear. During this period of initial wear, titanium from the ellipsoid surface and nickel from the coating surface is transferred to the opposing surface. Fig 8.4 shows the scanning electron microscope (SEM) images of typical nickel coating wear tracks after just 10 and 100 cycles of gross slip fretting against a Ti6Al4V ellipsoid. After 10 fretting wear cycles, some of the transferred fragments of titanium can be as large as 50 μm in size. However, these adhered titanium particles can grow to be as large as 200 μm in size after 100 cycles of

unlubricated wear. Fig 8.5 shows a side by side comparison of the wear on the Ti6Al4V ellipsoid and the wear on the Ni coating after 100 cycles. This figure again shows the titanium adhered to the Ni coating, but it also shows the exact regions of the counterface where the titanium was removed. The white regions in Fig 8.5B are Ni that has transferred to the ellipsoid.

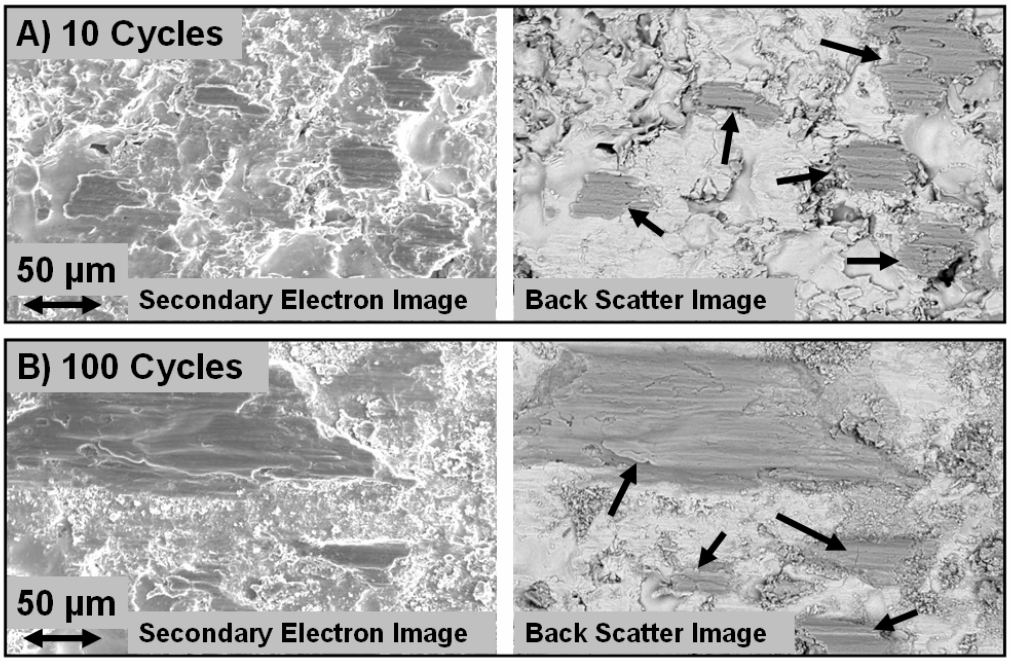

Fig. 8.4. Magnified secondary electron and back scatter images of the boxed regions in the Ni coating wear tracks shown in Fig 11A and 11B. Arrows point to dark regions that were identified as Ti-alloy using energy dispersive spectroscopy.

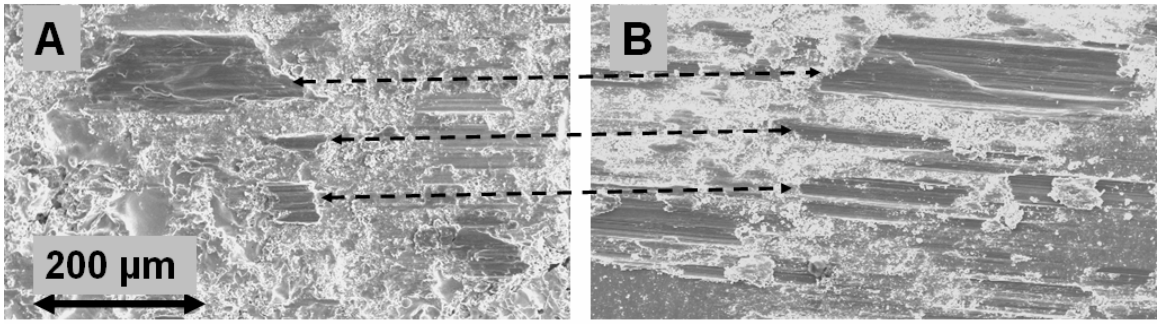

Fig. 8.5. Side by side images of the Ni coating and Ti6Al4V mated wear tracks after 100 cycles of fretting wear at room temperature. The arrows show directly where the adhered Ti6Al4V in A) was removed from the surface in B).

After approximately 1,000 cycles of gross slip fretting, debris accumulation in the contact caused the primary wear mechanism to transition from an adhesive type to a 3rd body type wear. Fig 8.6 and Fig 8.7 show a chronology of the wear tracks on the Ni coating and Ti6Al4V ellipsoid surfaces (respectively) after 10, 100, and 1,000 cycles of fretting wear. After 100 cycles, the adhered metallic material on both surfaces becomes so severely deformed that it breaks up into debris. Because of the nature of fretting wear, the majority of these wear debris are trapped within the interface and gets broken down into smaller and smaller particles. Most of these particles eventually oxidize and continue to damage both the Ni coating and the Ti6Al4V surfaces.

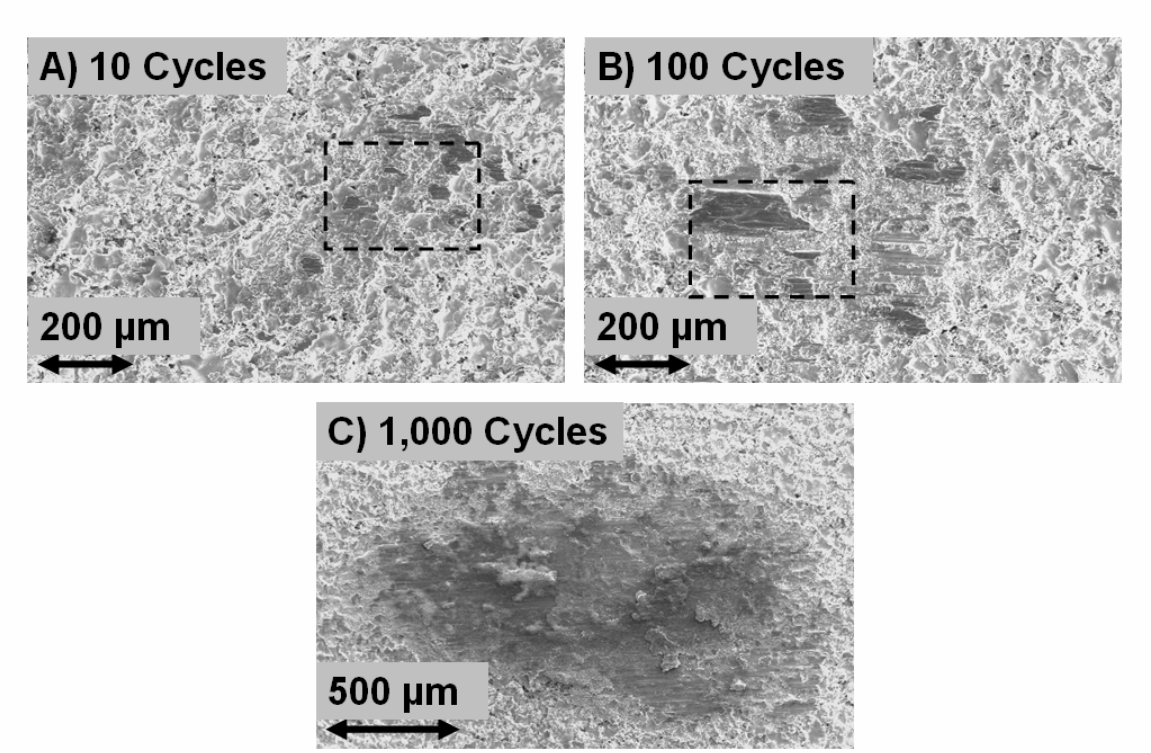

Fig. 8.6. Images of the Ni coating tested at room temperature after A) 10 cycles, B) 100 cycles, and C) 1,000 cycles against an uncoated Ti6Al4V ellipsoid.

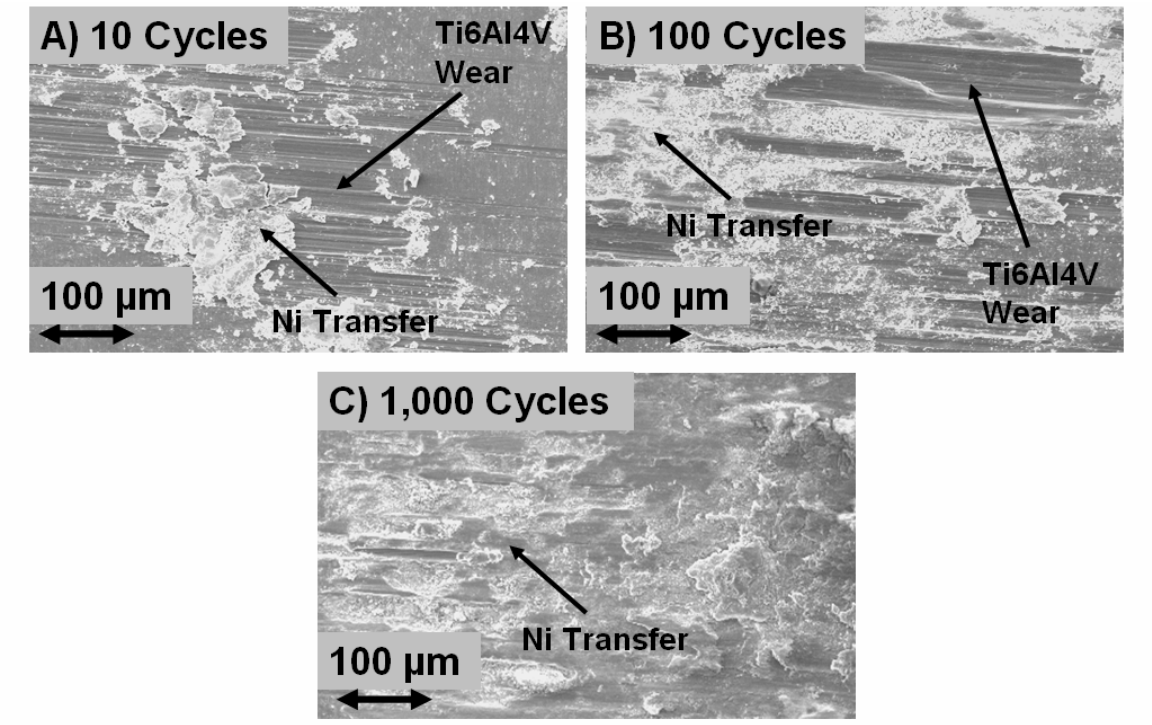

Fig. 8.7. A cyclic accumulation of fretting wear damage on the surface of the Ti6Al4V ellipsoid mated with the Ni surfaces depicted in Fig 9 respectively.

In order to combat the aforementioned wear mechanisms that were identified in the fretting wear of Ti6Al4V and Ni coated surfaces, the adhesive wear between the surfaces must be eliminated. One mitigation strategy, investigated herein, was to make a self-lubricating composite coating with a nickel matrix. For proof of concept, NiG-A composite coatings were tested under the same fretting wear conditions against Ti6Al4V. Fig 8.8 shows the chronology of the wear on the Ti6Al4V mated surfaces after 10, 100, 1,000, and 10,000 fretting wear cycles against the NiG-A coatings. The low friction exhibited by these coatings is guided by the formation of a transfer film that gradually smears onto the mated Ti6Al4V surface. Unlike the commercially pure Ni coating wear tracks, the NiG-A coatings did not cause any galling at the interface and induced very minimal damage to the Ti6Al4V ellipsoid surface. Even after 100,000 cycles of wear,

shown in Fig 8.9, the ellipsoid still exhibited a stable lubricious transfer film. The surface of the NiG-A coating was also smooth and there wasn't any evidence of 3rd body wear.

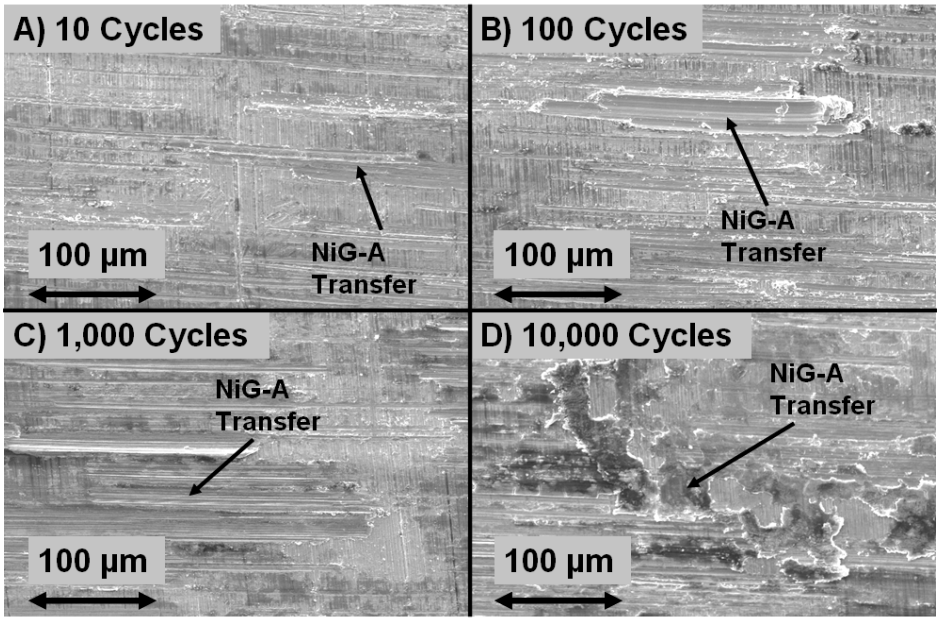

Fig. 8.8. Ti6Al4V wear track images after A) 10 cycles, B) 100 cycles, C) 1,000 cycles, and D) 10,000 cycles against the NiG-A composite coating at room temperature.

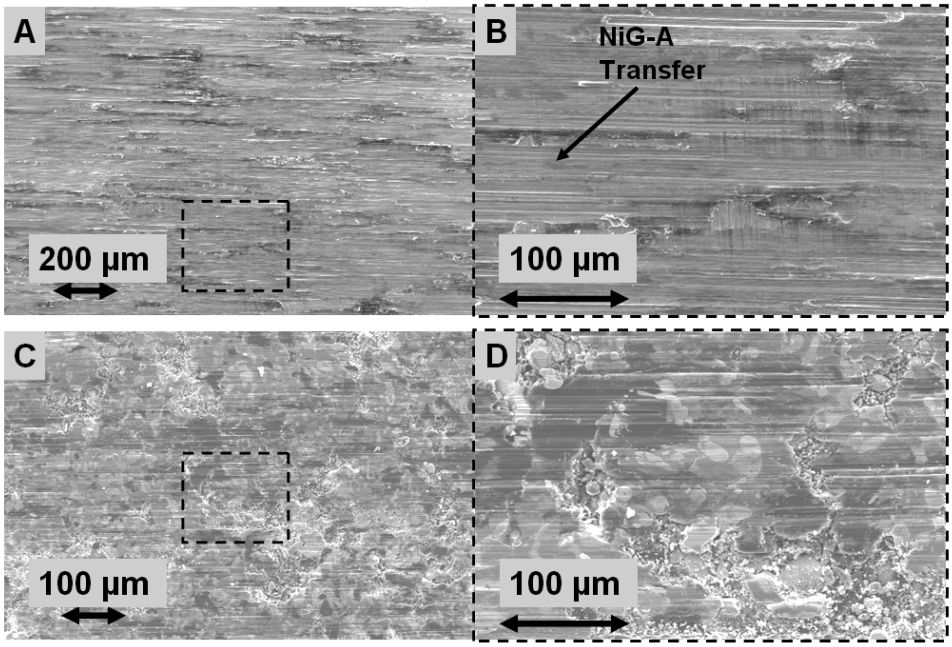

Fig. 8.9. Ti6Al4V (A and B) and NiG-A (C and D) wear track images after 100,000 room temperature fretting wear cycles. The images on the right are magnifications of the boxed regions on the left.

The NiG-A coating successfully ameliorated the gross slip fretting wear during the room temperature experiments, but the wear rate of the coatings was not acceptable. Therefore, the 10% pre-spray mixture NiG-10 coatings were tested under the same room temperature fretting wear conditions. Fig 8.10 shows the chronology of the NiG-10 wear on the Ti6Al4V ellipsoid surface. Although there was some moderate adhesive wear damage during the first 10 cycles, these worn regions were quickly filled in by the formation of a lubricious transfer film (similar to that seen in the NiG-A wear tracks). This transfer film continued to expand its coverage of the interface throughout the duration of the fretting wear experiments. The formation of this film protected the Ti6Al4V ellipsoids from further wear. After 100,000 cycles, the transfer film virtually covered the entire contact region, Fig 8.11. In addition, the NiG-10 wear track was still smooth without any evidence of 3rd body debris accumulation or wear.

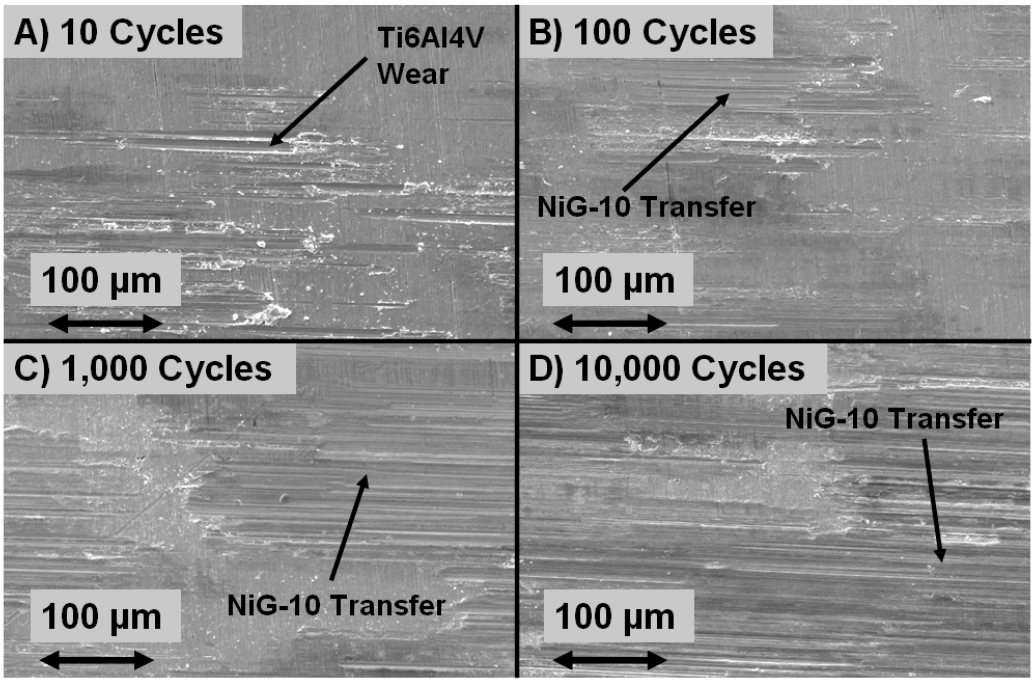

Fig. 8.10. Ti6Al4V wear track images after A) 10 cycles, B) 100 cycles, C) 1,000 cycles, and D) 10,000 cycles against the NiG-10 composite coating at room temperature.

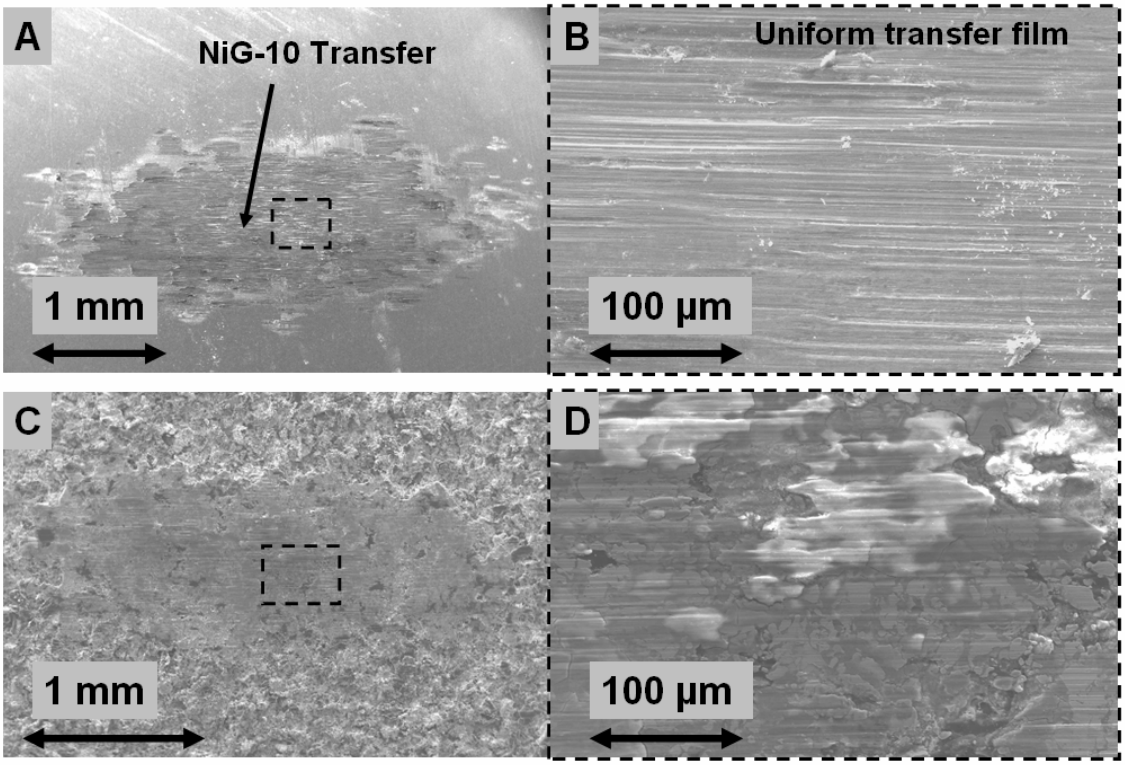

Fig. 8.11. Ti6Al4V (A and B) and NiG-10 (C and D) wear track images after 100,000 room temperature fretting wear cycles. The images on the right are magnifications of the boxed regions on the left.

At room temperature the added graphite in the NiG-10 coatings reduced the coefficient of friction from 0.8, with commercially pure Ni coatings, down to just under 0.35. At 450°C, the addition of graphite in the composite NiG-10 coatings reduced the friction from just above 0.5, with commercially pure Ni coatings, down to approximately 0.45. This difference appears modest; however, the reduction in wear on the Ti6Al4V interface was very significant. Fig 8.12 shows the chronology of the wear on a Ti6Al4V ellipsoid that was worn against a NiG-10 coating at 450°C. The wear was very similar to what was exhibited at room temperature, but there was even less damage to the Ti6Al4V

surface during the first 10 cycles of fretting. There was also a significant transfer film after just 10 wear cycles. This tribofilm took approximately 100 cycles to form on the Ti6Al4V ellipsoid surfaces during the room temperature tests. Fig 8.13 shows the wear tracks on both the Ti6Al4V and NiG-10 surfaces after 100,000 cycles of wear. Even after 100,000 cycles of fretting there was still a stable transfer film on the Ti6Al4V ellipsoid, and the NiG-10 wear track was smooth and uniformly worn. For comparison to the baseline, Fig 8.14 shows the same chronology of wear on a Ti6Al4V ellipsoid mated with a commercially pure Ni coating at 450°C. After 10 cycles of wear, the Ni coating caused significant adhesive wear on the Ti6Al4V surface. In addition, fragments of the Ni coating were adhered to the ellipsoid wear track. As the wear progressed, a tribofilm was eventually formed on the Ti6Al4V ellipsoid. The creation of this tribofilm reduced the further degradation of the Ti6Al4V surface. However, the tribofilm created by the Ni coatings was not as stable as the tribofilm formed by the NiG-10 coatings.

Chapter 7 showed that thick nickel oxide films need to break up and reform into nanocrystalline tribofilms, via tribo-sintering, in order to provide low friction. Fig 8.14 shows the fine debris within the wear track that has been combined into the smooth localized tribofilms. However, the NiG-10 surfaces do not appear exhibit any fine wear debris in any of the wear tracks. All of the wear debris in the NiG-10 wear tracks is around the edges of the contact area.

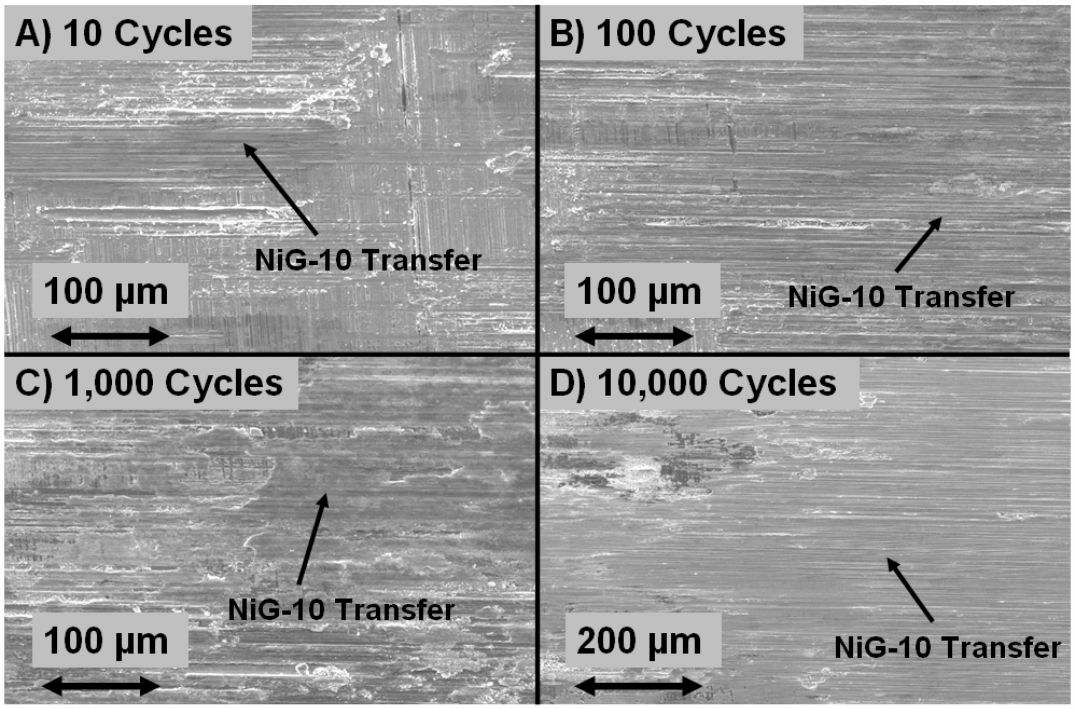

Fig. 8.12. Ti6Al4V wear track images after A) 10 cycles, B) 100 cycles, C) 1,000 cycles, and D) 10,000 cycles against the NiG-10 composite coating at 450°C.

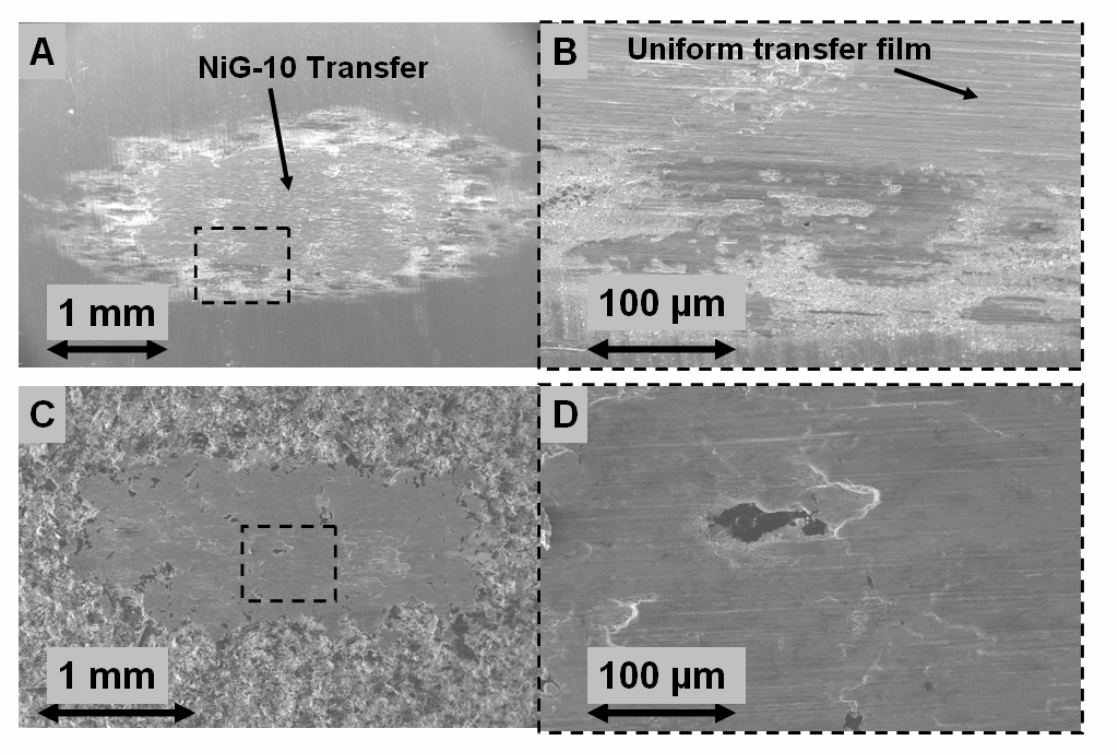

Fig. 8.13. Ti6Al4V (A and B) and NiG-10 (C and D) wear track images after 100,000 fretting wear cycles at 450°C. The images on the right are magnifications of the boxed regions on the left.

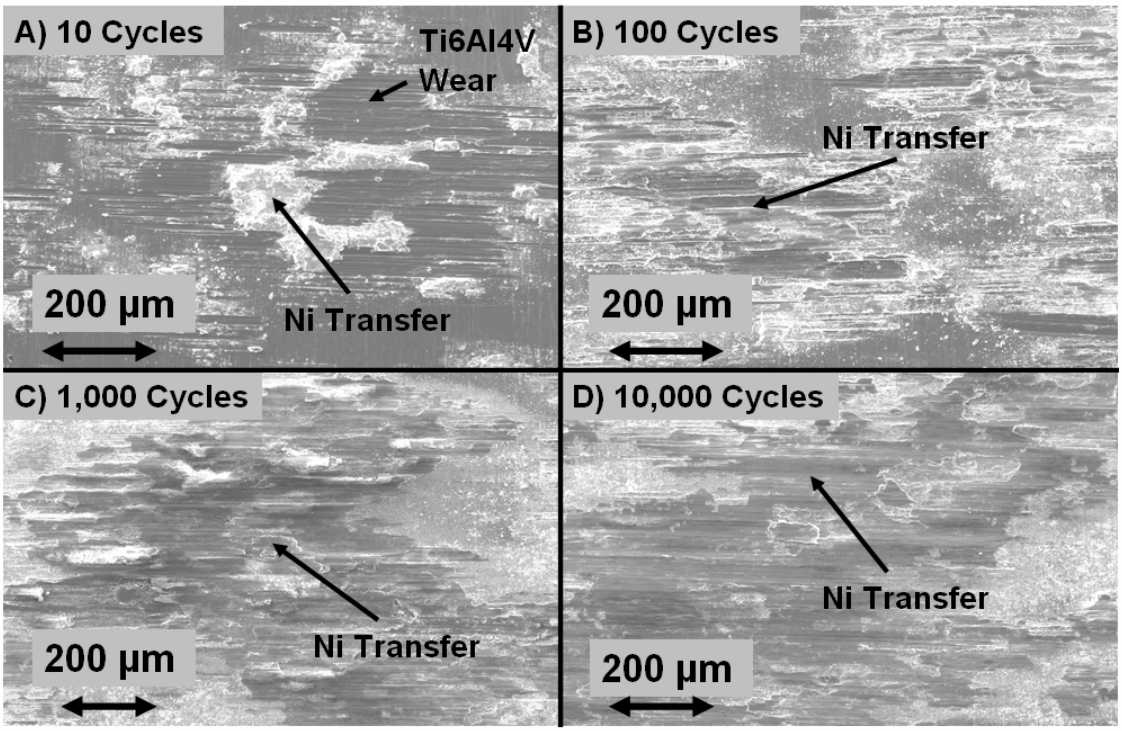

Fig. 8.14. Ti6Al4V wear track images after A) 10 cycles, B) 100 cycles, C) 1,000 cycles, and D) 10,000 cycles against the commercially pure Ni coating at 450°C.

8.5 Surface Chemistry

XPS for nickel-oxygen compositions have been well characterized in the literature [105, 107-109]. Using XPS for surface analysis, Kim et al found that there is always some Ni_2O_3 present in the surface oxide at temperatures below 250°C in air, with an increased ratio of NiO to Ni_2O_3 with increased temperature [107]. The ratio increases because Ni_2O_3 is reduced thermally to NiO, since NiO is thermodynamically favored at higher temperatures.

At the conclusion of the fretting wear experiments, x-ray photoelectron spectroscopy (XPS) of the worn NiG-10 coatings and Ti6Al4V ellipsoids was performed to determine the effect that the combination of fretting and increased bulk temperature had on the surface chemistry in the wear track. Fig 8.15 shows the survey scans taken in the wear

tracks of the mated surfaces. The most noticeable difference between the room temperature and 450°C worn surfaces was the fact that there were more intense Ni 2p peaks (labeled as nickel) in spectra from the 450°C wear tracks. The high resolution XPS scans of the NiG-10 coating wear track are shown in Fig 8.16. The Ni 2p peaks show definitively that the NiG-10 coating surface, worn at 450°C, contained predominantly NiO within the wear track. However, the slight evidence of nickel oxide present in the room temperature experiments suggested a higher oxidative state (the presence of Ni_2O_3). When Ni_2O_3 is present, the Ni $2p_{3/2}$ peak at ~ 855.5 eV becomes more intense relative to the Ni $2p_{3/2}$ peak at ~ 854 eV (both peaks are marked with dotted lines in Fig 8.16A). This shift in relative Ni $2p_{3/2}$ peak intensity is followed by an increase in intensity of an O 1s peak at ~ 531.7 eV. This change is shown in Fig 8.16B. NiO yields a spectrum with a more intense O 1s peak at ~ 529.5 eV. In addition, Fig 8.16C shows the high resolution scans of the carbon C 1s peaks, to show that there was not a bulk shift in the entire scan across all eV values.

High resolution scans of the Ti6Al4V ellipsoid wear tracks, shown in Fig 8.17, were taken in order to more accurately define the transfer film within the wear track after the room temperature and 450°C experiments. This analysis shows that the transfer films on the Ti6Al4V surfaces after the room temperature experiments were defined as containing carbon, TiO_2, and trace amounts of Ni_2O_3. The transfer films on the worn Ti6Al4V surfaces tested at 450°C contained mostly NiO and carbon, with trace amounts of TiO_2. The nickel oxide states are defined by the Ni 2p and O 1s peaks shown in Fig 8.17A and Fig 8.17B respectively. These peaks are almost identical to the peaks that were identified in the NiG-10 coating wear tracks after tests at the same respective temperatures.

The presence of TiO_2 is defined by the shift of the Ti 2p peaks to ~ 458.8 eV, as shown in Fig 8.17C.

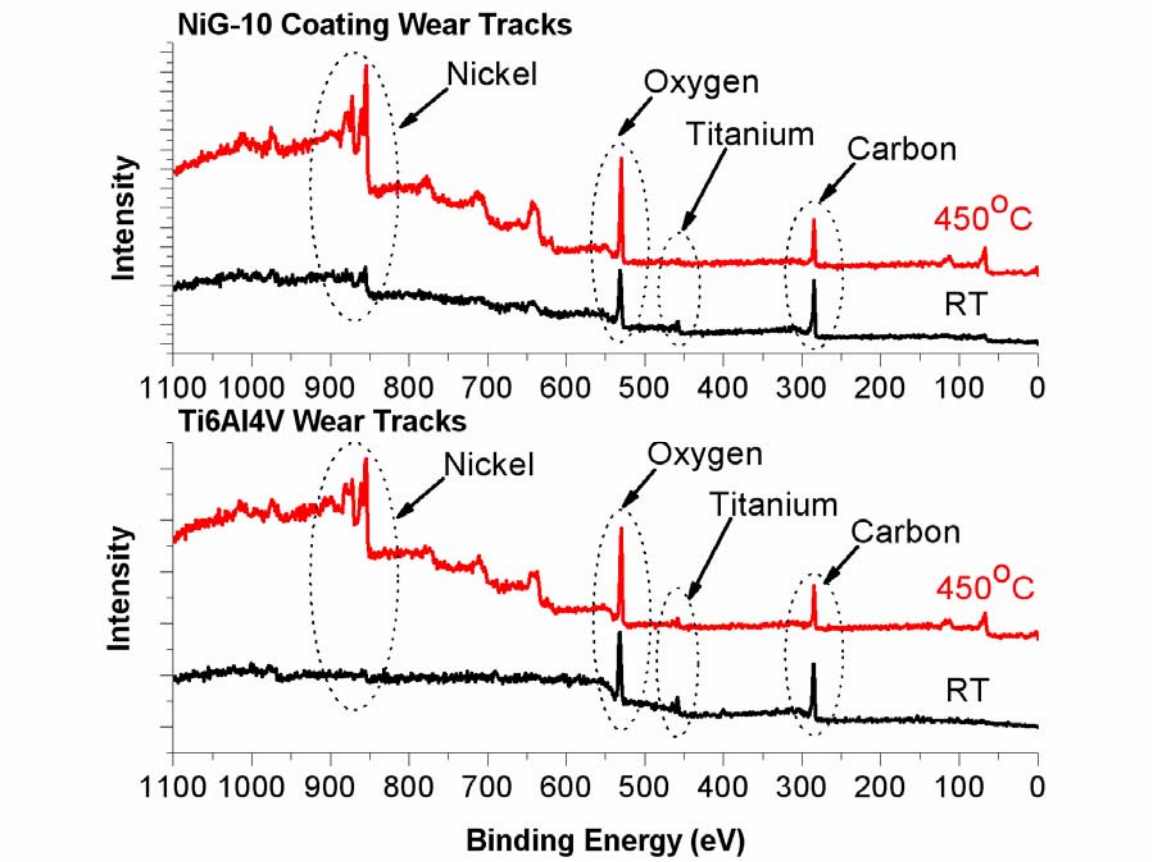

Fig. 8.15. XPS survey scans in the fretting wear tracks of samples tested at room temperature (RT) and 450°C after 10,000 cycles.

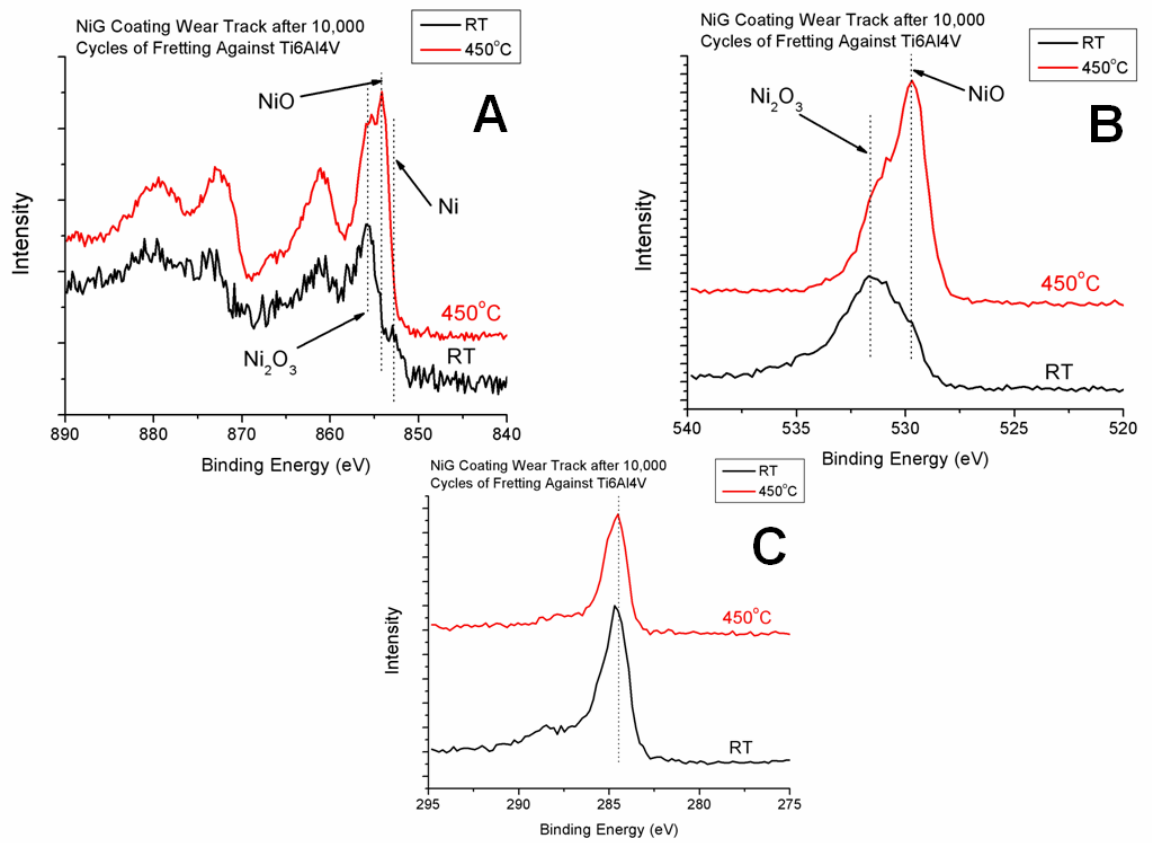

Fig. 8.16. High resolution XPS scans in the NiG-10 coating wear tracks of samples tested at room temperature (RT) and 450°C after 10,000 cycles. A) Shows the Ni 2p peaks. B) Shows the O 1s peaks. C) Shows the C 1s peak.

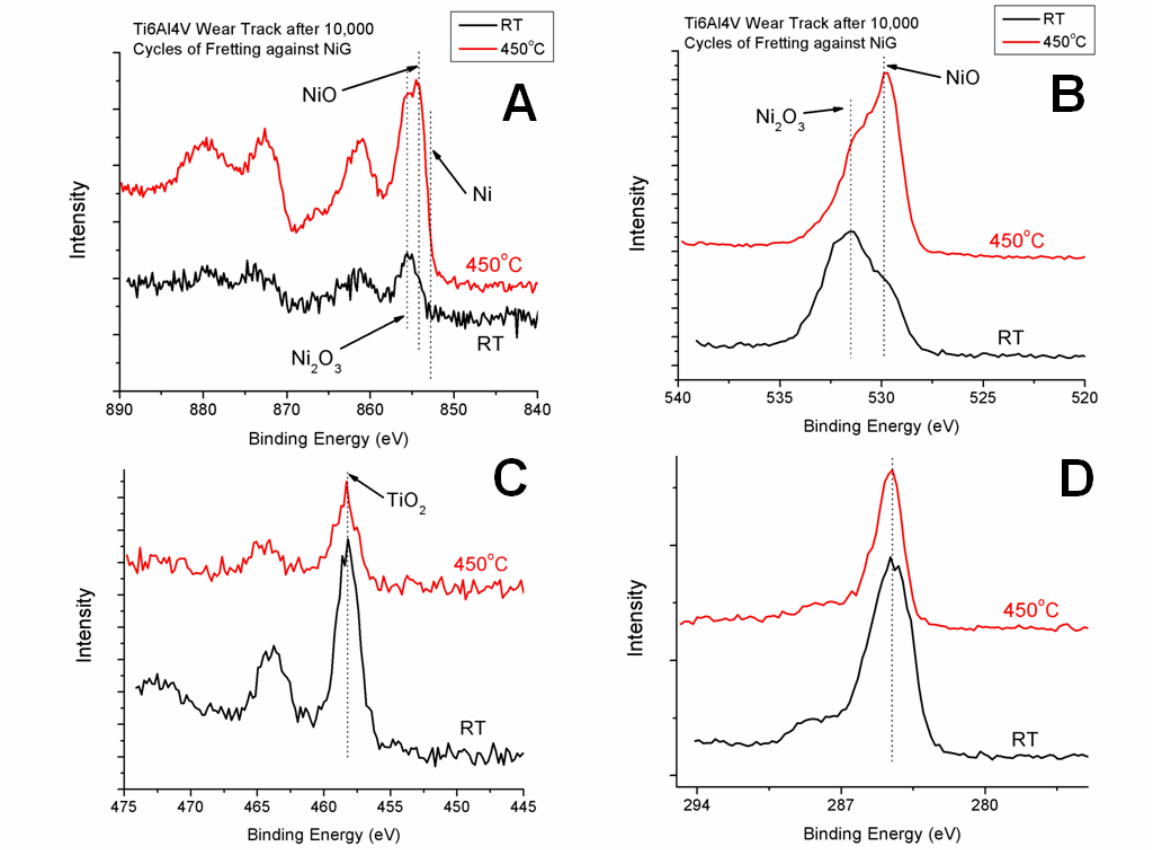

Fig. 8.17. High resolution XPS scans in the Ti6Al4V ellipsoid fretting wear tracks of samples tested at room temperature (RT) and 450°C after 10,000 cycles. A) Shows the Ni 2p peaks. B) Shows the O 1s peaks. C) Shows the Ti 2p peaks. D) Shows the C 1s peak.

In the literature there is mention of a binary or double oxide that may form with the mixture of titanium and nickel oxides at high temperatures [100,102, 133-134]. This complex oxide is not well characterized and is defined as $NiTiO_3$ or nickel titanate. However, one XPS study of this complex oxide suggested that it has a Ni^{2+} peak at (854.8 eV) and a Ti^{3+} peak at (457 eV) [134]. The 854.8 eV peak would be located between the Ni $2p_{3/2}$ peaks that describe NiO and Ni_2O_3, and is not apparent in the spectra shown in Fig 8.16A and Fig 8.17A. In addition, the Ti $2p_{3/2}$ peak at 457 eV is clearly not present in any of the spectra from the Ti6Al4V surfaces, as shown in Fig 8.17C. Therefore, there is no

current evidence of the formation of this complex oxide in the XPS data obtained in this study.

In addition to XPS, a Raman microscope with a 514 nm wavelength laser was also used to analyze the NiG-10 and Ti6Al4V wear tracks, and better define the state of carbon within the wear tracks. Fig 8.18 shows the Raman spectra collected from the smooth lubricious regions in the NiG-10 coating wear tracks, as well as spectra from the transfer films on the Ti6Al4V ellipsoids. The analysis showed that a graphitic film did form in the NiG-10 and mated Ti6Al4V wear tracks, during the room temperature experiments. This helped to confirm that graphite particles within the composite did in fact lubricate the interface, and reduce the friction and wear.

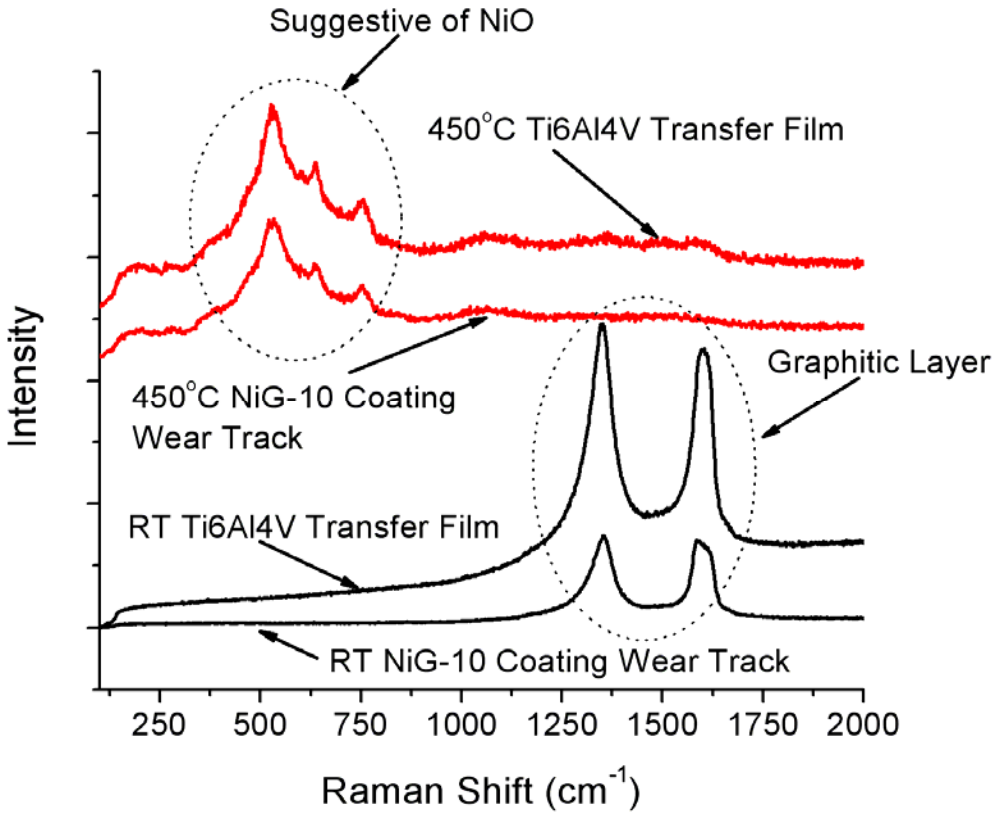

Fig. 8.18. Raman laser spectroscopy scans in the fretting wear tracks of samples tested at room temperature (RT) and 450°C after 10,000 cycles.

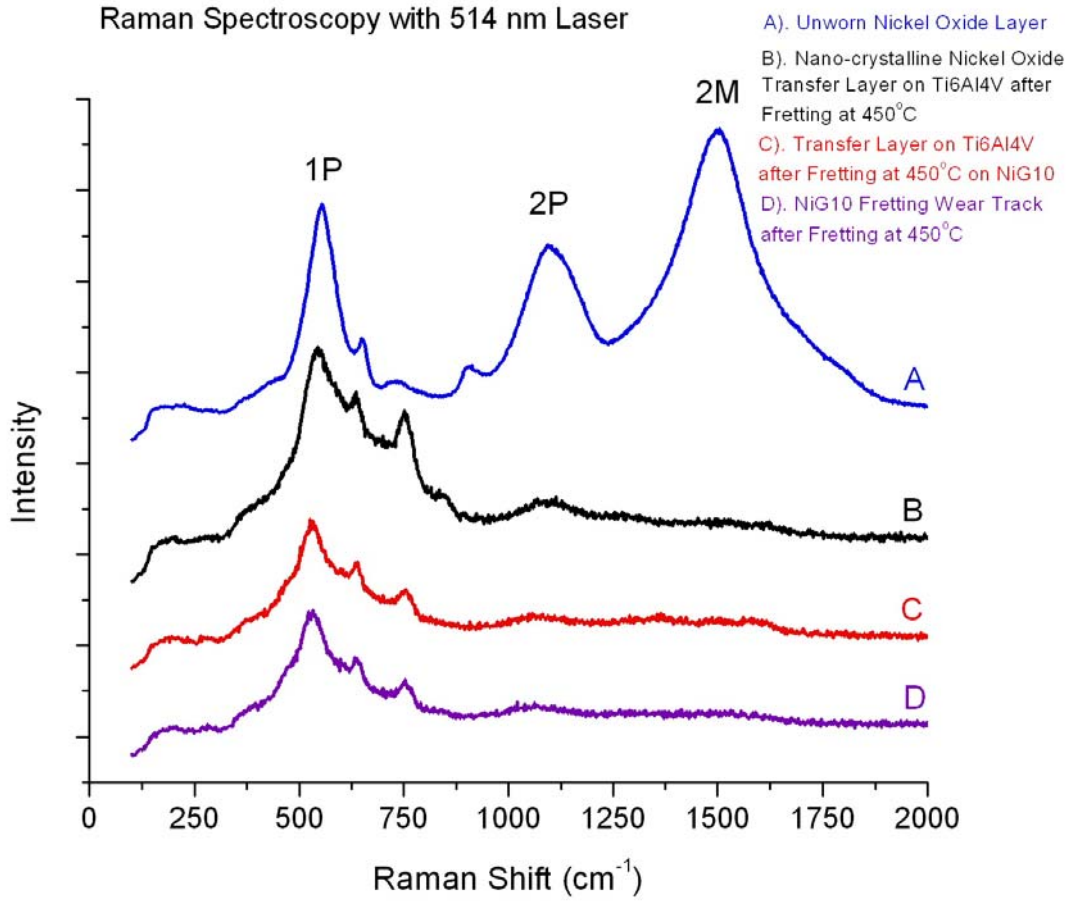

Fig. 8.19. Raman laser spectroscopy scans in the fretting wear tracks of: A) the unworn nickel oxide layer from Chapter 7, B) the nanocrystalline nickel oxide tribofilm formed on the mated Ti6Al4V surface at 450°C, C) the tribofilm on the mated Ti6Al4V surface after fretting at 450°C against NiG-10, and D) the NiG-10 surface after fretting at 450°C.

At 450°C, the Raman data suggests that the wear tracks of both the mated surfaces were composed of NiO [135]. This result is consistent with the XPS data from these surfaces. Fig 8.19 shows the comparison of the Raman data from the NiG-10 wear tracks (after fretting at 450°C) as compared to the date from the unworn nickel oxide and nanocrystalline tribofilms from Chapter 7. This shows that the nickel oxide tribofilms formed by the NiG-10 coatings at 450°C have the same structure as the nanocrystalline tribofilms formed at 450°C by the thick nickel oxide surfaces. However, it is important to

note the difference of these spectrums from the Raman spectrum from the unworn oxide. The spectrum from the unworn surface is characteristic of a typical nickel oxide surface with some excess oxygen (or in this case, some presence of Ni_2O_3 as described in Chapter 7). In the literature it has been shown by Mironova-Ulmane et al that nickel oxide with grain sizes between 1500 nm and 100 nm do not yield a 2 magnon (2M) peak [136]. The spectrum from the nickel oxide transfer film formed on Ti6Al4V at 450°C (spectrum B in Fig 8.19) is known to have a grain size of 5-20 nm. This establishes a known precedence as to why the 2M peak is absent from the tribofilm spectrums. However, the further decrease in grain size, from 100 nm in the literature, also explains the absence of the 2 phonon (2P) peak as well. As the size of the nanocrystallites get smaller, the amount of lattice symmetry is also diminished. This would severely reduce the likely hood that the Raman would detect a 2P shift. The reduction of the 2P peaks could also occur due to distortions in the lattice structure cause by interfacial shearing of the nanocrystalline layer.

8.6 Discussion

In overview, the goal of this research was to mitigate gross slip fretting wear in Ti6Al4V mated interfaces from room temperature up to 450°C, through the use of nickel graphite composite thermal sprayed coatings. The inclusion of graphite particles into the nickel coating matrix reduced the interfacial friction at both room temperature and 450°C. The combination of microstructural and surface chemistry analysis showed that during the room temperature fretting wear tests the nickel graphite composite coatings reduced the wear on the mated Ti6Al4V surfaces by minimizing the initial adhesive wear and facilitating the formation of a graphitic transfer film. The NiG-10 coatings were tested as-sprayed, or without surface modification. The inherent surface roughness of the coatings

caused the minimal adhesive wear that was observed during the first 10 cycles of wear at room temperature, Fig 8.10A. During the initial wear cycles, asperities were sheared and a smooth wear track was formed. It was during this phase of wear that the mated Ti6Al4V ellipsoid was damaged. While the asperities were being deformed, the imbedded graphite particles were also sheared and a lubricious graphite transfer film was formed at the interface. Although the graphitic transfer film reduced the coefficient of friction down to 0.35 at room temperature, this is much higher than the traditional 0.2 coefficient of friction that is measured during graphite lubrication. The friction was not able to reach 0.2 because the transfer film is not a purely graphite film, as it contains small amounts Ni_2O_3 and TiO_2 (from the initial wear damage).

Lower friction with the same coating may be possible by burnishing some graphite onto the coating surface prior to fretting or by controlling the coating roughness. Burnishing graphite onto the coating would fill the asperity gaps with graphite and reduced the number of cycles required to form a lubricious graphitic transfer film. Another approach could be to control the asperity sized and distribution during the coating process, or by post process grinding/polishing. A smooth interface may accelerate the graphite transfer film formation by bringing the imbedded graphite particles closer to the initial contact surface.

At 450°C, the initial adhesive wear was minimized further by the formation of a transfer film that was composed primarily of nickel oxide (NiO). Although the surface chemistry does not suggest that graphitic lubrication occurred at the interface, the presence of the carbon has enhanced the formation of a continuous transfer film. The experiments conducted with the commercially pure Ni coatings at 450°C did form a lubricious NiO

transfer film, but it was not continuous or uniform. Instead it was patchy with localized regions of wear debris. This was likely due to the tribo-sintering mechanism that was described in Chapter 7. In contrast, the NiG-10 coated surfaces yielded more uniform tribofilms with minimal debris. It is believed that this occurs due to a very small amount of retained nickel within the interface. The sintering of submicron oxide particles will occur more readily with a very small amount of nickel particles added to the mixture. In addition, these trace amounts of nickel would allow for even more plasticity in the nanocrystalline tribofilm. Yang et al, showed that nickel oxide can be reduced to metallic nickel in ball milling at temperatures as low as 350°C, with the addition of graphite into the interface [137]. It is possible that as nickel oxide particles are formed/sintered into the tribofilm, there is some retention of nanocrystalline nickel particles through this reduction reaction. This would enhance the plasticity of the tribofilms during formation. However, at 450°C the graphite and the retained nickel would only remain for a very short duration. That is why the post test XPS analysis does not detect any nickel in the tribofilms. The fine nickel nanocrystallites would have been oxidized as the tribofilm sheared at the interface.

8.7 Conclusions

The use of nickel graphite composite coatings for gross slip fretting wear mitigation was researched through experimentation, wear morphology, and surface chemistry analysis. From this work it can be concluded that nickel graphite composite coatings effectively reduced wear on the mated Ti6Al4V surfaces at room temperature and 450°C by the formation of lubricious graphitic and nickel oxide (NiO) based transfer films respectively. In addition, compositions of 5% to 20% graphite in the pre-spray powder

mixture were similarly effective in reducing the friction between the Ni based thermal sprayed coatings and the mated Ti6Al4V interfaces.

At 450°C the inclusion of graphite particles in the nickel coatings enhanced the formation of a uniform and continuous NiO based transfer film. It is believed that the enhanced tribofilm formation was due to a reduction of some of the formed nickel oxide back to metallic nickel. Although the nickel would eventually oxidize, the retention of small amounts of metallic nickel would enhance the formation and plasticity of the nickel oxide tribofilms.

Chapter 9

DISSERTATION SUMMARY AND FUTURE WORK

This dissertation was focused on the mechanisms of nickel based coatings for the mitigation of fretting wear in Ti6Al4V interfaces. One of the most prevalent places for fretting wear to occur in aerospace systems is at the dovetail interface of compressor bladed disk assemblies. This work started with fundamental research on the fretting wear mechanisms associated with mated Ti6Al4V surfaces at room temperature and 450°C, through various fretting wear regimes. This base understanding of the degradation of the uncoated Ti6Al4V surfaces was followed by more wear mechanistic research into how Ti6Al4V is damaged when mated with unlubricated CuNiIn and Al-Bronze coatings. Current fretting wear mitigation strategies utilize these coatings with solid lubricant overcoats. However, the wear analysis in Chapters 3 and 4 determined that the soft CuNiIn and Al-bronze coatings will not provide any fretting wear protection once the applied lubricants wear out. Therefore, it is more advantageous to have a coating system that does not have this limitation.

The body of literature on the friction and wear of nickel based materials suggested that nickel oxides may provide some wear protection at elevated temperatures. However, limited work has been done experimentally in the fretting wear of pure nickel materials. This lead to research focused on the wear mechanisms and surface chemistry of lubricious nickel oxide tribofilms formed at elevated temperatures on cold sprayed commercially pure nickel coatings. In this work it was determined that at elevated temperatures smooth nickel oxide tribofilms formed on both the coating and the mated Ti6Al4V surfaces. These tribofilms served to protect the Ti6Al4V interface at temperatures in excess of 450°C.

However, the surface chemistry showed that a second phase of nickel oxide (Ni_2O_3) was also present in the wear track at intermediate temperatures. As the temperature was increased, the friction decreased along with the Ni_2O_3 content in the tribofilms.

In order to determine what the mechanism for tribofilm formation was and what the effect of Ni_2O_3 was, fretting wear experiments were conducted on thick nickel oxide films with the same surface chemistry as the low friction films that formed on the cold sprayed nickel coatings. The results from this work concluded that the nickel oxide tribofilms were had a nanocrystalline structure and were formed via a tribo-sintering mechanism. This meant that the pressure, temperature, and speed had more influence on the friction and wear of the interface than the amount of Ni_2O_3 in the wear track. In addition, this work showed that bulk nickel oxide films would not be more beneficial than metallic nickel coatings. This is because the natural oxide growth is not such that nanocrystalline grain boundary sliding or grain rotation can enhance the plasticity of the oxide scale. Therefore, nickel oxide is not lubricious at the tested temperatures until the nanocrystalline structure is obtained.

Although nickel based coatings provided low friction and fretting wear protection of the Ti6Al4V surface at elevated temperatures, the dovetail joints of compressor bladed disk assemblies must be able to with stand operation at low temperatures as well. Therefore, the final step was to enhance the performance of the nickel coatings by imbedding graphite particles into the coating. This proved to yield low friction and wear at room temperature and up to 450°C.

In summary, the contributions of this work fall into three categories: testing methodology, fundamental oxide lubrication, and the application of self lubricating

coatings for fretting wear mitigation. The fundamental work on Ti6Al4V interfaces established a fretting wear test methodology that used maximum energy dissipation to identify the transition from mixed fretting to gross slip fretting wear. This approach can be used to map wear regimes for materials tested at various temperatures. The surface chemistry and wear analysis of the nickel oxide surfaces determined that the shear accommodation in lubricious tribofilms is facilitated by a nanocrystalline structure. This mechanism explains why preoxidation of many surfaces does not yield any tribological benefit. Finally, the validation of nickel graphite composite coatings for fretting wear mitigation over wide temperature ranges presents a potential paradigm shift in the protection of titanium alloy compressor bladed disk assemblies. The application of this composite coating methodology mitigates the problems associated with lubricant wear and lubricant degradation in the current coating systems. The work presented in this dissertation clearly shows that with out solid lubrication, soft metallic coatings do not provide any wear protection for the mated Ti6Al4V surfaces. Composite coatings do not have this problem, as they are continuously lubricious until the entire thickness of the coating has worn away.

Although this project may seem complete, there are many avenues for future work. From a fundamental research stand point; this work is the first in the literature to develop an understanding of how tribofilms form on bulk nickel oxide surfaces. However, the tests were all conducted in lab air. The impact of the formation of Ni_2O_3 at low temperatures could be better understood with more research on the wear of these materials in the absence of oxygen (either in dry nitrogen or in a vacuum). It would also be of great importance to understand what affect (if any) the oxygen in the atmosphere has on the tribo-sintering

process. Is oxygen required to form these tribofilms?

From a more conventional point of view, the nickel graphite coatings were not optimized. In order to make this coating a viable aerospace solution, other aspects of the coating performance need to be understood. These factors are the type lubricant, surface roughness, and quantity of lubricant. This work only utilized graphite as an imbedded lube. There maybe some benefit to using another lubricant such as MoS_2, or maybe mix MoS_2 and graphite as imbedded lubricants. How much lubricant needs to be in the coating? This work suggests approximately 10%, but how is this affected by surface finish. Does the coating require more or less lubricant with a finer surface finish?

Finally, the formation of nickel oxide films could be studied through thin film deposition. Prasad and Zabinski et al showed that the deposition of nanocrystalline ZnO films yielded low friction at room temperature [127-130]. Is it possible to get similar performance from physical vapor or chemical vapor deposited nickel oxide thin films? These types of coatings could have many uses. Although nickel oxide in this work is used to mitigate fretting wear, nickel oxides are widely used for their semi-conductive properties. By controlling how much Ni_2O_3 is in the films, you can control the conductivity of the coating. This could allow for the deposition of lubricious wear resistant coatings with tunable electrical conductivity.

REFERENCES

[1] G. X. Chen, Z. R. Zhou, Study on transition between fretting and reciprocating wear, *Wear* 250 (2001) 665-672.

[2] M. Varenberg, G. Halperin, I. Etsion, Different aspects of the role of wear debris is fretting wear, *Wear* 252 (2002) 902-910.

[3] R. D. Mindlin, *J. Appl. Mech*., 16 (1949) 259.

[4] Z. R. Zhou, L. Vincent, Mixed fretting regime, *Wear* 181-183 (1995) 531-536.

[5] O. Vingsbo, On fretting maps, *Wear*126 (1988) 131-147.

[6] I. Hutchings, Tribology: Friction and wear of engineering materials, CRC Press, Boca Raton, 1992.

[7] C. Hager, Jr., J. Sanders, and S. Sharma, "Characterization of Mixed and Gross Slip Fretting Wear Regimes in Ti6Al4V Interfaces at Room Temperature," *Wear*, 257 (2004) 167-180.

[8] F. Bowden, A. Moore, D. Tabor, The ploughing and adhesion of sliding metals, *Journal of Applied Physics* 14 (1943) 80-91.

[9] P. Blau, Mechanisms for transitional friction and wear behavior of sliding metals, *Wear* 72 (1981) 55-66.

[10] P. Blau, Glossary of Terms, in: Friction, Lubrication, and Wear Technology, ASM Handbook Volume 18, ASM International, pp, 1-21, 1998.

[11] P. Hurricks, The mechanisms of fretting – a review, *Wear* 15 (1970) 389-409.

[12] P. Blanchard, C. Colombie, V. Pellerin, S. Fayayeulle, L. Vincent, Material effects in fretting wear: Application to iron, titanium, and aluminum alloys, *Metallurgical Transactions* 22A (1991) 1535-1544.

[13] P. Blau, E. Doyle, Metallographic evidence for the nucleation of subsurface microcracks during unlubricated sliding of metals, *Wear* 117 (1987) 381-387.

[14] N. Suh, The delamination theory of wear, *Wear* 25 (1973) 111-124.

[15] C. Colombie, Y. Berthier, A. Floquet, L. Vincent, M. Godet, Fretting: Load Carrying Capacity of Wear Debris, *Transactions of the ASME Journal of Tribology* 106 (1984) 194-201.

[16] C. Hager, Jr., J. Sanders, and S. Sharma, "Unlubricated Gross Slip Fretting Wear of Metallic Plasma Sprayed Coatings for Ti6Al4V Surfaces," *Wear*, 265 (2008) 439-451.

[17] S. Fayeulle, P. Blanchard, L. Vincent, Fretting behavior of titanium alloys, *Tribology Transactions* 36 (1993) 267-275.

[18] E. Sauger, S. Fouvry, L. Ponsonnet, P. Kapsa, J. Martin, L. Vincent, Tribologically transformed structure in fretting, *Wear* 245 (2000) 39-52.

[19] R. Waterhouse, Fretting fatigue, *International Materials Reviews*, 37 (1992) 77-97.

[20] C. Hager, Jr., J. Sanders, and S. Sharma, Gross Slip Fretting Wear Analysis of Aluminum Bronze Coatings for Ti6Al4V Aerospace Components, *Conference Proceedings of the 19th International Conference of Surface Modification Technologies*, August 1-3, 2005 St. Paul Minnesota, pg 10-16.

[21] H. Privett III, S. Fujishiro, Coating studies for prevention of fretting fatigue in jet engine titanium compressor blade dovetails, *Metallurgy and technology of practical titanium alloys*, (1994) 401-410.

[22] A. Freimanis, A. Segall, J. Conway Jr., E. Whittney, Elevated temperature evaluation of fretting and metal transfer between coated titanium components, *Tribology Transactions* 43 (2000) 653-658.

[23] F. Stott, D. Lin, G. Wood, The Structure and Mechanism of Formation of the 'Glaze' Oxide Layers Produced on Nickel-Based Alloys During Wear at High Temperatures, *Corrosion Science* 13 (1973) 449-469.

[24] D. Lin, F. Stott, G. Wood, K. Wright, J. Allen, The Friction and Wear Behavior of Nickel-Base Alloys in Air at Room Temperature, *Wear* 24 (1973) 261-278.

[25] F. Stott, D. Lin, G. Wood, C. Stevenson, The Tribological Behavior of Nickel-Chromium Alloys at Temperatures From 20°C to 800°C, *Wear* 36 (1976) 147-174.

[26] F. Stott, G. Wood, The Influence of Oxides on the Friction and Wear of Alloys, *Tribology International* 11 (1978) 211-218.

[27] S. Harris, M. Overs, J. Gould, The Use of Coatings to Control Fretting Wear at Ambient and Elevated Temperatures, *Wear* 106 (1985) 35-52.

[28] J. Jiang, F. Stott, M. Stack, Some Frictional Features Associated with the Sliding Wear of the Nickel-Base Alloy N80A at Temperatures to 250°C, *Wear* 176 (1994) 185-194.

[29] J. Jiang, F. Stott, M. Stack, The Role of Triboparticulates in Dry Sliding Wear, *Tribology International* 31 (1998) 245-256.

[30] I. Inman, S. Datta, H. Du, J. Burnell-Gray, Q. Luo, Microscopy of Glazed Layers Formed During High Temperature Sliding Wear at 750°C, *Wear* 254 (2003) 461-467.

[31] T. Lindley, Fretting fatigue in engineering alloys, *International journal of fatigue*, 19 (1997) 39-49.

[32] D. Hoeppner, Mechanisms of fretting fatigue and their impact on test methods development, *ASTM*, STP 1159 (1992) 23-32.

[33] M. Szolminski, J. Matlik, T. Farris, Effects of HCF loading on fretting fatigue crack nucleation, *International Journal of Fatigue*, 21 (1999) 671-677.

[34] O. Jin, S. Mall, Effects of independent pad displacement on fretting fatigue behavior of Ti6Al4V, *Wear*, 253 (2002) 585-596.

[35] O. Jin, S. Mall, Influence of contact configuration on fretting fatigue behavior of Ti6Al4V under independent pad displacement condition, *International Journal of Fatigue*, 24 (2002) 1243-1253.

[36] M. Long, H. Rack, Friction and surface behavior of selected titanium alloys during reciprocating sliding motion, *Wear*, 249 (2001) 158-168.

[37] J. DeMasi-Marcin, D. Gupta, Protective coatings in the gas turbine engine, *Surface and Coatings Technology* 68-69 (1994) 1-9.

[38] A. Freimanis, A. Segall, J. Conway Jr., E. Whittney, The influence of temperature and wear mode on the deterioration of coatings used for titanium aircraft engine components, *Tribology Transactions* 45 (2002) 193-198.

[39] D. Liu, B. Tang, X. Zhu, H. Chen, J. He, J. Celis, Improvement of the fretting fatigue and fretting wear of Ti6Al4V by duplex surface modification, *Surface and Coatings Technology* 116-119 (1999) 234-238.

[40] Y. Fu, A. Batchelor, Y. Wang, K. Khor, Fretting wear behavior of thermal sprayed hydroxyapatite (HA) coating under unlubricated conditions, *Wear* 217 (1998) 132-139.

[41] S. Fourvy, P. Kapsa, L. Vincent, Fretting behavior of hard coatings under high normal load, *Surface and Coatings Technology*, 68-69 (1994) 494-499.

[42] J. Carton, A. Vannes, L. Vincent, Basis of a coating choice methodology in fretting, *Wear* 185 (1995) 47-57.

[43] Y. Fu, N. Loh, A. Batchelor, D. Liu, X. Zhu, J. He, K. Xu, Improvement in fretting wear resistance of Ti6Al4V by application of several surface treatments and coatings, *Surface and Coatings Technology* 106 (1998) 193-197.

[44] L. Swadzba, A. Maciejny, B. Formanek, P. Liberski, P. Podolski, B. Mendala, H. Gabriel, A. Poznanska, Influence of coatings obtained by PVD on the properties of aircraft compressor blades, *Surface and Coatings Technology* 78 (1996) 137-143.

[45] Y. Fu, J. Wei, A. Batchelor, Some considerations on the mitigation of fretting damage by the application of surface modification technologies, *Materials Processing Technology* 99 (2000) 231-245.

[46] V. Fridrici, S. Fouvry, P. Kapsa, Fretting wear behavior of CuNiIn plasma coating, *Surface and Coatings Technology* 163-164 (2003) 429-434.

[47] K. Miyoshi, B. Lerch, S. Draper, Fretting wear of Ti-48Al-2Cr-2Nb, *Tribology International* 36 (2003) 145-153.

[48] H. Deresiewicz, R. D. Mindlin and applied mechanics, Pergamon Press Inc., New York, 1974.

[49] O. Vingsbo, S. Söderberg, in Ludema KC, *Wear of Materials 1987,* ASME (1987) 885-894.

[50] A. Ramalho, J. Celis, Fretting laboratory tests: Analysis of the mechanical response of test rigs, *Tribology Letters* 14 (2003) 187-196.

[51] S. Fouvry, P. Kapsa, L. Vincent, Analysis of sliding behavior for fretting loadings: determination of transition criteria, *Wear* 185 (1995) 35.

[52] Z. Zhou, E. Sauger, J. Liu, L. Vincent, Nucleation and early growth of tribologically transformed structure (TTS) induced by fretting, *Wear* 212 (1997) 50-58.

[53] M. Gardos, Magnéli phases of anion-deficient rutile as lubricious oxides. Part 1. Tribological behavior of single-crystal and polycrystalline rutile (Ti_nO_{2n-1}), Tribology Letters 8 (2000) 65-78.

[54] R. Boyer, G. Welsch, E. Collongs, Materials Properties Handbook: Titanium Alloys, ASM International, Materials Park, OH. 1994.

[55] R. Bowers, W. Zisman, Pressure effects on the friction coefficient of thin-film solid lubricants, *Journal of Applied Physics* 39 (1968) 5385-5395.

[56] R. Bowers, Coefficient of friction of high polymers as a function of pressure, *Journal of Applied Physics* 42 (1971) 4961-4970.

[57] I. Singer, R. Bolster, J. Wegand, S. Fayeulle, B. Stupp, Hertzian stress contribution to low friction behavior of thin MoS_2 coatings, *Applied Physics Letters* 57 (1990) 995-997.

[58] D. R. Swalla, R. W. Neu, D. L. McDowell, Microstructural Characterization of Ti6Al4V Subjected to Fretting, *Journal of Tribology* vol 126 (2004) 809-816.

[59] A. Hutson, T. Nicholas, R. John, Fretting fatigue crack analysis in Ti6Al4V, *International Journal of Fatigue* 27 (2005) 1582-1589.

[60] C. Hager, Jr., J. Sanders, and S. Sharma, Gross Slip Fretting Wear Analysis of Aluminum Bronze Coatings for Ti6Al4V Aerospace Components, *Conference Proceedings of the 19th International Conference of Surface Modification Technologies*, August 1-3, 2005 St. Paul Minnesota, pg 10-16.

[61] A. Hutson, M. Niinomi, T. Nicholas, D. Eylon, Effect of various surface conditions on fretting fatigue behavior of Ti6Al4V, *International Journal of Fatigue*, 24 (2002) 1223-1234.

[62] B. P. Conner, T. Nicholas, Using a Dovetail Fixture to Study Fretting Fatigue and Fretting Palliatives, *Journal of Engineering Materials and Technology*, 128 (2006) 133-141.

[63] D. Rigney, J. Hirth, Plastic deformation and sliding friction of metals, *Wear* 53 (1979) 345-370.

[64] N. Tomashov, *Theory of Corrosion and Protection of Metals*, Macmillan, London, 1966.

[65] R. Antoniou, T. Radtke, Mechanisms of fretting-fatigue of titanium alloys, *Materials Science & Engineering*, A237 (1997) 229-240.

[66] N. Suh, S. Jajanmir, E. Abrahamson, and A. Turner, Further investigation of the delamination theory of wear, *Journal of Lubrication Technology* October (1974) 631-637.

[67] N. Suh, S. Jajanmir, and E. Abrahamson, Microscopic observations of the wear sheet formation by delamination, *Wear* 28 (1974) 235-249.

[68] R. Waterhouse and D. Taylor, Fretting debris and the delamination theory of wear, *Wear* 29 (1974) 337-344.

[69] S. Earles, M. Hayler, Wear Characteristics of Some Metals in Relation to Surface Temperature, *Wear* 20 (1972) 51-57.

[70] E. Bisson, C. Lipson, L. Colwell, Handbook of Mechanical Wear, University of Michigan Press, 1961.

[71] M. Hamdy, R. Waterhouse, The Fretting Wear of Ti6Al4V and aged Inconel 718 at elevated temperatures, *Wear* 71 (1981) 237-248.

[72] R. Waterhouse, Fretting at High Temperatures, *Tribology International* (1981) 203-207.

[73] P. Hurricks, The Fretting Wear of Mild Steel from 200 to 500°C, *Wear* 30 (1974) 189-212.

[74] A. Iwabuchi, Fretting Wear of Inconel 625 at High Temperature and in High Vacuum, *Wear* 106 (1985) 163-175.

[75] J. Jiang, F. Stott, M. Stack, Some Frictional Features Associated with the Sliding Wear of the Nickel-Base Alloy N80A at Temperatures to 250°C, *Wear* 176 (1994) 185-194.

[76] J. Jiang, F. Stott, M. Stack, A Mathematical Model for Sliding Wear of Metals at Elevated Temperatures, *Wear* 181-183 (1995) 20-31.

[77] S. Ikeno, I. Siota, M. Nobuki, M. Nakamura, Wear Properties of Oxide Dispersion Strengthened Nickel Alloys, *Journal of Materials Science* 30 (1995) 4401-4406.

[78] D. Chaudhuri, D. Xie, A. Lakshmanan, The Influence of Stacking Fault Energy on the Wear Resistance of Nickel Based Alloys, *Wear* 209 (1997) 140-152.

[79] J. Jiang, F. Stott, M. Stack, The Effect of Partial Pressure of Oxygen on the Tribological Behavior of a Nickel Based Alloy, N80A, at Elevated Temperatures, *Wear* 203-204 (1997) 615-625.

[80] J. Jiang, F. Stott, M. Stack, The Role of Triboparticulates in Dry Sliding Wear, *Tribology International* Vol. 31, No. 5 (1998) 245-256.

[81] J. Lawen, S. Calabrese, O. Dinc, Wear Resistance of Super Alloys at Elevated Temperatures, *ASME Journal of Tribology* 120 (1998) 339-344.

[82] H. Berns, S. Koch, High Temperature Sliding Abrasion of a Nickel-Base Alloy and Composite, *Wear* 225-229 (1999) 154-162.

[83] S. Kim, J. Kim, Effects of Temperature and Contact Stress on the Sliding Wear of Ni-base Deloro 50 Hardfacing alloy, *Journal of Nuclear Materials* 288 (2001) 163-169.

[84] X. Xu, Y. Yu, XPS and SEM Characterization of Wheel/Workpiece Interface in Grinding of Superalloy, *Surface and Interface Analysis* 33 (2002) 343-350.

[85] F. Stott, High Temperature Sliding Wear of Metals, *Tribology International* 35 (2002) 489-495.

[86] I. Inman, S. Datta, H. Du, J. Burnell-Gray, Q. Luo, Microscopy of Glazed Layers formed During High Temperature Sliding Wear at 750°C, *Wear* 254 (2003) 461-467.

[87] H. Xie, G. Yang, P. La, W. Hao, J. Fan, W. Liu, L. Xu, Microstructure and Wear Performance of Ni-20 wt% Pb Hypomonotectic Alloys, *Materials Characterization* 52 (2004) 153-158.

[88] I. Inman, S. Datta, H. Du, J. Burnell-Gray, Q. Luo, Studies of High Temperature Sliding Wear of Metallic Dissimilar Interfaces, *Tribology International* 38 (2005) 812-823.

[89] I. Inman, S. Rose, P. Datta, Studies of High Temperature Sliding Wear of Metallic Dissimilar Interfaces II: Incoloy MA956 versus Stellite 6, *Tribology International* 39 (2006) 1361-1375.

[90] T. Hejwowski, Sliding Wear of Fe, Ni, and Co Based Alloys for Plasma Deposition, *Vacuum* 80 (2006) 1326-1330.

[91] P. Alison, H. Wilman, The Different Behavior of Hexagonal and Cubic Metals in their Friction, Wear, and Work Hardening During Abrasion, *British Journal of Applied Physics* 15 (1964) 281-289.

[92] H. Goto, D. Buckley, The Influence of Water Vapour in Air on the Friction Behavior of Pure Metals During Fretting, *Tribology International* vol 18, no 4 (1985) 237-245.

[93] J. Takadoum, C. Roques-Carmes, Influence of the Oxidation Activity of Metals on Friction and Wear of Ceramic-Metal Systems, *Surface and Coatings Technology* 52 (1992) 153-158.

[94] D. Moore, J. Flitter, Friction and Wear of Plasma-Sprayed NiO Based Coatings, *Journal of Vacuum Science Technology* vol 11, no 4 (1974) 754-758.

[95] S. Harris, M. Overs, A. Gould, The Use of Coatings to Control Fretting Wear at Ambient and Elevated Temperatures, *Wear* 106 (1985) 35-52.

[96] J. Lankford, W. Wei, R. Kossowsky, Friction and Wear Behavior of Ion Beam Modified Ceramics, *Journal of Materials Science* 22 (1987) 2069-2078.

[97] D. Gawne, U. Ma, Wear Mechanisms in Electroless Nickel Coatings, *Wear* 120 (1987) 125-149.

[98] M. Ahmed, R. Abd El-Karim, S. El-Raghy, F. El-Refaie, A. El-Mehairy, Wear Resistance of Plasma Coatings on Mild Steel, *Journal of Materials Science* 26 (1991) 517-522.

[99] J. Sue, T. Chang, Friction and Wear Behavior of Titanium Nitride, Zirconium Nitride, and Chromium Nitride Coatings at Elevated Temperatures, *Surface and Coatings Technology* 76-77 (1995) 61-69.

[100] D. Taylor, P. Fleig, S. Schwab, R. Page, Sol-Gel Derived, Nanostructured Oxide Lubricant Coatings, *Surface and Coatings Technology* 120-121 (1999) 465-469.

[101] L. Jun, W. Yiyong, W. Dianlong, H. Xinguo, The Microstructure and Wear Resistance Characteristics of Electroformed Nickel and Partially Stabilized Zirconia Composite Coatings, *Journal of Materials Science* 35 (2000) 1751-1758.

[102] D. Taylor, P. Fleig, R. Page, Characterization of Nickel Titanate Synthesized by Sol-Gel Processing, *Thin Solid Films* 408 (2002) 104-110.

[103] M. Chao, E. Liang, Effect of TiO_2-Doping on the Microstructure and the Wear Properties of Laser-Clad Nickel-Based Coatings, *Surface and Coatings Technology* 179 (2004) 265-271.

[104] K. Kumar, R. Chandramohan, D. Kalyanaraman, Effect of Heat Treatment on Cobalt and Nickel Electroplated Surfaces with Cr_2O_3 Dispersions, *Applied Surface Science* 227 (2004) 383-386.

[105] K. Kim, R. Davis, Electron Spectroscopy of the Nickel-Oxygen System, *Journal of Electron Spectroscopy and Related Phenomena* 1 (1972) 251-258.

[106] G. Wood, I. Wright, J. Ferguson, The Oxidation of Ni and Co and of Ni/Co Alloys at High Temperatures, *Corrosion Science* 5 (1965) 645-661.

[107] K. Kim, N. Winograd, X-Ray Photoelectron Spectroscopic Studies of Nickel-Oxygen Surfaces Using Oxygen and Argon Ion-Bombardment, *Surface Science* 43 (1974) 625-643.

[108] S. Uhlenbrock, C. Scharfschwerdt, M. Neumann, G. Illing, H. Freund, The Influence of Defects on the Ni 2p and O 1s XPS of NiO, *Journal of Physics: Condensed Matter* 4 (1992) 7973-7978.

[109] B. Payne, A. Grosvenor, M. Biesinger, B. Kobe, N. McIntyre, Structure and growth of oxides on polycrystalline nickel surfaces, *Surface and Interface Analysis* 39 (2007) 582-592.

[110] G. Zambelli, A. Levy, Particulate Erosion of NiO Scales, *Wear* 68 (1981) 305-331.

[111] M. Roy, K. Ray, G. Sundararajan, An Analysis of the Transition from Metal Erosion to Oxide Erosion, *Wear* 217 (1998) 312-320.

[112] E. Gulbransen, K. Andrew, High Temperature Oxidation of High Purity Nickel Between 750°C and 1050°C, *Journal of the Electrochemical Society* Vol. 104 No. 7 (1957) 451-454.

[113] F. Rhines, R. Connell Jr., Role of Grain Growth in the Oxidation of Nickel, *Journal of the Electrochemical Society* Vol .124 No. 7 (1977) 1122-1128.

[114] R. Lewis, Hawley's Condensed Chemical Dictionary (14th Edition), John Wiley & Sons.

[115] A. Iwabuchi, K. Hori, H. Kubosawa, The Effect of Oxide Particles Supplied at the Interface Before Sliding on the Severe-Mild Wear Transition, *Wear* 128 (1988) 123-137.

[116] A. Iwabuchi, H. Kubosawa, K. Hori, The Dependence of the Transition from Severe to Mild Wear on the Load and Surface Roughness When the Oxide Particles are Supplied Before Sliding, *Wear* 139 (1990) 319-333.

[117] A. Iwabuchi, The Role of Oxide Particles in the Fretting Wear of Mild Steel, *Wear* 151 (1991) 301-311.

[118] A.E. Segall, A. Papyrin, J.C. Conway, Jr., and D. Shapiro*, "A Cold Gas Spray Coating Process for Enhancing Titanium," *Proceedings of the Symposium on Innovations in Titanium held at the 127th TMS Annual Meeting*, San Antonio, TX, , pp. 52-54, February 15-19, 1998.

[119] M. F. Amateau and T. J. Eden, "High Velocity Particle Consolidation Technology", *iMAST Quarterly 2000 No. 2*, 3-6.

[120] C. Hager, Jr., J. Sanders, and S. Sharma, "Effect of high temperature on the characterization of fretting wear regimes at Ti6Al4V interfaces," *Wear*, 260 (2006) 493-508.

[121] F. Cheng, P. Shi, H. Man, Nature of oxide layer formed on NiTi by anodic oxidation in methanol, *Materials Letters* 59 (2005) 1516-1520.

[122] K. Adachi, K. Kato, Formation of Smooth Wear Surfaces on Alumina Ceramics by Embedding and Tribo-Sintering of Fine Wear Particles, *Wear* 245 (2000) 84-91.

[123] K. Kato, K. Komai, Tribofilm Formation and Mild Wear by Tribo-Sintering of Nanometer Sized Oxide Particles on Rubbing Steel Surfaces, *Wear* 262 (2007) 36-41.

[124] R. Rhines, J. Wolf, The Role of Oxide Microstructure and Growth Stresses in High Temperature Scaling of Nickel, *Metallurgical Transactions* vol 1 June (1970) 1701-1710.

[125] M. Nagl, W. Evans, The Mechanical Failure of Oxide Scales Under Tensile or Compressive Load, *Journal of Material Science* 28 (1993) 6247-6260.

[126] A. Sergueeva, N. Mara, A. Mukherjee, Plasticity at Really Diminished Length Scales, *Material Science and Engineering A* 463 (2007) 8-13.

[127] S. Prasad, J. Zabinski, Tribological Behavior of Nanocrystalline Zinc Oxide Films, *Wear* 203-204 (1997) 498-506.

[128] S. Prasad, J. Nainaparampil, J. Zabinski, Lubricious Zinc Oxide Films Grown by Pulsed Laser Deposition: Lateral Force Microscopy of Wear Surfaces, *Journal of Materials Science Letters* 19 (2000) 1979-1981.

[129] J. Zabinski, J. Sanders, J. Nainaparampil, S. Prasad, Lubrication Using a Microstructurally Engineered Oxide: Performance and Mechanisms, *Tribology Letters* (2000) 103-116.

[130] S. Prasad, S. Walck, J. Zabinski, Microstructural Evolution in Lubricious ZnO Films Grown by Pulsed Laser Deposition, *Thin Solid Films* 360 (2000) 107-117.

[131] M. Romanes, T. Scharf, Lubricious Oxides Grown by Atomic Layer Deposition, *to be submitted to Tribology Letters* (2008).

[132] J. Sullivan, N. Granville, Reciprocating Sliding Wear of 9% Cr Steel in Carbon Dioxide at Elevated Temperatures, *Tribology International* (1984) 63-71.

[133] M. Woydt, A. Skopp, I. Dorfel, K. Witke, Wear engineering oxides/anti-wear oxides, *Wear* 218 (1998) 84-95.

[134] F. Cheng, P. Shi, H. Man, Nature of oxide layer formed on NiTi by anodic oxidation in methanol, *Materials Letters* 59 (2005) 1516-1520.

[135] R. Dietz, G. Parisot, A. Meixner, Infrared Adsorption and Raman Scattering by Two-Magnon Processes in NiO, *Physical Review B* vol 4 n7 (1971) 2302-2310.

[136] N. Mironova-Ulmane, A. Kuzmin, I. Steins, J. Grabis, I. Sildos, M. Pars, Raman Scattering in Nanosized Nickel Oxide NiO, *Journal of Physics: Conference Series* 93 (2007) 1-5.

[137] H. Yang, P. McCormick, Mechanically Activated Reduction of Nickel Oxide with Graphite, *Metallurgical and Materials Transactions B* vol 29B April (1998) 449-455.

[138] A. Evans, D. Rajdev, and D. Douglass, The Mechanical Properties of Nickel Oxide and Their Relationship to the Morphology of Thick Oxide Scales Formed on Nickel, *Oxidation of Metals* vol. 4 No. 3 (1972) 151-171.